# NEURON ADHESION PATTERNING ON POLYMERS BY NEGATIVE-ION IMPLANTATION( Dissertation_全文 )

AUTHOR(S):

SOMMANI, Piyanuch

# NEURON ADHESION PATTERNING ON POLYMERS

# BY

# NEGATIVE-ION IMPLANTATION

**Piyanuch SOMMANI**

**2007**

# ABSTRACT

Many conventional methods have been used to modify the wettability of the polymeric surfaces for the biomedical applications of the artificial bionic organ. Those methods are the chemical treatment, the ultraviolet (UV) irradiation, the plasma process and the ion implantation. Many artificial bionic organs, for example, an artificial heart, an artificial blood vessel, a device for prevention of thrombosis stent and an artificial endocranium have been developed for the physical or mental disability. For development of the high function of an artificial bionic organ, the data transmission between the brain neuron cells and the external electrical circuit, and the high biocompatible materials for the interface between brain and electrode are required. It is related to the technology of brain-computer interface (BCI), sometimes called a direct neural interface or a brain-machine interface. In case of the brain-controlled devices, the study of the brain memory is necessary. Then, the artificial pattern network of the brain cells cultured on the surface in vitro for simulation of the brain function is the concerned issue. The arrangement of a lot of neuron on a detection electrode is required. So, a formation method of the artificial neural network that arranged a neuron as technology for this purpose is demanded

As for the neuron arrangement, there were the reports about the immobilization of neuron by fabrication of the three-dimension structure, and they could be divided into two methods from their manipulation. One is the arrangement with one-by-one manipulation and the other is the arrangement with self-assembly. The former method is the fabrication of many micro-structures and then arranged a neuron in a desired position with one-by-one manipulation to for a neuron network. For the brain memory stimulation, however, the neuron network from more than 10 millions of neurons is required. So, this method is not suitable. The latter is the fabrication of the carbon nanotube pillar to immobilize the neurosphere with self-assembly adhesion. Although this method could be formed the large neuron network, the neurosphere consists of several 1,000 cells. So, it is very difficult to analyze the mechanism of data transformation. In contrast, by surface modification even if on the same surface to modify a geometric pattern, the cells can adhere along the modified pattern by using single culture on such surface. The neuron will migrate itself to adhere on the pattern. The self-assembly adhesion occur. This method is very useful for the neuron arrangement method.

The surface modification of the polymeric materials to pattern the cell adhesion area as a network has been taken place by using many techniques such as the plasma process, the irradiations of UV and X-ray and the ion implantation. The ion implantation technique into the polymeric-material surface has more advantage than the other techniques since its abilities to control the micro-area, and to break down the tight bonding of polymer material. The ion

implantation with positive ion without charge neutralization results in a charge-up problem due to the insulating properties of most polymers. This charge-up problem exerts a bad influence on the implantation control of ion dose and ion energy. The negative-ion implantation occurs almost "charge-up free" even if no external charge compensation. Then, the negative-ion implantation into polymeric surface has a very precise control to obtain very fine pattern. So, it is expected to control the adhesion size of about single cells (about several 10 μm). Since this study will be used for the application in the biomedical fields, the ion element should be considered to be harmless for the living body. Then, carbon is selected since it is main component of polymer materials and more familiar to cells.

As above described, in this thesis, I use the carbon negative-ion implantation to modify the polymeric surface to obtain the pattern of the neuron with self-assembly-adhesion. As for the polymeric material in the biomedical fields, I selected polystyrene (PS) and silicone rubber (SR). In this research, the fundamental parameters for cell adhesion on the modified surface by carbon negative-ion implantation were described (Chapters 3, 4 and 5). As for the fundamental issue, the wettability relating to the atomic bonding state of the new functional group and the surface morphology (Chapter 3), the protein adsorption (Chapter 4), and also the adhesion of nerve-like cells on the pattern (Chapter 5) were examined. In these chapters, I clarified the relationship among them and the negative-ion implantation. Then, based on these phenomena, I have developed the new application techniques by negative-ion implantation for the adhesion patterning of neuron (Chapters 6 and 7). In the development of these techniques, I have proposed two methods since the neuronal cells required the special base surface to adhere. One is degradation method of the special base surface by which I tried to make an artificial neuron network (Chapter 6). The other is the patterning of the stem cell adhesion and differentiation into neuron with maintaining the adhesion position. So, the neuron patterns were formed on the pattern (Chapter 7). The obtained results are summarized as the following.

In Chapter 3, the surfaces of the PS and SR were implanted by carbon negative ions at the energies of 5 – 20 keV and the doses of $1\times10^{13}$ – $3\times10^{16}$ ions/cm$^2$. After the implantation, the change in the physical surface properties, relating to the adsorption properties of adhesive proteins, was described. The new atomic bonding, the surface morphology and the wettability were studied by XPS analysis, AFM and contact angle measurement, respectively. XPS analysis showed the formation of new oxygen function groups of hydroxyl and carbonyl on the implanted surfaces from the adsorption of the oxygen in the residual gas and in the moisture in the air on the ion-induced defects. These new bonds refer to the hydrophilicity for the wettability. The ion implantation sputtered and changed the surface morphology of surface roughness in order of several nm that dose not interfere to the protein adsorption and to cell culture. The wettability properties of the $C^-$-implanted surfaces of SCPS and SR were evaluated by measuring the

change in contact angle. At first, the angles were measured by the water drop method. The contact angles of PS measured by water drop method decreased from 91° to 86° for the non-implantation to the implantation, respectively. Those of SR also decreased from 100° to 86° for the non-implantation to the implantation, respectively, even if the main chain bonds in SR are stronger than that in PS. The hydrophilic surfaces of PS and SR were obtained by carbon negative-ion implantation. Then, the contact angles were measured by the air bubble method. The sample was dipped in the water and the bubbles were injected on the surface. Then, the angle was evaluated from the arc circular of the bubble. After dipping in the water for 24 h, the average value of the angles decreased to 64° and to 52° for PS and SR, respectively. The more clearly hydrophilic properties were observed.

In Chapter 4, I checked the adsorption properties of the adhesive protein and the poly-D-lysine (PDL) on the implanted surface. Generally, in the cell adhesion, the adhesive proteins exist between the cell surface and the surface. On the cell membrane, cells have specific receptors that anchor to the specific protein. So, the adsorptions of the adhesive proteins are necessary for the cell adhesion. In nature, protein has both hydrophobic and hydrophilic groups. Thus, the ultra hydrophobic and ultra hydrophilic surfaces are not suitable for protein adsorption. The adhesive proteins for the cell adhesion generally prefer to be adsorbed on the hydrophilic surface, which the contact angle is in the range of 40° – 80°. I evaluated the adsorption properties of adhesive protein such as type-I collagen, fibronectin and laminin and that of PDL on the modified surfaces of PS and SR by detecting the nitrogen atom with using XPS analysis. As a result, the adsorptions of the adhesive protein were almost improved with 1.2 – 3.3 times by carbon negative-ion implantation.

In Chapter 5, the nerve-like cells of PC12h (rat adrenal pheochromocytoma) were cultured on the $C^-$-implanted surfaces of PS and SR to find out the fundamental condition for the neuron network formation. As a results, PC12h cells and their neurite outgrowth showed the self-assembly adhesion along the implanted pattern on both of PS and SR. The suitable condition of the ion implantation for the adhesion patterning of PC12h cells was about $1\times10^{15}$ – $3\times10^{15}$ ions/cm$^2$. Almost no effect of energy in the range of 5 – 20 keV on the cell adhesion was observed. The effective minimum line width of the implanted region for the adhesion of single cell-body and single neurite outgrowth were about 5 and 2 μm, respectively.

In Chapter 6, the brain neuronal cells require the specific surface culture, such as PDL. So, in this chapter, I used PDL coating on the PS and degraded it by the carbon negative-ion implantation. Two kinds of brain neuronal cells were used. One is newborn mouse brain neuronal cells (1 day) and the other is rat embryo brain cortex neuronal cells (16 – 18 days). As a result, I obtained the effective ion dose for degradation of the adhesion at $1\times10^{14}$ ions/cm$^2$. The adhesion patterning of brain neuronal cells on the unmodified pattern of PDL could be achieved by carbon

negative-ion implantation.

In Chapter 7, I cultured the adult stem cells of rat mesenchymal stem cells (MSC), which has the multipotential to differentiation into many kinds of cell lines, especially into neuron, on the pattern region of the $C^-$-implanted surfaces of PS and SR. As a results, MSCs showed the self-assembly adhesion along the implanted pattern of PS and SR. Comparing to the adhesion patterning of PC12h cells, the adhesion patterning of MSCs required a lower ion dose to implant on the polymeric surfaces. By culturing with the culture medium supplementing withβ-Mercaptoethanol (BME) at concentration of 1 mM, the MSCs were induced to differentiate into neuronal cells. The adhesion patterning of the neuron-differentiated cells maintained on the implanted region was observed. By staining with anti-neuron-specific enolase, these differentiated cells were neurons.

From all investigation, I clarified the change in the physical surface properties after the carbon negative-ion implantation into the polymeric surface and the mechanisms mentioned above. I showed the surface modification to obtain the hydrophilic surface by the ion-induced effect. This hydrophilic surface improved the protein adsorption properties. By using nerve-like cells, the ion implantation affecting to the cell adhesion were clarified. By the implantation through the micro-pattern mask, the cells adhered along the implanted pattern. The cells could adhere on the implanted area that was smaller than the cell size and their neurite also could adhere on the narrowed implanted area. So, I can obtain the self-assembly separation pattern of cell body adhesion and neurite outgrowth. For the application of patterning of real neuron, I coated the special surface with PDL and degraded it from patterning the negative-charge site on it by using carbon negative-ion implantation through a micro-pattern mask. I could pattern and form the neuron network of the brain neuron on the unmodified PDL. On the other hand, for the MSC, I also achieved the adhesion patterning by using carbon negative-ion implantation through a micro-pattern mask, and I succeeded the patterning of the neuron-differentiated cells from the adhered MSC with maintaining their adhesion pattern. As a conclusion, from all these researches, I achieved the cell-self-assembly adhesion and the patterning of the neuron network formation on the polymeric surfaces by using carbon negative-ion implantation.

# Acknowledgements

I would like to express my deep gratitude to my advisor, Professor Dr. Junzo Ishikawa, Department of Electronic Science and Engineering, Kyoto University for his supervision, extensive fruitful suggestions and discussion throughout this work. I acknowledge Professor Dr. Gikan Takaoka from Photonics and Electronic Science and Engineering Center, Kyoto University and Professor Dr. Tetsuo Kobayashi from Department of Electrical Engineering, Kyoto University for their critical reading of the manuscript and valuable comments.

I am deeply indebted to Assistant Professor Hiroshi Tsuji from Ishikawa's Laboratory for his co-supervision, continuous guidance, helpfully fruitful suggestions, discussion, comments on this work and the critical reading of the manuscript.

I am grateful to Associate Professor Yasuhito Gotoh and Assistant Professor Toyotsugu Ishibashi for their kind management and organization of the support academic works in Ishikawa's Laboratory.

I am also very obliged to Research Associate Dr. Hiroko Sato for continuous guidance, suggestions and discussion about the cell culture on this work.

I am thankful to Miss Ayako Tanaka, a secretary of Ishikawa's Laboratory for her management of the general work in Ishikawa's Laboratory.

Sincere thanks also go to all student members of Ishikawa Laboratory. In particular, I wished to express my great appreciation to Mr. Tetsuya Yamada (M2), Mr. Hiroyuki Kojima (M1), Mr. Mitsutaka Hattori (graduated), Mr. Tsuyoshi Kitamura (graduated) and Mr. Takashi Mutoh (graduated), for their collaborations, to Nobutoshi Arai (D3) for his kind translation of Japanese languages in filling up some applications and to Mr. Hiroyuki Nakatsuka (graduated) for his kindly tutoring in Japanese life and translation of Japanese conversations.

Experiments were partially assisted by facilities of index center, Kyoto University Venture Business Laboratory for the XPS analysis.

I am grateful to Assistance Professor Ryosuke Kakinoki, Dr. Ken Nakayama, Dr Tomoyuki Yamakawa and Dr. Yoshihide Morimoto from Department of Orthopedic Surgery, Kyoto University for their derivation of rat mesenchymal stem cells. I am also grateful to Mr. Junji Nakamura, Institute for Frontier Medical Science, Kyoto University for his cryopreservation of newborn mouse brain neuronal cells.

The partial financial supports from the Japan Student Services Organization (JASSO) for the Japanese government (Monbukagakusho: MEXT) scholarship are very much appreciated.

Lastly, I am indebted to my beloved father, who passed away since I was a high school student, for being a great model and giving me inspiration as well as my beloved mother, my elder sister, my aunts and my uncles for their consistent encouragements and supports.

Piyanuch Sommani

# Contents

# Abbreviation

| | |
|---|---|
| AFM | Atomic force microscopy |
| BCI | Brain-computer interface |
| BME | β-Mercaptoethanol |
| BSA | Bovine serum albumin |
| CA | Contact angle |
| CAM | Cell adhesion molecule |
| CNS | Central nervous system |
| Co-I | Type I collagen |
| Da | Atomic mass unit |
| DAPI | 4′, 6-diamino-2-phenylindole |
| DIW | De-ionized water |
| DMEM | Dulbecco's modified Eagle medium |
| DP | Diffusion pump |
| ECM | Extracellular matrix |
| EDTA | Ethylenediamine tetraacetic acid |
| ES | Embryo stem |
| F-actin | Actin filament |
| FBS | Fetal bovine serum |
| FITC | Fluorescein isothiocyanate |
| FN | Fibronectin |
| HS | Horse serum |
| IC | Integrated circuit |
| LN | Laminin |
| MSC | Mesenchymal stem cell |
| NGF | Nerve-growth factor |
| NIABNIS | Neutral and ionized alkaline metal bombardment type heavy negative-ion source |
| N-medium | Neurobasal medium |
| NSE | Neuron-specific enolase |
| NTPS | Non-treat polystyrene |
| PBS | Phosphate-buffered saline |
| PC12h | Rat adrenal pheochromocytoma |

| | |
|---|---|
| PDL | Poly-D-lysine |
| PEI | Polyethyleneimine |
| PNS | Peripheral nervous system |
| PS | Polystyrene |
| SCPS | Spin-coated polystyrene |
| SR | Silicone rubber |
| TCPS | Tissue-culture polystyrene |
| TMP | Turbo molecular pump |
| TRIM | Transport of ions in matter |
| Triton-X | Polyethylene glycol p-(1, 1, 3, 3-tetramethylbutyl)-phenyl ether |
| Tr-X phalloidin | Texas Red-X phalloidin |
| UV | Ultraviolet |
| XPS | X-ray photoelectron spectroscopy |

# Symbols

| | |
|---|---|
| $a$ | Screening parameter; radius of water drop in the contact angle measurement |
| $b$ | Height of water drop in the contact angle measurement |
| $c$ | Radius of air bubble in the contact angle measurement |
| $C_0$ | Constant value for calculation of sputtering yield |
| $d$ | Height of air bubble in the contact angle measurement |
| $c_k$ | Correction factor |
| $E$ | Ion implantation energy |
| $E_D$ | Energy deposited in the solid |
| $\Delta E$ | Energy transferred at the penetrated depth |
| $k_{CA}$ | Constant value for calculation contact angle |
| $k_{LS}$ | Lindhard-Scharff constant |
| $M$ | Mass (index 1 for ion, index 2 for target atom) |
| $N$ | Atomic density |
| $N(OH)$ | Number of hydrophilic groups induced by the implantation |
| $N_s$ | Dose concentration of the implantation ion |
| $N(x)$ | Concentration of the implanted substrate |
| $p$ | Impact collision parameter |
| $R$ | Range distribution (index $i$ for the $i^{th}$ component in compound material) |
| $R_p$ | Projected range (index $i$ for the $i^{th}$ component in compound material) |
| $\Delta R_p$ | Standard deviation (index $i$ for the $i^{th}$ component in compound material) |
| $S$ | Stopping power (index $e$ for electronic stopping power, index $n$ for nuclear stopping power) |
| $T$ | Transferred energy (index $m$ for maximum, index $e$ for electronic stopping power, index $n$ for nuclear stopping power) |
| $U_0$ | The surface binding energy |
| $v$ | Particle velocity |
| $W_{12}$ | Work of adhesion between solid and liquid |
| $x$ | X-direction |
| $X_i$ | Fraction of the total mass of the $i^{th}$ component in compound material |
| $Z$ | Atomic number |
| $Y_S$ | Sputtering yield |
| $\alpha(M_2/M_1)$ | Efficiency of energy transfer |
| $\gamma$ | Transfer efficiency of the ion (index $i$ for the $i^{th}$ component in compound |

| | |
|---|---|
| | material); surface free energy (index 1 for solid, index 2 for liquid, index *w* for water, index 0 for solid at the initial state, index *i* for solid after implantation, superscript index *a* for dispersion force, superscript index *b* for polar force, superscript index *c* for hydrogen bonding force, superscript index *f* for the $f^{th}$ component of surface forces) |
| $\Delta\gamma$ | Different value of surface free energy for solid (superscript index *a* for dispersion force, superscript index *b* for polar force, superscript index *c* for hydrogen bonding force, superscript index *f* for the $f^{th}$ component of surface forces) |
| $\lambda$ | Constant value for calculation of sputtering yield |
| $\Phi$ | Deflection angle in the center-of-mass system |
| $\theta$ | Contact angle (index 1 for the angle measured by water drop method, index 2 for the angle measured by air bubble method, index 0 for the initial angle before implantation, index *i* for the angle after implantation) |
| $\Delta\theta$ | Different value of the contact angle |

# Chapter 1

# Introduction

## 1.1 Background and Idea to Solve the Problem

Nowadays, many researchers and many doctors put a lot of efforts to develop many helpful technologies for many patients. Many artificial bionic organs, for example, eyes, ears, nose and limbs have been developed for the physical or mental disability [1-5]. Such artificial organs require the data transmission between the brain nerve cells and external electrical circuit and need the control by the brain. Then, the technology for brain-computer interface (BCI), sometimes called a direct neural interface or a brain-machine interface has been started [6]. The BCI is a direct communication pathway between a human or animal brain (or brain cell culture) and an external device. For the data communication, the high biocompatible materials for the interface between brain and the electrode are required. In case of the brain-controlled devices, the memory mechanism in the brain as neuron network has to be studied. Then, the artificial pattern network of the brain cells cultured on the surface *in vitro* for simulation of the brain function is the concerned issue. The arrangement of the neuron on the desired pattern is required.

There are many conventional methods for enhancement of cell adhesion or for improvement of biocompatibility of polymeric materials. In general, the chemical treatment, the ultraviolet (UV) irradiation and gas plasma process have been applied for these purposes. Recently, the ion implantation technique has been also examined for improvement of the biocompatibility. Although the chemical treatment, which is a coating of the extracellular matrix (ECM) on the surface by imprinting method [7] and by photolithography [8], is a rapid and easy process for treatment of the large area, but it is difficult to pattern a fine area. When dipping in the culture medium, the pattern fabricated from this method will be immersed. Next to the UV irradiation, this method is also a rapid process for the treatment of the large area and can pattern the fine area, but it is difficult to pattern the area on the tight bonding of polymeric material such as silicone rubber (SR). The gas plasma process, including the chemical vapor deposition and sputtering process, can pattern the area on the tight bonding material of SR, but it has a poor controllability for fabrication of a fine area. So, these three methods are not good to use for the neuron arrangement. In case of the ion implantation technique, this method not only can pattern the fine area on the tight bonding material of SR, but also has a good controllability for fabrication of the fine area. Therefore, the ion implantation technique is considered to be the best

candidate method for pattern the cell adhesion. As for the neuron arrangement, some researchers reported the some immobilization techniques by using the micro-fabrications of the three-dimension structures such as a pillar and a groove [9, 10]. They seeded one neuron into the fabricated structure. This method is the immobilization of the neuron with one-by-one cell manipulation. It is very difficult to form the neuron network by this method. Therefore, the formation of the neuron network requires the self-assemble adhesion, which cells assembled adhere on the certain pattern of the surface by cell-self. The self-assemble adhesion will be established by control of biocompatibility.

In the ion implantation, both types of positive and negative ions can be used to modify the polymeric surfaces. Generally, many researchers apply the positive-ion implantation to modify the polymeric surface [11-14]. They almost used the positive ion for implantation into the polymeric surface at very high energy of several hundred-keV [11-14]. Applying positive-ion implantation without charge neutralization results in a charge-up problem due to the insulating properties of most polymers. This charge-up problem exerts a bad influence on the implantation control of ion dose and ion energy [15-20]. In contrast in the negative-ion implantation into the polymeric surface, the "charge-up free" implantation is possible even if no external charge compensation [21-24]. Then, the implantation dose and energy can be precisely controlled even if at a much lower ion-energy such one to several tens of keV. Therefore, negative-ion implantation is a promising method for the surface modification of polymer materials.

Tsuji *et al.* reported the control of endothelial cell adhesion on the polymeric surface by using the negative-ion implantations of silver because they had expected an antibacterial of the silver atoms [21-24]. However, the heavy metal, including silver, can be harmful to the living body. Comparing to silver, carbon is a lighter element, mainly component of polymer materials and more familiar to cells. It will be harmless for the living body. Therefore, the implantation with the carbon negative-ions is better to be used to modify the polymeric surface for application in the biomedical field.

As for the neuron arrangement, the carbon negative-ion implantation is used to modify the biocompatibility of the polymeric surface, and the neuron will adhere on the modified polymeric surface. The idea of the self-assembly arrangement of the neuron with their neurite outgrowth on the polymeric surface by carbon negative-ion implantation is purposed. The adhesion pattern of both of the cell bodies and their neurite outgrowth on the modified surface is as shown in Fig. 1.1. The neurons are expected to adhere and to extend their neurite only on the modified surface. Therefore, the self-assembly patterning of the neuron network will be obtained.

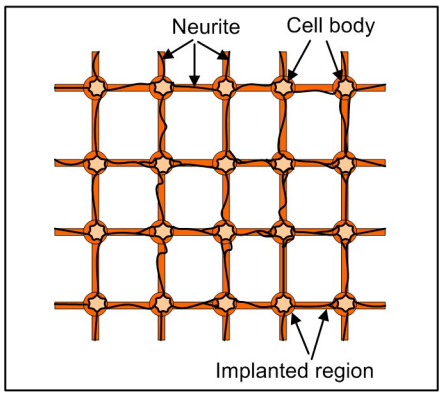


Fig. 1.1 Schematic diagram of the neuron network pattern.

## 1.2 Cell Adhesion and Negative-Ion Implantation Effect

For the achievement of the cell adhesion pattern, one of the important factors for the cell adhesion that should be considered is the mechanism of cell adhesion. Fig. 1.2 shows the schematic diagram of cell adhesion junction. In nature, there are two types of cell adhesion junctions [25-27]. One is the adhesion between cells. The other is the adhesion between cell and the extracellular matrix (ECM) adsorbed on the substratum. The cells adhere to each other and to the extracellular matrix through the intracellular attachment proteins and the cell-surface proteins of the cell adhesion molecules (CAMs). The cell-surface proteins can bind to the specific protein so that sometimes they are so-called the cell-surface receptors. They can be cell-cell adhesion molecules or cell-matrix adhesion molecules. Types of the intracellular attachment protein and

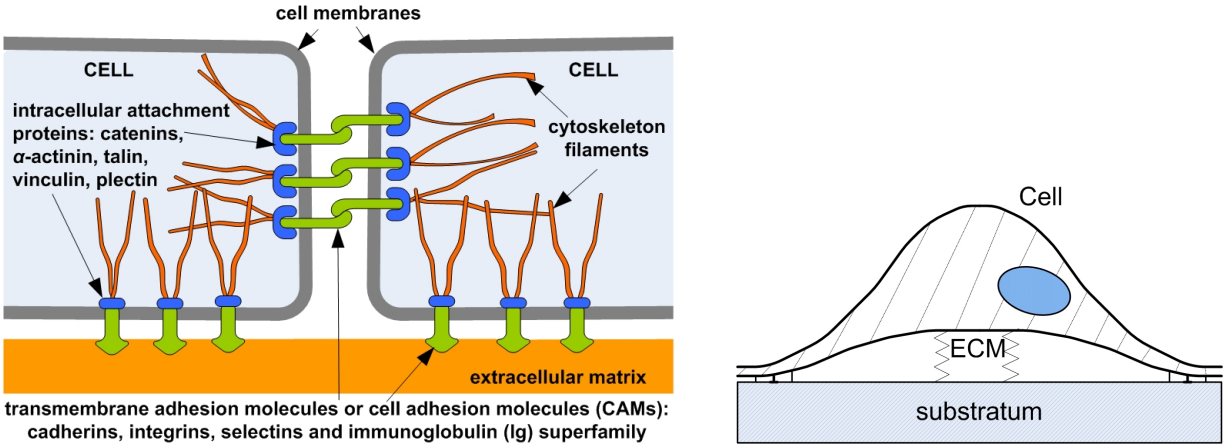


(a) Cell-cell adhesion (b) Cell-ECM-substratum adhesion

Fig. 1.2 Schematic diagram of cell adhesion junction between: (a) cell-cell; and (b) cell-ECM-substratum.

the CAMs are different for the adhesion of cell-cell and cell-ECM-substratum. As for cell-cell adhesion, the intracellular attachment protein and CAMs usually are catenins and cadheirns, respectively. As for cell-ECM-substratum adhesion, those usually are talin and integrins, respectively. Integrins generally anchor to the fibronectin, which have a domain binding to collagen. From the cell adhesion mechanism, the important parameter for the cell adhesion on the surface is the ECM. As for the ECM, the main components of ECM are collagen, proteoglycans and other glycoproteins, such as fibronectin and laminin [27]. The ECM serves as a structural element in tissues and also influences their development and physiology. In the *in vitro* culture, the ECM is delivered from the supplement of serum in the culture medium and from the cell release. However, the ECM released from cells is very small amount. Almost ECM adsorption on the surface for the cell adhesion is first from the culture medium.

The adhesive proteins in the ECM are a main point for the cell adhesion. For the cell-adhesion patterning, the promoting of the protein adsorption on the surface is required. In natural, all proteins consist of both hydrophobic and hydrophilic bonds [28], and those are randomly absorbed on the surface. Therefore, both of the ultra hydrophilic surface and the ultra hydrophobic surface are not good for the promoting adsorption of protein. The hydrophobic-hydrophilic properties correspond to the high-low contact angle. The suitable contact angle for the cell adhesion is generally in the range of 40° – 80° [29]. It indicates that the adhesive proteins prefer to be adsorbed on the hydrophilic surface. Therefore, if the contact angle of the polymeric surface can be modified to be in this rage, the adhesive proteins are expected to be adsorbed on the modified area, resulting in possible cell adhesion pattern on this area. The schematic diagram of the cell adhesion patterning is shown in Fig. 1.3. The adhesive proteins in ECM are immobilized on the modified surface (Fig. l.3 (a)), resulting in the adhesions of cells on these immobilized ECM (Fig. 1.3 (b). Then, the self-assembly adhesion of cells are obtained.

The contact angle of the polymeric surface could be modified by the negative-ion implantation [21-24], even if the silver ions were used. After the negative-ion implantation, both of the increasing or lowering of the contact angle could be possible, depending on the surface properties of the basic polymeric materials. In case of the hydrophobic surface, the lowering of the contact angle was obtained after the ion implantation by controlling of the ion dose and


(a) The immobilized ECM on the modified surface (b) Cell adhesions on the immobilized ECM

Fig. 1.3 Schematic diagram of the cell adhesion patterning: (a) the immobilized ECM on the modified surface; and (b) cell adhesions on the immobilized ECM.

energy [22]. In contrast, in case of the hydrophilic surface, the increasing of the angle occurred [23]. The improvement and degradation of the protein adsorption could be controlled.

In case of the carbon negative-ion implantation, the implantation into the normal hydrophobic surface of polymeric material with using a micro-pattern mask might pattern the cell adhesion on the implanted region. The lowering of the contact angle and the improvement of the protein adsorption on the implanted region was expected. The adhesion pattern of both of the cell bodies and their neurite outgrowth should be obtained as shown in Fig. 1.1.

From the speculation of the cell adhesion patterning on the modified surface, the carbon negative-ion implantation should be used to pattern the neuron adhesion. In the real formation of neuron network, however, there are many influence factors. So, the properties of the physical surface, the protein adsorption and the cell adhesion on the modified surface have to be studied.

## 1.3 Objectives

In this work, I applied the carbon negative-ion implantation to modify the polymeric surfaces of polystyrene and silicone rubber. Polystyrene and silicone rubber were used since these polymeric materials are widely used in the biomedical fields. Polystyrene is generally used in the field of medical equipment such as the cell culture dish and it is safety for the *in vitro* experiment. Silicone rubber is generally used in the medical fields since it is a stable biomaterial with the inactive against to the living body and it is very flexible in shape. Both of these polymers have a difference in main chain bonding. The main chain bond of polystyrene is the C-C bond, and that of silicone rubber is the Si-O. After the implantation, the fundamental properties relating to the cell adhesion were studied. The physical surface properties relating to ECM adsorption and cell adhesion, the new atomic bonding, the surface morphology and the wettability were examined. The adsorption properties of the adhesive proteins in ECM were evaluated. The fundamental conditions for the cell adhesion pattern properties were studied. After the fundamental conditions were obtained, the real neuron adhesion patterning on the polymeric surface by carbon negative-ion implantation would be done.

As for the changes in the physical surface properties relating to ECM adsorption and cell adhesion, I firstly investigated of the changes in the atomic bonding state by using X-ray photoelectron spectroscopy (XPS) to reveal the reason of the wettability change. Then, I studied the changes in the surface morphologies of the surface roughness by using atomic force microscope (AFM) to clarify the related reason of the protein adsorption and the cell adhesion. Finally, I evaluated the suitable condition of the carbon negative-ion implantation for the suitable wettability for the expected cell adhesion. The changes in the wettabilities were evaluated by measuring the contact angle of the de-ionized water. The contact angles were measured by the

water drop method and the air bubble method for study of the circumstance dependence. The water drop method is the measuring of the angle in the air within 2 h just after implantation. The air bubble method is the measuring of the angle in the de-ionized water (DIW) after dipping in DIW with the different time for study of the time dependence of the changes in contact angle.

As for the study of the adsorption of the ECM affecting the selective cell adhesion properties, I evaluated the adsorption properties of the adhesive proteins and poly-D-lysine (PDL) on the modified surfaces by detecting the amount of nitrogen atoms adsorbed on both of the implanted and unimplanted regions to investigate the possibility for the clear selective cell adhesion pattern. The studied adhesive proteins were type-I collagen, fibronectin and laminin. The suitable concentrations of the coating concentration and the ion dose for the selective adsorption ratio are evaluated by using XPS analysis.

As for the first study of the cell adhesion patterning, I selected the nerve-like cell of the rat adrenal pheochromocytoma cell (PC12h). Since this clone cell has the same specific characteristics of neurite extension similar to neuron ones [25, 30] and a strong ability to survival in the long term culture with an increase in the number, it is suitable for the essential assessment of study. To find the fundamental conditions for the good properties for cell adhesion and neurite outgrowth and for the immobilization, I investigated the culture of PC12h cells on the polymeric surfaces modified by the carbon negative-ion implantation at the various ion doses and energies with many micro-pattern masks. The properties of cell adhesion and neurite outgrowth were observed by using phase-contrast microscopy. The effects of ion dose, ion energy, additional adhesive protein coating, and the implanted line width on the properties were studied. Finally, the suitable condition for simple neuron network pattern was presented. From these fundamental assessments, I could predict the adhesion of other cell line by using culture at some conditions.

As for the adhesion patterning of the real neuron, there is one of the important issues that the brain neuronal cells can adhere only on the specific surface of the polycation polymers of PDL or polyethyleneimine (PEI) [31-34]. The other issue is the adsorption property of such polycation polymers on polystyrene. In this part, the carbon negative ions would be implanted into the polycation polymers to degrade it, so that the brain neuronal cells could not adhere on it. The patterned adhesion of the brain neuronal cells was expected to be on the non-modified region. To check the possibility for patterning the degradation of PDL, the decrease of the positive-charge sites relating to the nitrogen atoms should be evaluated by XPS analysis. In order to enhance PDL adsorption on the surface, the pre-treated surface by carbon negative-ion implantation before PDL coating was done. The suitable coating concentrations of the PDL solution for the cell adhesion were examined by culturing the newborn mouse brain neuronal cells. The adhesion properties of the newborn mouse brain neuronal cells on the coating surfaces of PDL were studied by phase-contrast microscopy and fluorescent microscopy. Then, I tried to

make a neuron patterning by using the rat embryo brain cortex neuronal cells. The properties of cell adhesion and neurite outgrowth were observed by phase-contrast microscopy and fluorescent microscopy. I used the immunofluorescent techniques to confirm the neurons by staining with antibodies for neuro marker and dyes.

The neuron network can be formed not only from the neurons of the brain cells, but also from the neurons that are differentiated from the stem cells. Stem cells not only retain the self renewal ability [35], but also the ability of unlimited potency to differentiate into a wide range of specialized cell types [36-37], especially, into neurons. Three broad categories of the stem cells are composed of the embryonic stem cell (ES), adult stem cells and cord blood stem cells. Recently, the stem cell, especially the adult stem cells such as mesenchymal stem cell (MSC) have the multipotential for the differentiation characteristic, are going to be used in the medical therapies [38-42]. MSCs are on the research since their potency of differentiation into neuron of peripheral nervous system and into other cells that support the nerve regeneration. These cells can be derived from the bone marrow [43-44] and the umbilical cord blood [38], so that they have no limitation in the ethic usage. The adhesion patterning of MSC on the polymeric surface and the differentiation into neuronal cells as keeping an adhesion site on the pattern can be one method for the formation of the neuron network.

As for the adhesion patterning of the real neuron from stem cell differentiation, at first, the suitable implantation conditions for the adhesions of MSC on the patterned polymeric materials by the carbon negative-ion implantation were investigated and then the differentiation into neuronal cells as keeping an adhesion site on the pattern was done. To study the implantation condition, the rat MSCs were cultured on the patterned polymeric surfaces. By considering some adhesion properties of MSC and the fundamental assessment obtained by PC12h culture in the previous work, I could predict the tendency to obtain the good adhesion properties. After I obtained the suitable implantation conditions for the adhesion pattering of MSC, the adhered MSCs were differentiated into neuronal cells. As for the differentiation, the β-Mercaptoethanol (BME) was used [45]. The adhesion patterning of MSC and the differentiated cells were observed by phase-contrast microscopy and fluorescent microscopy. I used the immunofluorescent techniques to confirm the neurons by staining with antibodies for neuro marker and dyes.

## 1.4 Chapter Organization

This thesis consists of many chapters that are corresponding to the previous objectives. The flowchart of chapter organization and the relationship among chapters are illustrated in Fig. 1.4.

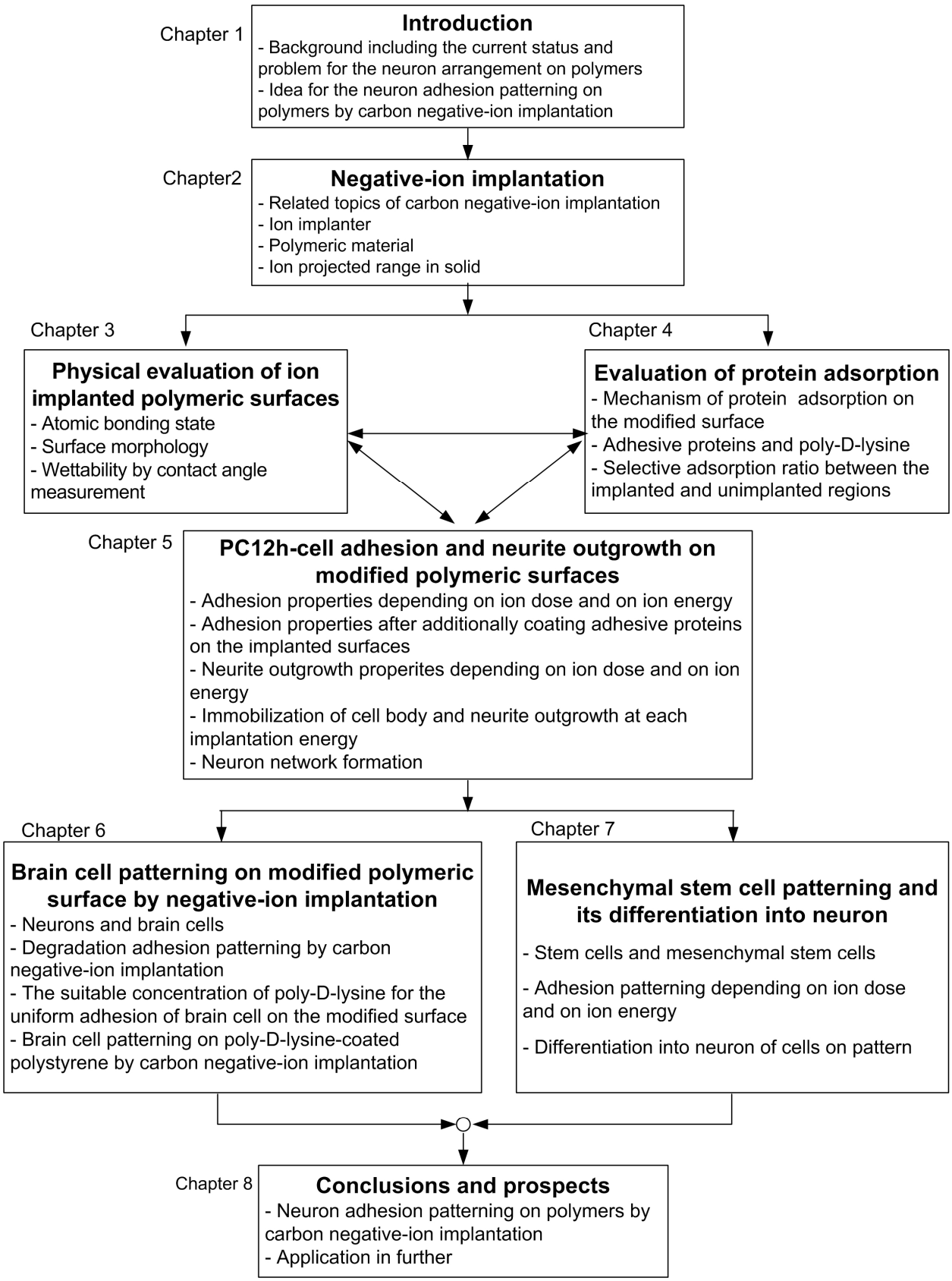


Fig. 1.4 Flowchart of chapter organization.

From the objectives, this thesis can be classified into two main parts of the fundamental phenomena (Chapters 3, 4 and 5) and the applications of the neuron adhesion patterning (Chapters 6 and 7), in addition to the introduction (Chapter 1), the implantation apparatus explanation (Chapter 2) and the conclusion (Chapter 8). Brief explanations of each chapter are as follows:

In Chapter 1, the background for the current status and the problem for the arrangement of the neuron as a pattern on the polymeric surface, the idea for neuron adhesion patterning on polymers by carbon negative-ion implantation, the speculation of the cell adhesion patterning on the modified surface and the objectives of each experiment for obtaining the neuron adhesion pattern are described.

In Chapter 2, the apparatus of the carbon negative-ion implantation and the details of the polymeric surfaces such as polystyrene and silicone rubber for the experiments, including the ion-projected range in solid, process of energy loss and the TRIM calculation of range distribution are described.

In Chapter 3, the evaluation of the changes in the physical surface properties, relating to the adsorption of the adhesive proteins and the cell adhesion are described. Those are the atomic bonding state by XPS analysis, the surface morphology of surface roughness by AFM and the wettability by measurement of the contact angles. The circumstance dependence and the time dependence of the change in the contact angles are described.

In Chapter 4, The evaluation of the adsorption properties for the ECM of adhesive protein and PDL on the $C^-$-modified polymeric surfaces are studied. At first, I describe the mechanism of protein adsorption on the $C^-$-modified polymeric surfaces. The preparation and evaluation process of protein-coated modified surface are explained. The details and the structure of the importance of adhesive protein such as type-I collagen, fibronectin and laminin, and those of PDL are described. The adsorption properties for such adhesive proteins and PDL on the $C^-$-modified polymeric surfaces of polystyrene and silicone rubber are evaluated by detecting amount of nitrogen atom from protein/PDL with XPS analysis. The relation between the physical surface properties of each surface and the adsorption properties of each adhesive protein and PDL are described.

In Chapter 5, the fundamental condition for the adhesion and neurite-outgrowth properties by the cultivation of PC12h cells on the $C^-$−modified polymeric surfaces of polystyrene and silicone rubber are described. The details of PC12h cell line, the cell-adhesion and neurite-outgrowth properties on each modified polymeric surface with various ion implantation conditions, the improvement and degradation of the selective adhesion properties of cells on the additional protein-coated modified surfaces, the immobilization of cell body and neurite, and the formation of neuron network on the $C^-$-implanted polymeric surfaces are

described. The relation between the physical surface properties, the protein adsorption ratio and the selective adhesion properties of PC12 cells on the $C^-$-implanted polymeric surfaces are used to describe the results.

In Chapter 6, the confirmation of the brain neuronal cell adhesion patterning on modified polymeric surface by negative ion implantation is described. The details of neuron and brain neuronal cells are explained. The measured fundamental assessment for degradation of the positive-charge site of PDL by carbon negative-ion implantation and the culture of brain neuronal cells to observe the suitable coating concentration of PDL for the uniform adhesion are studied. The relation between the PDL adsorption properties in Chapter 4 and the carbon negative-ion implantation for patterning the surface are explained. The brain neuronal cell adhesion patterning on the patterned PDL surface by carbon negative-ion implantation is described.

In Chapter 7, the adhesion properties and differentiation of MSC on the modified polymeric surfaces of polystyrene and silicone rubber are stated. The details of MSC, the adhesion pattern on each modified polymeric surface with various ion implantation conditions are studied. The success of the differentiation induction of MSC into neuronal cell on the $C^-$-implanted polymeric surfaces are described.

In Chapter 8, the conclusions of all results and prospects for the application in further are described. The achievements of the adhesion patterning of the different neurons on the polymeric surface by using carbon negative-ion implantation are described. The possibilities to use the patterning of stem cell adhesion and its differentiation into neuronal cells for application of the artificial bionic organ and on the neurological disease treatment in the further are described.

## References


[1] W.H. Dobelle, “Artificial Vision for the Blind by Connecting a Television Camera to the Visual Cortex”, J.ASAIO, vol. 46, pp. 3-9, 2000.

[2] L. Gärtner, C. Frohne-Büchner, A. Büchner, R. Heermann, T. Stöver, B. Schwab, R.D. Battmer and T.s Lenarz “Advanced Bionics New HiRes90K Cochlear Implant: Clinical Experience”, Proc. VIII International Cochlear Implant Conference in International Congress Series, vol. 1273, November 2004, pp. 97-100, 2004.

[3] Q. Liu, H. Cai, Y. Xu, Y. Li, R. Li and P. Wang, “Olfactory cell-based biosensor: A First Step towards a Neurochip of Bioelectronic Nose”, Biosens. Bioelectron., vol. 22, issue 2, pp. 318-322, 2006.

[4] D. Graham-Rowe, “Artificial Limbs Wired Direct to the Brain”, The New Scientist, vol.

192, issue 2573, pp. 30-31, 2006.

[5] X. Jia, M.A. Koenig, X. Zhang, J. Zhang, T. Chen and Z. Chen, “Residual Motor Signal in Long-Term Human Severed Peripheral Nerves and Feasibility of Neural Signal-Controlled Artificial Limb”, J. Hand Surg. vol. 32, issue 5, pp. 657-666, 2007.

[6] S.P. Levine, J.E. Huggins, S.L. BeMent, R.K. Kushwaha, L.A. Schuh, M.M. Rohde, E.A. Passaro, D.A. Ross, K.V. Elisevich, and B.J. Smith, “A Direct Brain Interface Based on Event-Related Potentials”, IEEE Trans Rehabil Eng, vol. 8, pp. 180-185, 2000.

[7] J.C. Chang, G.J. Brewer and B.C. Wheeler, “Neuronal Network Structuring Induces Greater Neuronal Activity through Enhanced Astroglial Development”, J. Neural Eng., vol. 3, pp. 217-226, 2006.

[8] P. Fromherz and H. Schaden, “Defined Neuronal Arborizations by Guided Outgrowth of Leech Neurons in Culture”, Eur. J. Neurosci, vol. 6, pp. 1500-1504, 1994.

[9] G. Zeck and P. Fromherz, “Noninvasive Neuroelectronic Interfacing with Synaptically Connected Snail Neurons Immobilized on a Semiconductor Chip”, Proc. Natl. Acad. Sci. USA 98, pp. 10457-10462, 2001.

[10] M. Merz and P. Fromherz, “Polyester Microstructures for Controlling Outgrowth and Synapse Formation of Individual Snail Neurons”, Adv. Mater., vol. 14, 141-144, 2002.

[11] Y. Suzuki, M. Kusakabe, K. Kusakabe, H. Akiba, and M. Iwaki, “In vivo Evaluation of Antithrombogenicity for Ion Implanted Silicone Rubber using Indium-111-Tropolone Platelets”, Nucl. Instrum. Methods Phys. Res. B, vol. 59-60, pp. 698-704, 1991.

[12] Y. Suzuki, M. Kusakabe, J.S. Lee, M Kusakabe, M. Iwaki, and H. Sasabe, “Endothelial Cell Adhesion to Ion Implanted Polymers”, Nucl. Instrum. Methods Phys. Res. B, vol. 65, pp. 142-147, 1992.

[13] R.S. Bhattacharya, “Evaluation of High Energy Ion-Implanted Polycarbonate for Eyewear Applications”, Surf. Coat. Technol., vol. 103-104, pp. 151-155, 1998.

[14] F.Z. Cui and Z. S. Luo, “Biomaterials Modification by Ion-Beam Processing”, Surf. Coat. Technol., vol. 112, pp. 278-285, 1999.

[15] H. Tsuji, T. Taya, J. Ishikawa, and T. Takagi, “Neutral and Ionized Cesium Bombardment Type Negative Ion Source”, in: T. Takagi (Ed.), Proceedings of the International Ion Engineering Congress, ISIAT ’83 & IPAT ’83, Kyoto, 12–19 September 1983, vol. 1, Institute of Electrical Engineers of Japan, IEEEJ, pp. 141–146, 1983.

[16] J. Ishikawa, and H. Tsuji, “Carbon Negative Ion Implantation into Silicon”, Nucl. Instrum. Methods Phys. Res. B, vol. 74, pp. 118-122, 1993.

[17] J. Ishikawa, H. Tsuji, Y. Toyota, Y. Gotoh, K. Matsuda, M. Tanjo, and S. Sakai, “Negative-Ion Implantation Technique”, Nucl. Instrum. Methods Phys. Res. B, vol. 96, pp. 7-12, 1995.

[18] H. Tsuji, Y. Toyota, J. Ishikawa, S. Sakai, Y. Okayama, S. Nagumo, Y. Gotoh, and K. Matsuda, "Charging Voltage Measurement of an Isolated Electrode and Insulators during Negative-Ion Implantation", in: S. Coffa, G. Ferla, F. Priolo, and E. Rimini. (Eds.), Proc. of the 10th Int. Conf. on Ion Implantation Technology 94, Elsevier, New York, pp. 612-615, 1995.

[19] H. Tsuji, J. Ishikawa, S. Ikeda, and Y. Gotoh, "Slightly Negative Surface Potential and Charging Model of Insulator in the Negative-Ion Implantation", Nucl. Instrum. Methods Phys. Res. B, vol. 127-128, pp. 278-281, 1997.

[20] H. Tsuji, Y. Gotoh, and J. Ishikawa, "Secondary Electron Emission and Surface Potential of $SiO_2$ Film Surface by Negative-Ion Bombardment", Nucl. Instrum. Methods Phys. Res. B, vol. 141, pp. 645-651, 1998.

[21] H. Tsuji, H. Satoh, S. Ikeda, N. Ikemoto, Y. Gotoh, and J. Ishikawa, "Surface Modification by Silver-Negative-Ion Implantation for Controlling Cell-Adhesion Property of Polystyrene", Surf. Coat. Technol., vol. 103-104, pp. 124-128, 1998.

[22] H. Tsuji, H. Satoh, S. Ikeda, Y. Gotoh, and J. Ishikawa, "Contact Angle Lowering of Polystyrene Surface by Silver-Negative-Ion Implantation for Improving Biocompatibility and Introduced Atomic Bond Evaluation by XPS", Nucl. Instrum. Methods Phys. Res. B, vol. 141, pp. 197-201, 1998.

[23] H. Tsuji, H. Satoh, S. Ikeda, S. Ikemura, Y. Gotoh, and J. Ishikawa, "Negative-Ion Beam Surface Modification of Tissue-Culture Polystyrene Dishes for Changing Hydrophilic and Cell-Attachment Properties", Nucl. Instrum. Methods Phys. Res. B, vol. 148, pp. 1136-1140, 1999.

[24] H. Sato, H. Tsuji, S. Ikeda, N. Ikemoto, J. Ishikawa, and S. Nishimoto, "Enhanced Growth of Human Vascular Endothelial Cells on Negative-Ion (Ag-)–Implanted Hydrophobic Surfaces", J. Biomed. Mater. Res. vol. 44, pp. 22-30, 1999.

[25] H. Lodish, A. Berk, L.S. Zipursky, P. Matsudaira, D. Baltimore and J. Darnell, **Molecular Cell Biology**, 4th ed, New York: W. H. FREEMAN and Company, 2000.

[26] G.M. Cooper, **The Cell: A Molecular Approach**, 2nd ed, Sunderland, Massachusetts, USA: Sinauer Associates, Inc., 2000.

[27] B. Alberts, A. Johnson, J. Lewis, M. Raff, K. Roberts and P. Walter, **Molecular biology of the cells**, 4th ed., New York: Garland Science, 2002.

[28] **Protein Chemistry for Conservators,** CL. Rose and D.W. von Endt, edts., Washington D.C.: American Institute for Conservation of Historic and Artistic Works, 1984.

[29] **Chapter 9 of Fundamental & Application of Polymer Surfaces volume 2**, Y. Ikada ed., Kagaku Dozin co., ltd. JP, 1998, p. 186.

[30] L.A. Greene, A.S.Tischler, "Establishment of a Noradrenergic Clonal Line of Rat Adrenal

Pheochromocytoma Cells which Respond to Nerve Growth Factor", Proc. Natl. Acad. Sci. USA, Jul 1976, vol. 73(7), pp. 2424-2428, 1976.

[31] E. Yavin and Z. Yavin, "Attachment and Culture of Dissociated Cells from Rat Embryo Cerebral Hemispheres on Polylysine-Coated Surface", J. Cell Biol, vol. 62, pp. 540-546, 1974.

[32] P. C. Letourneau "Possible Roles for Cell-to-Substratum Adhesion in Neuronal Morphogenesis", Dev Biol., vol. 44, no. 1, pp. 77-91, 1975.

[33] A.R. Vancha, S. Govindaraju, K.VL Parsa, M. Jasti, M. González-García, and R.P. Ballestero, "Use of Polyethyleneimine Polymer in Cell Culture as Attachment Factor and Lipofection Enhancer", BMC Biotechnology 2004, vol. 4, no. 23, Published online 2004, doi:10.1186/1472-6750-4-23.

[34] Y. Bledi, A.J. Domb and M. Linial, "Culturing Neuronal Cells on Surfaces Coated by a Novel Polyethyleneimine-Based Polymer", Brain Res. Protoc., vol. 5, issue 3, pp. 282-289, 2000.

[35] R.L. Gardner, "Stem Cells: Potency, Plasticity and Public Prception", J. Anat., vol. 200 (3), pp. 277-282, 2002.

[36] H. Shin, S. Jo, and A.G. Mikos, "Synthetic Biodegradable Polymer Networks Modulating Marrow Stromal Osteoblast Adhesion", in **Biomaterials for Drug Delivery and Tissue Engineering**, S. Mallapragada, M. Tracy, B. Narasimhan, E. Mathiowitz, and R. Korsmeyer, Eds., MRS Symposium Proceedings, vol. 662, Materials Research Society, Warrendale, 2001, pp. LL6.5.1-LL6.5.6, 2001.

[37] A. Kadner, Simon P. Hoerstrup, G. Zund, K. Eid, C. Maurus, S. Melnitchouk, J. Grunenfelder, M.I. Turin,"A New Source for Cardiovascular Tissue Engineering: Human Bone Marrow Stromal Cells", Eur. J. Cardiothorac. Surg., vol. 21, pp. 1055-1060, 2002.

[38] B.E. Tuch, "Stem Cells--a Clinical Update", Aust. Fam. Physician, vol. 35 (9), pp. 719-21, 2006.

[39] A.J. Becker, E.A. McCulloch, J.E. Till, "Cytological Demonstration of the Clonal Nature of Spleen Colonies Derived from Transplanted Mouse Marrow Cells", Nature vol. 197, pp. 452-454, 1963.

[40] L. Siminovitch, E.A.McCulloch, J.E.Till, "The Distribution of Colony-forming Cells among Spleen Colonies", J. Cell. Comp. Phy., vol. 62, pp. 327-336, 1963.

[41] A.J. Friedenstein, U.F. Deriglasova, N.N. Kulagina, A.F. Panasuk, S.F. Rudakowa, E.A. Luria, I.A. Ruadkow, "Precursors for Fibroblasts in Different populations of Hematopoietic Cells as Detected by the In Vitro Colony Assay Method", Exp. Hematol., vol. 2 (2) pp. 83-92, 1974.

[42] S. Bobis, D. Jarocha and M. Majka, "Mesenchymal Stem Cells: Characteristics and

Clinical Applications", Folia Histochemica Et Cytobiologica, vol. 44, no. 4, pp. 215-230, 2006.

[43] SL.Gerson, "Mesenchymal Stem Cells: No Longer Second Class Marrow Citizens", Nat Med., vol. 5, pp. 262–264, 1999.

[44] E.A. McCulloch, J.E. Till, "The Radiation Sensitivity of Normal Mouse Bone Marrow Cells, Determined by Quantitative Marrow Transplantaiton into Irradiated Mice", Radiation Research, vol. 13, pp.115-125, 1960.

[45] D. Woodbury, E.J. Schwarz, D.J. Prockop, and I.B. Black, "Adult Rat and Human Bone Marrow Stromal Cells Differentiate into Neurons", J. Neurosci. Res., vol. 61, pp. 364-370, 2000.

# Chapter 2

# Negative-Ion Implantation

## 2.1 Carbon Negative-Ion Implantation into Polymeric Surface

The ion implantation techniques with positive and negative ions into the polymeric-material surface have been applied to modify the biocompatibility for a prevalent application in the biomaterial field since 1990s [1-8]. The surface modifications for the biocompatible properties, such as antithrombogenicity, cell adhesion, antibacterial etc., were carried out [1-8]. Many techniques such as ion implantation, gas-plasma process and irradiations of UV and X-ray can use to modify the polymeric surface for the biocompatility. The ion implantation has the advantages of abilities to control the micro-structure and to reproduce the modified surface by controlling the ion dose and current, comparing to the gas-plasma process. Comparing to the irradiations of UV and X-ray, the ion implantation has ability to break down the tight bonding of polymer material such as silicone rubber by controlling the ion dose at the wide energy range from low-to-high keV. Therefore, the ion implantation is better to use for modification of the polymeric surface. Generally, many researchers use the positive-ion implantation. The positive-ion implantation into the polymeric surface for modifying properties almost applied at very high energy of several hundred-keV to the polymeric surface [1-4]. Applying very high voltage in positive-ion implantation without any charge compensation results in a charge-up problem between insulator surfaces and isolated electrodes due to the insulating properties of most polymers. This charge-up problem affects to the implantation control of ion dose and energy [9-14]. The fine pattern of the modified surfaces can not be obtained by using the positive-ion implantation [15-16]. In contrast, the negative-ion implantation into the polymeric surface for improvement of the biocompatible properties occurs almost “charge-up free” even if no external charge compensation [5-8]. The charge-up free occurs because the secondary electrons at the surface went out when the negative-ions implanted into the surface. Then, the implantation dose and energy can be precisely controlled even if at a much lower ion-energy such one to several tens of keV. This results in a possibility to obtain the fine pattern of modified polymeric surface with a low defect. Therefore, negative-ion implantation is a promising method for the surface modification of polymer materials. Tsuji *et al.* reported the control of endothelial cell adhesion on the polymeric surface by using the negative-ion implantations of silver because they had expected an antibacterial of the silver atoms [5-8].

However, the heavy metal, including silver, can be harmful to the living body. Comparing to silver, carbon is a lighter element, mainly component of polymer materials and more familiar to cells. It matches to the lattice of the polymer. It will be harmless for the living body. Therefore, the implantation with the carbon negative-ions is better to use to modify the polymeric surface for application in the biomedical field. In this works, the patterning of the real neuron cell adhesion on the polymeric surface was investigated, and the real neuron cells are very sensitive. Therefore, the carbon negative-ion implantation should be better to use to modify the polymeric surfaces for real neuron cell adhesion patterning.

## 2.2 Ion Implanter

In this experiment, the negative-ion implantation technique is used to modify the biocompatible property of the polymeric materials for patterning neuron adhesion. Our developed negative-ion implanter is shown in Fig.2.1.

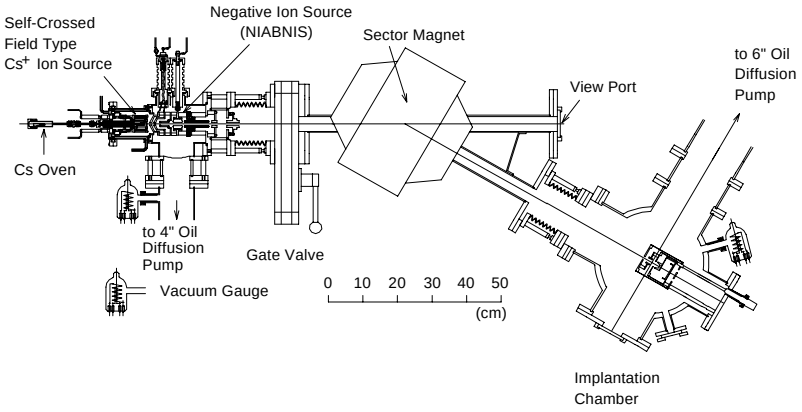


Fig 2.1 Schematic diagram of negative-ion implanter

This implanter is composed of negative-ion source, sector magnet for mass separation, and implantation chamber. Firstly, negative-ion beam is generated by cesium sputtering in the negative-ion source. Only the desired ion species in ion beam from the negative-ion source is then selected at the mass separation part. Finally, the selected negative-ion beam is induced to irradiate on samples in the implantation chamber.

### 2.2.1 Negative-Ion Source

The carbon negative ion is produced in the negative-ion source called the neutral and ionized alkaline metal bombardment type heavy negative-ion source (NIABNIS). The structure of NIABNIS and the power supply placement are shown in Figs. 2.2 and 2.3, respectively.

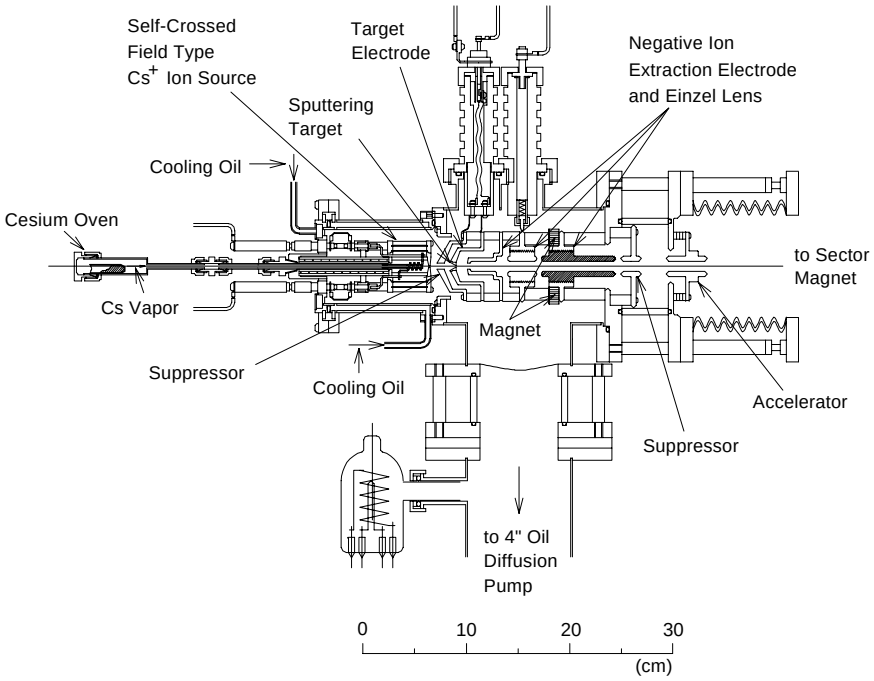


Fig 2.2 Schematic diagram of NIABNIS

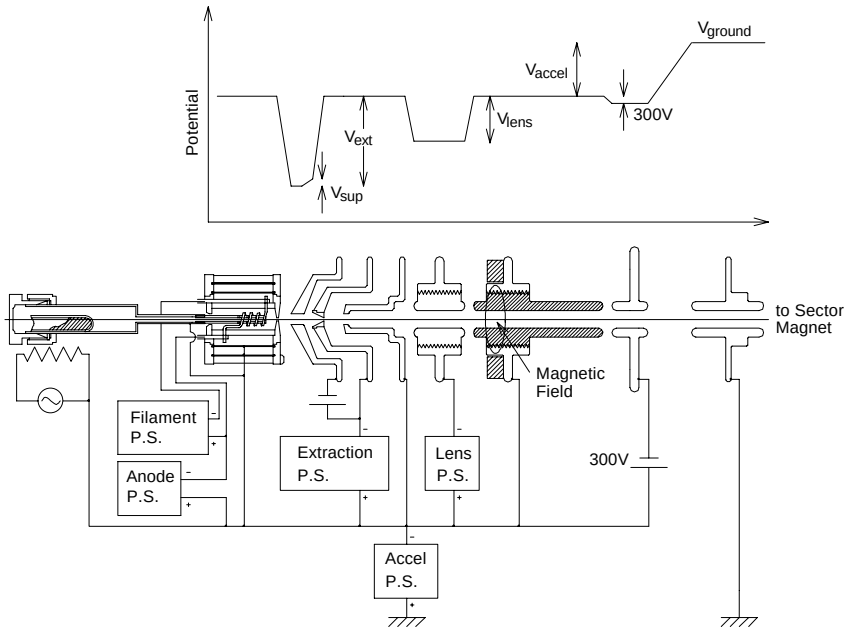


| | |
|---|---|
| Extraction P.S. | MAX. 20kV 30mA |
| Lens P.S. | MAX. 30kV 20mA |
| Filament P.S. | MAX. 35V 30A |
| Anode P.S. | MAX. 150V 3A |
| Accel P.S. | MAX. 30kV 20mA |

Fig 2.3 Schematic diagram of power supply placement for NIABNIS

From Figs. 2.2 and 2.3, the micro sheath heater wires of 1.0 mm in the diameter were wrapped around the oven of cesium (Cs). After flowing the current by increasing the power supply to heat the heater wire, Cs vapor is generated. Generated Cs vapor is then supplied to the plasma generation chamber through the center anode pipe. Around the front edge of this pipe, the filament wire made of tungsten (W) of 0.5 mm in diameter was rolled as a spiral. At this part, the negative bias voltage is connected to the filament, and the higher potential bias voltage is connected to the center anode pipe. Hot electrons emitted from the filament are accelerated to the center anode by the positive potential and plasma is generated by ionizing collision between electrons and Cs atoms. In addition, at the same time, the spin movement of electron is induced by the axial magnetic field caused by the current flow in a spiral filament. As a result, the flying range of the electron and the collision frequency with electron are increased, so the improvement of the plasma generation efficiency has been achieved.

Next, the extracted $Cs^+$ from the ion extraction hole in the plasma generation chamber is accelerated to irradiate to the sputtering target placed at the center of extraction electrode to which a high negative voltage is connected. After the $Cs^+$ sputtered to target, the presence of Cs vapor on the target surface forms the electric double layer, which results in decreasing in work function at the sputtering target surface and more efficiency to generate the negative ion of the sputtered target element.

The sputtered negative ion is passed through the center hole of target by the electric field of the extracted electrode which is connected to a positive voltage. After that the negative ion is focused by Einzel lens and then transported to mass separation part. At this time, not only the negative-ion beam, but also the secondary electrons are extracted. But the secondary electrons are removed from the beam by the magnetic field from a permanent magnet that is placed next the electrode of Einzel lens. Moreover, more biasing the negative voltage to the whole negative-ion source can be done by increasing the more negative potential between the negative-ion source and the mass separation part. Therefore, the negative ion can be post accelerated to 30 keV.

### 2.2.2 Mass Separation Part

Mass separation part is composed of electric sector magnet. Changing magnetic field of electric magnet can separate the negative-ion beam by different orbit of each mass. By this separation, only the desired ion can be selected and transported to the implantation chamber. Curvature radius and bending angle of this electric sector magnet are 300 mm and 30°, respectively. The maximum magnetic flux density is 8200 Gauss in gap of 27 mm. When using carbon as a sputtering target, the mass separation spectrum is shown in Fig. 2.4.

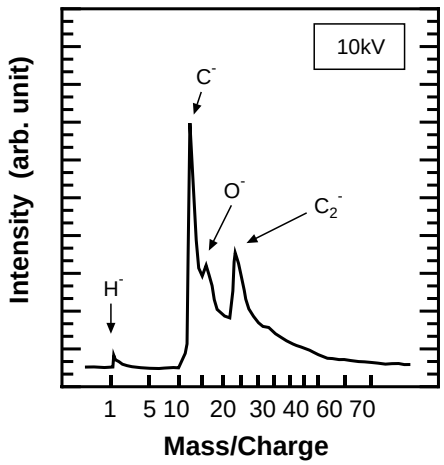


Fig 2.4 Mass separation spectrum

### 2.2.3 Implantation Chamber

Faraday cup in the implantation chamber is composed of limiter, collector cup, suppressor, shutter and current monitor and sample holder. Schematic diagrams of implantation chamber and of Faraday cup with the circuit for the negative-ion measurement are shown in Figs. 2.5 and 2.6, respectively.

Since the hole of limiter is 11.28 mm in diameter, the beam irradiation area on the sample is limited to about 1 $cm^2$. In the experiment, the sample is polymeric material that is an insulator. So, it is impossible to measure irradiated ion directly by using collector cup. Then, we

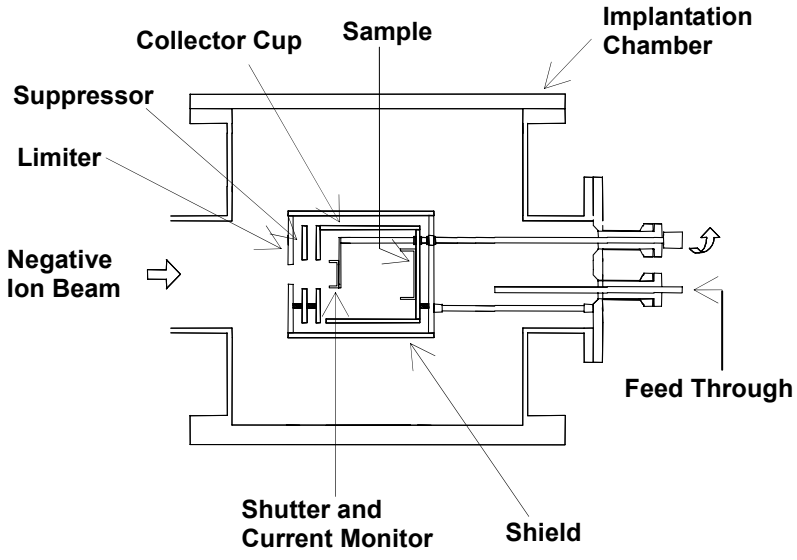


Fig 2.5 Schematic diagram of implantation chamber.

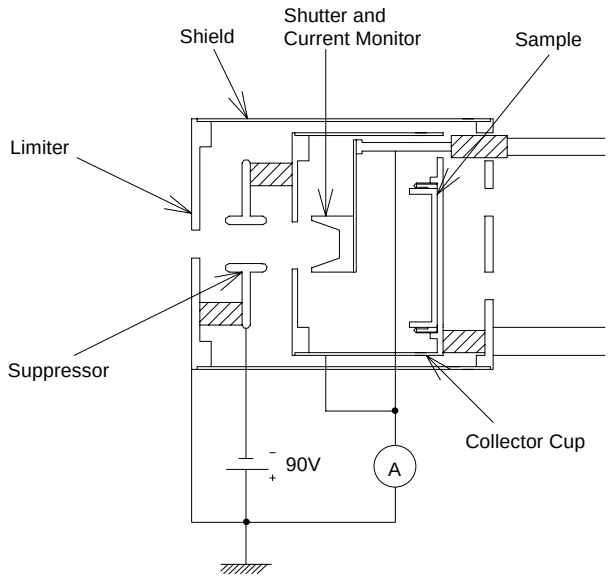


Fig 2.6 Schematic diagram of Faraday cup and circuit for the negative-ion measurement.

measure the irradiated ions by current monitor before irradiation. After irradiation, we can measure the ion current by detecting both currents of secondary electrons and ions in the collector cup. An electrostatic shield is set up to prevent the floating electron outside of the collector cup. In addition, there are some generated gases during ion implantation into the polymeric material. These gases can release from collector cup through many holes of 4 mm in diameter at the collector cup and electrostatic shield and through the Au sheet mesh of 1 mesh/mm$^2$ that surround the holes. Ion dose is calculated from integration value of amount of the current flow on the collector cup, so it is necessary to measure amount of the current correctly. The suppressor next the limiter have a hole of 14 mm in diameter and bias with the negative voltage to push back the secondary electron from both of limiter and collector cup. As a result, it is possible to precisely measure collector current. Moreover, a shutter controlled from outside is set up in order to control ion dose. Even in the case of closing this shutter, this shutter works as collector, so the beam current can be measured by the current flow at the shutter. In addition, the movable sample holder that can be manipulated from the outside of chamber enables to implant many samples at one evacuation by a freely moving rod in transversal direction to the beam axis. Schematic diagram of the movable sample holder is shown in Fig. 2.7. The sample holder, of cause, insulated from the moving rod.

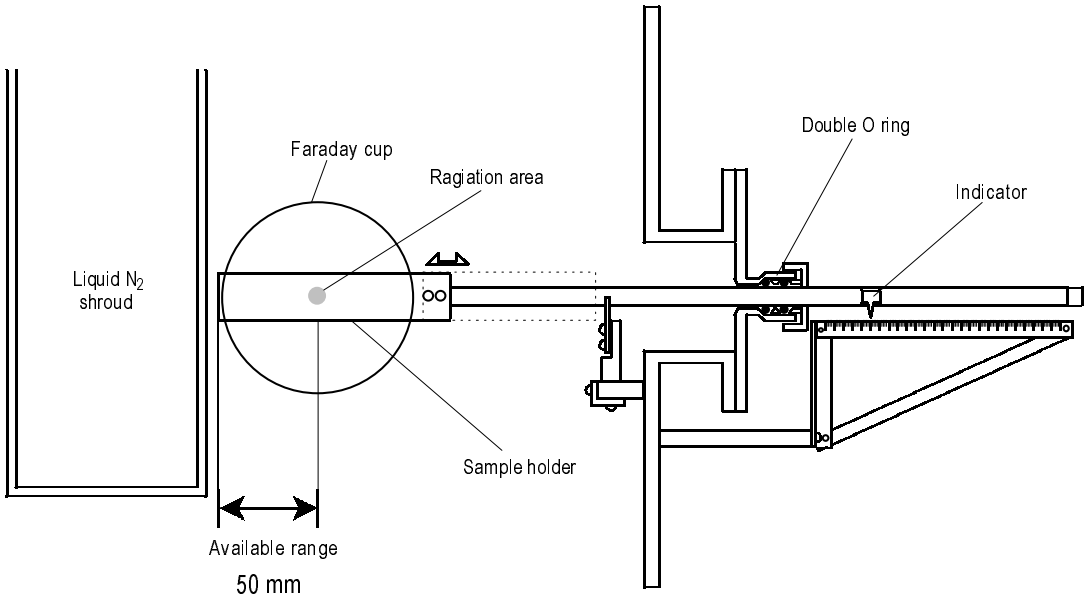


Fig 2.7 Schematic diagram of the movable sample holder.

### 2.2.4 Implantation Condition

In this implanter, the negative-ion source chamber and the implantation chamber are evacuated. Diffusion pump (DP) of 4 inch in diameter with liquid nitrogen trap is used for the negative ion source chamber, while turbo molecular pump (TMP) is used for the implantation chamber to prevent the contamination of oil to the sample surface. Moreover, the mass separation part is always connected to the implantation chamber, so mass separation part is also evacuated by TMP. Typical gas pressures inside the implantation chamber and ion source chamber are about $2\times10^{-4}$ and $3\times10^{-4}$ Pa, respectively, during implantation.

The carbon negative ion is chosen to implant into the polymeric material, since the purpose of this research is to apply to the bio-interface. Therefore, the implantation atoms should be harmless or at least have only little influence with human body. In this experiment, the applied implantation energy is in the range of 5 to 20 keV, and the implant dose is in the range of $1\times10^{13}$ and $3\times10^{16}$ ions/cm$^2$. Beam current is less than 400 nA/cm$^2$ to prevent the melting of polystyrene surface at high temperature. The typical conditions are shown in Table 2.1.

Table 2.1 Implantation conditions

| | |
|---|---|
| Species of ion | $^{12}C^-$ |
| Ion energy | 5 – 20 keV |
| Current density | less than 400 nA/cm$^2$ |
| Ion dose | $1\times10^{13} – 3\times10^{16}$ ions/cm$^2$ |
| Gas pressure (Implantation chamber) | $2\times10^{-4}$ Pa |
| Gas pressure (Ion source chamber) | $3\times10^{-4}$ Pa |

## 2.3 Mask for Patterning the Polymeric Surface

As for the neuron cell adhesion patterning on the polymeric surfaces by carbon negative-ion implantation, the carbon negative ions were implanted through a mask to pattern the implanted region on the polymeric surface. In this work, the used masks were made of the alloy of Ni and Cu. The sheet of the alloy has a thickness of about 50 μm. Many masks were used to pattern the implanted region for the different purpose examination. In studies of the changes in the properties of physical surface and protein adsorption, the normal metal sheet as a mask was used to pattern a half-moon-shaped area of the implanted region. In studies of the properties of the selective cell adhesion, the micro-pattern masks were used to pattern the different shaped area of the implanted region instead. Mainly two types of the normal micro-pattern mask were used. One consists of a period pattern of 200 μm in width from many rectangle-shaped slit apertures of 50 μm in width and 70 μm in spacing with the area of 5×10 mm$^2$. Other consists of a period pattern of 200 μm in width from many rectangle-shaped slit apertures of 50 μm in width and 150 μm in spacing with the area of 5×15 mm$^2$. The different patterns of the implanted region were used to study the selective cell adhesion properties, the immobilization of cell body and neurite outgrowth, and the formation of neuron network. The normal patterns of the rectangle-shaped area of the implanted region were obtained by the implantation in one time through this normal micro-pattern mask. The other patterns such as the ridge and the grid shapes could be obtained by set and rotation of the normal micro-pattern mask with the number of the implantation. The ridge-shaped pattern or wedge-shaped pattern could be achieved by the implantation in one time through a double mask set, which was obtained from alignment of two normal micro-pattern masks consisting of a 120 μm in period and their array of ridge-shaped apertures gradually changes the line width from 40 to 0 μm. The grid-shaped pattern could be achieved by the implantation in two times through the rotation of a normal micro-pattern mask consisting of a 200 μm in period. The applied masks, the applied patterns and their patterning methods in each chapter of this work are shown in Table 2.2.

Table 2.2 Types of the applied masks, the patterns of the implanted region and the patterning methods

| Types of mask | Line width (μm) | | Patterns of the region | Line width (μm) | | Patterning method | Chapter |
|---|---|---|---|---|---|---|---|
| | Slit aperture | Spacing | | The implanted region | The unimplanted region | | |
| Thin metal sheet | - | - | A half moon | - | - | Once implantation through the thin metal sheet, which cover a half implantation area | 3, 4, 6 |
| Rectangle pattern | 50 | 70 | Stripes | 50 | 70 | Once implantation through this micro-pattern mask | 5, 6, 7 |
| | | | Ridges | 40 ~ 0 | 70 ~ 120 | Once implantation through a double-mask set with array of ridge shaped aperture | 5 |
| Rectangle pattern | 50 | 150 | Stripes | 50 | 150 | Once implantation through this micro-pattern mask | 5, 7 |
| | | | Grids | 50 | 150 | Twice implantation through the alignment and rotation of the micro-pattern mask | 5 |

## 2.4 Polymeric Material

In this work, the carbon negative-ion implantations into the polymeric materials of polystyrene and silicone rubber were studied. Details of each polymeric material are described in the following section.

### 2.4.1 Polystyrene

Polystyrene (PS) is one of useful polymeric materials that is generally used in the field of medical equipment and experimental materials and etc., because of the economic price, the simple fabrication in any shape and its safety for *in vitro* experiment. Polystyrene is a polymerized styrene (vinyl benzene, or phenyl ethylene). The molecular form has two carbon atoms in the main chain with the side chain of phenyl groups as shown in Fig. 2.8.

Since polystyrene can be dissolved in toluene solution, the thin polystyrene film is easy to be formed by spin-coating. The spin-coated polystyrene (SCPS) films on glass substrate are adaptable to use as a substrate for study of the neuron cell adhesion patterning. In the experiment, the films were obtained from spin-coating with the 7% of polystyrene (PS Nacalai Tesque, Inc., Japan) in toluene on glass substrate (#7059, Corning) by spinner (1H-2, Mikasa co., ltd.) at the conditions of 1000 rpm and 20 seconds. We repeated the spin-coating for 3 times to obtain the SCPS film with the thickness of about 600 nm. In addition to this SCPS, the carbon negative ions were also implanted into the commercial polystyrene surface of Non-treated polystyrene dish (NTPS, Corning, 450389) to compare the surface morphology properties between the SCPS films and the commercial PS.

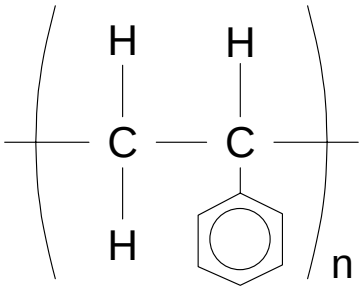


Fig 2.8 Molecular form of polystyrene.

### 2.4.2 Silicone Rubber

Silicone rubber (SR) is the chemically stable biomaterial with the inactive against to the living body, resulting in being harmless to use in human body. It is very flexible in shape and has heat-resistance. Therefore, the graft and breast plastic surgery has generally used the silicone rubber. Almost all parts of silicone rubber have polydimethylsiloxane that the molecular form is shown in Fig. 2.9.

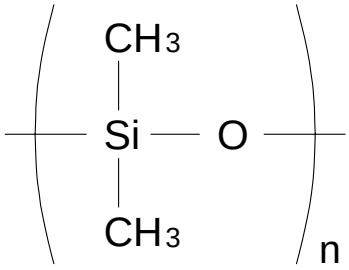


Fig 2.9 Molecular form of silicone rubber.

The main chain of silicone rubber is composed of the siloxane bonding between the atoms of silicon and oxygen, and the side chains are composed of the methyl groups. However, this methyl group in the silicone rubber can be replaced by the phenyl or carbide groups, depending on the commercial company. In this experiment, the silicone rubber sheets are obtained from Wacom electric co., ltd. (Chapters 3 – 5 and 7) and Fuji system (Chapters 3, 5 and 7), and there is only the methyl group in the side chain.

## 2.5 Ion Projected Range in Solid

In this work, the carbon negative-ion implantation into polymeric surface is done for the cell adhesion patterning. To understand and predict the suitable condition for the purpose, the effects of the ion implantation on the surface modification for cell adhesion are studied.

The ion implantation into the solid generally causes two effects. One is doping effect of the new atom implantation and other is radiation effect of the new atomic bonding formation at the surface.

In ion implantation into solid, the ions break down the surface bond and penetrate into the bulk of the material. The average depth, which the ions can penetrate into the bulk material, is calculated by Monte-Carlo simulation method and is ion projected range. As for the relation between the cell adhesion property at the surface and doping effect of the ions, cells adhere at the

surface, but the doping atoms are inside the material. Therefore, the doping effect should not influence the cell adhesion properties. The stopping position of the atom in the bulk material refers to the ion projected range in solid, which is related to the energy loss in solid. The process of energy loss of ion in the solid can be described as follows:

### 2.5.1 Process of Energy Loss

In the implantation, several different phenomena occur during penetration of ion in solid [17]. Those are the inelastic collision with bound electrons of the target atom, the inelastic collisions with nuclei, the elastic collisions with bound electrons and the elastic collisions with nuclei or whole atoms, etc. Since the inelastic nuclear collision and elastic collisions with electrons cannot efficiently stop the particles. Only two phenomena of the inelastic collisions with electron (electronic stopping) and elastic nuclear collisions (nuclear stopping) are main process in energy loss. Both of them are as the function of the energy and the mass of the accelerated particles, as well as upon the mass and the atomic number of the medium. The simple equation for the energy stopping calculation can be expressed simply by Eq 2.1.

$$S(E) = -\frac{1}{N}\left(\frac{dE}{dx}\right) \tag{2.1}$$

where $S(E)$ is the stopping power, $N$ is the atomic density, $E$ is the energy of the ion implantation and $x$ is the x-direction.

As described above, the stopping power mainly consists of the electronic stopping power and the nuclear stopping power. Then, Eq. 2.1 can be rewritten to be Eq. 2.2.

$$-\left(\frac{dE}{dx}\right) = N\left|S_n(E) + S_e(E)\right| \tag{2.2}$$

where $S_n(E)$ and $S_e(E)$ are the nuclear and electronic stopping. The consideration and calculations of each stopping power are as follows:

### Nuclear Stopping Power

The energy loss of an ion by elastic nuclear interaction, in a layer of x-direction, is proportional to the atomic density as well as to the total energy transferred in all individual collision. Therefore, the nuclear stopping power can be expressed simply by Eq. 2.3.

$$S_n(E) = -\frac{1}{N}\left(\frac{dE}{dx}\right)_n = \int_0^\infty T_n(E, p)\, 2\pi p\, dp \tag{2.3}$$

where $T_n$ is a total energy transferred in all individual and $p$ is the impact collision parameter.

The total energy transferred in all individual related the ion implantation energy, the masses of the ion and target, and the deflection angle in the center-of-mass system. Therefore, it can be expressed by Eq. 2.4.

$$T_n(E,p) = E\frac{2M_1M_2}{(M_1+M_2)^2}(1-\cos\Phi) \tag{2.4}$$

where $M_1, M_2$ are the masses of ion and target, and $\Phi$ is the deflection angle in the center-of-mass system. $\Phi$ relates to the interatomic potential and the impact parameter. If $\Phi$=180°, a maximum transferable energy for the center collision are obtained as shown by Eq. 2.5.

$$T_m = \frac{4M_1M_2}{(M_1+M_2)^2}E = \gamma E \tag{2.5}$$

where $T_m$ is a maximum transferable energy for the center collision and $\gamma$ is the transfer efficiency of the ion.

## Electronic Stopping Power

Based on the assumption for low implantation energy by Lindhard and Winter [17-19], the electronic-stopping cross-section is proportional to the velocity of the ions, and therefore proportional to the root of the energy. The model for calculation of the electronic stopping power can be simply expressed by Eq. 2.6.

$$S_e(E) = -\frac{1}{N}\left(\frac{dE}{dx}\right)_e = c_k k_{LS}\sqrt{E} \tag{2.6}$$

where $c_k$ is a correction factor, which is in the range of 0.6 – 1.3 for the low energy light ions in light targets ($Z_2 < 10$), and $k_{LS}$ is the Lindhard-Scharff constant. $c_k k_{LS}$ relates to the atomic numbers of ion and target ($Z_1$ and $Z_2$).

However, Firsov developed the different model [20] to explain oscillations in $S_e(E)$ [21]. He assumed that the ion and the target atom form a auasi-molecule during collision. For this model, the energy loss results from the electronic interaction between particles having the nuclear charges, and integration of over all impact parameters. The model can be expressed by Eq. 2.7.

$$S_e(E) = -\frac{1}{N}\left(\frac{dE}{dx}\right)_e = \int_0^\infty T_e(E,p)\,2\pi p\,dp \tag{2.7}$$

where $T_e$ is the energy loss resulting from the electronic interaction between particles. The energy loss of the incident particle (or ion) during formation of a quasi-molecule takes place through the transfer of momentum and energy to electrons of the target particle. When the incident particle passes from $-\infty$ to $+\infty$ via the target particle, the approximated $T_e$ can be

calculated by Eq. 2.8.

$$T_e = \frac{4.3\times10^{-8}\left(Z_1+Z_2\right)^{\frac{5}{2}}}{\left|1+3.1\times10^{7}\left(Z_1+Z_2\right)^{\frac{1}{2}}p\right|^{5}}v \quad \text{(eV)} \tag{2.8}$$

where $v$ is a particle velocity in a unit of cm/s, and $p$ is in cm.

By replacing Eq. 2.7 with Eq. 2.8 and integration, the electron stopping power for the stopping cross-section is obtained as shown in Eq. 2.9.

$$S_e(v) = 2.34\times10^{-23}\left(\mathrm{Z}_1+\mathrm{Z}_2\right)v \qquad (\text{eV cm}^2) \tag{2.9}$$

The range distribution can be obtained according to this model together with a suitable $S_n$.

## 2.5.2 Calculation of Range Distributions

From Eq. 2.1 and Eq. 2.2, we can rearrange the equation in form

$$N\int_{o}^{R} dx = -\int \frac{dE}{S_n(E)+S_e(E)} \tag{2.10}$$

where $R$ is range distribution of implanted ion. Then, the range distribution of implanted ion can be expressed by Eq. 2.11.

$$R = \frac{1}{N}\int_{0}^{E_0} \frac{dE}{S_n(E)+S_e(E)} \tag{2.11}$$

The range distribution of implanted ion relates to the concentration of the implanted substrate, which is obtained from the average range or so-called projected range, the standard deviation, and the implanted dose. Then, the concentration of the implanted substrate is calculated by Eq. 2.12.

$$N(x) = \frac{N_s}{\sqrt{(2\pi)}\,\Delta R_p}\exp\left[-\frac{\left(x-R_p\right)^2}{2\,\Delta R_p^2}\right] \tag{2.12}$$

where $N(x)$ is the concentration of the implanted substrate, $R_p$ is the ion projected range, $\Delta R_p$ is the standard deviation and $N_s$ is the implantation dose. From the above relationship, the ion projected range can be expressed by Eq. 2.13.

$$R_p = \frac{1}{N}\int_{0}^{\infty} x\, f(x)\, dx \tag{2.13}$$

In case of the compound material, the estimations of the range and straggling may be calculated from the average stopping powers of nuclear stopping power and electronic stopping power [22]. The range and straggling can be calculated by

$$\frac{1}{R_p} = \sum_i \frac{X_i}{R_{pi}} \tag{2.14}$$

and

$$\frac{R^2}{\Delta R^2} = \left[\sum_i \gamma_i \frac{Xi\ R_i^2}{R_i\ \Delta R_i^2}\right]\left[\sum_i \gamma_i \frac{X_i}{R_i}\right]^{-1} \tag{2.15}$$

where

$$\gamma_i = \frac{4M_1M_i}{(M_1 + M_i)^2} \tag{2.16}$$

$X_i$ is the fraction of the total mass of the $i^{th}$ component. Even if the elements involved do not have the same energy dependence for the stopping cross sections, these estimates are generally accurate within 10%.

The ion range in solid can be calculated from the energy stopping power of the more complicated equations from this simple equation. The Monte-Carlo simulation programs such as TRIM process such ability and are worldwide used [23].

### 2.5.3 TRIM Calculation of Range Distributions

Based on TRIM calculation, the relationship between stopping power and ion energy of the $C^-$-implanted PS and that of the $C^-$-implanted SR are shown in Fig. 2.10. The densities of polystyrene and silicone rubber for the calculation were set at 1.0600 and 1.1267 g/cm$^3$, respectively.

From Fig. 2.10, the stopping powers from electron and nuclear stopping are as the function of implantation energy. The nuclear stopping power decreases with an increase in the ion implantation energy, but the electron stopping power increases with an increase in the ion energy. Then, at low energy the stopping power is mainly due to the nuclear stopping. By using curve fitting, the approximate equation for calculation of the nuclear stopping power ($S_n(E)$) and the electronic stopping power ($S_e(E)$) of each polymer at the surface are follows:

For polystyrene, $S_n(E) = 4.67 + 8.68\exp^{-0.0575E}$ and $S_e(E) = 2.8295(E)^{\frac{1}{2}}$.

For silicone rubber, $S_n(E) = 4.83 + 8.6\exp^{-0.06E}$ and $S_e(E) = 2.829(E)^{\frac{1}{2}}$.

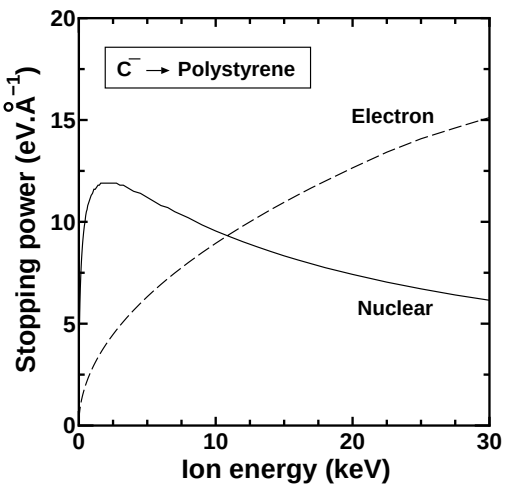


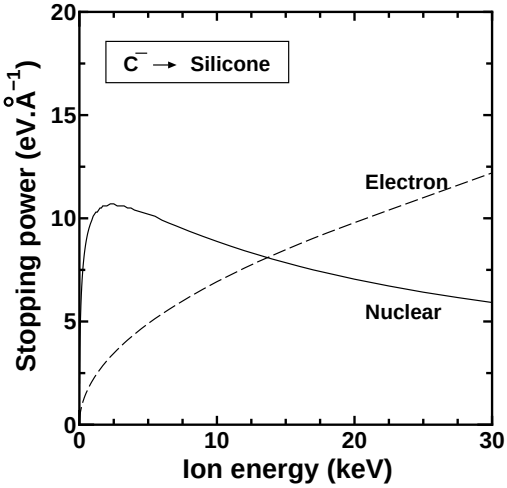


(a) $C^-$-implanted PS (density = 1.0600 g/cm$^3$) (b) $C^-$-implanted SR (density = 1.1267 g/cm$^3$)

Fig 2.10 Relationship between stopping power and ion energy by calculation of TRIM for (a) $C^-$-implanted PS; and (b) $C^-$-implanted SR.

The effect of the implantation energy on the nuclear stopping power can be neglected. Then, the radiation effect at the surface from the transferred energy is due to the electronic stopping power, and it is proportional to the root of the implantation energy.

The depth profiles of atomic carbon composition on the $C^-$-implanted surfaces of PS and SR at dose of $3\times10^{15}$ ions/cm$^2$ and energies of 5 – 30 keV were calculated by using Eq. 2.12 and the standard deviation obtained from TRIM calculation. They are shown in Fig. 2.11.

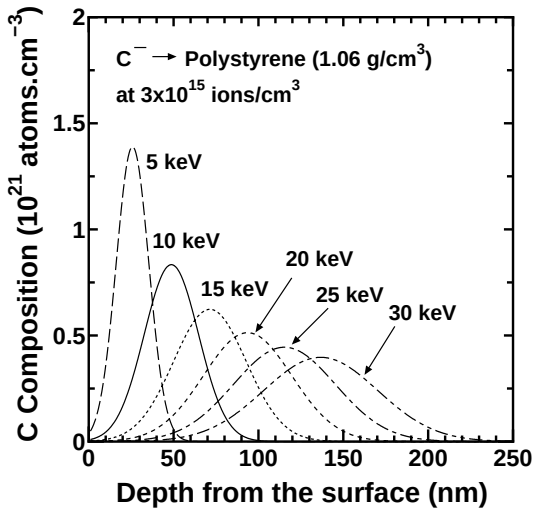


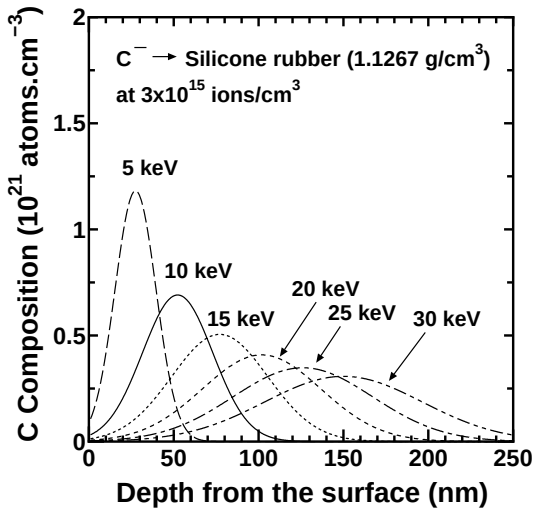


(a) $C^-$-implanted PS (b) $C^-$-implanted SR

Fig 2.11 Depth profile of implanted carbon composition at implantation dose of $3\times10^{15}$ ions/cm$^2$ by calculation of Eq. 2.12 with standard deviation from TRIM for: (a) $C^-$-implanted PS; and (b) $C^-$-implanted SR.

Based on calculation, the depth profile of atomic carbon composition on the $C^-$-implanted PS at energies of 5 – 30 keV is as a function of ion energy implantation. When increasing in the ion energy, the ion projected range becomes deep into the bulk material. In Fig. 2.11 (a), the ion projected range is 25 nm at low implantation energy of 5 keV, and becomes to 50 nm at the typical implantation energy of 10 keV. The different ion-projected range was almost twice.

As for the $C^-$-implanted SR, the depth profiles at the implantation dose of $3\times10^{15}$ ions/cm$^2$ and energies of 5 – 30 keV are shown in Fig. 2.11 (b). Similar to the depth profile for the $C^-$-implanted PS, the depth profile of the atomic carbon composition on the $C^-$-implanted SR by the calculation also shows that almost all doped atoms penetrated inside the solid. The ion projected ranges are 27 and 52 nm at low energy of 5 keV and at typical energy of 10 keV, respectively. The penetration of ions in the solid of SR is a little longer than that of PS and the atomic carbon composition for SR smaller than that for PS at the shallow depth of the surface.

The difference in the depth profiles between both materials of polystyrene and silicone rubber was considered to be due to the differences in the masses and atomic numbers of them that relates to the collision stopping power as described above. The possibility of the collision between the ion and target atom for polystyrene is higher than that for silicone rubber. This is because the main component of polystyrene is carbon, which is the same element of the implantation ion.

As described above that the carbon negative-ion implantation into polymeric surface is done for the application in cell affinity. The adhesion of cells takes place just on the surface area in which there is almost no distribution of the implanted atom. The doping effect of the implanted atoms are considered not to affect to cell adhesion property since the small amount of doped atoms at the top surface layer and almost doped atoms penetrated inside the solid.

As for the radiation effect, the energy loss at the surface polymers is considered, and it is caused by the ionization at the surface and in the shallow depth in solid. The energy loss from ionization for the $C^-$-implanted PS surfaces at the implantation energies of 5 – 30 keV by calculation of TRIM is shown in Fig. 2.12. A large amount of energies is transferred at the surface, and caused to break down the atomic bond at the surface. During the energy transfers, many dangling bonds are occurred at the top surface. After that, the new atomic bonding on these ion-induced defects is formed by the adsorption of gases from the residual gas during implantation and from the air after implantation. As described that the adhesion of cells takes place just on the surface area in which there is almost plenty of the new atomic bonding. Therefore, the effect of the new atomic bonding formation at the surface is expected to improve the cell affinity property. The detail of the atomic bonding state and the evaluation of the physical surface properties will be described in Chapter 3.

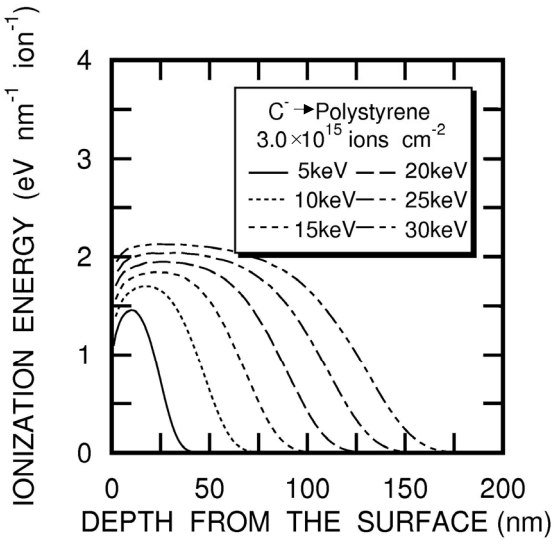


Fig 2.12 Depth profile of energy loss from ionization on the $C^-$-implanted PS at implantation dose of $3\times10^{15}$ ions/cm$^2$ by calculation of TRIM.

## References


[1] Y. Suzuki, M. Kusakabe, K. Kusakabe, H. Akiba, and M. Iwaki, "In vivo Evaluation of Antithrombogenicity for Ion Implanted Silicone Rubber using Indium-111-Tropolone Platelets", Nucl. Instrum. Methods Phys. Res. B, vol. 59-60, pp. 698-704, 1991.

[2] Y. Suzuki, M. Kusakabe, J.S. Lee, M Kusakabe, M. Iwaki, and H. Sasabe, "Endothelial Cell Adhesion to Ion Implanted Polymers", Nucl. Instrum. Methods Phys. Res. B, vol. 65, pp. 142-147, 1992.

[3] R.S. Bhattacharya, "Evaluation of High Energy Ion-Implanted Polycarbonate for Eyewear Applications", Surf. Coat. Technol., vol. 103-104, pp. 151-155, 1998.

[4] F.Z. Cui and Z. S. Luo, "Biomaterials Modification by Ion-Beam Processing", Surf. Coat. Technol., vol. 112, pp. 278-285, 1999.

[5] H. Tsuji, H. Satoh, S. Ikeda, N. Ikemoto, Y. Gotoh, and J. Ishikawa, "Surface Modification by Silver-Negative-Ion Implantation for Controlling Cell-Adhesion Property of Polystyrene", Surf. Coat. Technol., vol. 103-104, pp. 124-128, 1998.

[6] H. Tsuji, H. Satoh, S. Ikeda, Y. Gotoh, and J. Ishikawa, "Contact Angle Lowering of Polystyrene Surface by Silver-Negative-Ion Implantation for Improving Biocompatibility and Introduced Atomic Bond Evaluation by XPS", Nucl. Instrum. Methods Phys. Res. B, vol. 141, pp. 197-201, 1998.

[7] H. Tsuji, H. Satoh, S. Ikeda, S. Ikemura, Y. Gotoh, and J. Ishikawa, "Negative-Ion Beam Surface Modification of Tissue-Culture Polystyrene Dishes for Changing Hydrophilic and Cell-Attachment Properties", Nucl. Instrum. Methods Phys. Res. B, vol. 148, pp.

1136-1140, 1999.

[8] H. Sato, H. Tsuji, S. Ikeda, N. Ikemoto, J. Ishikawa, and S. Nishimoto, “Enhanced Growth of Human Vascular Endothelial Cells on Negative-Ion (Ag-)–Implanted Hydrophobic Surfaces”, J. Biomed. Mater. Res. vol. 44, pp. 22-30, 1999.

[9] H. Tsuji, T. Taya, J. Ishikawa, and T. Takagi, “Neutral and Ionized Cesium Bombardment Type Negative Ion Source”, in: T. Takagi (Ed.), Proceedings of the International Ion Engineering Congress, ISIAT ’83 & IPAT ’83, Kyoto, 12–19 September 1983, vol. 1, Institute of Electrical Engineers of Japan, IEEEJ, pp. 141–146, 1983.

[10] J. Ishikawa, and H. Tsuji, “Carbon Negative Ion Implantation into Silicon”, Nucl. Instrum. Methods Phys. Res. B, vol. 74, pp. 118-122, 1993.

[11] J. Ishikawa, H. Tsuji, Y. Toyota, Y. Gotoh, K. Matsuda, M. Tanjo, and S. Sakai, “Negative-Ion Implantation Technique”, Nucl. Instrum. Methods Phys. Res. B, vol. 96, pp. 7-12, 1995.

[12] H. Tsuji, Y. Toyota, J. Ishikawa, S. Sakai, Y. Okayama, S. Nagumo, Y. Gotoh, and K. Matsuda, “Charging Voltage Measurement of an Isolated Electrode and Insulators during Negative-Ion Implantation”, in: S. Coffa, G. Ferla, F. Priolo, and E. Rimini. (Eds.), Proc. of the 10th Int. Conf. on Ion Implantation Technology 94, Elsevier, New York, pp. 612-615, 1995.

[13] H. Tsuji, J. Ishikawa, S. Ikeda, and Y. Gotoh, “Slightly Negative Surface Potential and Charging Model of Insulator in the Negative-Ion Implantation”, Nucl. Instrum. Methods Phys. Res. B, vol. 127-128, pp. 278-281, 1997.

[14] H. Tsuji, Y. Gotoh, and J. Ishikawa, “Secondary Electron Emission and Surface Potential of $SiO_2$ Film Surface by Negative-Ion Bombardment”, Nucl. Instrum. Methods Phys. Res. B, vol. 141, pp. 645-651, 1998.

[15] M. Kusakabe, Y. Suzuki, A. Nakao, M. Kaibara, M. Iwaki, and M. Scholl, “Control of Endothelial Cell Adhesion to Polymer Surface by Ion Implantation”, Polym. Adv. Technol., vol. 12, pp. 453-460, 2001.

[16] A. Ohl, K. Schroder, D. Keller, A. Meyer-Plath, H. Bienert, B. Husen, and G.M. Rune, “Chemical Micropatterning of Polymeric Cell Culture Substrates using Low-Pressure Hydrogen Gas Discharge Plasmas”, J. Materials and science: Materials in Medicine, vol. 10, pp. 747-754, 1999.

[17] H. Ryssel and I. Ruge, **Ion Implantaion**, translation eds., Great Britain: John Wiley & Sons, 1986.

[18] **Fundamentals of Ion-Irradiated Polymers,** Springer Series in Materials Science, D. Fink Ed. Germany: Springer, p. 356, 2004.

[19] J. Lindhard, Mat. Fys. Medd. Dan. Vid Selsk. vol. 28 [8], 1954, and J. Lindhard and M.

Scharff, “Energy dissipation by ions in the keV region”, Phys. Rev., vol. 124, pp. 128-130, 1961.

[20] O.B. Firsov, Sov. Phys. JETP, vol. 36, p. 1076, 1959.

[21] L. Eriksson, J.A. Davies, and P. Jespersgard, Phys. Rev. vol. 161, p. 219, 1969.

[22] P.D. Townsend, J.C. Kelly, N.E.W. Hartley, **Ion Implantation, Sputtering and their Applications**, London, Great Britain: Academic Press, 1976.

[23] J.F. Ziegler, J.P. Biersack, W. Littmark, **The Stopping and Range of Ions in Solids**, New York: Pergamon Press., Chapter 4, p. 109, 1985.

# Chapter 3

# Physical Evaluation of Ion Implanted Polymeric Surface

In the carbon negative-ion implantation into the polymeric surface, the implanted ions bombard, sputter, create the defect on the surface, and then go to stop in the bulk material. These phenomena affect the structure of the material at the surface. The atomic bonding at the surface, which is modified by the implantation, refers to the change in the physical surface properties. The changes in the physical surface properties may give an effect on the adsorption properties of extracellular matrix (ECM) and the cell-adhesion properties. Therefore, the evaluation of the physical surface properties such as the surface atomic bonding state, the surface morphology and the surface wettability after implantation are considered to be useful for estimation method to predict the adsorption properties of ECM and the cell-adhesion properties. In this chapter, the changes in the surface atomic bonding state, the surface morphology and the surface wettability of the surfaces of spin-coated polystyrene (SCPS) and silicone rubber (SR) before and after carbon negative-ion implantations are described.

## 3.1 Surface Atomic Bonding State by XPS

Since the ion bombardment and surface sputtering make the defect on the surface, the structure or the atomic bonding at the surface will be changed. Atomic composition changes of the polymer surfaces of SCPS and SR between before and after the implantation at 10 keV and $3\times10^{15}$ ions/cm$^2$ were investigated by X-ray photoelectron spectroscopy (XPS; AXIS-165, Shimadzu/Kratos, Kyoto). The XPS survey spectra ranging from 1000 to 0 eV in binding energy for surface elements, and the XPS C 1s detailed spectra ranging from 295 to 280 eV were measured with the X-ray of monochromatic Al K$\alpha$ (photon energy = 1486.6 eV) at a relatively weak intensity for avoiding the X-ray-induced damage. Since the polymeric materials are an insulator, charge neutralizer was used to set the C 1s peak from C-C(H) bond to 285.0 eV [1].

Based on XPS analysis, only a peak of C 1s appeared in the XPS survey spectrum of the unimplanted SCPS as shown in Fig. 3.1 (a). In XPS C 1s spectrum (Fig. 3.1 (b)), two peaks of the main peak and small peak appeared at 285.0 and 291.6 eV, respectively. The main peak was from C-C(H) bond, and the small peak was from the shake-up satellite peak of conjugated $\pi$-$\pi^*$ orbital electrons of bonding carbon atoms in the phenyl group [2]. These correspond to the molecular form of polystyrene (PS), which is composed of only C and H with the side chain of

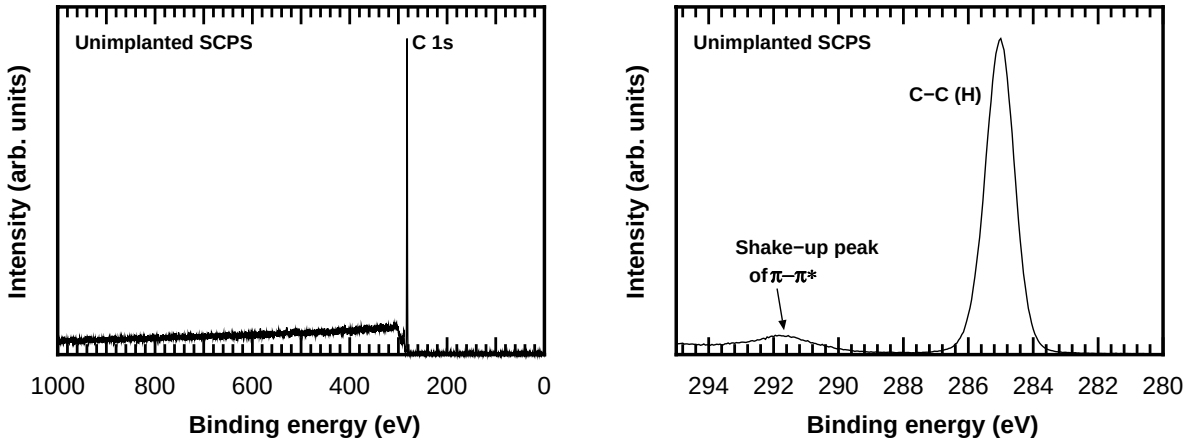


(a) Unimplanted SCPS (XPS survey spectrum) (b) Unimplanted SCPS (XPS C 1s spectrum)

Fig. 3.1 XPS spectra of the unimplanted SCPS: (a) survey spectrum and (b) C 1s spectrum.

phenyl group as described in Chapter 2.

After the implantation at 10 keV and $3\times10^{15}$ ions/cm$^2$, the peaks of C 1s and O 1s appeared in the XPS survey spectra as shown in Fig. 3.2 (a). In XPS C 1s spectrum, the peak from phenyl group at 291.6 eV was fully disappeared and the broadening of the main C 1s peak to 290 eV was appeared as shown in Fig. 3.2 (b). These phenomena presented the changes in the atomic bonding at the surface. The disappeared peak at 291.6 eV can be explained by breaking down the chemical bonds and by sputtering out the carbon atoms in phenyl group during the implantation. The broadening of the main C 1s peak presented the new atomic boding formation.

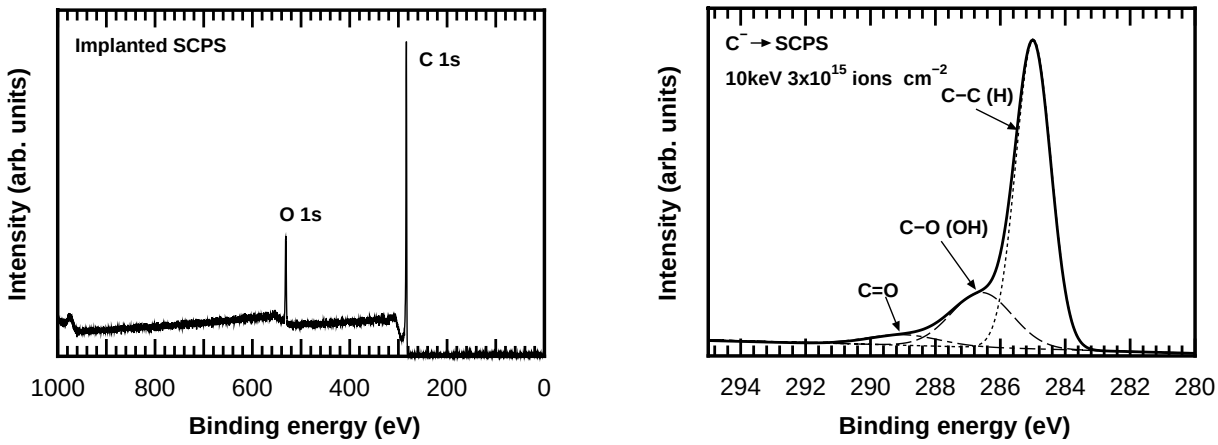


(a) $C^-$-implanted SCPS (XPS survey spectrum) (b) $C^-$-implanted SCPS (XPS C 1s spectrum)

Fig. 3.2 XPS spectra of the C-implanted SCPS at 10 keV and $3\times10^{15}$ ions/cm$^2$: (a) survey spectrum and (b) C 1s spectrum.

Based on curve fitting, the broadening was from the peaks at 286.5 and 289 eV, which two peaks correspond to the bonding of C-O and C=O at chemical shift in the ranges of 1.45 – 1.65 and 2.9 – 4.26 eV [3], respectively. Then, this bonding of C-O and C=O were from the formation of oxygen functional groups on the surface. After ion bombardment and recoils, many dangling bonds and defect occurred. The formation of the oxygen functional group such as C-O and C=O on these dangling bonds and defects from the residual gas during implantation and from oxygen gas and moisture in the environment after implantation occurred. The bonding of the negative polar functional group such as C-O and C=O refers to the hydrophilic property from the polarized dipole. The property of the wettability of the SCPS should be then changed from hydrophobic to hydrophilic after implantation. Therefore, the carbon negative-ion implantation into polystyrene is expected to modify and improve the surface wettability to be hydrophilic, which may lead to the lowering of the contact angle of water after implantation.

In case of silicone rubber surface, the XPS measured spectra are shown in Fig. 3.3. The peak of C 1s, O 1s, Si 2s and Si 2p appeared in the XPS survey spectrum of the unimplanted SR as shown in Fig. 3.3 (a). The atomic compositions of carbon, silicon and oxygen from the calculation of the peak intensities of C 1s, Si 2p and O 1s with their sensitivity factors of XPS were about 51%, 22% and 27%, respectively. Then, their composition ratio of C:Si:O was 2.3:1:1.2. Only bonding of C-Si and C-C(H) appeared in the XPS C 1s spectrum as shown in Fig. 3.3 (b). These also corresponds to the molecular form of silicone rubber, which is composed of Si, C, O and H as described in Chapter 2.

After the implantation at 10 keV and $3\times10^{15}$ ions/cm$^2$, Fig. 3.4 (a) also show the same element peaks of C 1s, O 1s, Si 2s and Si 2p in the XPS survey spectrum. The atomic

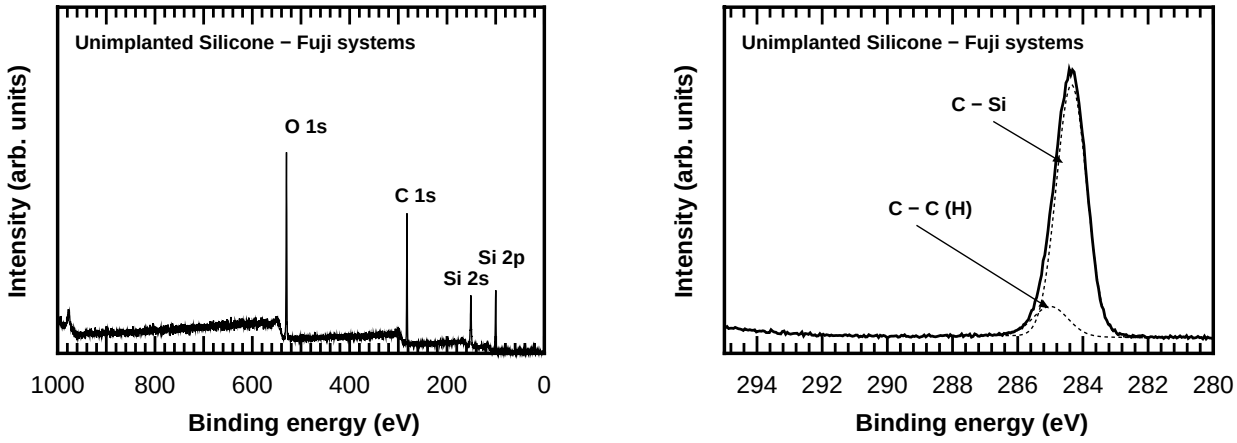


(a) Unimplanted SR (XPS survey spectrum) (b) Unimplanted SR (XPS C 1s spectrum)

Fig. 3.3 XPS spectra of the unimplanted SR: (a) survey spectrum and (b) C 1s spectrum.

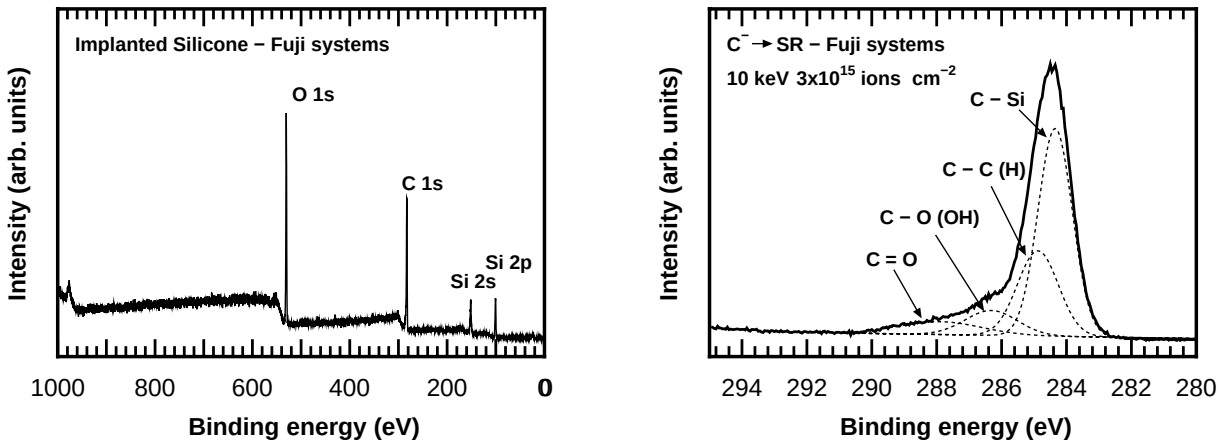


(a) $C^-$-implanted SR (XPS survey spectrum) (b) $C^-$-implanted SR (XPS C 1s spectrum)

Fig. 3.4 XPS spectra of the C-implanted SR at 10 keV and $3\times10^{15}$ ions/cm$^2$: (a) survey spectrum and (b) C 1s spectrum.

composition of carbon, silicon and oxygen were about 52%, 16% and 32%, respectively. The composition ratio of C:Si:O was changed to be 3.3:1:1.2. The changes in the compositions between carbon, oxygen and silicon should be considered to be from the increase in the atoms of carbon and oxygen, or from the decrease in the atom of silicon. In respects of the bond-strength energy [4-5], breaking down the bonds of C-H and C-Si in the side chain was easier than that of Si-O in the main chain. Then, the changes in these compositions were considered to be from the increase in the intensity of carbon and oxygen. The increase of carbon atoms was from the implanted atoms and the adsorbed hydrocarbon atoms, which are from the broken-down bonds of C-H in the side chain of molecular from of silicone rubber, in the residual gas during implantation. Similar to the $C^-$-implanted surface of SCPS, the broadening of C 1s also appeared in the XPS C 1s spectrum of the $C^-$-implanted surface of SR as shown in Fig. 3.4 (b). Based on curve fitting, the broadening was from the peaks at 286.4 and 288 eV. These correspond to the bonding of C-O and C=O [3], respectively. Although there is oxygen atom in the main chain of molecular form, there is no such bonding in the main chain before the implantation. After the implantation, the oxygen functional group formation such as C-O and C=O were also obtained by the adsorption of oxygen atoms from the residual gas during implantation and from oxygen gas and moisture in the environment after implantation on the dangling bonds and on the other ion-induced defects at the surface, and this resulted in increase in the intensity of oxygen atoms. The new oxygen functional groups of C-O and C=O at the surface are hydrophilic groups. Therefore, the carbon negative-ion implantation into silicone rubber made the surface property to be hydrophilic.

The negative polar characteristics in the oxygen functional groups of C-O and C=O refer to the hydrophilic properties due to their polarized dipole. As for these evaluations, the $C^-$-modified surfaces, which have such the hydrophilic functional groups, are expected to be hydrophilic surfaces.

## 3.2 Surface Morphology by AFM

Not only the formation of the hydrophilic bond at the surface, but also the surface morphology can affect adsorption of extracellular matrix (ECM) that influence the cell affinity property. If the surface is smooth, for example, the uniformity adsorption of ECM may occur. In contrast, if the surface is very rough, the adsorption of ECM may be non-uniform resulting in the partial adhesion of cells. Therefore, the evaluation of the surface morphology of $C^-$-implanted polymeric material is necessary. In this research, the polystyrene substrate was prepared by spin-coating on the mirror polished glass as described in Chapter 2. Then, the surface morphology of the spin-coated polystyrene (SCPS) may be different from the normal commercial polystyrene dish. To confirm the morphology to the normal commercial polystyrene, the non-treated polystyrene dish (NTPS, Corning) was examined. The surface morphologies of the polymer surfaces of NTPS dish, SCPS and SR between before and after implantation at 10 keV and $3\times10^{15}$ ions/cm$^2$ were investigated by atomic force microscope (AFM, SPI3800, Seiko instruments Inc.).

The surface morphologies of the unimplanted NTPS dish and the $C^-$-implanted NTPS dish are shown in Fig. 3.5. On the image area of $1.5\times1.5$ μm$^2$ and depth scale of 20 nm, the

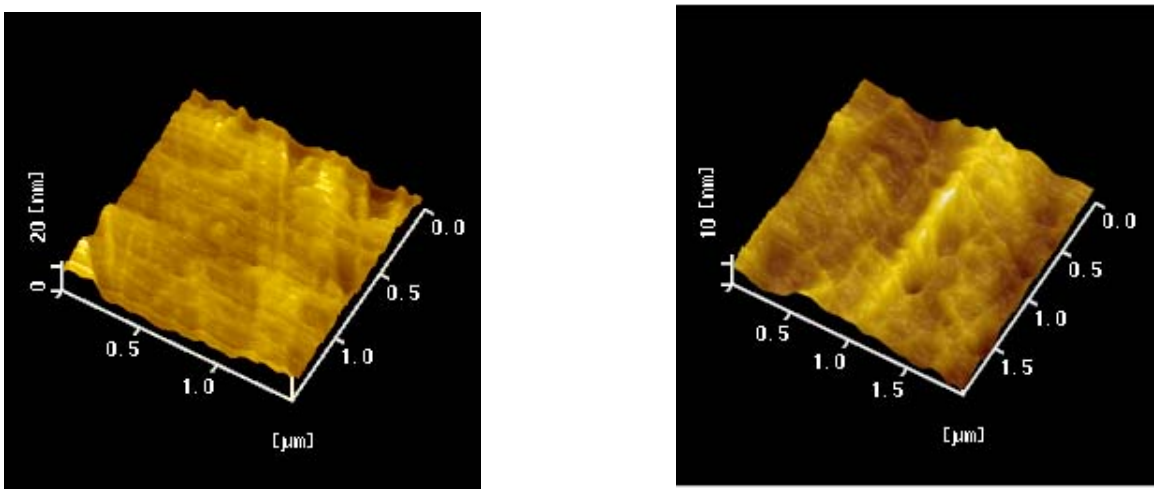


(a) Unimplanted NTPS dish (b) $C^-$-implanted NTPS dish

Fig. 3.5 AFM images of NTPS dish: (a) before and (b) after implantation at 10 keV and $3\times10^{15}$ ions/cm$^2$.

surface of the unimplanted NTPS was almost smooth and had some local depression areas with 1 μm in width and 10 nm in depth as shown in Fig. 3.5 (a). The local depression areas may be from the molding into dish shape. The surface roughness (Ra) measured within the area of 1×1 $\mu m^2$ was about 1.75 nm. After implantation at 10 keV and $3\times10^{15}$ ions/$cm^2$, no different surface appeared as shown in Fig. 3.5 (b). The peak-to-valley depth was about 10 nm.

In case of the SCPS, the surface of the unimplanted SCPS (Fig. 3.6(a)) was very smooth and had no local depression area comparing to the unimplanted NTPS dish. After implantation at 10 keV and $3\times10^{15}$ ions/$cm^2$, no different surface also existed as shown in Fig. 3.6 (b). The surface roughness (Ra) measured within the area of 1×1 $\mu m^2$ was 0.14 nm, and the peak-to-valley depth was about 1.5 nm.

In case of SR, the surface of the unimplanted SR was relatively rough, and had some local depression areas with 1 μm in width and several hundreds nm in depth as shown in Fig. 3.7 (a). While on other areas the peak-to-valley of the surface with about 300 nm in width and about 50 nm in depth existed. Thus, the surface roughness by peak-to-valley depth was several nm. After implantation at 10 keV and $3\times10^{15}$ ions/$cm^2$, the surface contour of SR is shown in Fig. 3.7 (b). The surface was very smooth within the area of 1×1 $\mu m^2$. The peak-to-valley of the surface was about 50 nm in depth and no small rip existed.

From the results, the surface roughness on the implanted polystyrene and the smoother surface on the implanted silicone rubber were due to the effect of sputtering, which occurred from the nuclear collision as well as the electronic excitations. Sputtering is a function of many variables including the masses of the ion and the target atom, the ion implantation energy, direction of incidence to the face of the target, the target temperature and the ion-current density.

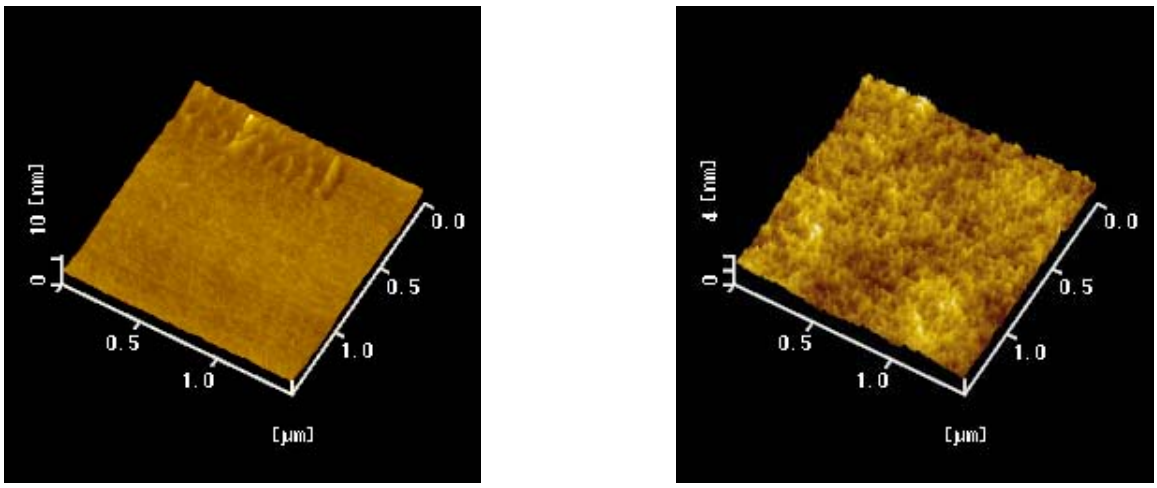


(a) Unimplanted SCPS (b) $C^-$-implanted SCPS

Fig. 3.6 AFM images of SCPS films: (a) before and (b) after implantation at 10 keV and $3\times10^{15}$ ions/$cm^2$.

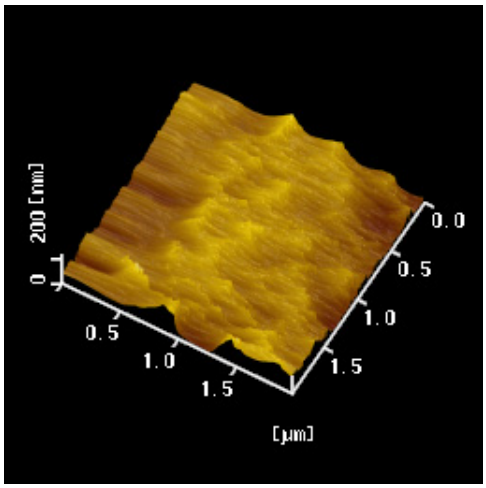


(a) Unimplanted SR

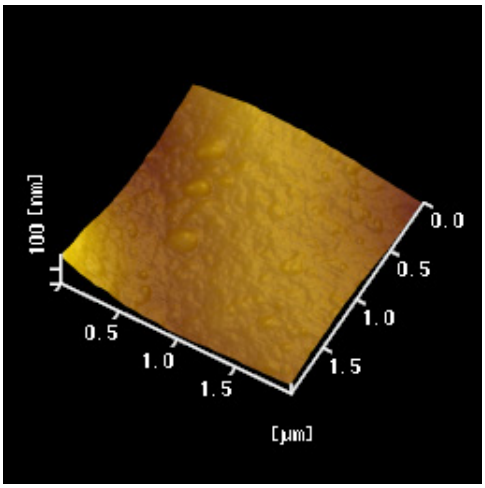


(b) $C^-$-implanted SR

Fig. 3.7 AFM images of SR: (a) before and (b) after implantation at 10 keV and $3\times10^{15}$ ions/cm$^2$.

Moreover, the measured sputtering yield will also depend on the background gas pressure, the previous history of the solid, including the ion implantation concentration and electrical fields existing at the surface. At low energies, sputtering from the nuclear collision is caused by elastic collision between incident ions and the target atom, followed by a cascade of collisions among a large number of atoms inside the solid. Therefore, the sputtering yield ($Y_S$) is directly proportional to the nuclear energy loss of nuclear stopping power ($S_n(E)$). The sputtering yields decreases beyond its peak value at a sputtering energy with increasing energy, consistent with the nuclear stopping power. Sigmund described the model for accuracy calculation of sputtering yield at implantation dose lower than $10^{16}$ ions/cm$^2$ [6-7]. He assumed that the sputtering yield depends on the stopping cross-section for displacement, the efficiency of energy transfer, and a surface binding energy. Hence, the sputtering yield can be expressed by Eq. 3.1.

$$Y_S = \frac{\lambda\, S_n(E)\, \alpha(M_2/M_1)}{U_0} \tag{3.1}$$

where $\lambda$ should be a calculable constant, $S_n(E)$ is a nuclear stopping power, $\alpha(M_2/M_1)$ is the efficiency of energy transfer and $U_0$ is a surface binding energy.

From the simply Eq. 2.3 in Chapter 2, Sigmund reduced the term of impact collision parameter by using a differential cross-section as shown in Eq. 3.2.

$$d\sigma = 2\pi\, p\, dp \tag{3.2}$$

By including the energy dependence of the nuclear and electronic scattering cross section, the power potential approximations of the Thomas-Fermi atomic model were used. Then, a solution for the differential cross section for energy transfer is given as Eq. 3.3.

$$d\sigma(T) = C E^{-m} T^{1-m}\, dT \tag{3.3}$$

where

$$C = C_m = \frac{\pi \lambda_m a^2}{2} \left( \frac{M_1}{M_2} \right)^m \left( \frac{2 Z_1 Z_2 e^2}{a} \right)^{2m} \tag{3.4}$$

The exponent $(1/m)$ in the power potential is chosen as $m = 1/2$, which is used for medium energies of ~10 to 100 keV [6]. However, when we consider to the surface binding energy and its influence on the energy spectrum of the ejected atom, the exponent (m) in the power potential and in the index in Eq. 3.4 are chosen as $m = 0$. Then, $\lambda_0 = 24$. $a$ is a screening parameter that is calculated from Bohr radius and atomic numbers of the ion and the target atom, and $a$ = 0.0219 nm. After we put Eqs. 3.3 and 3.4 into Eq. 2.3 and integrated from 0 to $T_m$ ($T_m = \gamma E$), the sputtering yield is given by Eq. 3.5.

$$Y_S = \frac{3}{4\pi^2} \frac{F(E)}{N C_0 U_0} \tag{3.5}$$

when

$$F(E) = \alpha \left( \frac{M_2}{M_1} \right) \left( \frac{dE}{dx} \right)_n = \alpha \left( \frac{M_2}{M_1} \right) N S_n(E) \tag{3.6}$$

where $F(E)$ is a damage distribution function. When we replaced Eq. 3.5 with Eq. 3.6, the sputtering yield can be expressed by Eq. 3.7.

$$Y_S = \frac{3}{4} \frac{S_n(E) \alpha (M_2/M_1)}{\pi^2 C_0 U_0} \tag{3.7}$$

Based on TRIM calculation, the sputtering yield on the polystyrene modified at the implantation energy of 10 keV was in the range of 0.3 and 0.4 atoms/ion. For the implantation at dose of $3\times10^{15}$ ions/cm$^2$, the sputtered atoms were 1.2 $\times10^{15}$ atoms/cm$^2$. The numbers of atoms are $9.8062\times10^{22}$ ions/cm$^3$. Therefore, the sputtering depth was approximate 0.122 nm. This is corresponding to the result of the surface roughness (Ra) of the implanted SCPS that was obtained by AFM.

In case of silicone rubber, the sputtering yield from TRIM calculation was in the range of 0.6 and 0.7 atoms/ion. At dose of $3\times10^{15}$ ions/cm$^2$, the sputtered atoms were $2.1\times10^{15}$ atoms/cm$^2$. The numbers of atoms are $9.1498\times10^{15}$ ions/cm$^3$. Then, the sputtering depth was about 0.229 nm. Since the initial surface was rough these sputtering almost occurred at the rough area. The surface was sputtered and the gas particles were emitted from the implanted area. Then, the surface shrank, leading to the smoother surface. However, if we increase the implantation time, the surface will become rough, again.

From all investigations of the surface morphology, the surfaces of NTPS and SCPS before implantation and after the implantation at 10 keV and $3\times10^{15}$ ions/cm$^2$ were almost

smooth, even if some local depression areas were found on the surface of NTPS. There was no difference in surface roughness between before and after the implantation at this condition. When comparing the roughness of NTPS and SCPS to the size of proteins and cells [8-10], this roughness was much more less than the size of proteins and cells. Therefore, the surface roughness of NTPS and SCPS is expected to be no effect on the protein adsorption and the cell adhesion. In case of the SR, the surface of SR before implantation is relatively rough. The surface consists of many local depression areas and many asperities. Such roughness was relatively large to the size of some adhesive protein [8-10], and this roughness is expected to effect on the protein adsorption and the cell adhesion. After implantation at 10 keV and $3\times10^{15}$ ions/cm$^2$, there is no difference in peak-to-valley depth of the surfaces, but the implanted surfaces of SR was smoother. So, the uniforms of protein adsorption and cell adhesion on the $C^-$-implanted SR are expected.

## 3.3 Wettability by Contact Angle Measurement

One of physical surface properties that relates to cell affinity is surface wettability, and it can be simply evaluated by contact angle measurement. After implantation, the formation of oxygen functional groups on the defect from the ion bombardment on the surface makes the contact angle of surface decrease. Then, the hydrophilic property is obtained. The formation of the oxygen functional group is illustrated in Fig. 3.8.

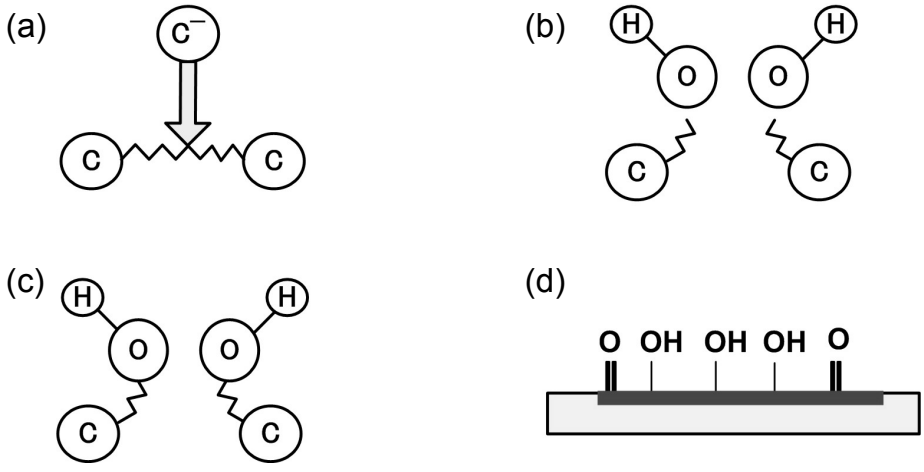


Fig. 3.8 Schematic diagram of formation for oxygen-functional group on the $C^-$-implanted polymeric surface from: (a) carbon negative-ion implantation into C-C bond; (b) a cut C-C bond induced with O-H; (c) bonding of hydroxyl; and (d) formation of carbonyl and hydroxyl on the implanted region.

The hydrophobic-hydrophilic properties correspond to the high-low contact angle. Generally, the adhesions of each cell line concern to the extracellular matrix (ECM) of many proteins absorbed on the surface as described in Chapter 4. In natural, all proteins consist of both hydrophobic and hydrophilic bonds [11], and those are randomly absorbed on the surface. However, the necessary proteins for the adhesion of cells are absorbed on the hydrophilic surface, which contact angle is in the range of 40° – 80° [12].

The contact angle of pure water distilled by a filter is widely measured by water drop method, which is measuring in the air. In the real cell culture, however, the $C^-$-implanted surface is in aqueous solution that affect to the contact angle. The real contact angle of surface in the aqueous solution should be considered. Then, the air bubble method for contact angle measurement is examined in this research.

### 3.3.1 Water Drop Method

The contact angles are generally measured by the stationary water drop method, so-called droplet. This method is done by taking the photo of droplet on the surface in the air from the horizontal direction and calculation of angle between the solid surface and water surface at the edge by using simple circular arc assumption of the simple equation. The schematic diagram of contact angle measurement method by droplet is shown in Fig. 3.9.

The $C^-$-implanted sample is set on the stage of jack. After setting light, position and the focus of microscope, a small drop of pure de-ionized water with less than 1-mm diameter or about 0.8-1.2 µl is put on the sample. The numerical contact angle values can be calculated from the width and height of a droplet assuming a circular shape as shown in Eq. 3.8.

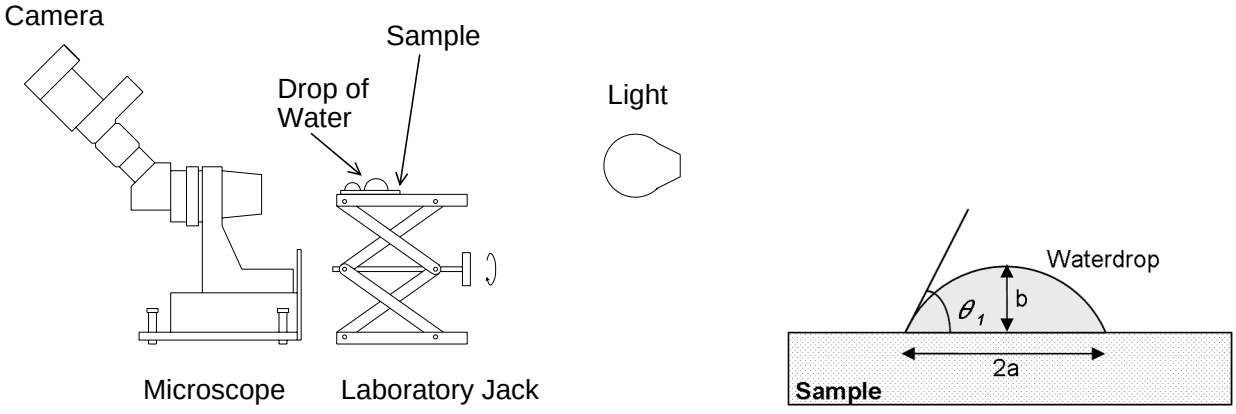


(a) Measurement method (b) Contact angle measurement

Fig. 3.9 Contact angle measurement by water drop method.

$$\theta_1 = \frac{\pi}{2} - \tan^{-1}\left(\frac{a^2 - b^2}{2ab}\right) \tag{3.8}$$

where $\theta_1$ is the contact angle of water drop method, and a and b are the radius and height of water drop, respectively.

In this work, more than eighteen values obtained from droplet pictures were averaged for each sample, excluding the maximum and minimum values.

### 3.3.2 Air Bubble Method

The contact angle in the aqueous state is also measured in this research by the air bubble method. The method is done by taking the photo of air bubble on the surface under the pure water from the horizontal direction and calculation by the simple equation. The schematic diagram of contact angle measurement bubble by air method is shown in Fig. 3.10.

The sample set on the sample holder is dipped upside-down in the pure de-ionized water with the distance from top surface of the water for 1 cm to control the pressure. After setting light, position and the focus of microscope, a small bubble with less than 1-mm diameter is putted on the sample. The numerical contact angle values can be calculated from the width and height of a air bubble assuming a circular shape as shown in Eq. 3.9.

$$\theta_2 = \tan^{-1}\left(\frac{c^2 - d^2}{2cd}\right) \tag{3.9}$$

where $\theta_2$ is the contact angle of air bubble method, and c and d are the radius and height of the bubble, respectively.

In this work, more than eighteen values obtained from droplet pictures were averaged for each sample, excluding the maximum and minimum values.

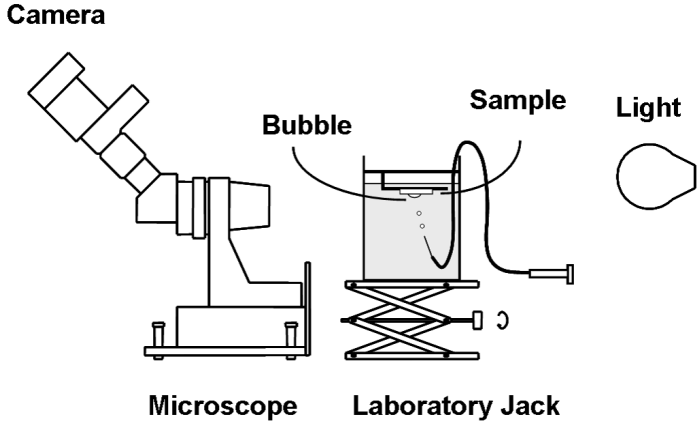


(a) Measurement method

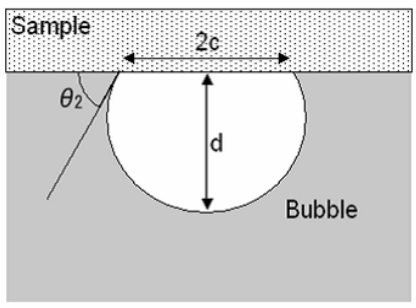


(b) Contact angle measurement

Fig. 3.10 Contact angle measurement by air bubble method.

### 3.3.3 Contact Angle of $C^-$-Implanted Polymeric Surface

In this experiment, two types of polymeric materials of polystyrene and silicone rubber were examined. The carbon negative ions were implanted into these samples to modify the surface properties. As described in section 3.1 and in Chapter 2, by implantation the carbon negative ions implantation break down the bonds of C-C, C-H, C-Si and Si-O on the polymeric surfaces and penetrate into the bulk material. Then after implantation, the relaxation or stabilization of the ion-implanted polymeric surface gradually occurs with time dependence by rearrangement and adsorption of oxygen atoms in the residual gas and in the circumstance after exposuring to the air or to aqueous solution to form the functional group of C=O and OH on the implanted surface. These rearrangement and stabilization of the surface result in gradually change in contact angle, especially, on the implanted surface. That means the change in contact angle of the implanted polymeric surfaces should depend on the ion dose and ion energy in the condition implantation. The change in their contact angles of pure de-ionized water (DIW) were measured by water drop method within 2 h just after implantation (as implanted) and by air bubble methods after dipping in pure water for 0, 2, 24, 36 and 48 h at 20°C.

### Contact Angle of $C^-$-Implanted Spin-Coated Polystyrene (SCPS) Films

In this section, the spin-coated polystyrene (SCPS) films on a commercial glass substrate with area of 24×24 $mm^2$ and thickness of 0.5 mm (#7059, Corning) were implanted by carbon negative ions at various energies of 5 – 20 keV and at various doses of $1\times10^{14}$ – $3\times10^{16}$ ions/$cm^2$ to study the effect of ion dose and energy on the change in contact angle.

The contact angles of DIW on the $C^-$-implanted SCPS at the low energy of 5 keV are shown in Fig. 3.11, which (a) is the angle measured by the water drop and air bubble method after the implantation within 2 h, and (b) is the angle measured by the air bubble method after dipping in DIW for 0, 2 and 24 h. From Fig. 1(a) as the ion dose increased the contact angle on the implanted SCPS decreased from 91° to 86° at the lowest in the case of the water drop method and from 86° to 73° in the case of the air bubble method. The lowest angle took place at the dose of $3\times10^{15}$ ions/$cm^2$. Over this ion dose, the angles increased with small degrees to 87° by water drop method and to 75° by air bubble method. The lowering of the contact angle in the water is larger than that in the air. Fig. 3.11(b) shows the time dependence of the contact angle in the water. After dipping the $C^-$-implanted SCPS at $3\times10^{15}$ ions/$cm^2$ in DIW for 24 h, the angle decreased from 73° to 65° and it was saturated at 62° after dipping in DIW for 48 h. The angle decreased with an increase in the dipping time.

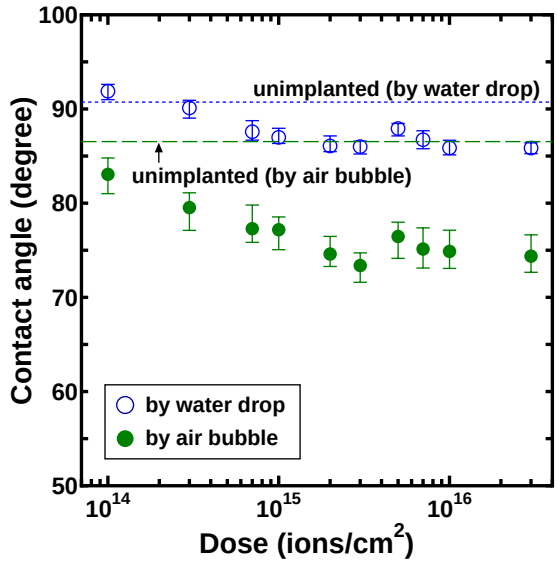


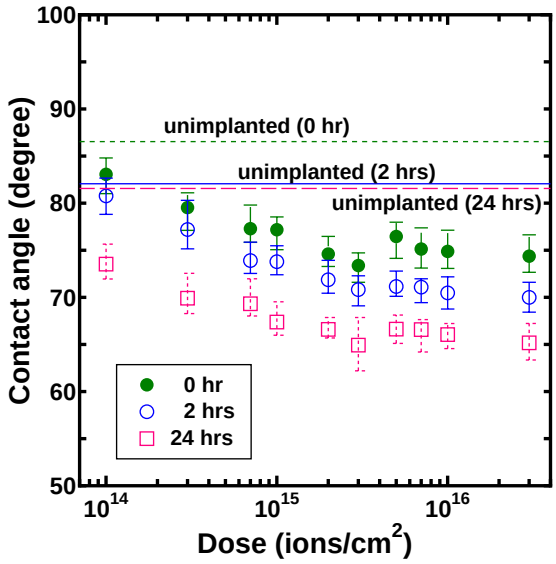


(a) by water drop and air bubble methods (b) by air bubble method after 0, 2, 24 h dipping

Fig. 3.11 Contact angle on $C^-$-implanted SCPS films as a function of the ion dose at 5 keV.

As the same results of implantation at the low energy of 5 keV, the contact angles of the $C^-$-implanted surfaces of SCPS at the typical implantation energy of 10 keV decreased with an increase in the implantation dose. The lowering of contact angles at the energy of 10 keV are shown in Fig. 3.12. The angle decreased as a function of ion dose from 91° to 85° at the lowest in the case of the water drop method and from 86° to that of 75° in the case of the air bubble method as shown in Fig. 3.12 (a). The lowest angle also took place at the $3\times10^{15}$ ions/cm$^2$.

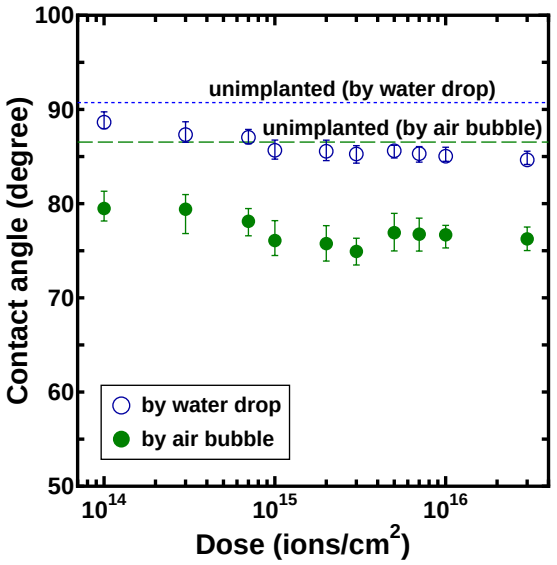


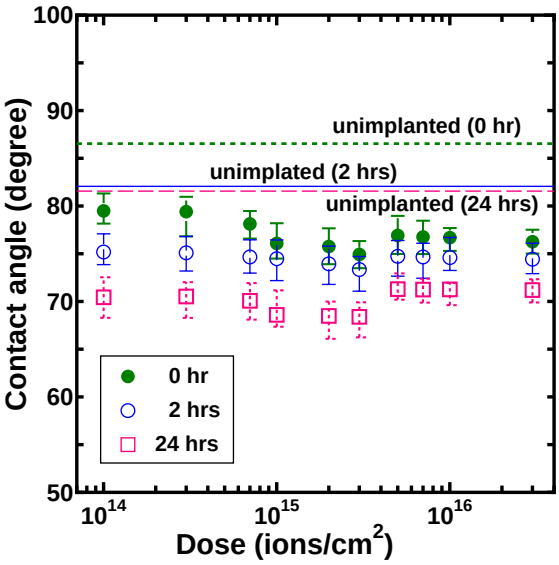


(a) by water drop and air bubble methods (b) by air bubble method after 0, 2, 24 h dipping

Fig. 3.12 Contact angle on $C^-$-implanted SCPS films as a function of the ion dose at 10 keV.

The angle of the higher dose-implanted samples became saturated around 85° by water drop method. Fig. 3.12(b) shows the time dependence of the contact angle in the water. After dipping in DIW for 24 h at $3\times10^{15}$ ions/cm$^2$, the angle decreased from 75° to 68° and it was saturated at 66° after dipping in DIW for 48 h. These decreases in contact angle at the implantation energy of 10 keV is similar to those of the energy of 5 keV.

At high implantation energies of 15 – 20 keV, the contact angles of the $C^-$-implanted surfaces of SCPS are shown in Figs. 3.13 and 3.14, respectively. Figs. 3.13 (a) and 3.14 (a) show the difference in lowering of contact angles by the water drop method and by air bubble method for the implantation energies at 15 and 20 keV, respectively. The angle also decreased as the function of ion dose from 91° to 84° at the lowest in the case of the water drop method and from 86° to 73° in the case of the air bubble method. The lowest angle at the implantation energies of 15 and 20 keV took place at the $7\times10^{15}$ and $2\times10^{15}$ ions/cm$^2$, respectively. The implantation dose for obtaining the lowest angle at the implantation energy of 20 keV is smaller than the dose at the energy of 15 keV. The angle of the higher dose-implanted samples became saturated around 85° by water drop method. Figs. 3.13(b) and 3.14 (b) shows the time dependence of the contact angle. After dipping in DIW for 24 h at $3\times10^{15}$ ions/cm$^2$, the angle decreased from 73° to 65° and it was saturated at 63° after dipping in DIW for 48 h.

As for the energy dependence of contact angle, the effect of ion energy implantation at a certain ion dose of $3\times10^{15}$ ions/cm$^2$ on the change in contact angle can be summarized. From the above data, the energy dependence is shown in Fig. 3.15, where (a) is the angle measured by the water drop and air bubble method after the implantation within 2 h, and (b) is the angle measured

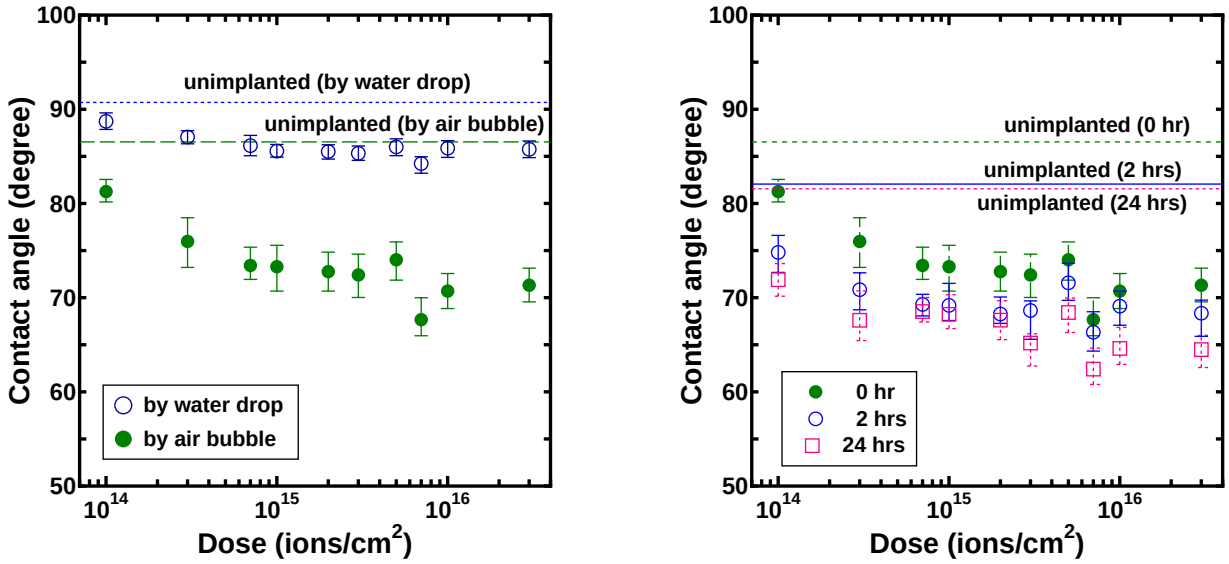


(a) by water drop and air bubble methods (b) by air bubble method after 0, 2, 24 h dipping

Fig. 3.13 Contact angle on $C^-$-implanted SCPS films as a function of the ion dose at 15 keV.

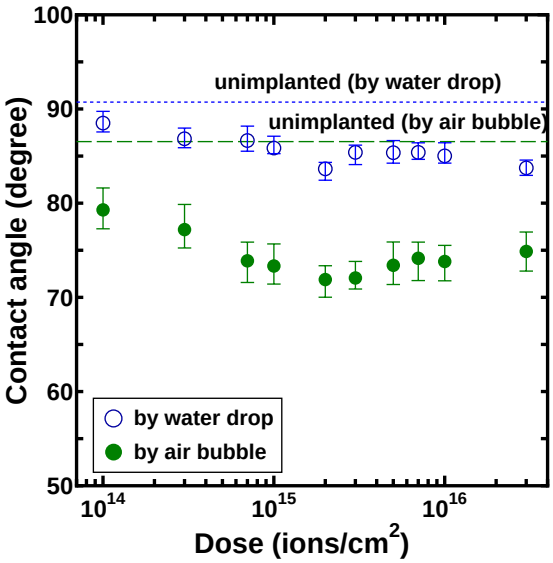


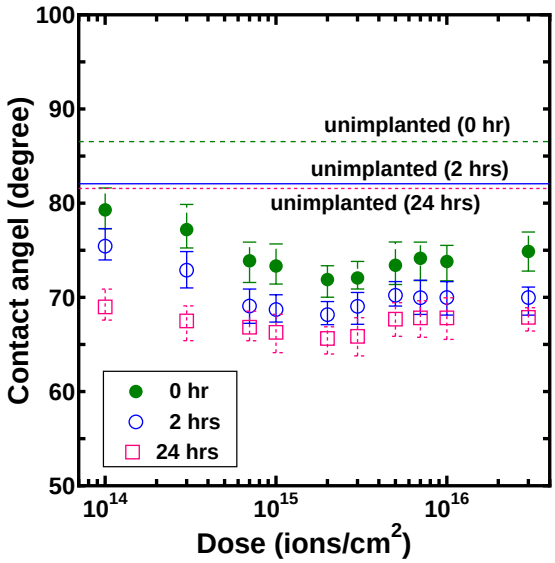


(a) by water drop and air bubble methods (b) by air bubble method after 0, 2, 24 h dipping

Fig. 3.14 Contact angle on $C^-$-implanted SCPS films as a function of the ion dose at 20 keV.

by the air bubble method after dipping in DIW for 0, 2, 24, 36 and 48 h. In Fig. 3.15 (a), the contact angles a little decreased and saturated as a function of the implantation energy for the data measured by the water drop method. They increased at 10 keV and then decreased as a little before saturated at 15 keV for the data measured by the air bubble method. However, the different was only 3° – 4° when increase in the ion energy.

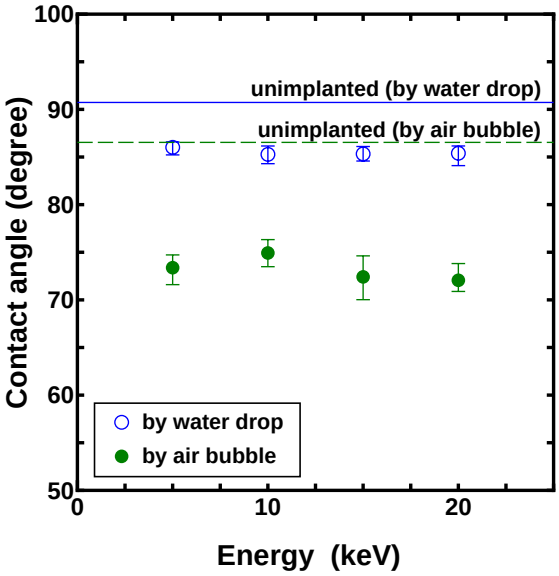


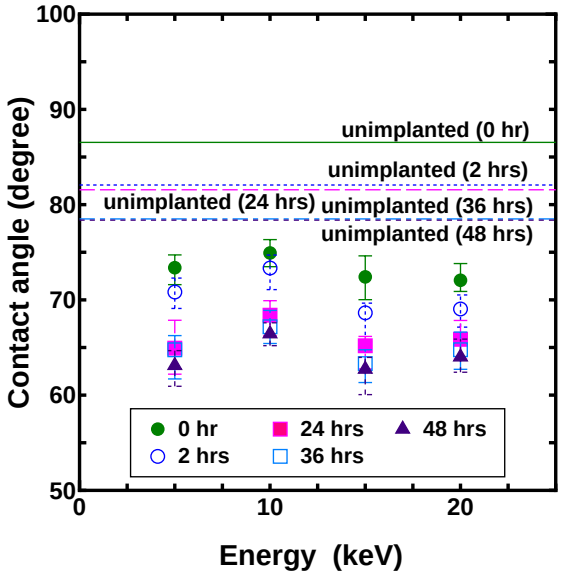


(a) by water drop and air bubble methods (b) by air bubble method after 0, 2, 24 h dipping

Fig. 3.15 Contact angle on $C^-$-implanted SCPS films as a function of the ion energy at $3\times10^{15}$ ions/cm$^2$.

In Fig. 3.15 (b), the data also confirmed that there was no insignificant decrease of contact angles after dipping in DIW for 0, 2, 24, 36 and 48 h when increase in the ion energy. After dipping all implanted polystyrene films in DIW, the angle rapidly decreased for 3° – 5° within first 2 h and then gradually decreased for the dipping time from 2 to 24 h, until to reach the saturation at around 63° after 48 h. For the implantation energies of 5 – 20 keV, the contact angles in the water slightly decreased after dipping in DIW for 24 and 48 h. Therefore, these mean the dipping time in DIW for the beginning of the saturation of the decrease in the contact angles was 24 h. This dipping time is expected to enough for obtaining the nearly saturation of the lowering of the contact angle.

The lowering of the contact angle after implantation resulted from the formation of the hydrophilic groups of hydroxyl and carbonyl on the implanted surface due to the radiation effect as described in section 3.1. It was a function of the radiation effect, which relates to the energy loss of the ion at the surface. By the process of energy loss to stopping the ion, the ion energy is transferred to the target atoms in solid. Such energy loss is so-called the energy deposition. As described in Chapter 2, energy loss at the surface and the shallow depth in solid are due to the ionization, as well as the collision. The ionization and the collision are the electronic and nuclear stopping powers, respectively. Then, the energy deposited in solid is proportional to the stopping power, the penetrated depth and the implantation dose, and it can be expressed by Eq. 2.10.

$$E_D = S_T(E)\,\Delta E\,N_s \tag{3.10}$$

where $E_D$ is the energy deposited in the solid, $S_T(E)$ is a total stopping energy and $\Delta E$ is a energy transfer at the penetrated depth.

For consideration of the radiation, we calculated only the energy deposited at the top surface. The term of $\Delta E$ is reduced. Then, the energy transfer is given by Eq. 2.11.

$$E_D = S_T(E)\,N_s = \{S_e(E) + S_n(E)\}\,N_s \tag{3.11}$$

when $S_e(E) = 2.8295(E)^{\frac{1}{2}}$ and $S_n(E) = 4.67 + 8.68\exp^{-0.0575E}$, which were obtained by curve fitting as described in Chapter 2.

Fig. 3.16 shows the increases of the energy deposited at the surface as the functions of ion energy and ion dose. By TRIM calculation Fig. 3.16 (a) shows that the deposited energy is a summary of the stopping powers at certain dose. The deposited energy increased with an increasing in the energy and became to saturate at beyond the energy of 10 keV. There is insignificant energy dependence for the energy deposition. Then, it is considered to have a very small effect of the ion energy on increase of radiation effect at the surface. In contrast, the deposited energy increased as a linear function of the ion dose at certain ion energy as shown in Fig. 3.16 (b).

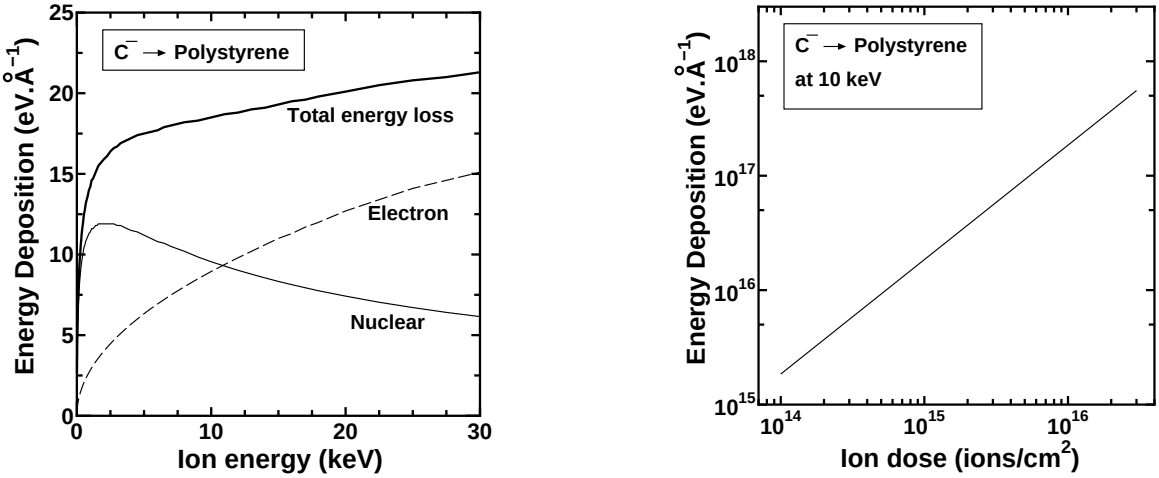


(a) Ion energy dependence (b) Ion dose dependence

Fig. 3.16 Energy deposition at the implanted surface of polystyrene by TRIM calculation as a function of: (a) ion energy; (b) ion dose at 10 keV.

From the calculation, the radiation effect was considered to be mainly due to the ion dose. When increasing in the ion dose, the radiation effect increased, leading to more formation of the hydrophilic groups of hydroxyl and carbonyl. The number of hydrophilic groups on the surface relates to the polar force, which is one of the surface free energy. The surface free energy is used to estimate the contact angle on each surface. Relationship between the contact angle and the balance between surface free energies is shown in Fig. 3.17.

From Fig. 3.17, the balance between the forces on the surface can be expressed by Young's equation as shown in Eq. 3.12.

$$\gamma_1 = \gamma_2 \cos\theta + \gamma_{12} \tag{3.12}$$

where $\gamma_1$ and $\gamma_2$ are surface free energies for the solid and liquid, respectively. $\gamma_{12}$ is interfacial free energy between the solid and liquid, and $\theta$ is contact angle.

Based on Fowkes'theory, the surface free energy and the interfacial free energy are the summations of the surface forces such as dispersion, polarized dipole and hydrogen bonding on each surface [13]. Each surface free energy is expressed by Eq. 3.13.

$$\gamma = \gamma^a + \gamma^b + \gamma^c \tag{3.13}$$

where $\gamma^a$, $\gamma^b$ and $\gamma^c$ are surface forces of dispersion, polarized dipole and hydrogen bonding, respectively.

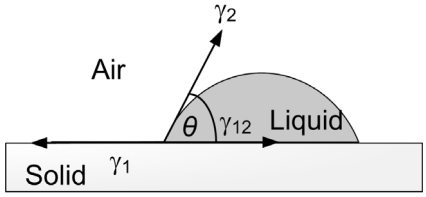


Fig. 3.17 Relationship between the contact angle and the balance between forces on the surface.

When Eq. 3.12 is expressed by the work of adhesion between the different surfaces of solid and liquid, the Young-Dupree Equation can be given by Eq. 3.14.

$$W_{12} = \gamma_1 + \gamma_2 - \gamma_{12} = \gamma_2 + \gamma_2 \cos\theta = \gamma_2(1+\cos\theta) \tag{3.14}$$

where $W_{12}$ is the work of adhesion between solid and liquid. The work of adhesion between solid and liquid is expressed by Eq. 3.15 [14].

$$W_{12} = 2\sqrt{\gamma_1^a \gamma_2^a} + 2\sqrt{\gamma_1^b \gamma_2^b} + 2\sqrt{\gamma_1^c \gamma_2^c} = 2\sum_f^{a\ to\ c}\sqrt{\gamma_1^f \gamma_2^f} \tag{3.15}$$

where $f$ is the $f^{\text{th}}$ component of surface forces.

After we replaced $W_{12}$ in Eq. 3.14 with $W_{12}$ from Eq. 3.15, the term of $\cos\theta$ is given by Eq. 3.16.

$$\cos\theta = \frac{2}{\gamma_2}\sum_f^{a\ to\ c}\sqrt{\gamma_1^f \gamma_2^f} - 1 \tag{3.16}$$

Before implantation, the initial contact angle for polystyrene is about 90˚. After implantation, the obtained contact angle is the summation of the initial contact angle and the change value of contact angle, and it can be expressed by Eq. 3.17.

$$\theta_i = \theta_0 + \Delta\theta \approx \frac{\pi}{2} + \Delta\theta \tag{3.17}$$

where $\theta_0$, $\theta_i$ are the contact angles at the initial state and after implantation, respectively. $\Delta\theta$ is the different value of the angle. If $\Delta\theta$ is considered to be a small value, $\cos\theta_i \approx -\Delta\theta$. The surface free energy of solid after implantation is a summation of the initial surface free energy and the different value of surface free energy. In case of the water contact angle, the $\cos\theta_i$ can be expressed by Eq. 3.18.

$$\cos\theta_i = \frac{2}{\gamma_w}\sum_f^{a\ to\ c}\sqrt{\gamma_i^f \gamma_w^f} - 1 = \frac{2}{\gamma_w}\sum_f^{a\ to\ c}\sqrt{(\gamma_0^f + \Delta\gamma^f)\gamma_w^f} - 1 \approx -\Delta\theta \tag{3.18}$$

where $\gamma_0$ and $\gamma_i$ are surface free energies of the solid at the initial state and after implantation, respectively. $\gamma_w$ is surface free energy of water and $\Delta\gamma$ is the different value of surface free energy of the solid after implantation.

From this approximation and Eq. 3.16, the different value of the contact angle can be expressed by Eq. 3.19.

$$\begin{aligned}
-\Delta\theta &\approx \frac{2}{\gamma_w}\sum_f^{a\ to\ c}\sqrt{(\gamma_0^f+\Delta\gamma^f)\gamma_w^f} - 1 = \frac{2}{\gamma_w}\sum_f^{a\ to\ c}\sqrt{\gamma_0^f \gamma_w^f}\sqrt{\left(1+\frac{\Delta\gamma^f}{\gamma_0^f}\right)} - 1 \approx \frac{2}{\gamma_w}\sum_f^{a\ to\ c}\sqrt{\gamma_0^f \gamma_w^f}\left(1+\frac{1}{2}\frac{\Delta\gamma^f}{\gamma_0^f}\right) - 1 \\
&\approx \frac{2}{\gamma_w}\sum_f^{a\ to\ c}\sqrt{\gamma_0^f \gamma_w^f} - 1 + \frac{1}{\gamma_w}\sum_f^{a\ to\ c}\Delta\gamma^f\sqrt{\frac{\gamma_w^f}{\gamma_0^f}} \approx \cos\theta_0 + \frac{1}{\gamma_w}\sum_f^{a\ to\ c}\Delta\gamma^f\sqrt{\frac{\gamma_w^f}{\gamma_0^f}} \\
&\approx \frac{1}{\gamma_w}\sum_f^{a\ to\ c}\Delta\gamma^f\sqrt{\frac{\gamma_w^f}{\gamma_0^f}} = \frac{1}{\gamma_w}\left(\Delta\gamma^a\sqrt{\frac{\gamma_w^a}{\gamma_0^a}} + \Delta\gamma^b\sqrt{\frac{\gamma_w^b}{\gamma_0^b}} + \Delta\gamma^c\sqrt{\frac{\gamma_w^c}{\gamma_0^c}}\right)
\end{aligned} \tag{3.19}$$

In this work, the change value of the forces due to dispersion and hydrogen bonding were considered to be a small value, and they can be neglected. Then, the change value of surface free energy of the solid was due to the change of the polar force. When considering to the increase and decrease of the contact angle value after implantation, the plus-minus symbols have to put into Eq. 3.19. Then, the different value of the contact angle can be expressed by Eq. 3.20.

$$\Delta\theta \approx \mp \frac{\Delta\gamma^b}{\gamma_w}\sqrt{\frac{\gamma_w^b}{\gamma_0^b}} \tag{3.20}$$

If $\Delta\gamma^b$ is plus, $\Delta\theta$ will be minus, leading to the lowering of the contact angle. The increase of surface free energy means plus $\Delta\gamma^b$. From Eq. 3.20, the different value of the contact angle is proportional to the different value of the polar force on the solid surface. The polar force relates to the number of the hydrophilic groups on the surface, and it increases with an increase in the number of the hydrophilic groups. After the ion implantation, the polar force increased, resulting in the increase of surface free energy. The relation among the decrease of contact angle, the increase of surface free energy, number of hydrophilic groups and energy deposited in solid can be expressed by Eq. 3.21.

$$-\Delta\theta \propto \Delta\gamma^b \propto N(OH) \propto E_D \propto N_s \propto E^{1/2} \tag{3.21}$$

where $N(OH)$ is the number of hydrophilic groups induced by the implantation.

This also corresponded with the results that the contact angle decreased with an increasing in the ion dose. However, the lowering of the angle became saturation at dose order of $10^{15}$ ions/cm$^2$. This could be considered to be due to the high radiation effect or breaking-down the new formed bonding of hydroxyl and carbonyl groups during the implantation. The ratios between the breaking-down and the formation for hydroxyl and carbonyl groups are the important parameters to decide the change of contact angle. The total amount of the formation of hydroxyl and carbonyl groups became to saturate at the optimum value. Then, the lowering of the contact angle became to saturate at the optimum dose.

As a result and consideration, therefore, the relation among the different value of contact angle, the ion energy and the ion dose can be simply expressed by Eq. 3.22.

$$-\Delta\theta \begin{cases} \propto k_{CA}\left(\dfrac{S_e(E)}{E_i}+\dfrac{S_n(E)}{U_0}\right)N_s = k_{CA}\left[\sum_j^{Com}\dfrac{S_{ej}(E)}{E_{ij}}+\sum_j^{Com}\dfrac{S_{nj}(E)}{U_{0j}}\right]N_s & (\textit{for low dose}) \\ = \textit{const.} & \left(\textit{for medium dose of } 10^{15}\ \textit{ions/cm}^2\right) \end{cases} \tag{3.22}$$

where $k_{CA}$ is constant, *Com.* means compound element and $j$ is the $j^{\text{th}}$ component in compound material.

In case of measuring contact angle in the water, the results showed the more lowering of the angle after dipping in the water and increasing in the dipping time. It was considered to be due to the penetration of the water molecules into the shallow depth of the solid, leading to some rearrangement of the atoms at such area. Then, when considering about the radiation effect on the lowering of the contact angle in the water, we should include the energy deposited inside the solid or term of energy transferred at each penetrated depth into Eq. 3.11. From the increase of summation of $\Delta E$ in calculation, the deposited energy increased, leading to more decrease of the contact angle in water.

From the results, the lowering tendencies of the contact angles of water as a function of ion dose in the range of $10^{14}$ – $10^{16}$ ions/cm$^2$ and their minimum value at the ion implantation dose after dipping in DIW for 24 and 48 h for the implantation energies of 5 – 20 keV are summarized as shown in Table 3.1.

Table 3.1 The lowering tendencies of the contact angle (CA) of water as a function of ion dose and their minimum contact angle at the ion implantation dose after dipping in DIW for 24 and 48 h on the $C^-$-implanted SCPS for the implantation energies of 5 – 20 keV.

| Ion Energy (keV) | Tendency of CA at the ion dose range (ions/cm$^2$) | | | Minimum CA (°) | | Mininum CA at dose (ions/cm$^2$) |
|---|---|---|---|---|---|---|
| | $10^{14}$ | $10^{15}$ | $10^{16}$ | after 24 h dipping in DIW | after 48 h dipping in DIW | |
| 5 | ↘ | → | → | 65 | 62 | $3\times10^{15}$ |
| 10 | ↘ | → | → | 68 | 66 | $3\times10^{15}$ |
| 15 | ↘ | → | → | 65 | 63 | $7\times10^{15}$ |
| 20 | ↘ | → | → | 66 | 64 | $2\times10^{15}$ |

As a consequence of the contact angle measurement for $C^-$-implanted SCPS surface, the contact angle decreased as a function of ion dose from $1\times10^{14}$ – $1\times10^{15}$ ions/cm$^2$ before became to saturate at dose of about $2\times10^{15}$ – $5\times10^{15}$ ions/cm$^2$ for both measurement of water drop and air bubble methods. The decrease in the contact angle in the air was smaller than that in the angle in the water. These could be considered from the circumstance dependence of the stabilization of the ion-induced defects at the implanted surface. The stabilization rate at the surface for formation of the oxygen function group in the water was higher. At a certain dose implantation of $3\times10^{15}$ ions/cm$^2$, the contact angle insignificantly decreased with an increase in the ion energy from 5 – 20 keV. As for the time dependence, the contact angles on the $C^-$-implanted SCPS by the air bubble method decreased with an increase in the dipping time in the water. The lowering

of contact angle almost spent 24 h, and then it became to saturate. These indicated that the stabilization of the ion-induced defect at the shallow surface and inside of the solid of material required the time of about 24 h. By the measured angle values, the considerably suitable conditions with hydrophilic property for high possible cell-adhesion properties on the $C^-$-implanted SCPS should be $1\times10^{15} - 3\times10^{16}$ ions/cm$^2$ for 5 – 20 keV. The best condition was expected to be around $2\times10^{15} - 3\times10^{15}$ ions/cm$^2$.

## Contact Angle of $C^-$-Implanted Silicone Rubber (SR)

In this section, the silicone rubber sheets (SR, Wacom electric co., ltd.) with a thickness of 0.5 mm were implanted by carbon negative ion at 10 keV and at various doses of $1\times10^{13} - 1\times10^{16}$ ions/cm$^2$ to study the effect of ion dose on the changing of contact angle.

The contact angles of DIW on the $C^-$-implanted SR sheet at the typical implantation energy of 10 keV as a function of ion dose measured by the water drop method as implanted and by the air bubble method after dipping in DIW for 0, 2 and 24 h are shown in Fig. 3.18. The contact angles by water drop method gradually decreased with an increase in the ion dose and saturated in the dose range of $1\times10^{15} - 3\times10^{15}$ ions/cm$^2$ as shown in Fig. 3.18 (a). Comparing to the unimplanted SR, the angle values decreased from 100° to the lowest angle of 86° at $3\times10^{15}$ ions/cm$^2$. Over this ion implantation dose, the angle increased with a few degrees from the lowest angle. This lowering of the contact angle on the surface of silicone rubber modified by carbon negative-ion implantation has the same tendency and value of that of the angle on the surface modified by the gas plasma process [15-16].

After the surfaces were dipped in DIW for 0 h, the contact angles from air bubble method increased at very low implantation doses of $1\times10^{13}$ - $3\times10^{13}$ ions/cm$^2$ from 90° to 96°, and the angles over these very low implantation doses gradually decreased to the lowest angle of 61° with an increase in the ion dose as shown in Fig. 3.18 (b). The high angle value at very low implantation doses of $1\times10^{13}$- $3\times10^{13}$ ions/cm$^2$ showed the hydrophobic property of surface due to cleaning by sputtering. The more lowering of angle at high implantation dose of $1\times10^{16}$ ions/cm$^2$ might be caused by stabilization inside the solid of SR.

As for the time dependence in the water, the contact angles on the $C^-$-implanted SR as the function of ion dose at 10 keV after dipping in the DIW for 0, 2, and 24 h are also shown in Fig. 3.18 (b). After dipping all implanted SR sheets in DIW, the angle rapidly decreased for 3° – 8° within first 2 h, excepting at very low implantation dose that brought about decrease of angle of 2° – 4°. Then angle gradually decreased by 9° – 17° until saturate during dipping time from 2 h to 24 h. The lowest angle was 47° at $1\times10^{16}$ ions/cm$^2$ after 24 h dipping in DIW.

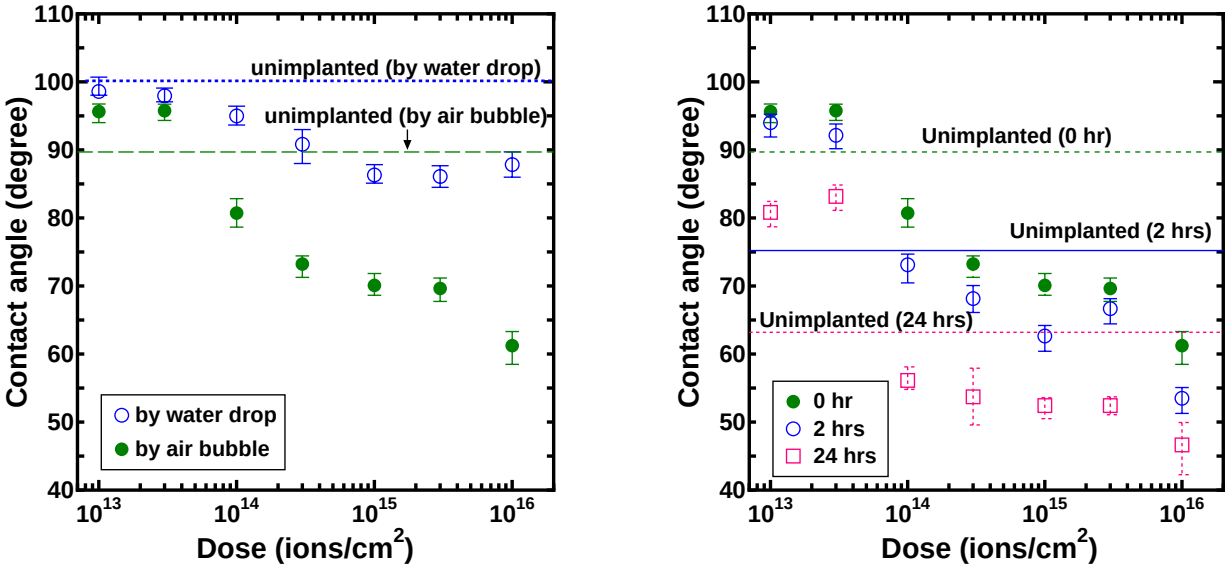


(a) by water drop and air bubble methods (b) by air bubble method after 0, 2, 24 h dipping

Fig. 3.18 Contact angle on $C^-$-implanted silicone rubber as a function of the ion dose at 10 keV.

As the same results of the change in the contact angle of the $C^-$-implanted SCPS surfaces at the implantation energy of 10 keV, the contact angles decreased with an increase in the implantation dose. The decrease in the angles of the $C^-$-implanted SCPS surfaces at the implanted energies of 5, 15 – 20 keV was similar to those at the energy of 10 keV. Then, the lowering of angles of the $C^-$-implanted SR surfaces at the energies of 5, 15 – 20 keV are expected to be similar to that of at the energy of 10 keV. The contact angles of the $C^-$-implanted SR surfaces the energies of 5, 15 – 20 keV are expected to decrease with an increase in the implantation dose and in the dipping time. Comparison of the lowering of the contact angle on the surfaces of SCPS and SR, the contact angle of the unimplanted SR was higher than that of the unimplanted SCPS. After implantation, the contact angles of both surface decreased with an increase in implantation dose. The lowering of the angles from the water drop method on the $C^-$-implanted surfaces of SCPS and SR at the implantation doses of $1\times10^{15}$ – $1\times10^{16}$ ions/cm$^2$ to the lowest angle and saturation was almost no different. After dipping in DIW, the lowering of the contact angles on the $C^-$-implanted SR surfaces at the implantation doses of $1\times10^{14}$ – $1\times10^{16}$ ions/cm$^2$ showed more decrease. Based on the consideration of the ion-projected range and the energy transfer as described in Chapter 2, the ion-projected range of the $C^-$-implanted SR is deeper than that of the $C^-$-implanted SCPS at the same implantation energy. So, the energy loss at the surface of the $C^-$-implanted SR should be smaller. Then, the ion-induced defects inside the $C^-$-implanted SR surface are more than that of the $C^-$-implanted SCPS, but the new atomic bonding at the surface of the $C^-$-implanted SR should be smaller. The more lowering of the contact angles in the water for the $C^-$-implanted SR might be considered to be from the effect of

the stabilization inside the solid of SR.

As a result, the considerably suitable dose conditions with hydrophilic property for high possible cell adhesion on the $C^-$-implanted SR should, therefore, be in the range of $1\times10^{15}$ – $1\times10^{16}$ ions/cm$^2$.

## 3.4 Summary

The carbon negative-ion implantation into polymeric surfaces of spin-coated polystyrene (SCPS) and silicone rubber (SR) could modify the surface wettability by introducing new oxygen function groups of hydroxyl and carbonyl on the ion-induced defect. This formation of new bonds on the surface could be confirmed by the evaluation of the surface atomic bond state with XPS analysis. Based on the AFM, the implantations into the surfaces of SCPS and the commercial non-treated polystyrene dish at 10 keV and $3\times10^{15}$ ions/cm$^2$ made some surface roughness on the surfaces of polystyrenes within the acceptable value that does not interfere to the adsorption of extracellular matrix (ECM) and cell culture. Whereas the implantation into the surface of SR at the same condition made the surface be smoother that might lead to the improvement of the adsorption of ECM and cell culture. The adsorption of ECM on the surface is related to the surface wettability properties, which can be simply estimated by the contact angle measurement. The changes in contact angle of the $C^-$-implanted surfaces of SCPS and SR at doses of $1\times10^{13}$ – $3\times10^{16}$ ions/cm$^2$ and energies of 5 – 20 keV were measured by the water drop method after implantation with 2 h and by the air bubble method after dipping in DIW for 0, 2, 24, 36 and 48 h. The lowering of contact angle was as a function of the ion dose for all implantation energies of 5 – 20 keV. There was little implantation effect of energy on the lowering of contact angle in case of the $C^-$-implanted SCPS at $3\times10^{15}$ ions/cm$^2$. The suitable implantation dose for the saturation of the contact angle was in the range of $1\times10^{15}$ – $3\times10^{16}$ ions/cm$^2$. The lowest angle of the $C^-$-implanted SCPS at 5 – 20 keV took place at the dose of around $2\times10^{15}$ – $3\times10^{15}$ ions/cm$^2$, excepting at 15 keV. The lowest angle of the $C^-$-implanted SR took place at the dose of $1\times10^{16}$ ions/cm$^2$. The considerably suitable implantation conditions with hydrophilic property for high possible cell-adhesion properties on the $C^-$-implanted surfaces of SCPS and SR should, therefore, be in the range of $1\times10^{15}$ – $1\times10^{16}$ ions/cm$^2$.

## References

[1] D. Briggs and M.P. Seah: Chapter 9 of **Practical Surface Analysis (the second edition), volume 1: Auger and X-ray Photoelectron Spectroscopy**, 2nd Ed., Chichester, UK: John Wiley & Sons, 1990, p. 444.

[2] P. 448 in Ref. [1]

[3] G. Beamson and D. Briggs, Appendix I – Primary C 1s Chemical Shifts (eV) Relative to Saturated Hydrocarbon (C 1s = 285.00 eV) – in **High Resolution XPS of Organic Polymers – The SCINTA ESCA 300 Database**, Chicehster, UK: John Wiley & Sons, 1992.

[4] **CRC Handbook of Chemistry and Physic**, 71st Ed., D.R. Lide, ed. Boca Raton, FL: CRC press Ins., 1990-1991.

[5] F. Rodriguez, C. Cohen, C.K. Ober and L.A. Archer, **Principle of Polymer Systems**, 5th Ed., New York: Taylor and Francis, 2003.

[6] P.D. Townsend, J.C. Kelly, N.E.W. Hartley, **Ion Implantation, Sputtering and their Applications**, London, Great Britain: Academic Press, 1976.

[7] H. Ryssel and I. Ruge, **Ion Implantaion**, translation eds., Great Britain: John Wiley & Sons, 1986.

[8] W.S. Klug and M. R. Cummings**, Concepts of Genetics,** 5th Ed**.**, Upper Saddle River, New Jersey: Prentice Hall, 1997.

[9] M.K. Magnusson, D.F. Mosher, "Fibronectin: Structure, Assembly, and Cardiovascular Implications", Arterioscler. Thromb.Vasc. Biol. 1998, vol. 18, issue 9, pp.1363-1370, 1998.

[10] W.M. Becker, L.J. Kleinsmith, J. Hardin, **The World of the Cell**, 5th Ed., Benjamin Cummings, 2002.

[11] **Protein Chemistry for Conservators,** CL. Rose and D.W. von Endt, edts., Washington D.C.: American Institute for Conservation of Historic and Artistic Works, 1984.

[12] **Chapter 9 of Fundamental & Application of Polymer Surfaces volume 2**, Y. Ikada ed., Japan, Kagaku Dozin co., ltd. 1998, p. 186.

[13] F.M. Fowkes; I. E. C., vol. 56, pp. 40-52, 1964.

[14] L.A. Girifalco and R.J. Good; J. Phys. Chem., vol. 61, pp. 904-909, 1957.

[15] H.M.L. Tan, H. Fukuda, T. Akagi, and T. Ichiki, "Surface Modification of Poly(dimethylsiloxane) for Coating Biological Cells' Adhesion using a Scanning radical microjet", Thin Solid Films, vol. 515, pp. 5172-5178, 2007.

[16] N. Patrito, C. McCague, P.R. Norton, and N.O. Peterson, "Spatially Controlled Cell Adhesion via Micropatterned Surface Modification of Poly(dimethylsiloxane)", Langmuir, vol. 23, pp. 715-719, 2007.

# Chapter 4

# Evaluation of Protein Adsorption by XPS Analysis

In the practice of cell adhesion on the polymeric surface, one of the required important parameters for the adhesive strength between cell membrane and the surface is adhesive proteins found in the extracellular matrix (ECM). As introduced in Chapter 1, all cells do not directly adhere to the surface. They adhere to the ECM adsorbed on the surface through their specific protein receptor at the cell membrane [1]. Therefore, the measurement of ECM adsorption properties on the modified surface can evaluate the cell-adhesion property before cell culture, and it is useful to form the cell adhesion patterning. In nature, the ECM for binding to the cell membrane mainly consists of collagen, proteoglycans and glycoproteins, such as fibronectin and laminin. For study of the neuron adhesion patterning, the adsorption properties of the interesting ECM, such as type I collagen (Co-I), fibronectin (FN) and laminin (LN), on the $C^-$-implanted polymeric surfaces of spin-coated polystyrene (SCPS) and silicone rubber (SR) were evaluated by detecting of the nitrogen atoms from proteins with the XPS analysis. In addition, polylysine, the synthesized polymer, is a useful base material for the central nerve cell adhesion [2]. Therefore, the adsorption of poly-D-lysine (PDL) on the $C^-$-implanted surfaces was also investigated. At first, in this chapter, the mechanism of protein adsorption on the $C^-$-implanted surfaces at the implantation condition for obtaining the best on the results of lowering of the contact angle in Chapter 3 are described. The procedure of the experiment and the studied proteins such as type I collagen, fibronectin and laminin are described. The brief in the functions, source and structures of these adhesive proteins and PDL are then explained. Finally, the results of their adsorption properties on the $C^-$-implanted polymeric surfaces of SCPS and SR are described.

## 4.1 Mechanism of Protein Adsorption on $C^-$-Implanted Polymeric Surface

Generally, a protein is composed of several hundreds to several thousands of the amino acid monomeric units covalently linked together in a specific sequence through peptide bonds [3]. These monomeric units are formed by the common amino acids of all carboxylic organic acids. The depiction of common amino acid can be shown in Fig. 4.1. The main chain of the common amino acid contains a carbon atom and terminal functional groups of a primary amine and of a carboxyl. The side chain is liked to this carbon atom and it can be any a chemical atom or atomic

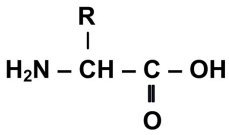


Fig. 4.1 Structure of the common amino acid.

group or acid group such as hydrogen, an alkyl chain and aromatic chain and the linked part is generally represented with the letter R. This part is defined the types of amino acids. Then, more than 20 individual amino acids are found in nature [3]. There are both of hydrophobic and hydrophilic sites in each amino acid. The terminal groups of a primary amine and a carboxyl show the hydrophilic sites of the positive charge and negative charge, respectively. Through such terminal groups the amino acids in protein can adsorb on the polymeric surface, and link together to form the protein and the extracellular matrix.

The protein adsorption on the polymeric surface is caused by the hydrogen bonding between the amino acids of protein and the hydrophilic sites of the polymeric surface. In case of the $C^-$-implanted polymeric surface, after implantation the hydrophilic groups of hydroxyl and carbonyl were introduced on the implanted surface as described in Chapter 3, and such hydrophilic sites are as shown in Fig. 4.2 (a). Generally, the hydrogen bonds in protein chain and that on the hydrophilic sites of the surface are always broken by the chemical or physical stress, and the new bonds between the weak positive charges of the –NH– in amino acid of protein and the weak negative charges of the C=O and the O-H on the surface then are reformed. The reformation of hydrogen bond can produce the strong cohesive forces between molecules that make the suitable interaction between the molecules. Such binding of hydrogen bond makes amino acids in protein adsorb on the hydrophilic surface (Fig. 4.2 (b).). After that, the amino acids in each protein also bind themselves with the same mechanism of breaking-reforming of hydrogen bonding between protein chains. Then, the extracellular matrix of protein was formed as shown in Fig. 4.2 (c). Since the reformation of the new hydrogen bond always occurred, amount of protein adsorption and the strong cohesive forces increase with an increase in the adsorption time.

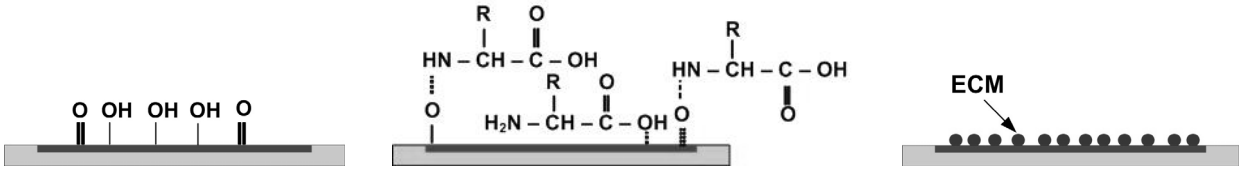


(a) Hydrophilic bonding (b) Amino acid binding to surface (c) ECM adsorption

Fig. 4.2 Mechanism of ECM adsorption on the $C^-$-implanted polymeric surface: (a) hydrophilic bonding after implantation; (b) binding of amino acid in protein to this bond; and (c) adsorption of ECM on surface.

Comparing to the hydrophobic surfaces of the SCPS and SR, carbon negative-ion implantation into such polymeric surfaces can therefore enhance the binding of the amino acids to the modified hydrophilic surfaces that bring about the improvement of ECM adsorption. In case of cell adhesion, since cells have a specific receptor to anchor the certain adhesive protein as introduced in Chapter 1, cells adhere to the specific adhesive protein adsorbed on the polymeric surface modified by the implantation.

## 4.2 Preparation and Evaluation Process of Protein-Coated Modified Surfaces

The protein adsorption properties on the $C^-$-implanted surfaces of SCPS and SR (Wacom Electric co., ltd) were evaluated by XPS analysis. Carbon negative-ion beam was implanted into the polymeric surfaces of SCPS and SR as a half moon shape. The operation conditions of residual gas pressure and ion-current density were those described in Chapter 2. In the adsorption procedure of protein and of PDL, the modified surfaces were dipped in a protein solution for 2 h, or in a PDL solution for 1 h. The protein concentration in the solution is one of the considered important parameters. Therefore, the suitable protein concentration was investigated at the constant implantation condition of 10 keV and $3\times10^{15}$ ions/cm$^2$, before studying the dependence of protein adsorption protein upon the ion implantation conditions. As for study of the suitable concentration, the adsorption properties of the adhesive proteins such as type I collagen, fibronectin and laminin, and that of poly-D-lysine were investigated. After implantation within 2 h or so-called as-implanted, the samples were dip-coated in these proteins at the various concentrations of 0.5 – 50 μg/ml for 2 h and were dried at 37°C for 30 min before surface analysis. The conditions of the protein coating and others are shown in Table 4.1. As for study of the suitable implantation dose, the implantation was set at 10 keV with the various doses of $1\times10^{14}$ – $1\times10^{16}$ ions/cm$^2$. After implantation within 2 h, the samples were dip-coated in these proteins at the obtained suitable concentration at the same coating process of each protein for surface analysis.

The surface of the protein-coated samples were analyzed by the X-ray photoelectron spectroscopy (XPS; AXIS-165, Shimadzu/Kratos, Kyoto). The XPS survey spectra for surface elements of N, C and O were evaluated with the X-ray source of monochromatic Al K$\alpha$ (1486.6 eV) at a relatively weak intensity for avoiding the state of surface modification by irradiation. Since the polymeric materials are an insulator, charge neutralizer was used to set the C1s peak from C-C(H) bond to 285.0 eV. The surfaces at the interface area between the unimplanted and implanted regions were scanned point by point from 1 to 10 for 10 pairs from the unimplanted region to the implanted region for evaluation of the XPS survey spectra as shown in Fig. 4.3.

Table 4.1 Experiment condition for study of the protein adsorption property

| ECM | Conditions | | | | | | Ion implantation dose (ions/cm$^2$) |
|---|---|---|---|---|---|---|---|
| | Protein coating | | | | | | |
| | Source | | Concentration in solution (μg/ml) | Dipping time (h) | Rinsing with DIW (time) | Drying time at 37°C (min) | |
| | Product code | Company | | | | | |
| Co-I | 9003 | Böttger GmbH, Berlin, Germany | 0.5 – 50 (in DIW or in 0.1M acetic acid) | 2 | 2 | 30 | $1\times10^{14} – 3\times10^{15}$ |
| FN | F1141 | Sigma-Aldrich, Inc. | 0.5 – 10 (in PBS) | 2 | 2 | 30 | $1\times10^{14} – 1\times10^{16}$ |
| LN | L2020 | Sigma-Aldrich, Inc. | 0.5 – 50 (in PBS) | 2 | 3 | 30 | $1\times10^{14} – 1\times10^{16}$ |
| PDL | P0899 | Sigma-Aldrich, Inc. | 0.5 – 50 (in DIW and PBS) | 1 | 2 | 30 | $1\times10^{14} – 1\times10^{16}$ |

Note: Co-I = type I collagen, FN = fibronectin, LN = laminin, PDL = poly-D-lysine, PBS = phosphate-buffered saline, DIW = de-ionized water

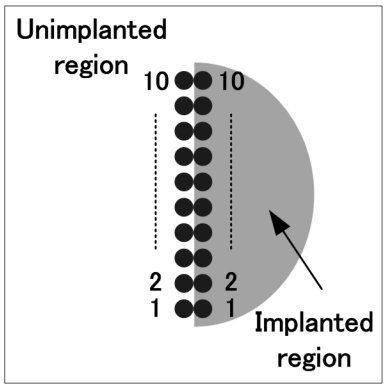


Fig. 4.3 Schematic diagram of the evaluated points on the $C^-$-implanted sample for XPS

As for protein adsorption, for example, the laminin-coated surface of the $C^-$-implanted SCPS (LN/C-SCPS) at 10 keV and $3\times10^{15}$ ions/cm$^2$ at 1 μg/ml is used. The XPS survey spectra of both regions of $C^-$-implanted SCPS at 10 keV and $3\times10^{15}$ ions/cm$^2$ at the center area or point 5 are shown in Fig. 4.4, where (a) is the spectrum on the unimplanted region and (b) is the spectrum on the implanted region after dipped in the protein solution such as laminin at concentration of 1 μg/ml. The XPS survey spectra of the unimplanted and implanted surface after dipping in the protein solution show three element peaks of C 1s, N 1s and O 1s. Before dipping, both of them had no peak of N 1s as shown in Chapter 3. The peak of N 1s after dipping was considered due to the nitrogen atoms in the protein. Based on XPS analysis condition; almost the same dual time at the nearly close adsorption and the selective adsorption ratio between the implanted surfaces of the implanted and unimplanted regions, we can evaluate the

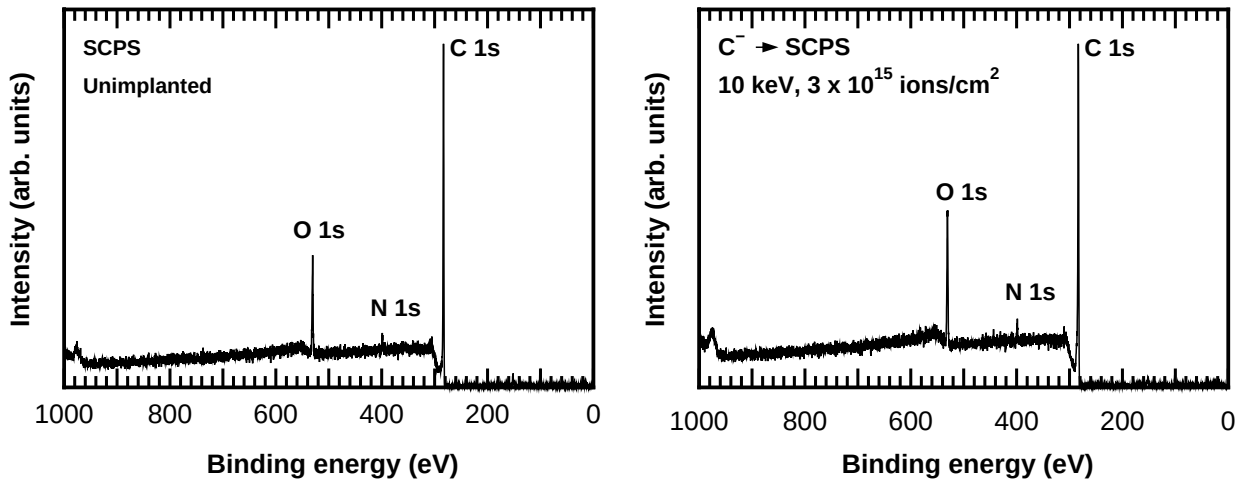


(a) LN/C-SCPS on the unimplanted region (b) LN/C-SCPS on the implanted region

Fig. 4.4 XPS survey spectra of the $C^-$-implanted SCPS after 2-h dipping in the laminin solution with 1 μg/ml: (a) on the unimplanted region and (b) on the implanted region at point 5.

amount of nitrogen atom and unimplanted surfaces. We found that the amount of nitrogen atom adsorption on the implanted region was higher than those on the unimplanted region. The ratio was about 1.35. These might be due to the rich of hydrophilic bonding such as the oxygen functional groups of hydroxyl and carbonyl on the implanted region as described in Chapter 3. The more adsorption of the nitrogen atoms from the amino acids in peptide chain of laminin was considered to be due to the reforming of the hydrogen bond between the hydrophilic sites in protein and those sites on the implanted surface as described in section 4.1.

In case of protein adsorption on the $C^-$-implanted SR, for example, the laminin-coated surface of the $C^-$-implanted SR (LN/C-SR) at 10 keV and $3\times10^{15}$ ions/cm$^2$ at 1 μg/ml is used. The XPS survey spectra of both regions of $C^-$-implanted SR at the center area are shown in Fig. 4.5, where (a) and (b) are the spectrum on the unimplanted and implanted regions, respectively. Three element peaks of C 1s, O 1s, Si 2s, Si 2p and N 1s also appeared on the XPS survey spectra of the implanted and unimplanted regions. Similar to the result of the $C^-$-implanted SCPS before dipping in the protein solution, there was no peak of N 1s on the XPS survey spectra of both unimplanted and implanted surfaces as shown in Chapter 3. These N 1s was considered due to the nitrogen atoms in laminin. From the evaluation, the amount of the amount of nitrogen atom adsorption on the implanted region was also higher than those on the unimplanted region. The ratio was about 1.64. The amount of nitrogen atom adsorption on the implanted surface of the $C^-$-implanted SR was smaller than that of the $C^-$-implanted SCPS, but the ratio of the $C^-$-implanted SR was higher. The former was considered due to more formation of the hydrophilic sites on the implanted surface of the $C^-$-implanted SCPS since the weaker

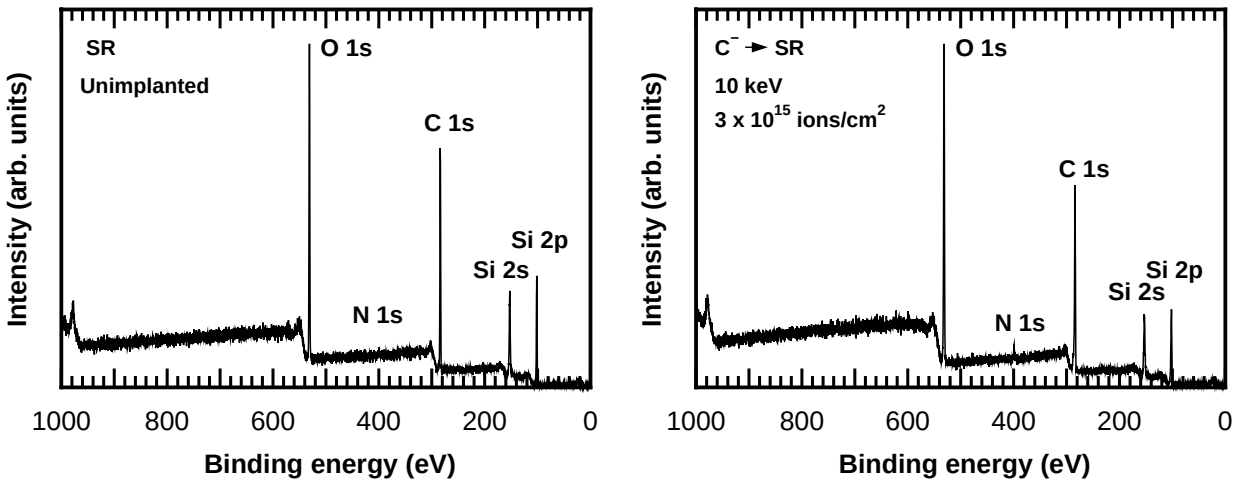


(a) LN/C-SR on the unimplanted region (b) LN/C-SR on the implanted region

Fig. 4.5 XPS survey spectra of the $C^-$-implanted SR after 2-h dipping in the laminin solution with 1 μg/ml: (a) on the unimplanted region and (b) on the implanted region at point 5.

bond strength in the main chain of SCPS as described in Chapter 3. The latter was considered due to high hydrophobic property on the unimplanted surface of the $C^-$-implanted SR that almost the contact angle was about 100° as shown in Chapter 3.

From these examples, the carbon negative-ion implantation into the polymer surfaces such as SCPS and SR could improve the protein adsorption property of the surfaces. Therefore, the assumption of the patterned cell adhesion with the stronger adhesive forces on the protein adsorbed on the $C^-$-implanted polymeric surface could be possible. Since the strength of these co-adhesive forces related to the number of the reformation of hydrogen bonding on the surface, the adsorption time, the types and concentration of the proteins and the physical surface property should be concerned. As for evaluation of the protein adsorption properties, the amount of nitrogen atoms was calculated from the N peak area of the XPS N 1s spectra on the implanted and unimplanted regions on the $C^-$-implanted surfaces of SCPS and SR. The adsorption ratio between amount of nitrogen atoms on the implanted and unimplanted regions from point-by-point scanning were calculated. The high adsorption ratio will indicate to the good selective adsorption properties of the protein on the implanted region, leading to the selective adhesion properties. The studied proteins and their adsorption properties on the $C^-$-implanted surfaces of SCPS and SR will be described in sections 4.3 and 4.4, respectively.

## 4.3 Types of Proteins and PDL for Experiment

### 4.3.1 Type I Collagen

Collagens are the most abundant protein in the human body, according for about 25% of the total amount of protein. They are a fibrous protein that is a structure support for most tissue in the body as the extracellular matrix. Particularly, they are abundant in connective tissue. The functions of collagens in connective tissue are to sheath muscles and attach them to bone through tendons or to attach skeletal elements together through cartilage. Collagens also form the bulk of the proteins found in hides and skin, and they have a vital role in many processes such as wound healing and glue. Cells in all the other tissue are also surrounded by finer collagen structures though the extracellular matrix. Therefore, collagens have a vital role also in cell proliferation, migration and differentiation. As a nature function, collagen has been also used in technical and medical applications as a model physiological surface for cell culture, implant biocompatibility and directed cell growth. The structure of collagen fiber formation is shown in Fig. 4.6 [4]. The primary feature of a typical collagen molecule is its long, stiff, triple-stranded helical structure, in which always three collagen polypeptide chains, called $\alpha$ chains, are wound around one another in a rope-like superhelix [1, 4]. Collagens are extremely rich in proline and glycine, both

of which are important in the formation of the triple-stranded helix. The ring structure of proline stabilizes the helical conformation in each $\alpha$ chain, while glycine is regularly spaced at every third residue throughout the central region of the $\alpha$ chain. While the smallest amino acid size for glycine allows the three helical $\alpha$ chains to pack tightly together to form the final collagen superhelix [1]. This superhelix sometimes called tropocollagen. Molecular weight of each tropocollagen is 300 kDa and its diameter is about 1.5 nm. Each terminal of tropocollagen is composed of the amine and carboxyl groups, so-called N-terminal and C-terminal, and here are no presence of the helical structure. The tropocollagen with these terminals is called procollagen.

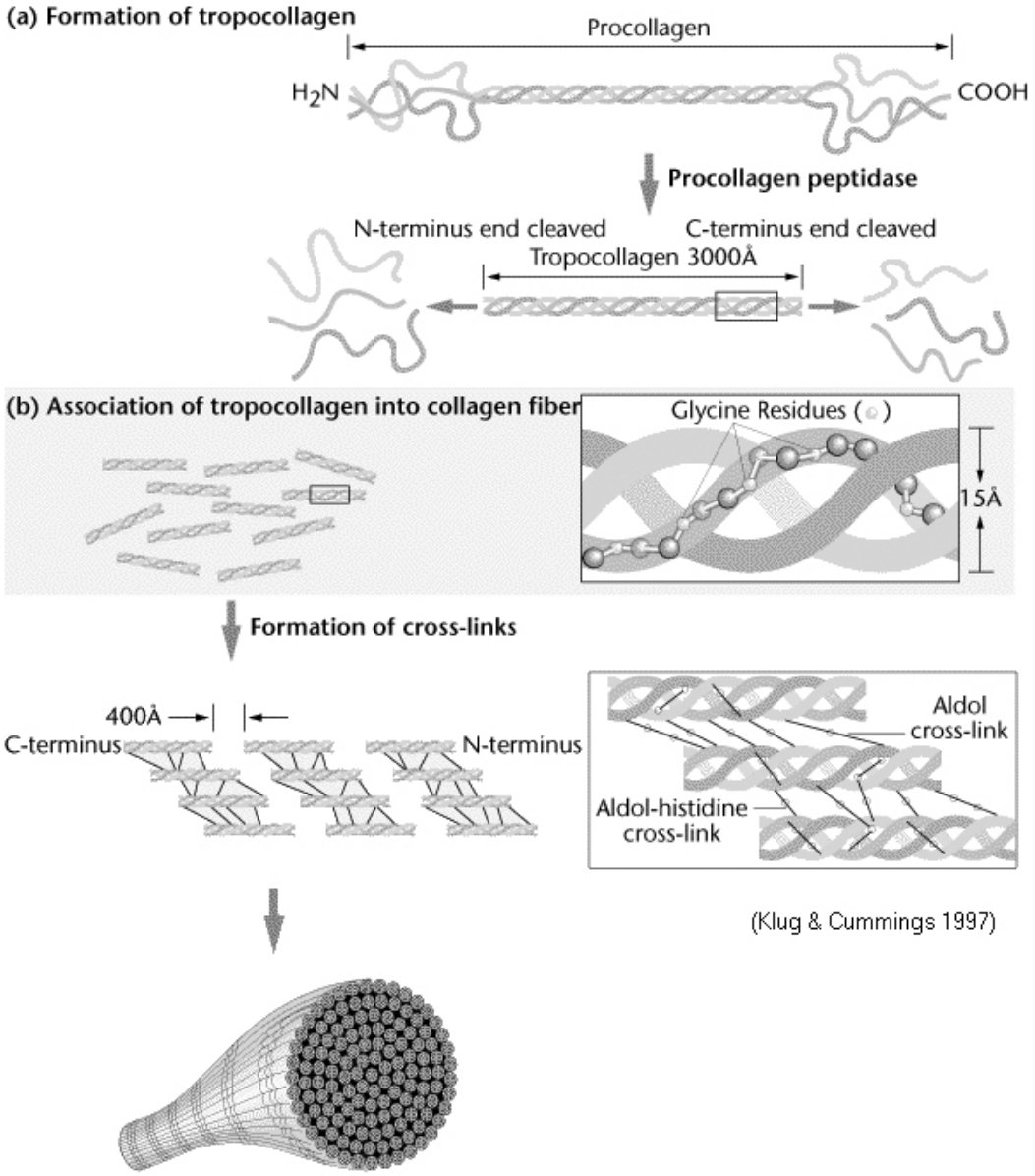


Fig. 4.6 Structure of collagen [4].

Each one procollagen is over 1000 amino acids long [1], and each triple-helical collagen molecule is 300 nm long [4]. The triple-stranded nanometer-sized protofibril can bind together from the cross-link between the N-terminal and C-terminal to form the collagen fibril [1, 4]. Abundant of collagen fibrils perform collagen fiber.

In natural, around 20 types of collagen molecules have been found [1]. The main types of collagen found in connective tissues are types I, II, III, V, and XI. These are the fibrillar collagens, or fibril-forming collagens, with the rope-like structure. The most common of over 85% collagen is type I that is found in skin, tendon, and bone. In type I collagen (Co-I), not only repeating of glycine and proline, specific amino acid of hydroxyproline is also repeated in the chain [1]. Deformation of collagen is induced by the temperature. When collagen is heated in water, collagen structure is lost by unwinding of triple-stranded helical structure and separating of three chains. Then, this denatured mass of tangled chain cools down, it soaks up all of the surrounding water. These chains try to reform the triple-stranded helical structure, but it can line up only in sections. The unaligned parts of the chain then align with parts of other chains until a network of the chain exits. This network held together by the hydrogen-bonded and short triple-stranded helical link is gelatin. Since collagens contain over 85% of type I collagen, the gelatin almost comes from type I collagen. Use of gelatin for study of the collagen adsorption property on the surfaces was also reported [5].

### 4.3.2 Fibronectin

Fibronectin (FN) is one of important protein for the process of cell adhesion since it will bind to the receptor proteins of integrins on cells that span the cell membrane. Moreover, it can bind to other macromolecule such as collagen, fibrin and heparin. Fibronectin is a large multidomain glycoprotein containing about 5% carbohydrate found in connective tissue, on cell surfaces, and in plasma and other body fluids. Fibronectin is composed of two peptide chains of approximately 275 kDa molecular weight which are linked through two interchain disulfide bonds at the COOH-terminal end of the molecule. Then, total molecular weight is about 550 kDa with 50 nm in length. The structure of fibronectin is characterized by three different types of repeating homologous sequence units as shown in Fig. 4.7 [6]. Three modules are type I, type II and type III. For stability and function of fibronectin, two disulfide bonds are found in each module of type I and II, while none is found in type III module.

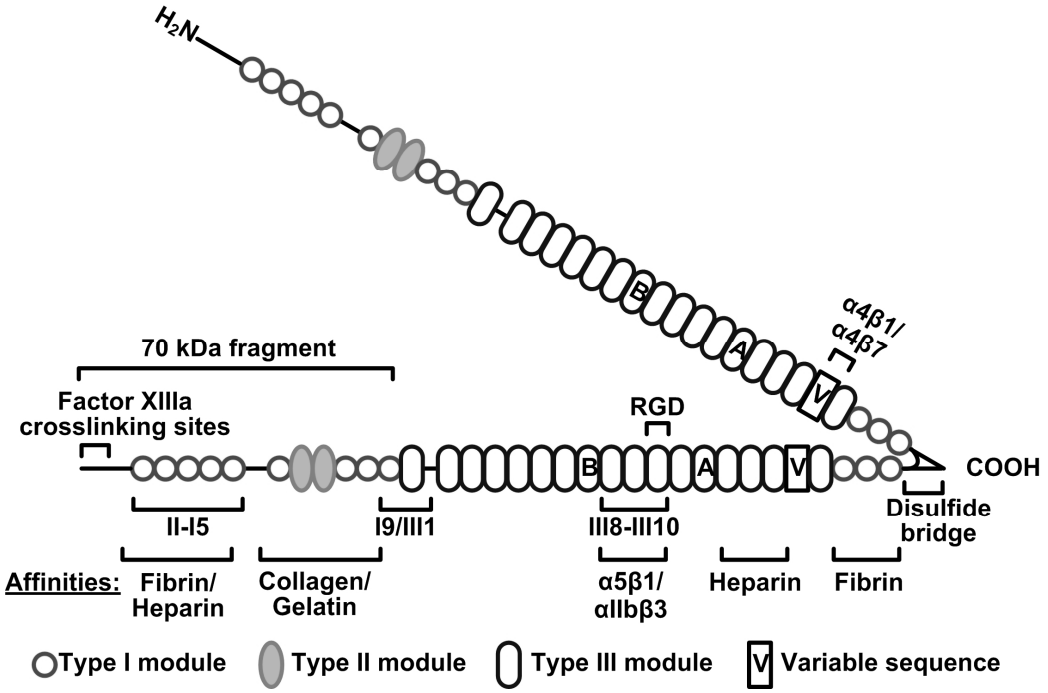


Fig. 4.7 Structure of fibronectin [6].

### 4.3.3 Laminin

Laminin (LN) is a basement membrane extracellular matrix macromolecule that provides an attachment substrate for both adhesion and migration in a wide variety of cell types, including epithelial cells, fibroblasts, neurons and leukocytes. Generally, laminin is composed of three different huge polypeptide chains so-called α, β and γ whose molecular weights are 400, 215 and 200 kDa, respectively [7]. The longest chain is the α chain, made up of 3,712 amino acids. The cohesion between these chains is the result of many inter- and intra-chain disulfide bonds. Together, they cause the molecule to look like a crucifix, so-called sometimes triple-stranded helical or α-helical coiled coil structure. The structure at this point is similar to the primary feather in the collagen structure. Laminin can be characterized to many types that composed of the different chains of α, β and γ. Each pair of polypeptide chains can bind to different laminin. The structure with the possibility of binding of laminin is shown in Fig. 4.8. Not only binding to itself, but also laminin can bind to the other proteins such as collagen binding, cell adhesion, heparin binding, and neurite outgrowth.

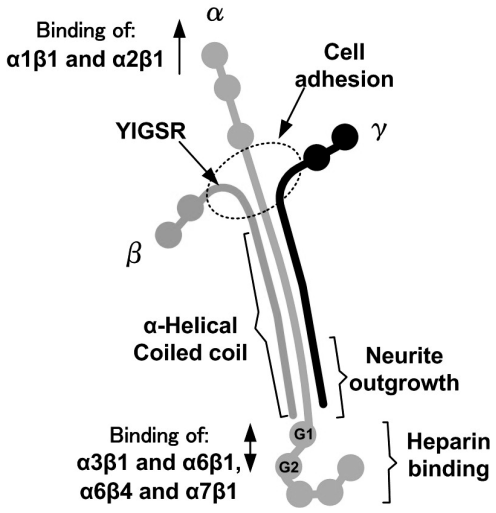


Fig. 4.8 Structure of laminin.

### 4.3.4 Poly-D-lysine (PDL)

Poly-lysine is a polycation which binds to DNA, red cell membrane and any negatively charged protein. Since it can enhance electrostatic interaction between negatively-charged ions of the cell membrane and positively-charged surface ions of attachment factors, which refer to the ECM, on the culture surface, it is typically used as a coating substrate for culture dishes to increase the number of positively charged sites available for cell binding. It is also used for the primary culture of the brain neuronal cells [2]. Poly-lysine has two type-forms, D- and L- forms. Both of their forms can be used as a coating substrate since poly-lysine is a nonspecific attachment factor for cells. However, certain cells can digest poly-lysine. In this case, poly-D-lysine should be used as the attachment factor so that the cells are not disrupted by excessive uptake of L-lysine. Three ranges of molecular weight for commercial synthesized poly-lysine are the lower molecular weight of 30 – 70 kDa, the mid-range molecular weight of 70 – 150 kDa and the high molecular weight more than 300 kDa. The suitable molecular weight for the convenient coating substrate for cell culture is the mid-range one since the low viscous in solution with high attachment sites per molecule. The molecular form of PDL consisted of carbon, oxygen, nitrogen and hydrogen atom as shown in Fig. 4.9. There is approximately one HBr per lysine residue for allowance of PDL to be crystalline solid and soluble in water. This HBr can be removed from the structure by dissolving in a neutral buffer such as PBS and one can dialyze to remove the salts. There may be a small amount of the $\beta$ structure because the HBr interferes with hydrogen bonding between the amino and carboxyl groups, or between the amino group and other N or O containing moieties.

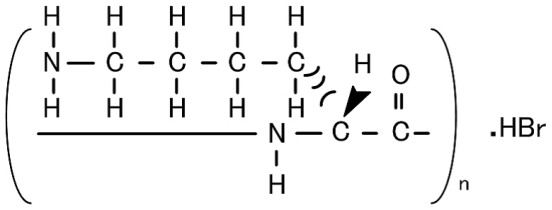

Fig. 4.9 Molecular form of poly-D-lysine

## 4.4 Results of Adsorption Property

After drying the coated surfaces, the adsorption properties of the proteins and PDL on the polymeric surfaces were evaluated by detecting amount of nitrogen atom with using XPS analysis. Based on calculation of the N peak areas on the XPS N 1s spectra of the implanted and unimplanted regions, the amount of nitrogen atoms adsorbed on the surfaces and the adsorption ratio of the nitrogen atoms between the implanted and unimplanted regions could be evaluated.

In case of the adsorption property of type I collagen, at first the concentration dependences on the Co-I adsorption properties for the $C^-$-implanted surfaces of SCPS and SR at the certain implantation conditions of 10 keV and $3\times10^{15}$ ions/cm$^2$ were studied. The amount of nitrogen atoms adsorbed on the implanted region of the $C^-$-implanted SCPS at 10 keV and $3\times10^{15}$ ions/cm$^2$ was in the range of 2400 – 12000, whereas that of the $C^-$-implanted SR at 10 keV and $3\times10^{15}$ ions/cm$^2$ was in the range of 1500 – 6300 (see Table 4.2). Almost twice was different. This corresponded to the more obtained hydrophilic bond on the $C^-$-implanted SCPS at the same implantation condition. Comparing to the Si-O bonds in the main chain of SR [8], the C-C(H) bonds in the main chain of SCPS have a weaker bond strength, and they were easily to be broken by the ion implantation. Therefore, the number of the formation of the oxygen functional groups such as the carbonyl and hydroxyl on the $C^-$-implanted SCPS was higher than that on the $C^-$-implanted SR. This led to more hydrophilic property on the $C^-$-implanted SCPS. The adsorption properties on the $C^-$-implanted SCPS were then better than those of the $C^-$-implanted SR.

From the amount of nitrogen atom adsorptions, the adsorption ratios of the amount of nitrogen atom between the implanted and unimplanted regions could be calculated and are shown Fig. 4.10 (a), where the closed and open circles are corresponding to the Co-I/C-SCPS and Co-I/C-SR, respectively. The adsorption ratio on the $C^-$-implanted SCPS at 10 keV and $3\times10^{15}$ ions/cm$^2$ was almost in the range of 1.1 – 1.25. That on the $C^-$-implanted SR at this implantation condition was almost in the range of 1.75 – 3.3. The adsorption ratio of type I collagen on the $C^-$-implanted SR was higher than that on the $C^-$-implanted SCPS, and almost 2

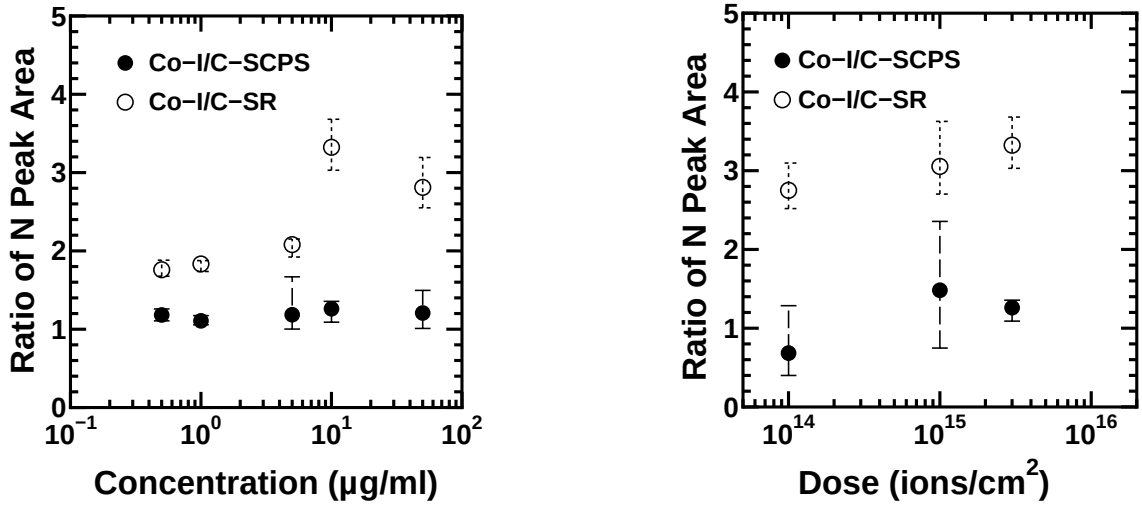


(a) Ratio vs. Co-I concentration (b) Ratio vs. ion dose

Fig. 4.10 Ratio of N peak areas between the implanted and unimplanted regions for the $C^-$-implanted surfaces of SCPS and SR after 2-h dipping in Co-I solution as a function of: (a) Co-I concentration at implantation condition of 10 keV and $3\times10^{15}$ ions/cm$^2$ and (b) ion dose at Co-I concentration of 10 μg/ml.

– 3 times were different. The high adsorption ratio of Co-I on the $C^-$-implanted SR was considered due to high hydrophobic property on the unimplanted surface of the $C^-$-implanted SR as described in section 4.2. The high adsorption ratios indicated that the selective adsorption properties of the $C^-$-implanted SR were much better than those of the $C^-$-implanted SCPS, and they led to the obtainable selective adhesion properties of cells on the implanted region. Both adsorption ratio increased with an increase in the concentration of type I collagen and tended to saturate at concentration of 10 μg/ml. Then, the Co-I concentration at 10 μg/ml was used to study the effect of ion dose on the collagen adsorption properties.

Considering to the adsorption properties of type I collagen as a function of ion dose, the amount of nitrogen atoms adsorbed on the implanted regions of the $C^-$-implanted surfaces of SCPS and SR at 10 keV with Co-I concentration of 10 μg/ml increased with an increase in the ion dose. The amount of nitrogen atoms adsorbed on the implanted region of the $C^-$-implanted SCPS was in the range of 5500 – 9900, whereas that of the $C^-$-implanted SR was in the range of 5200 – 6300 with an increase in the ion doses of $1\times10^{14}$ – $3\times10^{15}$ ions/cm$^2$ (see Table 4.3). Almost 1 – 1.67 times were different. The adsorption properties on the implanted regions of both of the $C^-$-implanted surfaces of SCPS and SR were improved with an increase in the ion dose, especially on the $C^-$-implanted SCPS.

As for the selective adsorption properties between the implanted and unimplanted regions, the adsorption ratios of the amount of nitrogen atoms between the implanted and

unimplanted regions as a function of the ion dose are shown in Fig. 4.10 (b), where the closed and open circles are corresponding to the Co-I/C-SCPS and Co-I/C-SR, respectively. The adsorption ratio on the $C^-$-implanted SCPS was almost in the range of 0.7 – 1.5. That on the $C^-$-implanted SR was in the range of 2.75 – 3.3. Almost 3 – 4 times were different. At the ion dose of $1\times10^{14}$ ions/cm$^2$, the adsorption ratio on the $C^-$-implanted SCPS was lower than 1. This might be due to the aggregation of rope-like structure of type I collagen on the unimplanted region. From Fig. 4.10 (b), the high adsorption ratios on the $C^-$-implanted SR proved the high selective adsorption properties leading to the clear selective adhesion properties of cells on the implanted region.

In case of the adsorption properties of the other proteins and PDL, Figs 4.11, 4.12 and 4.13 show the adsorption ratios of the fibronectin, laminin and PDL, respectively. The ratios as a function of coating concentration and as a function of ion dose are shown by Figs. 4.11 (a) – 4.13 (a) and Figs. 4.11 (b) – 4.13 (b), respectively. The closed and open circles of each figure are corresponding to the protein/C-SCPS and protein/C-SR, respectively. The Adsorption properties such as the amount of nitrogen atom and the selective ratio on the $C^-$-implanted surfaces of SCPS and SR at a certain implantation of 10 keV and $3\times10^{15}$ ions/cm$^2$ as a function of coating concentration, and those at the certain coating concentration for each protein and PDL as a function of ion dose can be summarized and are shown in Tables 4.2 and 4.3, respectively.

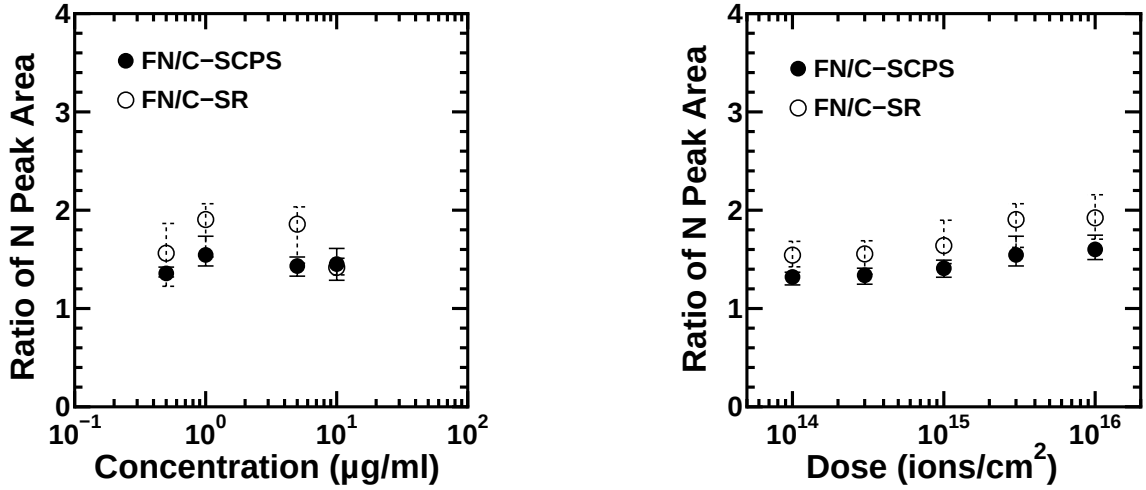


(a) Ratio vs. FN concentration (b) Ratio vs. ion dose

Fig. 4.11 Ratio of N peak areas between the implanted and unimplanted regions for the $C^-$-implanted surfaces of SCPS and SR after 2-h dipping in fibronectin solution as a function of: (a) fibronectin concentrations at implantation condition of 10 keV and $3\times10^{15}$ ions/cm$^2$ and (b) ion dose at fibronectin concentration of 1 μg/ml.

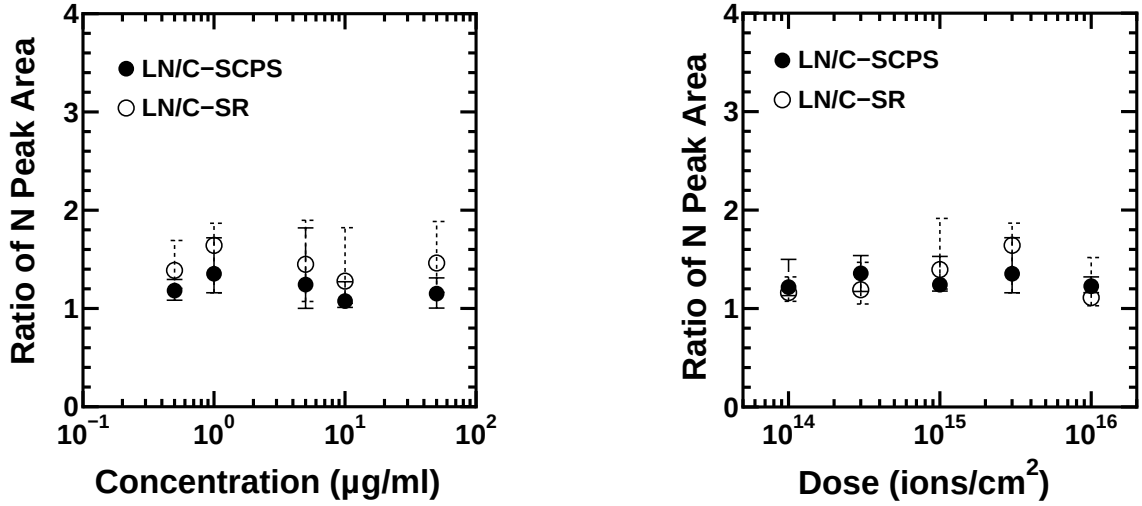


(a) Ratio vs. LN concentration (b) Ratio vs. ion dose

Fig. 4.12 Ratio of N peak areas between the implanted and unimplanted regions for the $C^-$-implanted surfaces of SCPS and SR after 2-h dipping in laminin solution as a function of: (a) laminin concentrations at implantation condition of 10 keV and $3\times10^{15}$ ions/cm$^2$ and (b) ion dose at laminin concentration of 1 μg/ml.

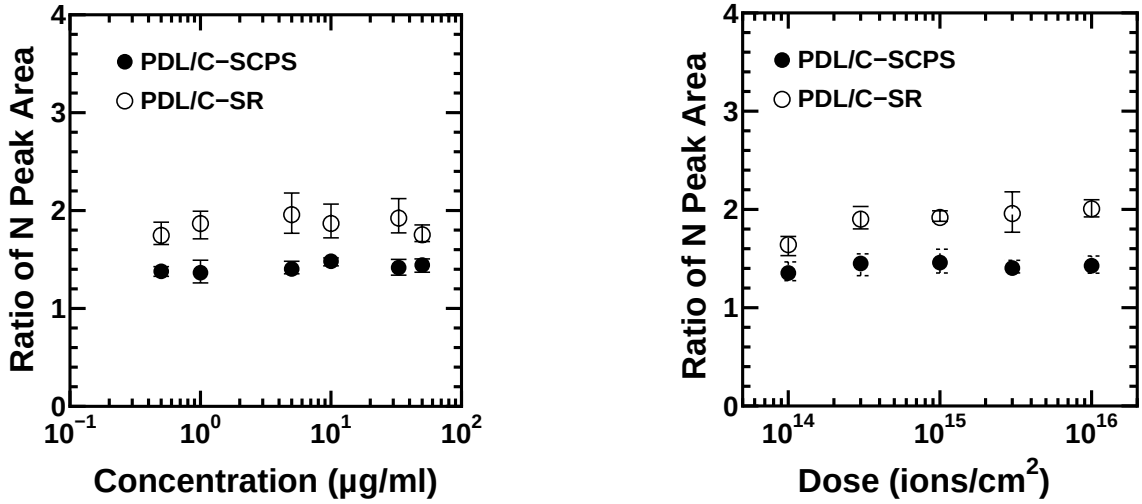


(a) Ratio vs. PDL concentration (b) Ratio vs. ion dose

Fig. 4.13 Ratio of N peak areas between the implanted and unimplanted regions for the $C^-$-implanted surfaces of SCPS and SR after 1-h dipping in PDL solution as a function of: (a) PDL concentrations at implantation condition of 10 keV and $3\times10^{15}$ ions/cm$^2$ and (b) ion dose at laminin concentration of 5 μg/ml.

Table 4.2 Adsorption properties on the $C^-$-implanted surfaces of spin-coated polystyrene (SCPS) and silicone rubber (SR) at 10 keV and $3\times10^{15}$ ions/cm$^2$ as a function of coating concentration.

| ECM | Adsorption property on the $C^-$-implanted polymers at 10 keV and $3\times10^{15}$ ions/cm$^2$ as a function of coating concentration | | | |
|---|---|---|---|---|
| | $C^-$-implanted SCPS | | $C^-$-implanted SR | |
| | Amount of nitrogen atom | Selective adsorption ratio | Amount of nitrogen atom | Selective adsorption ratio |
| Co-I | 2400 – 12000 | 1.1 – 1.25 | 1500 – 6300 | 1.75 – 3.3 |
| FN | 1300 – 1500 | 1.25 – 1.55 | 1100 – 1500 | 1.4 – 1.9 |
| LN | 3800 – 29000 | 1.1 – 1.4 | 1300 – 7900 | 1.26 – 1.6 |
| PDL | 1400 – 3400 | 1.37 – 1.5 | 1000 – 2200 | 1.75 – 1.96 |



Table 4.3 Adsorption properties on the $C^-$-implanted surfaces of SCPS and SR as a function of ion implantation dose.

| ECM | Concentration (μg/ml) | Adsorption property on the $C^-$-implanted polymers at 10 keV as a function of ion implantation dose | | | |
|---|---|---|---|---|---|
| | | $C^-$-implanted SCPS | | $C^-$-implanted SR | |
| | | Amount of nitrogen atom | Selective adsorption ratio | Amount of nitrogen atom | Selective adsorption ratio |
| Co-I | 10 | 5500 – 9900 | 0.7 – 1.5 | 5200 – 6300 | 2.75 – 3.3 |
| FN | 1 | 1200 – 1700 | 1.32 – 1.6 | 1200 – 1500 | 1.55 – 1.92 |
| LN | 1 | 1500 – 3800 | 1.22 – 1.36 | 1500 – 2400 | 1.1 – 1.64 |
| PDL | 5 | 1600 – 3000 | 1.35 – 1.46 | 1600 – 2200 | 1.64 – 2.0 |

Note: Co-I = type-I collagen, FN = fibronectin, LN = laminin, PDL = poly-D-lysine

From Tables 4.2 and 4.3, the nitrogen atom adsorptions for all proteins and PDL could be improved on the implanted regions of $C^-$-implanted surfaces of SCPS and SR, especially on the $C^-$-implanted SCPS. In contrast, the selective adsorption ratios of all proteins and PDL on the $C^-$-implanted SR were higher than those of the $C^-$-implanted SCPS as shown in Figs. 4.11 – 4.13.

As for study of the coating concentration dependences on the adsorption properties at a certain implantation of 10 keV and $3\times10^{15}$ ions/cm$^2$ in Table 4.2, the amounts of the nitrogen atoms on the implanted region of the $C^-$-implanted SCPS for fibronectin, laminin and PDL in the concentration ranges of 0.5 – 50 μg/ml were in the ranges of 1300 – 1500, 3800 – 29000 and 1400 – 3400, respectively. Those of the $C^-$-implanted SR for fibronectin, laminin and PDL were in the ranges of 1100 – 1500, 1300 – 7900 and 1000 – 2200, respectively.

When comparing to the nitrogen adsorption of type I collagen in the concentration range of 0.5 – 50 μg/ml, the amounts of nitrogen atom adsorption for fibronectin and PDL on the implanted regions of SCPS were lower than 4.2 – 6.6 and 1.7 – 3.53 times, respectively. That for laminin on the implanted regions of SCPS was higher than 1.6 – 2.4 times. In case of the $C^-$-implanted SR, the nitrogen atom adsorptions of fibronectin and PDL were also lower than that of type I collagen for 1.15 – 4.2 and 1.5 – 2.86 times, respectively. The adsorption of laminin was also higher than that of type I collagen for 0.9 – 1.25 times. The different nitrogen atom adsorptions for each protein and PDL on the same surface property were due to the differences in the structure and the amount of amino acid in one molecule of each protein and PDL. The capacities for binding to the implanted surfaces of fibronectin and PDL were lower than those of type I collagen. Although the implanted region of the $C^-$-implanted SCPS contained more hydrophilic bonds than that of the $C^-$-implanted SR, the amounts of nitrogen atoms adsorbed on the implanted regions of the surfaces were the same. Thus, there was the limitation for binding between the amino acid in fibronectin and hydrophilic bonds on the implanted region.

When comparing to the adsorptions on different implanted surfaces of SCPS and SR for coating with the same protein and PDL in the concentration ranges of 0.5 – 50 μg/ml, the insignificant difference in the nitrogen atom adsorption was obtained for fibronectin, but more significant differences for laminin and for PDL. The differences were in the ranges of 3 – 3.7 and 1.4 – 1.55 times for laminin and PDL, respectively. These were also considered to be due to the differences in the hydrophilic surface properties, and in the structure and the amount of amino acid in one molecule of each protein and PDL.

Considering to the selective adsorption properties in the concentration range of 0.5 – 50 μg/ml at a certain implantation of 10 keV and $3\times10^{15}$ ions/cm$^2$ in Figs. 4.11 (a) – 4.13 (a) and in Table 4.2, the adsorption ratios of the amount of nitrogen atoms between the implanted and unimplanted regions on the $C^-$-implanted SCPS for fibronectin, laminin and PDL were in the

range of 1.25 – 1.55, 1.1 – 1.4 and 1.37 – 1.5, respectively. Those on the $C^-$-implanted SR for fibronectin, laminin and PDL were in the range of 1.4 – 1.9, 1.26 – 1.6 and 1.75 – 1.96, respectively.

In Figs. 4.11 (a) – 4.13 (a), small differences in the adsorption ratios for fibronectin, laminin and PDL on both of the implanted surfaces were observed in the concentration ranges of 0.5 – 50 μg/ml. The adsorption ratios for fibronectin, laminin and PDL on the $C^-$-implanted SR were higher than those on the $C^-$-implanted SCPS for about 1.2, 1.14 and 1.3 times, respectively. These were also considered to be due to the high hydrophobic property of the unimplanted surface of the $C^-$-implanted SR. Comparing to the adsorption ratio for type I collagen, however, the ratios for fibronectin, laminin and PDL still were lower. The high adsorption ratios (nearly 2) of fibronectin and PDL on the $C^-$-implanted SR indicated to the selective adsorption properties and to the obtainable selective adhesion properties of cells on the implanted region. The adsorption ratios of fibronectin and laminin on both of the $C^-$-implanted surfaces of SCPS and SR increased with an increase in the concentration and tended to saturate at concentrations of 1 – 5 μg/ml. That of PDL on both of the surfaces increased with an increase in the concentration and tended to saturate at concentrations of 5 – 50 μg/m. The maximum ratio of fibronectin and laminin was at 1 μg/ml, but that of PDL was almost at 5 μg/ml. Then, the concentrations of fibronectin and laminin at 1 μg/ml and that of PDL at 5 μg/ml were used to study the effect of ion dose on the adsorption properties.

As for study of the ion implantation dose dependences on the adsorption properties at a certain coating concentration in Table 4.3, both of the nitrogen atom adsorptions on the implanted regions of SCPS and SR at 10 keV for coating with a certain concentration of each protein and PDL increased with an increase in the ion dose. The amounts of nitrogen atom adsorption for fibronectin, laminin and PDL on the implanted region of the $C^-$-implanted SCPS were in the range of 1200 – 1700, 1500 – 3800 and 1600 – 3000, respectively. Those for fibronectin, laminin and PDL on the $C^-$-implanted SR were in the range of 1200 – 1500, 1500 – 2400 and 1600 – 2200, respectively. All of them increased with an increase in the ion doses of $1\times10^{14}$ – $1\times10^{16}$ ions/cm$^2$. There was almost no difference in the adsorption between the implanted surfaces of SCPS and SR at the low implantation dose of $1\times10^{14}$. The adsorption properties on the implanted regions of both of the $C^-$-implanted surfaces of SCPS and SR were improved as a little when increasing in the ion dose. The nitrogen atom adsorptions of fibronectin, laminin and PDL on the implanted region of SCPS increased with an increase in doses from $1\times10^{14}$ – $1\times10^{16}$ ions/cm$^2$ for 1.4, 2.5 and 1.88 times, respectively. In contrast, those on the implanted region of SR also increased as a little for 1.25, 1.6 and 1.38 times, respectively. The smaller increase in the nitrogen atom adsorptions on the $C^-$-implanted SR than that on the $C^-$-implanted SCPS was considered to be due to the lower formation of the hydrophilic

functional groups on the implanted surface of SR since the stronger bond of the Si-O bond in the main chain of SR as described in Chapter 3.

Considering to the selective adsorption properties on the $C^-$-implanted surfaces of SCPS and SR at the doses of $1\times10^{14}$ – $1\times10^{16}$ ions/cm$^{2,}$ the adsorption ratios for fibronectin, laminin and PDL at a certain concentration are shown in Figs. 4.11 (b) – 4.13 (b), respectively and in Table 4.3. The adsorption ratio of the nitrogen atoms for fibronectin, laminin and PDL was almost in the range on the $C^-$-implanted SCPS of 1.32 – 1.6, 1.22 – 1.36 and 1.35 – 1.46, respectively. Those on the $C^-$-implanted SR was in the range of 1.55 – 1.92, 1.1 – 1.64 and 1.64 – 2.0, respectively. Similar to the adsorption ratio for type I collagen, the adsorption ratios of the $C^-$-implanted SR were higher than those of $C^-$-implanted SCPS for about 1.2 times. From Fig. 4.11 (b), the adsorption ratios for fibronectin on both implanted surfaces of SCPS and SR increased and became to saturate with an increase in the ion dose to $3\times10^{15}$ ions/cm$^2$. The adsorption ratios for laminin (Fig. 4.12 (b)) and PDL (Fig. 4.13 (b)) on the $C^-$-implanted SCPS almost saturated at doses of $3\times10^{14}$ ions/cm$^2$, while those on the $C^-$-implanted SR increased with an increase in doses of $1\times10^{14}$ – $3\times10^{15}$ ions/cm$^2$. The maximum adsorption ratio for the proteins and PDL on the $C^-$-implanted SCPS was almost obtained at dose of $3\times10^{14}$ ions/cm$^2$, excepting for fibronectin. But those on the $C^-$-implanted SR were almost obtained at dose of $3\times10^{15}$ ions/cm$^2$. This indicates that the ion implantation into SR required higher dose than that into SCPS for 10 times to obtain the same hydrophilic surface properties.

As a result, the carbon negative-ion implantation into polymeric surfaces of SCPS and SR can improve the adsorptions of protein and PDL. The adsorption properties of proteins such as type I collagen, fibronectin and laminin and those of PDL on the implanted regions could be improved, especially on the implanted surface of SCPS to which has more formation of the hydrophilic groups. The adsorption properties on the implanted regions of the SCPS and SR increased as a function of ion dose, and they increased with an increase in the ion dose from $1\times10^{14}$ to $1\times10^{16}$ ions/cm$^2$. However, the selective adsorption ratios between the implanted and unimplanted regions of the $C^-$-implanted surfaces of SCPS and SR were not high. The maximum ratios for all proteins and PDL on the $C^-$-implanted SCPS were almost lower than 1.6. Those on the $C^-$-implanted SR were lower than 2, excepting to the adsorption ratio for type I collagen that ratio could reach to 3.3.

## 4.5 Discussion and Summary

We evaluated the adsorption properties of some adhesive proteins of the extracellular matrix (ECM) by detecting the amount of nitrogen atoms on the modified surface with using XPS analysis to estimate and to predict the selective cell-adhesion properties. The important

adhesive proteins of type I collagen, fibronectin (FN) and laminin (LN), and the polycation polymer of poly-D-lysine (PDL) were selected to study their adsorption properties on the $C^-$-implanted surfaces of SCPS and SR. The proteins prefer to be adsorbed or to bind with the hydrophilic surface. The capacity of binding to the surface of the adhesive protein depends on the structure, the molecular weight and the concentration of each protein and on the physical surface properties of the substrate. The suitable concentrations of the coating concentration and ion implantation dose on the adsorption properties for selective cell-adhesion properties. Resulting from all observations, the adsorption properties of all proteins and PDL on the implanted region of the $C^-$-implanted SCPS and SR were improved by the implantation, especially of the $C^-$-implanted SCPS. Therefore, the cell-adhesion properties of the $C^-$-implanted SCPS should be better than those of the $C^-$-implanted SR at the same implantation. In this work, a clear difference between the unimplanted and implanted regions was obtained, but it was not so high. Almost the selective adsorption ratios of each protein were 1.25 – 1.6 for the coating surface of the $C^-$-implanted SCPS and were 1.6 – 3.3 for the coating surface of the $C^-$-implanted SR. The selective cell-adhesion properties on the $C^-$-implanted SR should be better than those of $C^-$-implanted SCPS. When considering to the low value of the adsorption ratios from the experiment, there is almost no difference for the selective cell-adhesion property.

There are two different important concerned factors between the experiment and the real cell culture. Those are the real contact angle and the real protein concentration in the cell culture. As for the contact angle, the dipping time for coating the proteins and PDL in the experiment was almost 1 - 2 h, but that in the real cell culture is almost more than 48 h. After the implantation, the contact angle in the water gradually decreased with an increase in the dipping time and it became saturate after dipping for 48 h as shown in Chapter 3. Although the lowering of the contact angle at 2 h dipping was enough to use for the observation in the experiment, the contact angle in the real cell culture are lower than that in the experiment for 10°. Then, the more clearly selective adsorption ratio should be obtained. As for the protein concentration, the adhesive proteins in real cell culture are obtained from the serum in the culture medium. Their concentrations are very low when comparing to the concentrations used in the experiment. At this very low concentration of the adhesive protein in the serum, we can not detect the small amount of nitrogen atom adsorption by using the XPS analysis technique. The real adsorption ratios of the adhesive protein in serum are expected to be higher than the results from the experiment. In addition, in real cell culture, the culture surface is disturbed by the replacement of the culture medium. Since the adsorption strength of the protein depends on the hydrophilic sites of the oxygen functional groups on the polymeric surface, the adsorbed protein on the unimplanted surface may detach with adhered cell. Therefore, the clear pattern of cell adhesion on the implanted region should be obtained.

## References


[1] B. Alberts, A. Johnson, J. Lewis, M. Raff, K. Roberts and P. Walter, **Molecular biology of the cells**, 4th ed., New York: Garland Science, 2002.

[2] E. Yavin, Z. Yavin "Attachment and Culture of Dissociated Cells from Rat Embryo Cerebral Hemispheres on Polylysine-Coated Surface", J. Cell. Biol., vol. 62, pp. 540-546, 1974.

[3] **Protein Chemistry for Conservators,** CL. Rose and D.W. von Endt, edts., Washington D.C.: American Institute for Conservation of Historic and Artistic Works, 1984.

[4] W. S. Klug and M. R. Cummings**, Concepts of Genetics,** 5th Ed**.**, Upper Saddle River, New Jersey: Prentice Hall, 1997.

[5] T. Yamada, **A Study of Protein Adsorptive Property onto Medical Polymer Improved by Carbon Negative-Ion Implantation,** Bachelor thesis, Department of Electronic Science and Engineering, Faculty of Engineering, Kyoto University.

[6] M.K. Magnusson, D.F. Mosher, "Fibronectin: Structure, Assembly, and Cardiovascular Implications", Arterioscler. Thromb.Vasc. Biol. 1998, vol. 18, issue 9, pp.1363-1370, 1998.

[7] W.M. Becker, L.J. Kleinsmith, J. Hardin, **The World of the Cell**, 5th Ed., Benjamin Cummings, 2002.

[8] F. Rodriguez, C. Cohen, C.K. Ober and L.A. Archer, **Principle of Polymer Systems**, 5th Ed., New York: Taylor and Francis, 2003.

# Chapter 5

# PC12h-Cell Adhesion and Neurite Outgrowth on Modified Polymeric Surface

Capability for cell adhesion to the polymer surface generally depends on many factors, especially, following things: (1) the physical surface property, (2) the extracellular matrix (ECM) of protein adsorption on the surface and (3) the kinds of issued cell line. Adhesion properties of each cell line are different due to specific anchoring between the cell receptors at its plasma membrane and the adhesive proteins. Such adhesive proteins, to which each specific cell receptor anchors, require the hydrogen bonding between their amine groups and the oxygen functional groups of the polymeric surface for binding and adsorption on the polymeric surface and each adhesive protein has a different ability to binding to the polymeric surface. Therefore, the cell adhesion properties on each polymeric surface depend on the different kinds of cell line. In this chapter, the fundamental properties of the implantation condition for the properties of neuron adhesion and neurite outgrowth were studied by using the nerve-like cells of rat adrenal pheochromocytoma (PC12h). The cell lines and PC12h cell are described. The adhesion properties of PC12h cells on the $C^-$-implanted surfaces of spin-coated polystyrene (SCPS) and silicone rubber (SR) without and with coating protein in details, the neurite-outgrowth properties on the $C^-$-implanted SCPS, the immobilization of cell body and neurite outgrowth for PC12h cells and the neuron network of PC12h cells on the $C^-$-implanted SCPS are stated in this chapter.

## 5.1 Cell Lines and PC12h Cell

In researches regarding to the modification of polymeric surfaces for the improvement of biocompatibility, of course, the *in vitro* cultivation of cells is required as the essential assessment. Many kinds of cell line, such as rat adrenal pheochromocytoma cell (PC12h), embryo stem cell (ES), mesenchymal stem cell (MSC), neuron, fibroblast, epithelial etc., are widely chosen according to each study, depending on their characteristics for the application purposes in further [1-10]. As for the development of neuron network and nerve regeneration, the cultivation of neuron is required. However, the culture of the real neuron is very delicates and there is no cell growth in vitro culture. The well-established clone cells were used for the fundamental assessment. One of them that are interesting for the study of the development is

PC12h cell line.

PC12h cell, so-called nerve-like cell, is a clone cell that has the same specific characteristics of differentiation of neurite extension similar to neuron ones in addition to cell growth [11-12]. Then, it is the well established and well-known useful cell line as a model system for studies of neuron differentiation, neurobiochemistry and neurobiology because it responds to nerve growth factor (NGF) [11]. This cell was first generated by Greene and Tischler in 1976 from a transplantable rat adrenal pheochromocytoma line [11]. PC12h cell line has a strong ability to survive in the long term culture with an increase in the number. Therefore, it is suitable for the essential assessment of study. The adhesion and the neurite outgrowth of PC12h cells on the tissue-culture polystyrene (TCPS, #25010, Corning) are shown in Fig. 5.1, where (a) adhesion of PC12h cells before differentiation and (b) neurite outgrowth after differentiation with NGF at 50 ng/ml. From Fig. 5.1, after differentiation, cells spread their body as a little and extended the neurite, which looked similar to the axon in neuron. The cell size is in the range of 15 – 25 μm in diameter. The average size of cells is almost 18 μm in diameter.

Although PC12h cell is a useful cell line for studies of some neuron activities, all of the responses shown by PC12h can not be compared with those of real neuron. Then, in some case, the essential assessments for studies of the neuron activities, the other cell lines that can differentiate into neuron were chosen. ES cell and MSC can differentiate into many other kinds of cells including neuron [10]. Therefore, stem cells can be applicable to the research on the development of neuron network.

As for the development of the neuron network and nerve regeneration, the neuron adhesion patterning on the polymeric surface is required. In this work, three kinds of cell lines; PC12h, neuron and MSC were chosen in the experiment of the cell cultivation on the polymeric

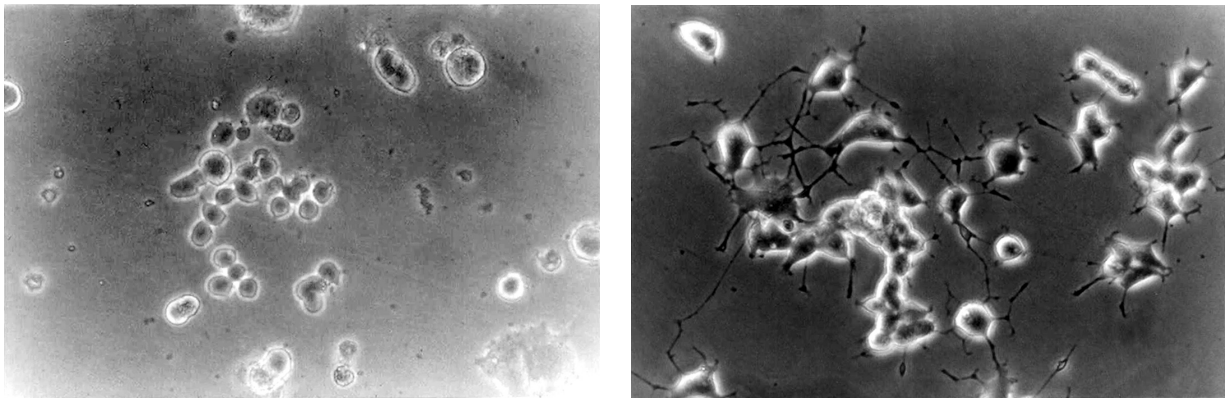

(a) Before differentiation (b) After differentiation with NGF

Fig. 5.1 Phase-contrast micrographs of PC12h cells: (a) before; and (b) after differentiation with NGF.

modified by carbon negative-ion implantation. At the first step, the study of the suitable implantation condition for the patterning was required. Many parameters such as the ion dose, energy, and pattern line-width in the implantation, as well as the effect of additional protein-coating on the modified pattern should be concerned. Prior to the cell culture with real neurons, which is very delicates and has no cell growth, I have performed the culture of nerve-like cell of PC12h on the $C^-$-implanted surfaces to find out these fundamental parameters since this cell line has some specific characteristics as neuron and a strong potential to survive. After obtained the suitable fundament parameters, the cell culture of real neurons, which are found in central nervous system (CNS) and peripheral nervous system (PNS), on the modified polymeric surface by carbon negative-ion implantation will be studied to find out the suitable condition for neuron adhesion patterning. The culture of the CNS neuron of the brain neuronal cells from mouse newborn and rat embryo were studied to form the neuron network on the pattern adhesion of the polymeric surface by carbon negative-ion implantation. Details will be described in Chapter 6. The culture of the PNS neuron of the neuronal cells from MSC differentiation was studied by patterning the adhesion of MSC on the $C^-$-implanted polymeric surfaces and by then differentiation into neuron. Details will be described in Chapter 7.

## 5.2 Cell-Adhesion Properties of PC12h on $C^-$-Implanted SCPS

The nerve-like cell line of PC12h was cultured on the modified spin-coated polystyrene (SCPS) by carbon negative-ion implantation to study the suitable implantation condition for the cell adhesion. The carbon negative ions were implanted into the SCPS films on glass at doses of $1\times10^{14}$ – $3\times10^{16}$ ions/cm$^2$ and energies of 5 – 20 keV through a micro-pattern mask, which is consisted of many slit apertures with 50-μm width and 70-μm spacing, to pattern the implanted lines. The other operation conditions of residual gas pressure and ion-current density were those described in Chapter 2. Each $C^-$-implanted sample was then fixed with a 35-mm non-treated polystyrene dish (NTPS, Corning) by the silicone adhesive and was left to dry in the clean bench preventing from dust at the room temperature for 2 days. All fixed dishes were sterilized by 70% ethanol, were rinsed three times with the sterilized DIW and were rinsed once with the phosphate buffered saline (PBS) before cell culture. PC12h cells with a number of $3.7\times10^3$ cells/dish were seeded and cultured on the sample dishes in Dulbecco's modified Eagle's medium (DMEM, Nissui, Japan) containing 5% heat-inactivated horse serum (HS, Biomedicals, USA), 5% fetal bovine serum (FBS, Bio-Wittker, USA), sodium hydrogen carbonate (1.8 mg/ml, Wako, Japan) with antibiotic of penicillin G and streptomycin for 2 days under 5% $CO_2$ at 37°C in incubator, as well as on type-I collagen-coated dish of tissue culture polystyrene (TCPS, Corning) as a control. Then, their cell adhesion properties on the $C^-$-implanted SCPS were observed by phase

contrast microscope (CK2, Olympus).

### 5.2.1 Effect of Ion Dose on Cell-Adhesion Properties on SCPS

As described in Chapters 3 and 4, the lowering of the contact angles and the improvement of the protein adsorption properties on the implanted region depending on the ion dose caused the improvement in the hydrophilicity of the SCPS surface with an increase in the ion dose. Then, at first, the effect of the ion dose on the cell-adhesion properties was checked. From the lowering of contact angle, we could expect that the cells should adhere on the implanted region and the cell adhesion properties should be improved with an increase in the ion dose. This expectation was confirmed with the cell culture.

Fig. 5.2 shows phase-contrast micrographs of cultured PC12h cells on the $C^-$-implanted SCPS at 10 keV and $3\times10^{15}$ ions/cm$^2$. Three things were observed. The first observation was the selective adhesion of almost all seeded PC12h cells on the implanted region, where is corresponding to the dark strip, as shown in Fig. 5.2. The second one was the some adhesion of cells at the boundary region between the unimplanted and implanted regions. These cells did not adhere to the surface, but they hanged to the adhered cells of the implanted region (see the magnified case of Fig. 5.2 (b)), so we called the hanging cells. The third one was the non-adhesion of cells and floating of cells all over area. Such floating cells could be removed after the replacement of the culture medium, so then the clean pattern can be obtained. This result was agreed with the first expectation that cell should adhere on the implanted region.

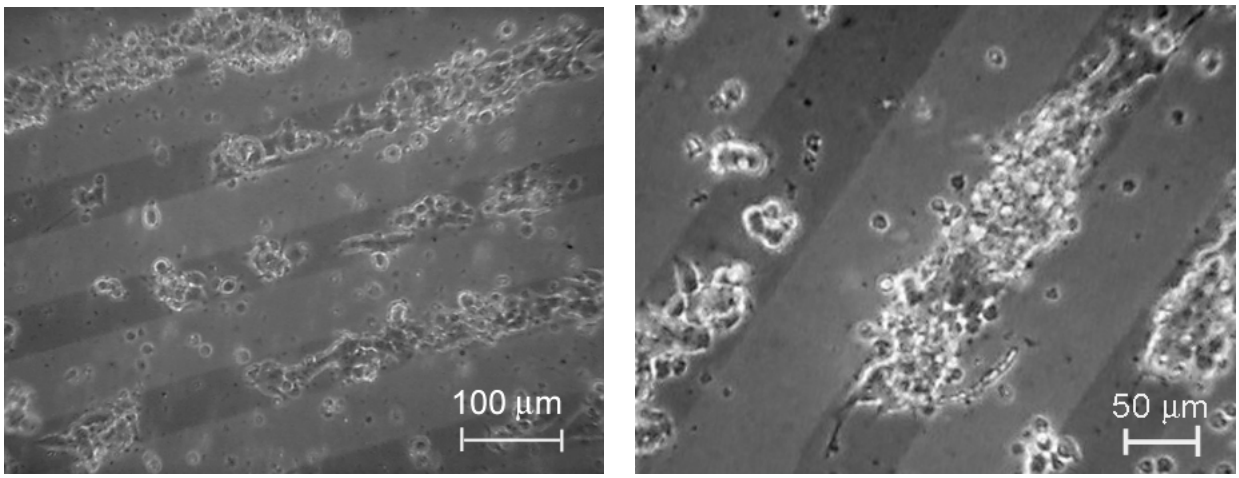


(a) C/SCPS (10 keV and $3\times10^{15}$ ions/cm$^2$) (b) C/SCPS (10 keV and $3\times10^{15}$ ions/cm$^2$, zoom)

Fig. 5.2 Phase-contrast micrographs of PC12h cells after 2-day culture on the implanted region of $C^-$-implanted SCPS at 10 keV and $3\times10^{15}$ ions/cm$^2$: (a) 10×10 magnification; and (b) zoom area of cell adhesion.

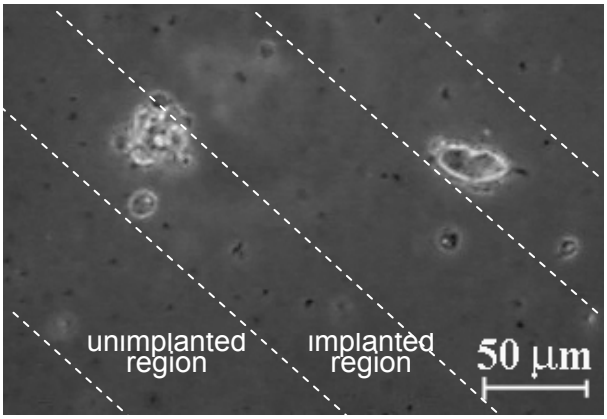


(a) C/SCPS (10 keV, $1\times10^{14}$ ions/cm$^2$)

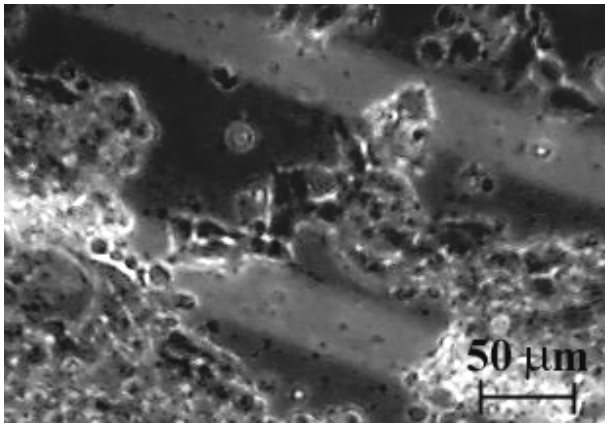


(b) C/SCPS (10 keV, $3\times10^{16}$ ions/cm$^2$)

Fig. 5.3 Phase-contrast micrographs of PC12h cells after 2-day culture on the $C^-$-implanted SCPS at 10 keV with: (a) $1\times10^{14}$; and (b) $3\times10^{16}$ ions/cm$^2$.

At the dose of the order of $10^{15}$ ions/cm$^2$, the cells also showed clear selective adhesion on implanted region (data not shown here), similar to the typical culture at $3\times10^{15}$ ions/cm$^2$ as shown in Fig. 5.2 (b), corresponding to a very low contact angle of these implanted regions as described in Chapter 3.

The adhesion properties of PC12h cells at other low and high ion doses are shown in Fig. 5.3. At the low dose of $1\times10^{14}$ ions/cm$^2$, very small amount of cells adhered on the surface as shown in Fig. 5.3(a). The small adhesion was corresponding to the small lowering of contact angle and small amount of adsorbed protein on the surface implanted with the low dose. At the high dose of $3\times10^{16}$ ions/cm$^2$, the selective adhesion properties of cell became poor, where cells adhered on both of the implanted and unimplanted regions as shown in Fig. 5.3 (b). Almost 65% of PC12h cells adhered on the implanted region. This decrease of the selective adhesion is considered to be due to the adsorption of the sputtered particles or the emitted gas particles from the implanted areas on the unimplanted areas. Such adsorption might lead to hydrophilicity on the unimplanted areas. So, the cells could adhere on the surface.

The adhesion properties of PC12h cells on the $C^-$-implanted SCPS at 10 keV could be summarized as shown in Fig. 5.4. The cell density on the implanted region increased with an increase in the ion dose in the dose range of $1\times10^{14} - 1\times10^{16}$ ions/cm$^2$ and became saturated. The cell density increased from 150 to 1100 cells/mm$^2$. The selective adhesion ratio in percent between the number of cells on the implanted region and the number of cells on both of the implanted and unimplanted regions increased with an increase in the ion dose from $1\times10^{14} - 3\times10^{15}$ ions/cm$^2$ and gradually decreased with an increase in the ion dose from $3\times10^{15} - 3\times10^{16}$ ions/cm$^2$. The selective adhesion ratio increased from 67% to 90% and decreased to 65%. In the dose range of $1\times10^{15} - 5\times10^{15}$ ions/cm$^2$, a lot of cells could adhere to the implanted region with

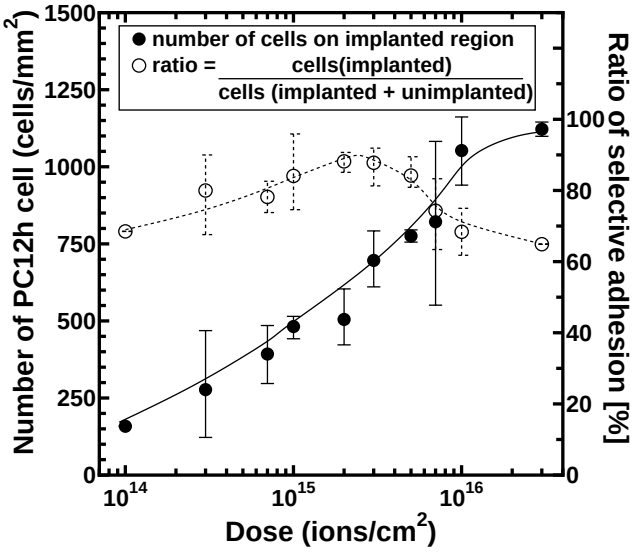


Fig. 5.4 Adhesion properties of PC12h cells for the number of cells adhered on the implanted region of the $C^-$-implanted SCPS and the selective adhesion properties as implantation at energy of 10 keV.

the high selective adhesion ratio of 80% –90%. From this observation, the suitable ion dose at 10-keV-energy implantation for the selective adhesion properties of PC12h cells was considered to be in the ion doses of $1\times10^{15}$ – $5\times10^{15}$ ions/cm$^2$. The best condition for the properties was at $3\times10^{15}$ ions/cm$^2$.

As described in Chapter 4, the adhesive proteins were required to adsorb on the surface for cell adhesion. For the presented experiment of selective cell-adhesion, the required proteins were delivered from the culture medium, especially from the supplement serum, in the initial state of cell culture, and were produced by cell self. The protein adsorption properties on SCPS was improved by the carbon negative-ion implantation about only factor of 1.2 – 1.6 in the ratio for each protein as shown in Chapter 4. However, it was found by the experiment in this section that such small improvement of protein adsorption worked well and they induced to a clear separation of cell adhesion on the $C^-$-implanted region.

### 5.2.2 Effect of Ion Energy on Cell-Adhesion Properties

Although the change in the implantation energy in the range of 5 – 20 keV gave a small difference in the lowering of contact angle at the same dose as described in Chapter 3, the effect of such the change on the cell adhesion properties of PC12h were also investigated.

Fig. 5.5 shows phase-contrast micrographs of cultured PC12h cells on the $C^-$-implanted SCPS at $3\times10^{15}$ ions/cm$^2$ with various energies in 5 – 20 keV. In every energy, almost all of the

cells selectively adhered on the implanted region. Some hanging cells at the boundary region between the unimplanted and implanted regions and the floating cells on all over areas were also observed on the unimplanted region. Such floating cells were also removed after the replacement of the culture medium, so the clear pattern was obtained. The selective adhesion properties of cells on the $C^-$-implanted SCPS at $3\times10^{15}$ ions/cm$^2$ with various energies of 5 – 20 keV were reflected by the number of adhered cells on the implanted and unimplanted region. Therefore, I counted the number of the cells on both of the regions. The results are shown in Fig. 5.6. The cell density on the implanted region increased with an increase in the ion energy from 5 to 10 keV and became saturated. The cell density increased twice from 350 to 700 cells/mm$^2$. The selective adhesion ratio between cells on the implanted region and all cells on both of the implanted and unimplanted region is also shown in Fig. 5.6, where the ratio decreased with an increase in the ion energy from 5 to 20 keV. The selective adhesion ratio decreased from 90% to 83%. In the energy range of 10 – 20 keV, a lot of cells could adhere to the implanted region with the high selective adhesion ratio of 80% – 90%. From this observation, the suitable ion energy at implantation dose of $3\times10^{15}$ ions/cm$^2$ for the selective adhesion properties of PC12h cells was

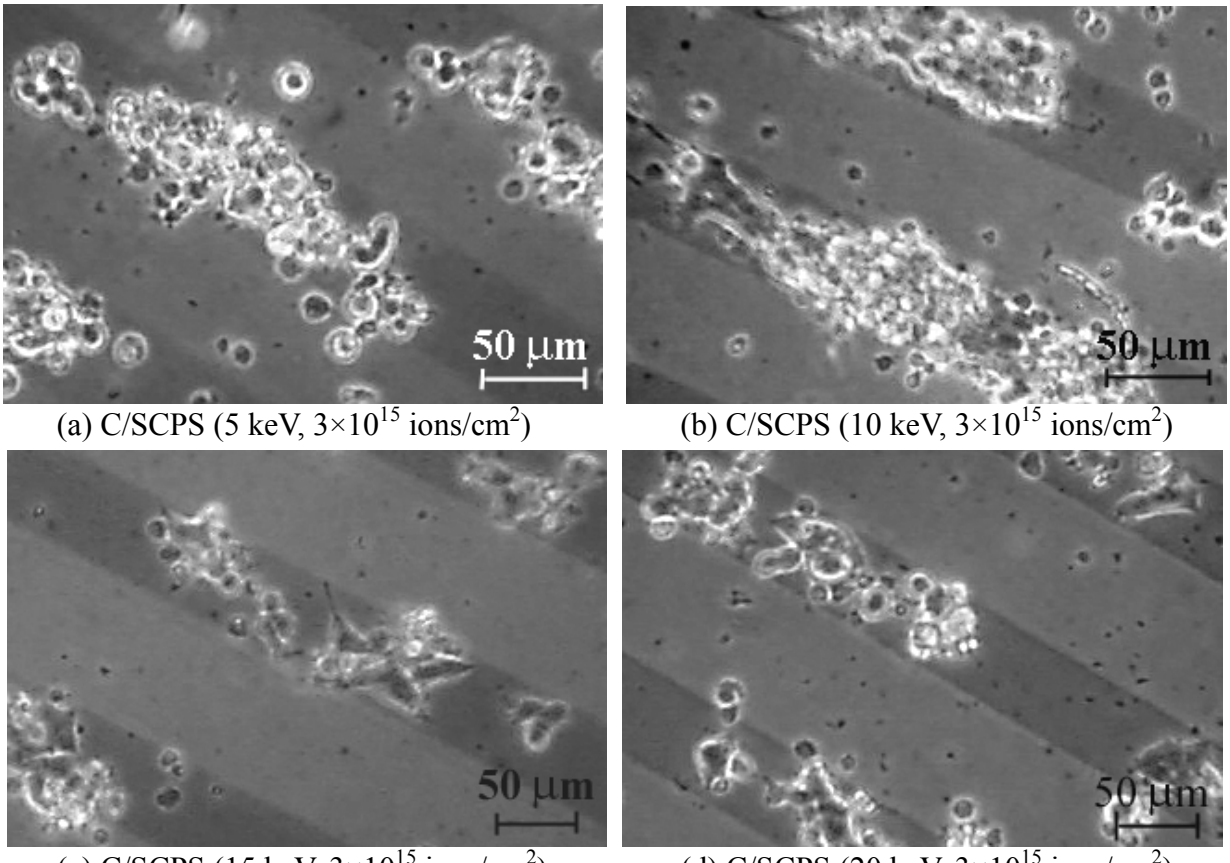


(a) C/SCPS (5 keV, $3\times10^{15}$ ions/cm$^2$) (b) C/SCPS (10 keV, $3\times10^{15}$ ions/cm$^2$)

(c) C/SCPS (15 keV, $3\times10^{15}$ ions/cm$^2$) (d) C/SCPS (20 keV, $3\times10^{15}$ ions/cm$^2$)

Fig. 5.5 Phase contrast micrograph of PC12h cells after 2-day culture on the $C^-$-implanted SCPS at $3 \times 10^{15}$ ions/cm$^2$ and: (a) 5; (b) 10; (c) 15; and (d) 20 keV.

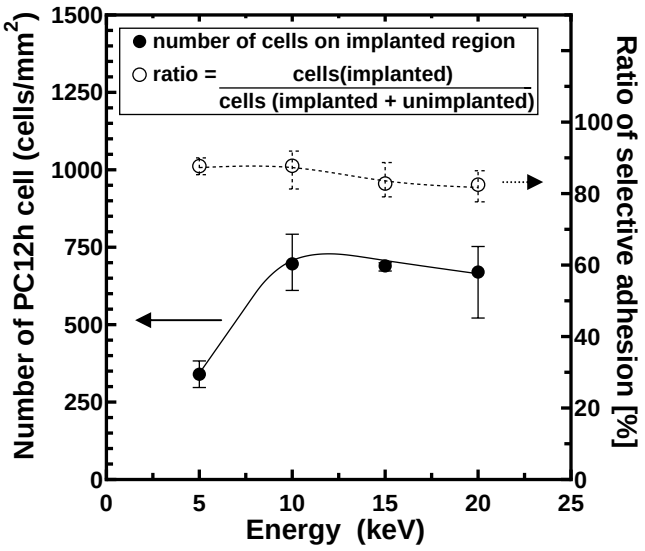


Fig. 5.6 Adhesion properties of PC12h cells for the number of cells adhered on the implanted region of the $C^-$-implanted SCPS and the selective adhesion properties as a function of implantation energy at dose of $3\times10^{15}$ ions/cm$^2$.

considered to be in the ion energy from 10 – 20 keV. The best condition for the properties was at 10 keV.

## 5.3 Cell-Adhesion Properties of PC12h on $C^-$-Implanted SR

The suitable implantation condition to silicone rubber (SR) for nerve cell adhesion was studied by the cell culture of the nerve-like cell line of PC12h. The carbon negative ions were implanted into the SR sheet (0.5 mm thickness, Fuji system) at doses of $1\times10^{14}$ – $1\times10^{16}$ ions/cm$^2$ and energies of 5 – 30 keV through a micro-pattern mask, which consists of many slit apertures with 50-μm width and 70-μm spacing, to pattern the implanted lines. The other operation conditions of residual gas pressure and ion-current density were those described in Chapter 2. After the implantation, the samples were set into PS dish and were sterilized, and PC12h cells were cultured on the samples. The procedures were the same as described in section 5.2. The type-I collagen-coated dish of tissue culture polystyrene (TCPS, Corning) was used as a control. PC12h cells were cultured for 2 days with the culture serum medium of DMEM and then the culture medium was replaced by the serum-free medium of DMEM supplemented with nerve growth factor for 50 ng/ml, hydrogen carbonate (1.8 mg/ml, Wako, Japan), and antibiotic of penicillin G and streptomycin. The cells were cultured for a further 2 days. Their cell-adhesion properties on the $C^-$-implanted SR were observed by phase contrast microscope (CK2, Olympus).

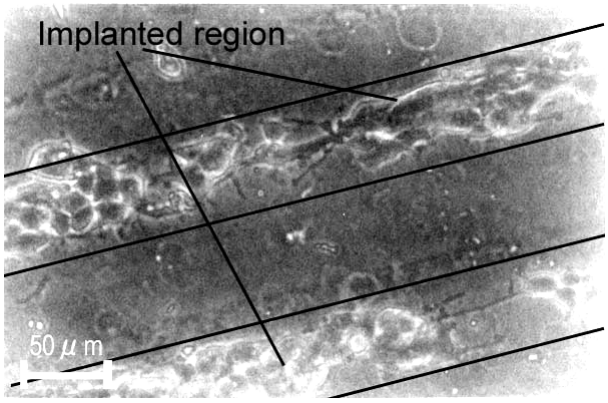


Fig. 5.7 Phase contrast micrographs of PC12h cells on the $C^-$-implanted SR (p-C/SR) at 10 keV and $3\times10^{15}$ ions/cm$^2$ after cultured for 4 days (NGF supplement for 2 days).

Fig. 5.7 shows PC12h cells with their neurite outgrowth after culturing for totally 4 days on the $C^-$-implanted films at 10 keV and $3\times10^{15}$ ions/cm$^2$. The cells and their neurite outgrowth adhered only on the implanted region due to the lowering of contact angle after implantation. The clear pattern of cell adhesion could be obtained. At the doses in the range of $1\times10^{15}$ – $1\times10^{16}$ ions/cm$^2$, PC12h cells should be considered to adhere on the implanted region since the enough in the lowering of the contact angle and more adsorption of ECM on the implanted region as described in Chapters 3 and 4.

After cultured for the first 2 days, no cell adhesion on the implanted region at a low implantation dose of $1\times10^{14}$ ions/cm$^2$ was observed, corresponding to the small lowering of contact angle at this dose. As described in Chapters 3 and 4, the ECM adsorption resulted due to binding between the amino acid in protein and the hydrophilic bond on the surface, and the formation of these hydrophilic bonds on the surface happened after the destruction of the atomic bonding in SR. However, the destruction of the main chain bonds of Si-O in SR required the high dose and high energy so that the implantation at 10 keV and $1\times10^{14}$ ions/cm$^2$ could not be satisfied as shown in Fig. 5.8 (a). The contact angle did not decrease so much. The ECM layer could not form on the very small amount of hydrophilic bond at this implantation condition. Therefore, the effective ECM adsorption on SR modified at the dose of $1\times10^{14}$ ions/cm$^2$ was not induced, so that the cells did not adhere on the implanted region.

At other energy implantation, since the contact angle decreased with an increase in the ion energy from 5 to 30 keV, the cell adhesion at high energy should be good. However, the cell adhesion on the implanted surface at $3\times10^{15}$ ions/cm$^2$ with higher energy of 30 keV was not good as shown in Fig. 5.8 (b). The abnormal cell adhesions were observed on the implanted region of the $C^-$-implanted SCPS at high energy implantation of 30 keV after cultured for 2 days. The very large size and abnormal shape, comparing to the normal cell on control, were found on the

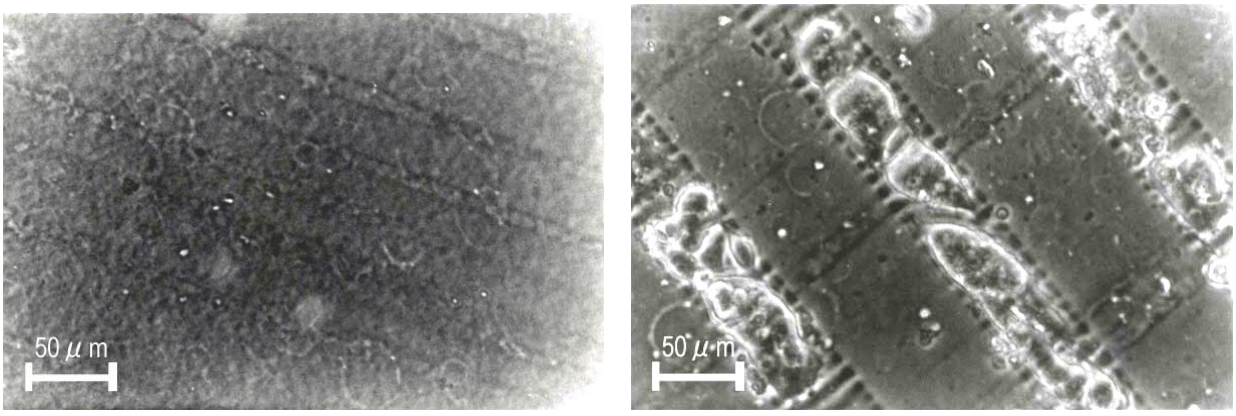


(a) p-C/SR (10 keV, $1\times10^{14}$ ions/cm$^2$) (b) p-C/SR (30 keV, $3\times10^{15}$ ions/cm$^2$)

Fig. 5.8 Phase contrast micrographs of PC12h cells on the $C^-$-implanted SR (p-C/SR) at (a) 10 keV and $1\times10^{14}$ ions/cm$^2$; and (b) at 30 keV and $3\times10^{15}$ ions/cm$^2$ after cultured for 2 days. Where the dark stripe is the implanted region.

implanted region and the cell death were observed soon. The high energy implantation gave an effect on the adhesion of cells, but the implantation at high energy was not suitable for adhesion of PC12h cells.

Resulting from all observation, the implantation at low dose or at high energy was not suitable for cell adhesion. The suitable ion dose condition at implantation at 10 keV for the good cell adhesion property should be $1\times10^{15} - 1\times10^{16}$ ions/cm$^2$. The best dose condition was $3\times10^{15}$ ions/cm$^2$.

## 5.4 Cell-Adhesion Properties of PC12h on Protein-Coated Modified Polymeric Surfaces

As described in Chapter 4, the carbon negative-ion implantation into SCPS could improve the adsorption property of Co-I, FN and LN, but the selective adhesion properties of these protein on the implanted region were not so much, especially the property of LN. The effects of additional protein adsorption on the $C^-$-implanted surfaces of SCPS and SR on the selective cell adhesion for enhancement of neuron pattern formation were studied by cultivation of PC12h cells on the protein-coated surfaces after the implantation. The carbon negative ions were implanted into SCPS films on glass and SR sheet (0.5 mm in thickness, Wacom Electric co., ltd.) at 10 keV and $3\times10^{15}$ ions/cm$^2$ through the micro-pattern mask. The other operation conditions of residual gas pressure and ion-current density were those described in Chapter 2. After the implantation, the samples were set into PS dish and were sterilized. The procedures were the same as described in section 5.2. The adhesive protein such as type I collagen (Co-I), fibronectin (FN) and laminin

(LN) were selected in an additional coating. In the additional protein coating, the implanted samples were dipped in each protein solution for 2 h and then were rinsed once with PBS before cell culture. The applied concentrations of solutions for Co-I, FN and LN were 10, 1 and 1 μg/ml, respectively. In case of LN, after coating the surfaces were dried at least 45 min before cell culture. In addition, the $C^-$-implanted surfaces of SCPS and SR without any protein coating were also tested as control. The cell culture of PC12h was executed as described in section 5.2. The cells were cultured for 4 days. Their cell adhesion properties on the $C^-$-implanted surfaces of SCPS and SR were observed by phase contrast microscope (CK2, Olympus).

### 5.4.1 Cell-Adhesion Properties on Protein-Coated SCPS

Figs. 5.9 shows phase-contrast micrographs of PC12h cells cultured for 1 day and 2 days on each additionally protein-coated SCPS after carbon negative-ion implantation at 10 keV and $3\times10^{15}$ ions/cm$^2$. The additional protein coating showed clear difference in the cell-adhesion properties of PC12h from those without the additional protein coating shown in the previous section.

In case of Co-I coated surface of $C^-$-implanted of SCPS (Co-I-C/SCPS), the cell adhesion property on the implanted region was much more improved, even only after 1-day culture (Fig. 5.9(a)). However, the selective adhesion property was degraded a little when comparing to cell adhesion properties on the non-coating surface of the control as shown in Fig. 5.9 (g). The improvement of the cell adhesion property and the degradation of the selective adhesion property were obviously observed after 2-day culture as shown in Fig. 5.9 (b).

As for FN-coated surface of $C^-$-implanted of SCPS (FN-C/SCPS), the cell adhesion and the selective adhesion properties on the implanted region was much more improved, corresponding to the high selective ratio of FN as described in Chapter 4, after cultured for 1 day (Fig. 5.9 (c)). However, the adhered cells increased in the number so quickly, leading to cell growth to the confluence state and detachment of cells from the surface after only 2 days as shown in Fig. 5.9 (d). The detachment of cells was related to the binding to the surface of the ECM. As described in Chapter 4, small amount of nitrogen atom adsorbed on the implanted region caused the low adsorption property of FN on the implanted region. Therefore, cells easily detached from the surface at the confluence state.

In case of LN-coated surface of $C^-$-implanted of SCPS (LN-C/SCPS), the cell adhesion properties were much more improved, even on the unimplanted region. This good LN adsorption from the additional LN coating caused the completely degradation of the selective cell-adhesion property as shown in Fig. 5.9 (e). In Fig. 5.9 (f), PC12h cells on both of implanted and unimplanted regions reached to the confluent state after culturing within 2 days and still adhered

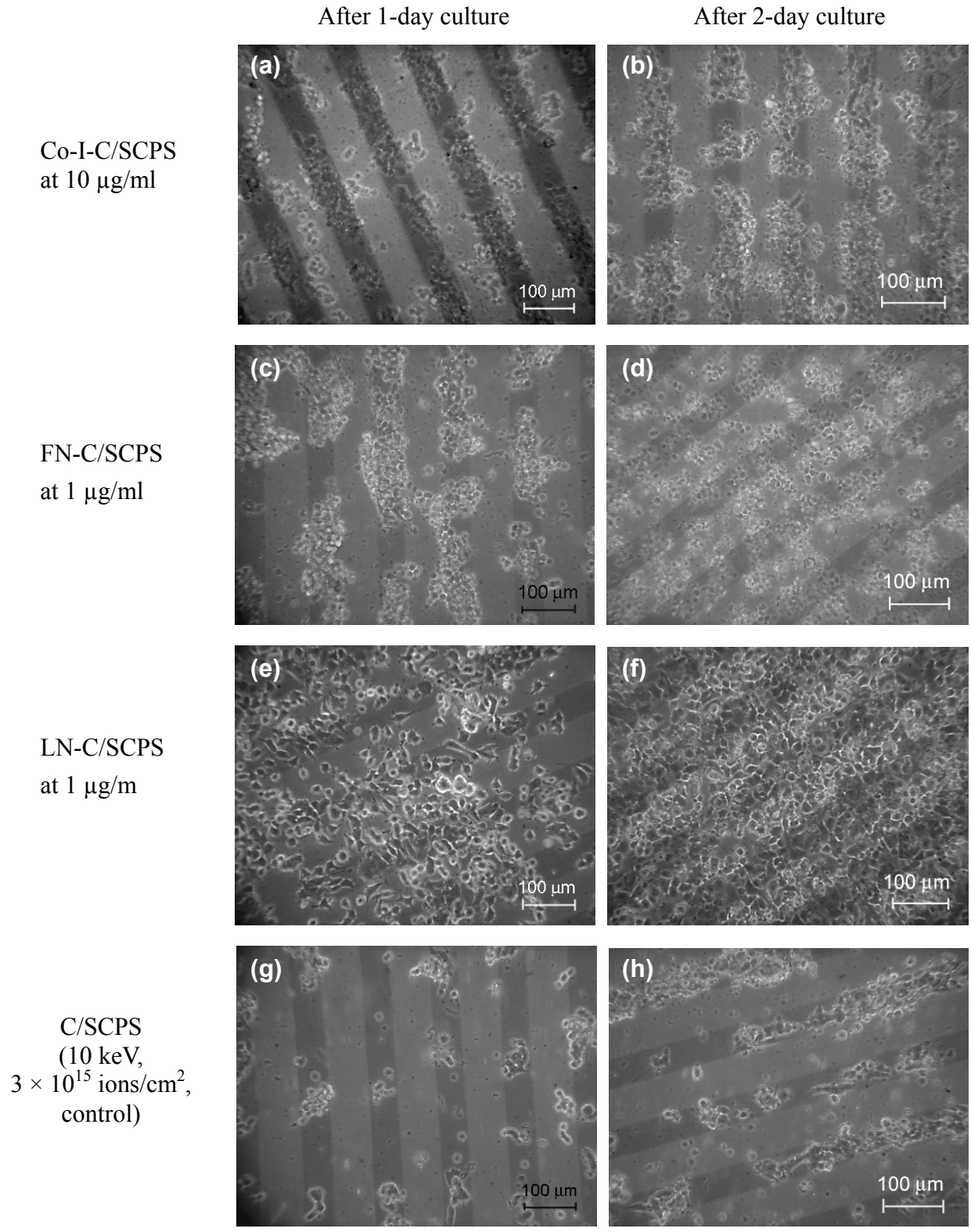


Fig. 5.9 Phase contrast micrograph of PC12h cells after 1- and 2-day culture on SCPS implanted at 10 keV and $3\times10^{15}$ ions/cm$^2$ coated with proteins of: (a), (b) type I collagen at 10 μg/ml; (c), (d) fibronectin at 1 μg/ml; (e), (f) laminin at 1 μg/ml; and (g), (h) on control.

on the surface. This result also agreed with the large amount of nitrogen atoms adsorbed on the surface of SCPS and with the poor selective adsorption property of laminin as described in Chapter 4.

As a result for protein-coated surface of $C^-$-implanted of SCPS, the additional protein coating had much effect on enhancing cell adhesion on both of the implanted and unimplanted surface of SCPS. The coating with Co-I might be suitable for improvement of the cell-adhesion properties, even if with a little degradation on the $C^-$-implanted of SCPS. Therefore, by using the suitable solution, might be less than 10 μg/ml, we will obtain the clear adhesion pattern.

### 5.4.2 Cell-Adhesion Properties on Protein-Coated SR

In case of silicone rubber (SR), although the amount of nitrogen atoms adsorbed on the implanted region at 10 keV and $3\times10^{15}$ ions/cm$^2$ were small, the selective adsorption properties of ECM on the $C^-$-implanted of SR were much better when comparing to those on the implanted region of the $C^-$-implanted of SCPS as described in Chapter 4. Therefore, the cell adhesion properties on the protein-coated surface of the $C^-$-implanted of SR should be better than those of SCPS. The adhesion properties of PC12h cells cultured on each protein-coated SR after 2 and 4 days are shown in Fig. 5.10.

Based on phased-contrast microscopy, the cell adhesion property on the Co-I coated surface of the $C^-$-implanted of SR (Co-I-C/SR) was improved with containing the selective adhesion property after culturing for 2 days as shown in Fig. 5.10 (a). However, after culturing for 4 days, the selective adhesion property was degraded as shown in Fig. 5.10 (b). PC12h cells adhered all over the implanted region and some of them also adhered on the boundary area next to the implanted region. Although the selective adsorption property of Co-I on the $C^-$-implanted of SR was very high as shown in Chapter 4, the degradation of the selective adhesion property of cells was found. This was considered to be due to the aggregation of type I collagen and the cell hanging out of the implanted region at the confluence state.

Whereas on the FN-coated surface of the $C^-$-implanted of SR (FN-C/SR), no improvement of the cell adhesion property was observed, even after culturing for 2 days (Fig. 5.10 (c)). In Fig. 5.10 (d), the cell adhesion property was improved with still containing the selective adhesion property after 4 days. The cells adhered and increased their number on the implanted region, resulting in a clear pattern adhesion. This was considered to be the weak bonding energy between FN and the unimplanted region due to the high contact angle. The adsorbed FN on the unimplanted surface detached easily when replacement of the culture medium. Therefore, the detachment of protein and the adhered cells on it could be removed. Then, clear adhesion pattern on the implanted region was obtained.

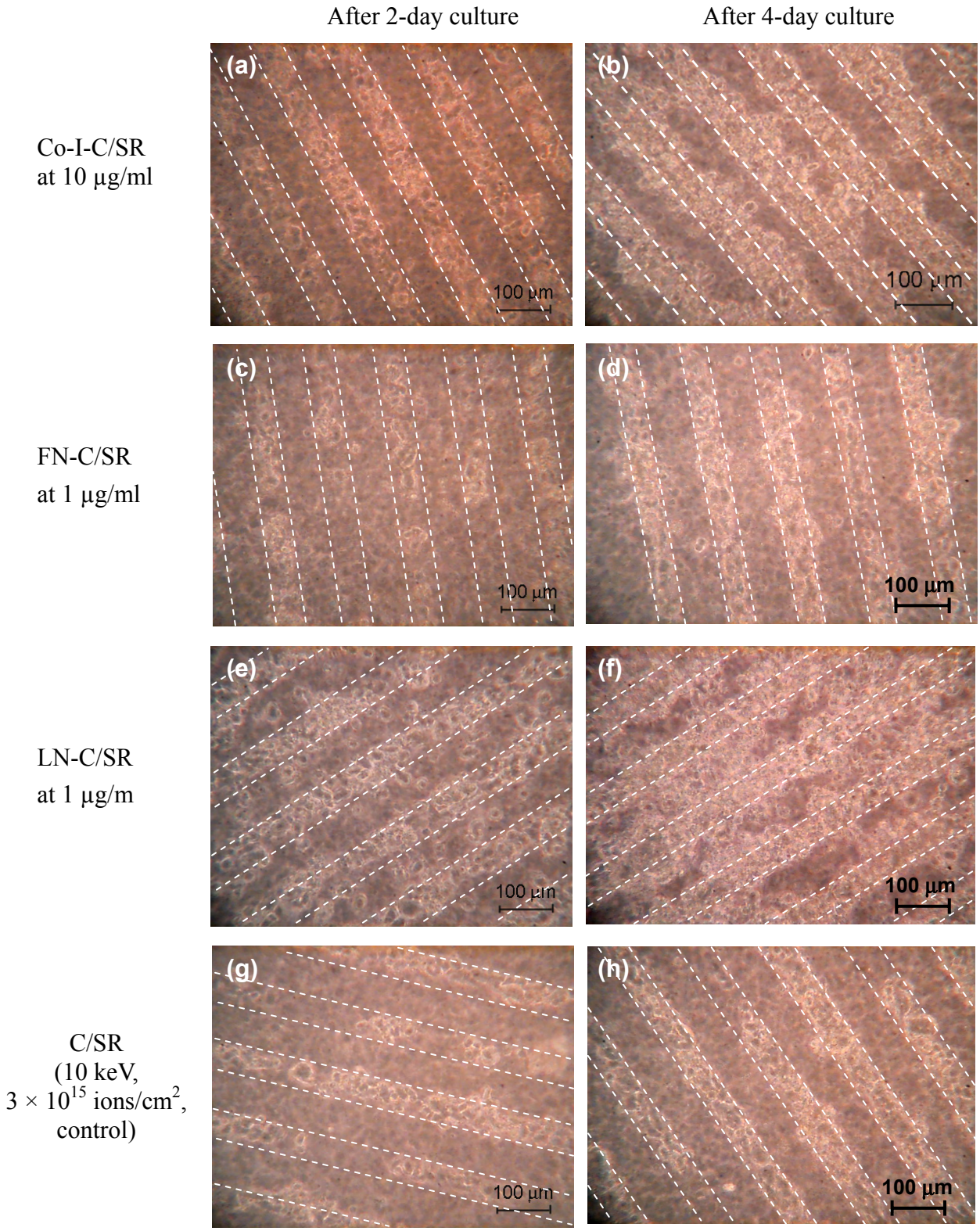


Fig. 5.10 Phase contrast micrograph of PC12h cells after 2- and 4-day culture on SR implanted at 10 keV and $3\times10^{15}$ ions/cm$^2$ coated with proteins of: (a), (b) type I collagen at 10 μg/ml; (c), (d) fibronectin at 1 μg/ml; (e), (f) laminin at 1 μg/ml; and (g), (h) on control.

As for the LN-coated surface of $C^-$-implanted of SR (LN-C/SR), the cell adhesion property on the implanted region was improved with a small degradation of the selective adhesion property within 2-day culture. Fig. 5.10 (e) shows the confluence state of the adhered cells on the implanted region and some adhered cells on the unimplanted region. After culturing for 4 days, however, the properties for the number of cell adhesion on the implanted and unimplanted regions were improved, resulting in the degradation of the selective adhesion property as shown in Fig. 5.10 (f). This is because laminin could be adsorbed on all over regions leading to the large amount adsorption and the poor selective adsorption as described in Chapter 4. Therefore, the LN coating could not be used for the improvement the selective cell-adhesion property. From all results for protein-coated surface of $C^-$-implanted of SR, the coating with FN was the best for improvement of the adhesion properties with remaining the selective adhesion property. Other suitable protein coating might be sequenced by Co-I for improvement of the adhesion properties with a little degradation of the selective adhesion property.

From all investigation, the protein coating on the $C^-$-implanted surfaces of SCPS and SR gave an enhancing effect on the cell-adhesion property, in the order of LN, FN and Co-I. The adhesion properties of cell could be improved by the additional protein coating. The aggregation properties of protein affected to the adhesion of cells on boundary area next to the implanted region, and it led to the degradation of the selective adhesion properties. In some case, however, the additional FN coating on the $C^-$-implanted SR could improve the adhesion and selective adhesion properties of cells. The additional coating of Co-I on the $C^-$-implanted surfaces of SCPS and SR, and that of FN on the $C^-$-implanted SR are useful for the condensed patterns of cell adhesion on the implanted surface. The clearer pattern on the additional coating of FN on the $C^-$-implanted SR was considered due to the easier detachment of protein adsorbed on the unimplanted region.

## 5.5 Neurite-Outgrowth Properties of PC12h Cell

The suitable implantation conditions for the neurite-outgrowth properties were continually studied from section 5.2. After PC12h cells were cultured on the $C^-$-implanted SCPS for 2 days, the culture serum medium was replaced by the serum free medium of DMEM supplementing with NGF for 50 ng/ml to promote the neurite outgrowth. Cells were cultured for a further 2 days. The neurite-outgrowth properties on the $C^-$-implanted SCPS were observed by phase contrast microscope (CK2, Olympus). Results are as follows:

Fig. 5.11 shows phase-contrast micrographs of PC12h cells with their neurite outgrowth on the $C^-$-implanted SCPS at 10 keV with various doses of $3\times10^{14}$ – $3\times10^{16}$ ions/cm$^2$. The numbers and the length of neurite outgrowth increase with an increase in the ion dose. At low

dose of $3\times10^{14}$ ions/cm$^2$, the cells sparsely adhered on the implanted region, which is the narrow region between white dotted lines, and some cells differentiated their body and extended the long neurite as shown in Fig. 5.11 (a). Those cells did not spread their body, and almost they have a cobble-shape. Therefore, the adhesion strength of the cells on this surface was weak. Neurite outgrowth on the implanted region at the medium dose of $3\times10^{15}$ ions/cm$^2$ for cell adhesion as described in section 5.2.1 is shown in Fig. 5.11 (b). The cells and their neurite outgrowth adhered only on the implanted region, where is the dark narrow strip. The cells spread their body as a stretched-shape that means the strong adhesion of cells on the implanted surfaces at this dose. At a high dose of $1\times10^{16}$ ions/cm$^2$, however, PC12h cells adhered on both of the implanted and unimplanted regions, but the neurite outgrowth still was on the implanted region as shown in Fig. 5.11 (c). As increasing in dose to $3\times10^{16}$ ions/cm$^2$, both of cells body and their neurite outgrowth

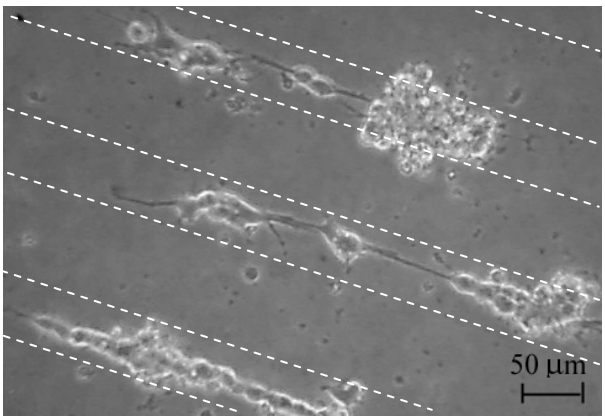


(a) C/SCPS (10 keV, $3\times10^{14}$ ions/cm$^2$)

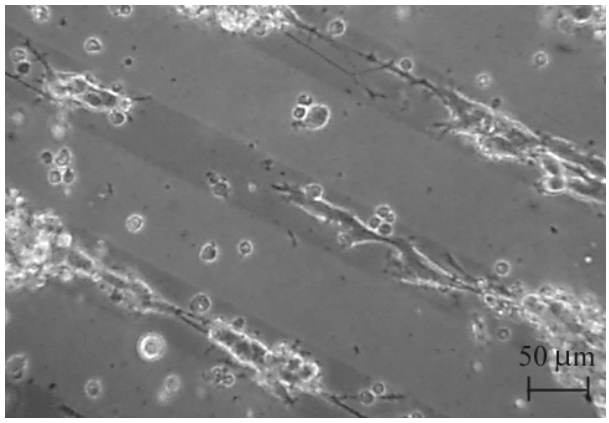


(b) C/SCPS (10 keV, $3\times10^{15}$ ions/cm$^2$)

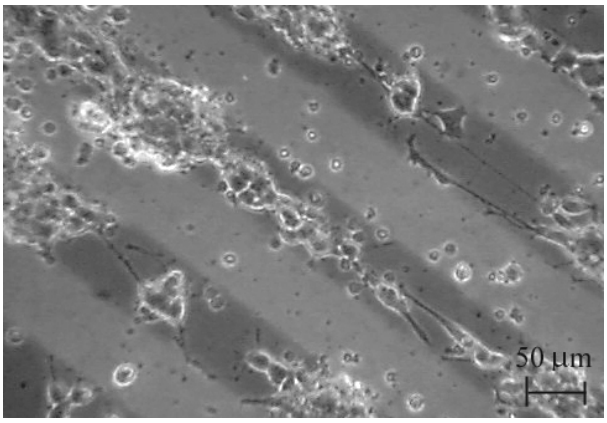


(c) C/SCPS (10 keV, $1\times10^{16}$ ions/cm$^2$)

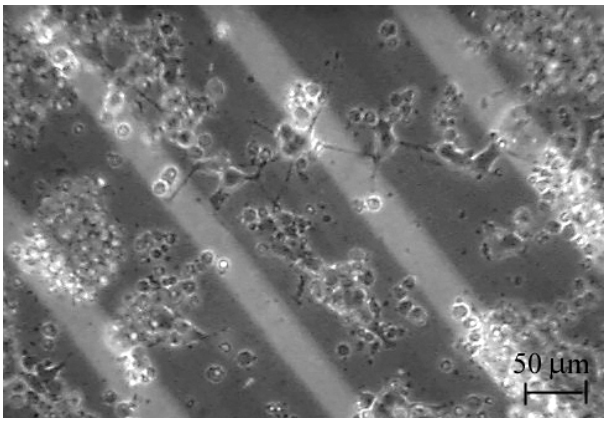


(d) C/SCPS (10 keV, $3\times10^{16}$ ions/cm$^2$)

Fig. 5.11 Phase contrast micrograph of PC12h cells with their neurite after 2-day NGF-supplemented culture on the C-implanted films at 10 keV as a function of ion dose at: (a) $3\times10^{14}$; (b) $3\times10^{15}$; (c) $1\times10^{16}$; and (d) $3\times10^{16}$ ions/cm$^2$.

adhered on both of the implanted and unimplanted regions as shown in Fig. 5.11 (d). Therefore, the good condition of the dose amount for the neurite outgrowth was obtained around $3\times10^{15}$ ions/cm$^2$. The neurite outgrowth properties depending on the implantation energies of 5 – 20 keV were studied at the same dose of $3\times10^{15}$ ions/cm$^2$. The phase-contrast micrographs of PC12h cells with their neurite outgrowth at $3\times10^{15}$ ions/cm$^2$ of all energy are shown in Fig. 5.12.

Among all case of various energies in 5 – 20 keV at $3\times10^{15}$ ions/cm$^2$, no significant difference in the neurite outgrowth was observed. A lot of PC12h cells also differentiated and extended their neurite only on the implanted region. The neurite outgrowth on the implanted region stopped at the edge of implanted region. No neurite on the unimplanted surface was found.

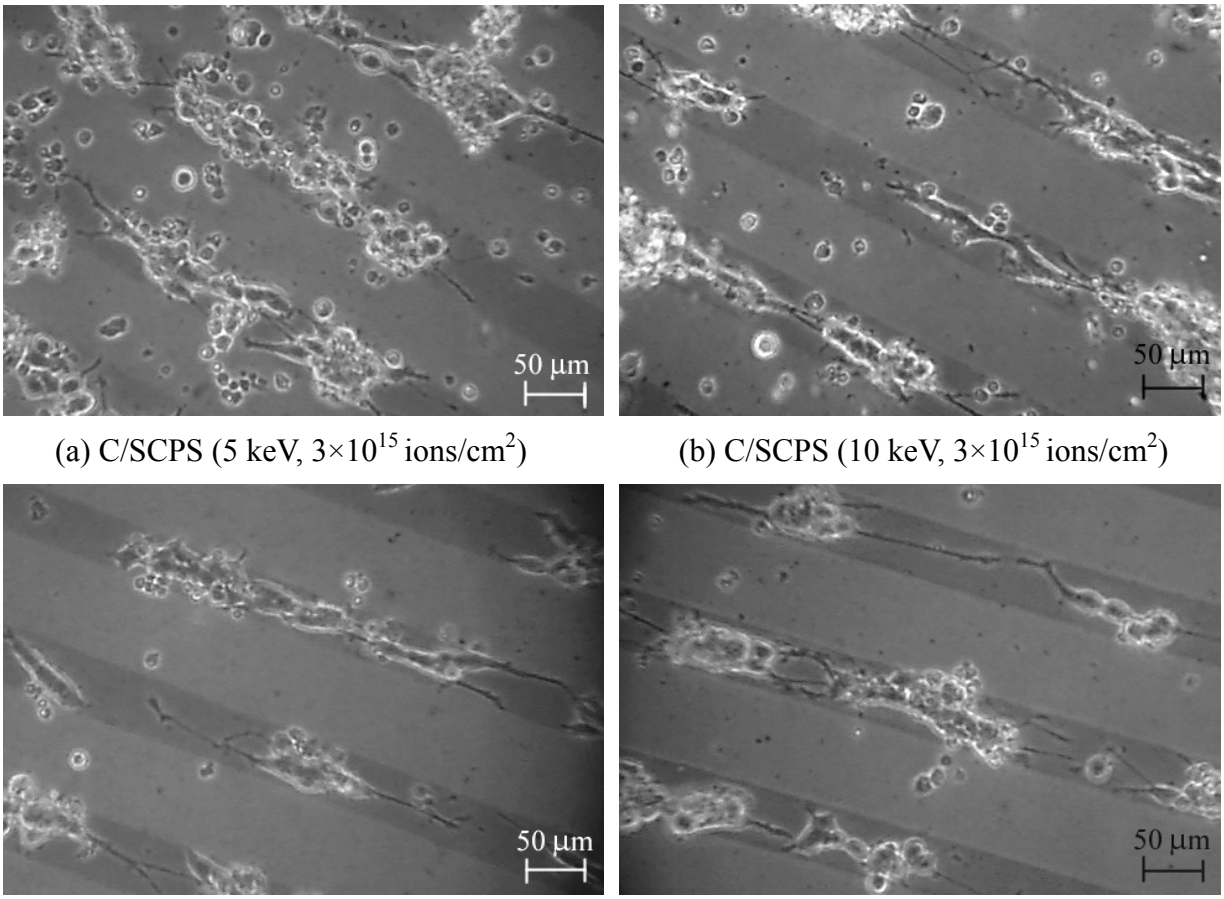


(a) C/SCPS (5 keV, $3\times10^{15}$ ions/cm$^2$) (b) C/SCPS (10 keV, $3\times10^{15}$ ions/cm$^2$)

(c) C/SCPS (15 keV, $3\times10^{15}$ ions/cm$^2$) (d) C/SCPS (20 keV, $3\times10^{15}$ ions/cm$^2$)

Fig. 5.12 Phase contrast micrograph of PC12h cells with their neurite after 2-day NGF-supplemented culture on the $C^-$-implanted films at $3\times10^{15}$ ions/cm$^2$ as a function of ion energy at: (a) 5; (b) 10; (c) 15; and (d) 20 keV.

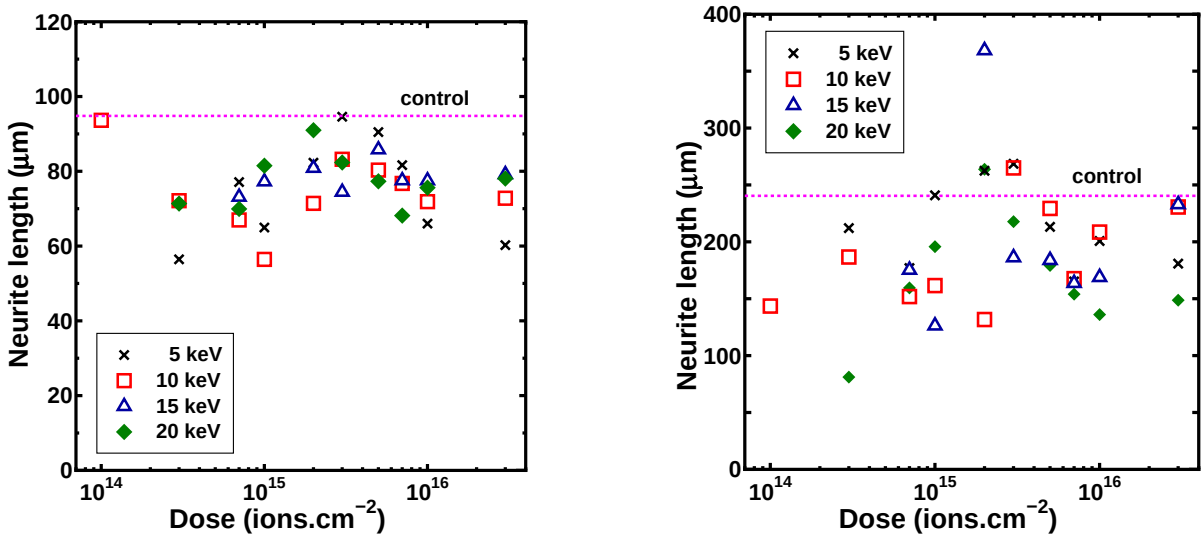


(a) The average neurite length (b) The maximum neurite length

Fig. 5.13 The neurite length of PC12h cells on the $C^-$-implanted polystyrene films at 5 – 20 keV as a function of ion dose when (a) the average length; and (b) the maximum length.

The average and the maximum neurite length of PC12h cells on the $C^-$-implanted SCPS at various ion doses and energies were measured and were summarized in Figs. 5.13 (a) and (b), respectively. The outgrowth of the average neurite length as a function of culture day is shown in Fig. 5.14.

After 2-day culture with NGF, the PC12h cells on the $C^-$-implanted SCPS at 5 – 20 keV with $2\times10^{15}$ – $3\times10^{15}$ ions/cm$^2$ could extend very long neurite length as same as that on control

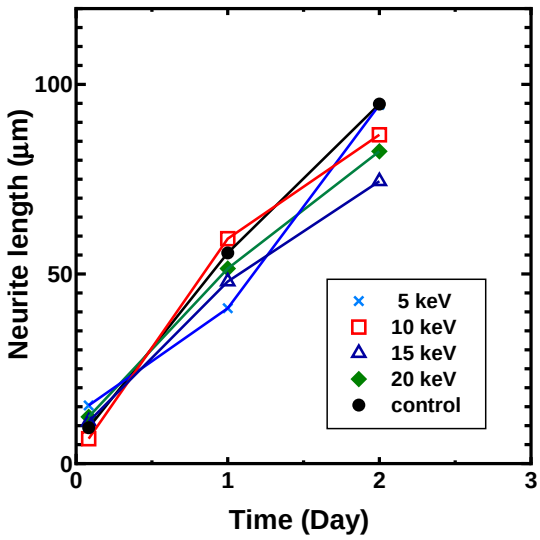


Fig. 5.14 The average neurite length for each day of PC12h cells on the $C^-$-implanted films at 5 – 20 keV with $3\times10^{15}$ ions/cm$^2$ after supplement NGF.

of the type-I collagen-coated dish. Therefore, carbon negative-ion implantation into polystyrene at 5 – 20 keV with $2\times10^{15}$ – $3\times10^{15}$ ions/cm$^2$ gave the same effect as type-I collagen coating for cell culture of PC12h . There was a few data at low dose of $1\times10^{14}$ – $3\times10^{14}$ ions/cm$^2$. Prior to the small number of PC12h cells with weak adhesion strength on the $C^-$-implanted SCPS at these low doses as described in section 5.2.1, therefore, these cells were easily removed during replacement of the culture medium. Then, there was no data for the neurite outgrowth of PC12h cells on the $C^-$-implanted SCPS at low dose such as $1\times10^{14}$ – $3\times10^{14}$ ions/cm$^2$ after 4-day culture for some energy.

The observation of neurite outgrowth for each day showed that PC12h cells started to differentiate their cell bodies to extend the neurite after supplement NGF within 2 h, so the average neurite-length within 2 h was 10 – 20 μm as the same length as the cell body. Data are shown in Fig. 5.14. After culturing with NGF for 1 and 2 days, the longer neurite length was obtained. The average neurite-length growth increased with an increase in day-by day, and the growth decreased at day 2. This was considered to be the saturation of the average neurite-length growth after culturing more than 2 days due to the cell ability to differentiation themselves and the outgrowth of neurite reaching the other cells. The average neurite-length growth for PC12h cells on the $C^-$-implanted SCPS at $3\times10^{15}$ ions/cm$^2$ and 5 – 20 keV were the same that corresponding to the nearly same contact angle at this dose. Moreover, they were similar to the outgrowth of the cells cultured on type-I collagen-coated dish.

The frequency distribution of neurite outgrowth from PC12h cells on the $C^-$-implanted SCPS at $3\times10^{15}$ ions/cm$^2$ and 10 keV after 2-day supplement with NGF is shown in Fig. 5.15. Neurite of PC12h cells grew into two ways; one is the continuous length extension from the

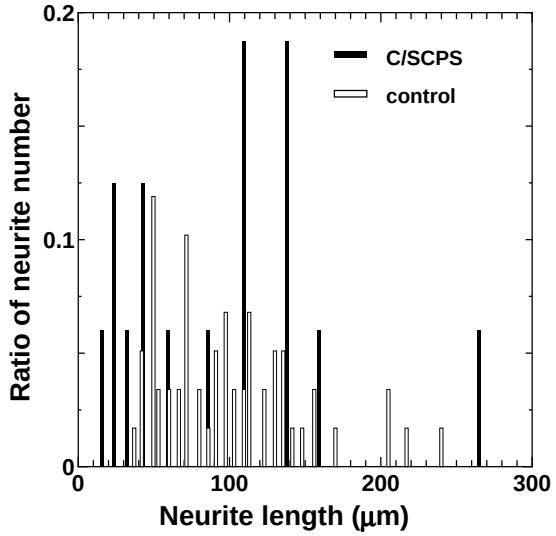


Fig. 5.15 Frequency distribution of neurite outgrowth on the $C^-$-implanted polystyrene films at 10 keV and $3\times10^{15}$ ions/cm$^2$ and on a reference dish after 2-day NGF supplement.

previous culture day, and the other is the new differentiation from the cell body. The obtained neurite from the former had very long length with many branches on the main neurite, while that from the latter had only the extended lengths with 10 to 15 μm from the cell body. From Fig. 5.15, 90% of frequency distribution of the average length were around 25 – 170 μm for both cells cultured on the $C^-$-implanted SCPS at 10 keV and $3\times10^{15}$ ions/cm$^2$ and on the control. The highest frequency in the length for the $C^-$-implanted SCPS was obtained around 110 and 140 μm, while that for control was around 50 μm. It means that almost all neurite lengths on the $C^-$-implanted SCPS at 10 keV with $3\times10^{15}$ ions/cm$^2$ increased by continuous length extension from the previous culture day. Only five percents of the distribution for the average neurite length were from the new differentiation from the cell body.

From all observation, neurite outgrowth property of PC12h cells on the $C^-$-implanted SCPS could be controlled by the ion implantation conditions such as dose and energy. The suitable dose for the neurite outgrowth property was in the order of $10^{15}$ ions/cm$^2$, and the best condition was around $2\times10^{15}$ – $3\times10^{15}$ ions/cm$^2$, as the same dose for the good adhesion properties as described in section 5.2. At this dose, the maximum value of the average neurite length of cells was equal to that of cells on control of type-I collagen-coated dish. Then, the carbon negative-ion implantation at the best conditions gave the same effect as type-I collagen coating.

## 5.6 Immobilization of Cell Body and Neurite on the Minimum Modified Area

The effective minimum modified implanted line width of the $C^-$-implanted SCPS for immobilization of cell body and neurite outgrowth was studied by the cultivation of PC12h cells on wedge-shape pattern of the $C^-$-implanted SCPS. Carbon negative ions were implanted into SCPS at $3\times10^{15}$ ions/cm$^2$ with the various energies of 5 – 20 keV through the special micro-pattern mask with the various triangle apertures from 0 – 40 μm in width (Fig. 5.16 (a)). Two line-and-space pattern masks were used to compose a wedge-shape pattern by lapping together with a very small angle. This lapping is shown in Fig. 5.16 (b). After the implantation, the samples were set into PS dish and were sterilized, and PC12h cells were cultured on the samples. The procedures were the same as described in sections 5.2 and 5.3. The type-I collagen-coated TCPS was also tested as a control. The cells were cultured totally for 4 days. Then, the cell-adhesion properties and neurite-outgrowth properties of PC12h cells on the $C^-$-implanted SCPS were observed by phase contrast microscope (CK2, Olympus).

After culturing for 4 days in total, PC12h cells were observed on the implanted region with cells hanging into the unimplanted region next to the adjacent implanted region for all of the implanted samples. All of the neurite outgrowth were seen on the implanted region. Fig. 5.7 shows phase-contrast micrographs of PC12h cells with neurite outgrowth on two area parts

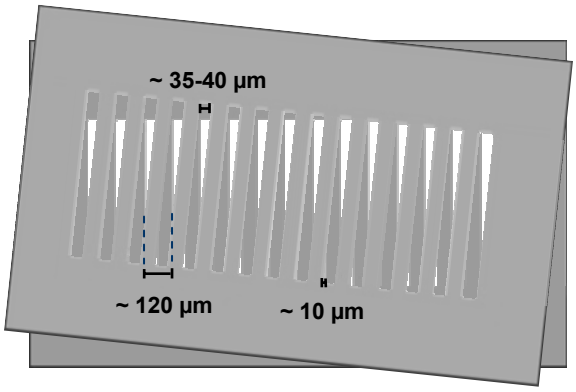


(a) A special micro-pattern mask

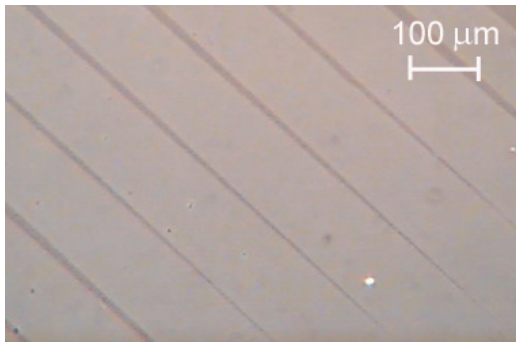


(b) The patterned surface

Fig. 5.16 A special micro-pattern mask: (a) schematic diagram of a special micro-pattern mask from the alignment of two original micro-pattern masks; and (b) phase contrast micrograph of the patterned surface from a special micro-pattern mask.

having different line widths at the implanted pattern at 10 keV and $3\times10^{15}$ ions/cm$^2$. A large number of cell group and their extended neurite along the pattern were found on the implanted region of about 20 – 35 μm in width as shown in Fig. 5.17 (a). On the very narrow implanted pattern, small amount of single cell and their extended neurite were observed on the implanted region of about 7 – 10 μm in width as shown in Fig. 5.17 (b). PC12h cells around the narrowed-implanted region could adhere and then differentiated on this boundary areas.

Although, the size of PC12h cells is about 18 μm, the cells could adhere on the narrowed-implanted region than the cell size. This reason was considered to be due to the

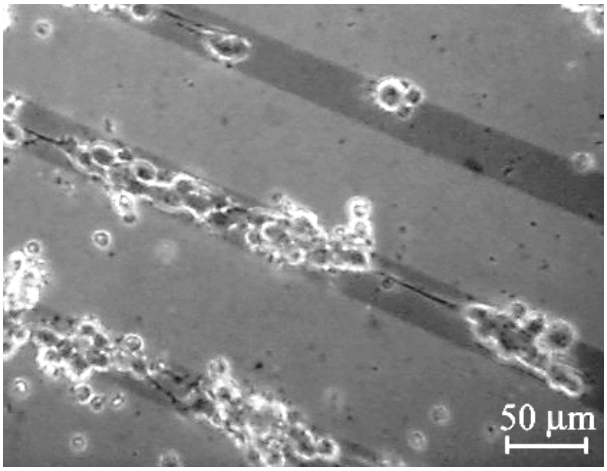


(a) 20 – 35 μm in width of C/SCPS (10 keV)

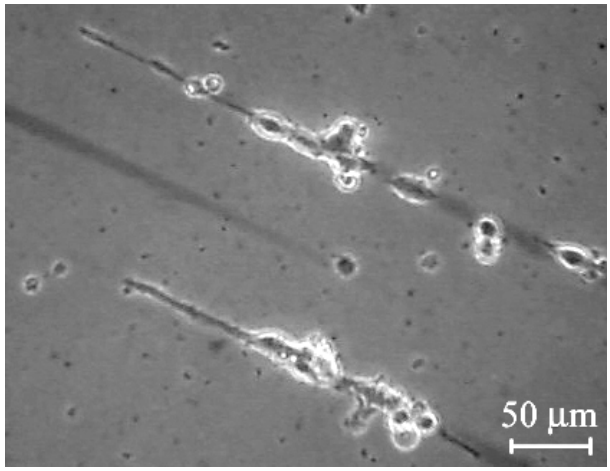


(b) 7 – 10 μm in width of C/SCPS (10 keV)

Fig. 5.17 Phase-contrast micrographs of PC12h cells and neurite after NGF supplement for 2 days on the $C^-$-implanted SCPS at $3\times10^{15}$ ions/cm$^2$ and 10 keV as a function of line width: (a) 20 – 35 μm in width; and (b) 7 – 10 μm in width.

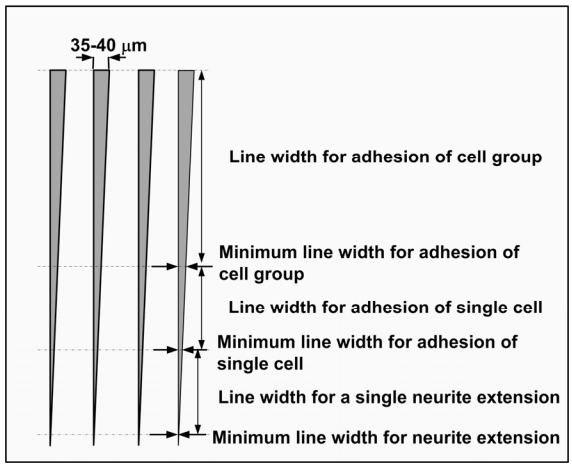


Fig. 5.18 Classification of modified-line width for cell attachment and neurite extension.

adsorption of the extracellular matrix (ECM) on the $C^-$-implanted SCPS. PC12h cells actually required such ECM on surface as a 'footing' site for their adhesion. Therefore, only some parts of cell adhered to the surface through anchoring of the cell receptor on the adhesive protein. As described in Chapter 4, the protein adsorption properties were improved by carbon negative-ion implantation. In addition, the proteins were also adsorbed on the boundary area next to the implanted region, resulting in the adhesion of cells on this boundary with hanging to the cells on the implanted region as shown in section 5.4. Therefore, the adhesion of PC12h cells on the narrowed-implanted region was considered to be due to the cell receptors almost anchored with the adhesive proteins on the implanted region and to some of them might anchor with the adhesive protein on the boundary area.

From the results, the modified line width of the $C^-$-implanted SCPS for cell adhesions and neurite outgrowth could be evaluated by the number of adhered cells and neurite outgrowth along the implanted region and it is as shown in Fig. 5.18. Three significant widths were existed, which are the minimum width for adhesions of a single cell, of the cell group and of the neurite. On the $C^-$-implanted SCPS at 10 keV and at $3\times10^{15}$ ions/cm$^2$, it was found that there existed three significant widths; one was the minimum width of 7 μm for single cell adhesion, the other was the minimum value of 20 μm for the cell group adhesion, and another was the minimum value of 5 μm for the neurite extension.

Fig. 5.19 shows the frequency distribution of adhere cells depending on the line width of the $C^-$-implanted SCPS at 10 keV and at $3\times10^{15}$ ions/cm$^2$. A lot of cell groups were found on the modified-implanted width in the range of 15 – 40 μm.

At other energies, the minimum line width for cell group adhesion was the same as the results at 10 keV. Fig. 5.20 shows the minimum line widths for both the single cell adhesion and their neurite outgrowth on the $C^-$-implanted SCPS as a function of implantation energy in the

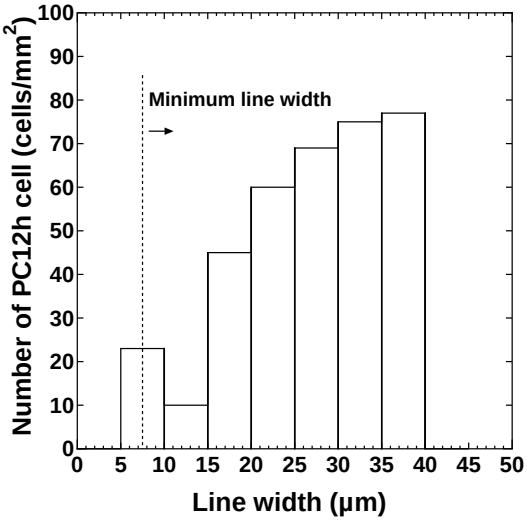


Fig. 5.19 Frequency distribution of cell adhesion on the different line width of the $C^-$-implanted SCPS at 10 keV and $3\times10^{15}$ ions/cm$^2$ after 2-day NGF supplement.

range of 5 – 20 keV. Both of the minimum line width showed a little decrease dependence on the ion energy in the range of 5 – 20 keV. The minimum line widths of $C^-$-implanted SCPS at 5 keV for the properties were the same as that of $C^-$-implanted SCPS at 10 keV. While those of $C^-$-implanted SCPS at 15 – 20 keV for the properties were 5 and 3 μm, respectively.

In case of neurite outgrowth, both of the maximum and average neurite lengths of cells on control were longer than those of group cells on the modified $C^-$-implanted region of 15 – 35 μm in width as shown in Fig. 5.21. The neurite length on the modified-region width a little

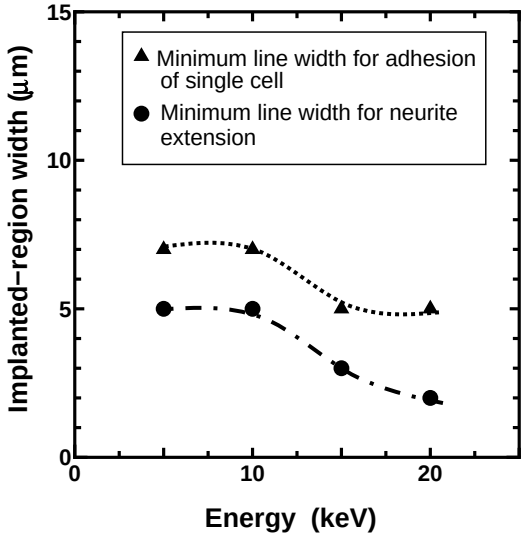


Fig. 5.20 Minimum line width for cells cultured on $C^-$-implanted SCPS with $3\times10^{15}$ ions/cm$^2$ at 5 – 20 keV.

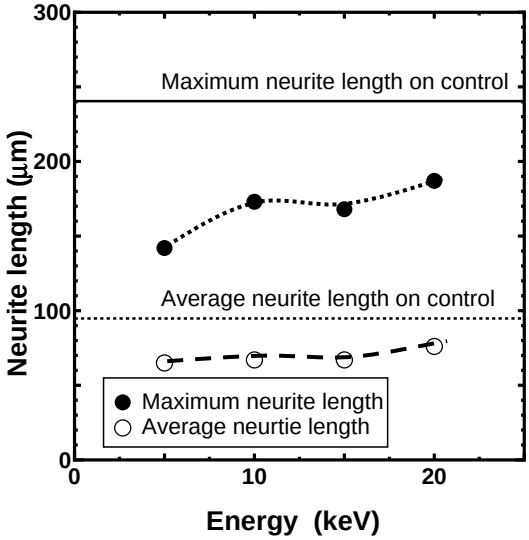


Fig. 5.21 Neurite length of cells cultured on modified-region width of $C^-$-implanted PS at $3\times10^{15}$ ions/cm$^2$ as a function of energy and on control.

increased with an increase in the energy. Especially, the maximum neurite length increased from 142 to 187 μm with an increase in the energy from 5 to 20 keV. Although the contact angle of $C^-$-implanted SCPS films a little decreased with an increase in ion energy as presented in Chapter 3, the ion-beam energy did not significantly affect to the cell adhesion and neurite outgrowth on the width region wider than 50 μm as shown in sections 5.2 and 5.5. However, this small lowering of contact angle affected to the cell adhesion and neurite outgrowth on much narrowed implanted region width of $C^-$-implanted SCPS because the adhesion area was much smaller than cell size. The lower angle, the more ECM adsorption should be obtained, corresponding to the protein adsorption properties in Chapter 4. The outgrowth of neurite concerns to the cell condition, including the adhesion property, and neurite also requires ECM as a 'footing' site. Since the ion energy affected to the adhesion of cells and ECM adsorption, it also affected to the neurite extension. Therefore, the modified line width of $C^-$-implanted SCPS and the ion-beam energy affected the nerve-like cell-affinity properties such as the adhesion and neurite outgrowth. As a result, the line width modification of the implanted region could clearly affect the immobilization of the cell-body adhesion and neurite outgrowth. The suitable widths for guidance and the immobilizations of cell-body adhesion and the neurite outgrowth were about 20 and 5 μm, respectively. The best energy condition for the adhesion and neurite outgrowth on the modified-line width was at 20 keV.

## 5.7 Neuron Network on Carbon Negative-Ion Implantation

The carbon negative-ion implantation into SCPS for patterning the neuron network was studied by culture of PC12h cells on a grid pattern implanted region of the $C^-$-implanted SCPS. Carbon negative ions were implanted into SCPS at 10 keV and at doses of $1\times10^{15}$ – $3\times10^{15}$ ions/cm$^2$ through the micro-pattern mask consisting of many slit apertures with 50-μm width and 150-μm spacing. Such these doses gave the suitable properties of the cell adhesion and the neurite outgrowth. The other operation condition of residual gas pressure and ion-current density were those described in Chapter 2. After the implantation, the samples were rotated at 90° on the sample holder and were again implanted at the same condition for obtaining the grid pattern. The samples were set into PS dish and were sterilized, and PC12h cells were cultured on the samples. The procedures were the same as described in sections 5.2 and 5.3. In this experiment, the number of plated cells was changed to about $7.4\times10^3$ cells/dish. The cells were cultured totally for 4 days. The patterns of the cell adhesion and neurite outgrowth on the $C^-$-implanted SCPS were observed by phase contrast microscope (CK2, Olympus).

Figs. 5.22 and 5.23 show the patterned adhesions of PC12h cells after culturing 2 days on $C^-$-implanted SCPS at 10 keV and doses of $1\times10^{15}$ and $3\times10^{15}$ ions/cm$^2$, respectively. At dose of $1\times10^{15}$ ions/cm$^2$, although almost 80% of plated PC12 cells adhered on the implanted region along the grid pattern, about 20% of them were floating and adhered on the boundary area, resulting in the weak pattern as shown in Fig. 5.22. After replacement of the culture medium, however, the clear patterned adhesions of PC12h cells on the $C^-$-implanted SCPS at 10 keV and

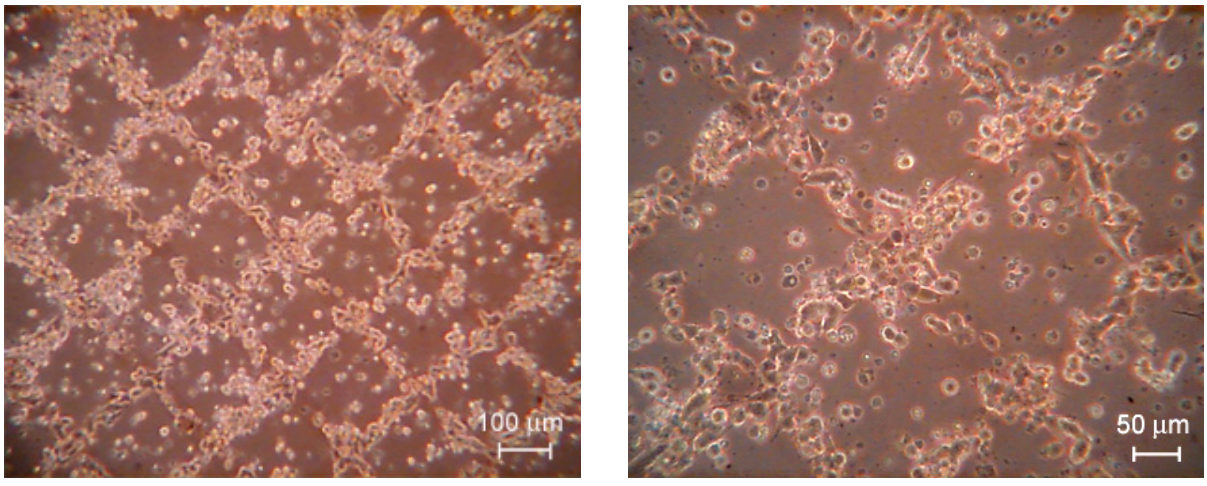


(a) 10 × 10 magnification (b) 10 × 20 magnification

Fig. 5.22 Phase-contrast micrographs of PC12h cells on the $C^-$-implanted SCPS at 10 keV and $1\times10^{15}$ ions/cm$^2$ as a grid pattern after cultured for 2 days with magnifications of: (a) 10×10; and (b) 10×20.

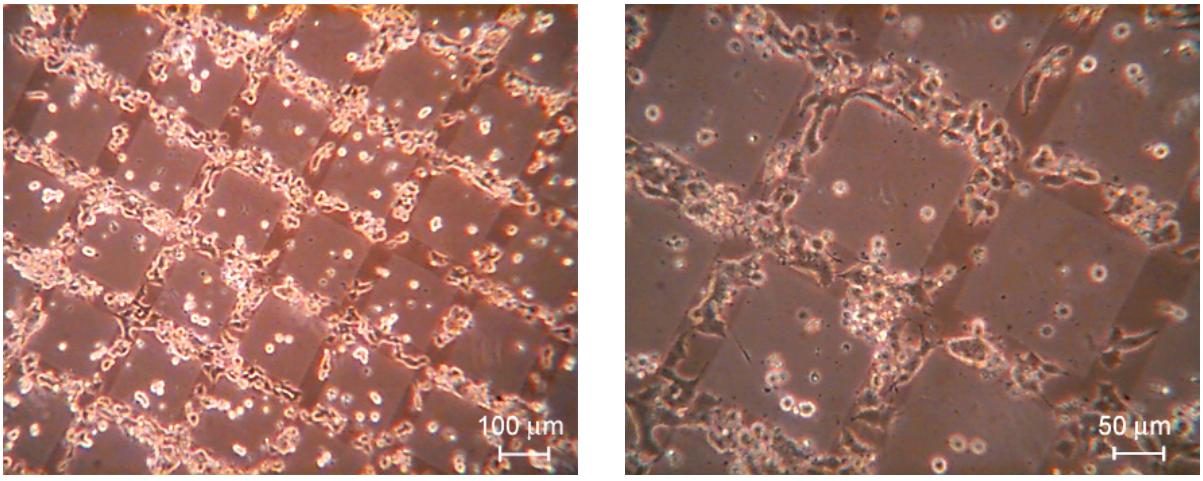


(a) 10 × 10 magnification (b) 10 × 20 magnification

Fig. 5.23 Phase-contrast micrographs of PC12h cells on the $C^-$-implanted SCPS at 10 keV and $3\times10^{15}$ ions/cm$^2$ as a grid pattern after cultured for 2 days with magnifications of: (a) 10×10; and (b) 10×20.

$1\times10^{15}$ ions/cm$^2$ was observed (data not shown here). At dose of $3\times10^{15}$ ions/cm$^2$, more than 93% of plated PC12h cells adhered on the implanted region along the grid pattern with only 7% of floating cells after culturing 2 days as shown in Fig. 5.23.

Figs. 5.24 and 5.25 show the patterned adhesion with neurite outgrowth of PC12h cells after culturing with NGF for 2 days on $C^-$-implanted SCPS at 10 keV and doses of $1\times10^{15}$ and $3\times10^{15}$ ions/cm$^2$, respectively. In Fig. 5.24, almost clear patterned adhesions of PC12h cells on

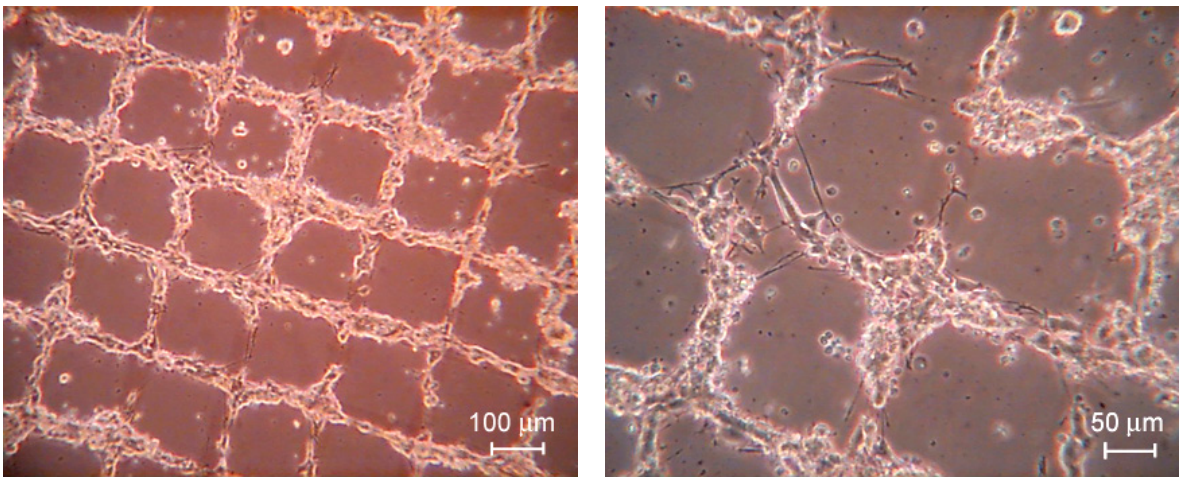


(a) 10 × 10 magnification (b) 10 × 20 magnification

Fig. 5.24 Phase-contrast micrographs of PC12h cells on the $C^-$-implanted SCPS at 10 keV and $1\times10^{15}$ ions/cm$^2$ as a grid pattern after NGF supplement for 2 days with magnifications of: (a) 10×10; and (b) 10×20.

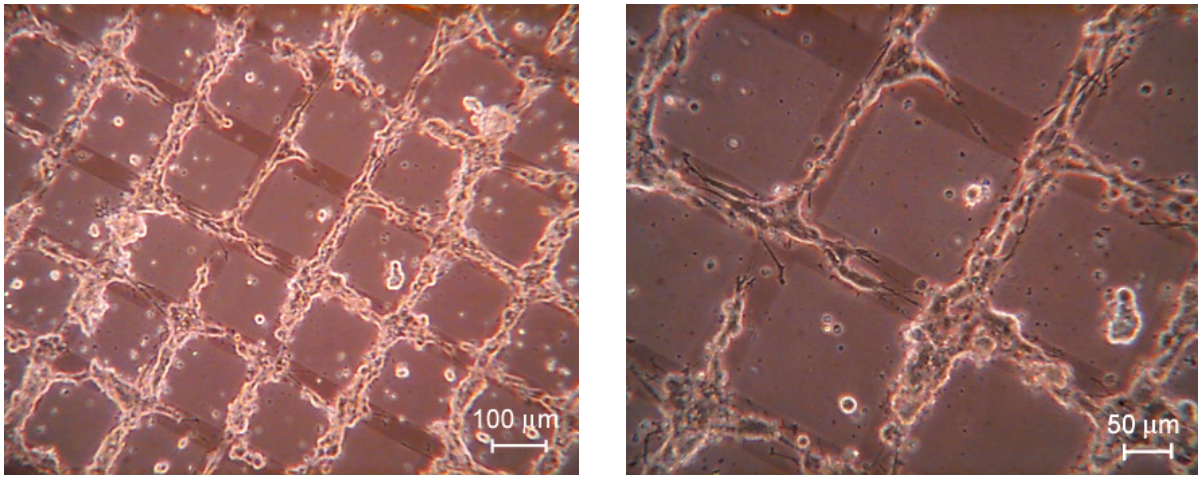


(a) 10 × 10 magnification (b) 10 × 20 magnification

Fig. 5.25 Phase-contrast micrographs of PC12h cells on the $C^-$-implanted SCPS at 10 keV and $3\times10^{15}$ ions/cm$^2$ as a grid pattern after NGF supplement for 2 days with magnifications of: (a) 10×10; and (b) 10×20.

the implanted region at dose of $1\times10^{15}$ ions/cm$^2$ could be observed, but some outgrowth of neurite on the unimplanted region between the cross implanted region were found, leading to pull some cell-bodies out from the implanted region. This was considered to be due to the small selective adsorption properties of adhesive protein on the implanted region at this dose as shown in Chapter 4. In Fig. 5.25, while the fine patterned adhesions and neurite outgrowth of PC12h cells only on the implanted region at dose of $3\times10^{15}$ ions/cm$^2$ could be observed. No outgrowth of neurite on the unimplanted region between the cross implanted region was observed. Neurite outgrowth adhered only on the implanted region. This was considered to be due to higher selective adsorption properties of adhesive protein and the enough of the protein adsorption on the implanted region at this dose. On the cross-section area of the implanted region, the selective adhesion property still remained, even if the dose amount was to $6\times10^{15}$ ions/cm$^2$. As a result, the clear patterned adhesion of PC12h cells on the $C^-$-implanted SCPS could be obtained at $3\times10^{15}$ ions/cm$^2$.

## 5.8 Summary

The nerve-like cells of rat adrenal pheochromocytoma cells (PC12h) were cultured on the $C^-$-implanted polymeric surfaces of SCPS and SR to find out the suitable implantation conditions and the suitable protein coating for patterning neuron adhesion in neuron network application. Results showed that the carbon negative-ion implantation into polymeric surfaces of SCPS and SR could improve and control the adhesion properties of PC12h cells on the implanted

region. The suitable dose and energy implantations for the selective adhesion properties of cells were dose order of $10^{15}$ ions/cm$^2$ and 10 – 20 keV. The best condition was at $3\times10^{15}$ ions/cm$^2$ and 10 keV. As for the additional protein coating with the cell-adhesion properties, the additional protein coating on the implanted surface at the best implantation condition improved the cell adhesion property, and only the coating with fibronectin at 1 μg/ml on the $C^-$-implanted SR more improved the cell adhesion properties with selectivity. While the coating with collagen at 10 μg/ml on the $C^-$-implanted surfaces of SCPS and SR improved the cell adhesion properties but degraded the selective adhesion properties. Neurite outgrowth properties of PC12h cells could be controlled by carbon negative-ion implantation of ion dose and energy at the same dose and energy for the selective adhesion properties. The ion dose, ion energy and implanted line width were the important parameters for patterning and immobilization of cell adhesion and neurite outgrowth. The suitable line width for adhesion of the cell-body and for only outgrowth of neurite on the $C^-$−implanted SCPS was about 20 and 5 μm, respectively. As for the cell adhesion on the grid pattern of the $C^-$-implanted SCPS at 10 keV, the suitable dose was at $3\times10^{15}$ ions/cm$^2$. From all results, the adhesion patterning of nerve-like cells on the $C^-$-implanted polymeric surfaces of SCPS and SR could be achieved. However, some characteristics of the nerve-like cells can not compare with those of real neuron as described in section 5.1. Therefore, the culture of real neuron is required to study the suitable condition for patterning adhesion in neuron network application. The study of neuron culture from the brain neuronal cells on the pattern adhesion by carbon negative-ion implantation will be described in Chapter 6. In addition, the culture of the multipotential mesenchymal stem cells and its differentiation into neurons on the $C^-$-implanted polymeric surfaces of SCPS and SR will be described in Chapter 7.

## References


[1] Y. Suzuki, M. Kusakabe, J.S. Lee, M Kusakabe, M. Iwaki, and H. Sasabe, “Endothelial Cell Adhesion to Ion Implanted Polymers”, Nucl. Instrum. Methods Phys. Res. B, vol. 65, pp. 142-147, March 1992.

[2] H. Tsuji, H. Satoh, S. Ikeda, N. Ikemoto, Y. Gotoh, and J. Ishikawa, “Surface Modification by Silver-Negative-Ion Implantation for Controlling Cell-Adhesion Property of Polystyrene”, Surf. Coat. Technol., vol. 103-104, pp. 124-128, 1998.

[3] H. Tsuji, H. Satoh, S. Ikeda, Y. Gotoh, and J. Ishikawa, “Contact Angle Lowering of Polystyrene Surface by Silver-Negative-Ion Implantation for Improving Biocompatibility and Introduced Atomic Bond Evaluation by XPS”, Nucl. Instrum. Methods Phys. Res. B, vol. 141, pp. 197-201, 1998.

[4] H. Tsuji, H. Satoh, S. Ikeda, S. Ikemura, Y. Gotoh, and J. Ishikawa, "Negative-Ion Beam Surface Modification of Tissue-Culture Polystyrene Dishes for Changing Hydrophilic and Cell-Attachment Properties", Nucl. Instrum. Methods Phys. Res. B, vol. 148, pp. 1136-1140, 1999.

[5] H. Sato, H. Tsuji, S. Ikeda, N. Ikemoto, J. Ishikawa, and S. Nishimoto, "Enhanced Growth of Human Vascular Endothelial Cells on Negative-Ion (Ag-)–Implanted Hydrophobic Surfaces", J. Biomed. Mater. Res. vol. 44, pp. 22-30, 1999.

[6] H. Shin, S. Jo, and A.G. Mikos, "Synthetic Biodegradable Polymer Networks Modulating Marrow Stromal Osteoblast Adhesion", in **Biomaterials for Drug Delivery and Tissue Engineering**, S. Mallapragada, M. Tracy, B. Narasimhan, E. Mathiowitz, and R. Korsmeyer, Eds., MRS Symposium Proceedings, vol. 662, Materials Research Society, Warrendale, 2001, pp. LL6.5.1-LL6.5.6, 2001.

[7] A. Kadner, Simon P. Hoerstrup, G. Zund, K. Eid, C. Maurus, S. Melnitchouk, J. Grunenfelder, M.I. Turin,"A New Source for Cardiovascular Tissue Engineering: Human Bone Marrow Stromal Cells", Eur. J. Cardiothorac. Surg., vol. 21, pp. 1055-1060, 2002.

[8] H. Tsuji, H. Sasaki, Y. Utsumi, H. Sato, Y. Gotoh, J. Ishikawa, "Extracellular Matrix Absorption Properties of Negative Ion-Implanted Polystyrene, Polydimethylsiloxane and Poly-Lactic Acid", Surf. Coat. Tech. 158–159, pp. 620 – 623, 2002.

[9] B.E. Tuch, "Stem Cells--a Clinical Update", Aust. Fam. Physician, vol. 35 (9), pp. 719-21, 2006.

[10] R.L. Gardner, "Stem Cells: Potency, Plasticity and Public Perception", J. Anat., vol. 200 (3), pp. 277-282, 2002.

[11] L.A. Greene, A.S.Tischler, "Establishment of a Noradrenergic Clonal Line of Rat Adrenal Pheochromocytoma Cells which Respond to Nerve Growth Factor", Proc. Natl. Acad. Sci. USA, Jul 1976, vol. 73(7), pp. 2424-2428, 1976.

[12] H. Lodish, A.Berk, L. S. Zipursky, P. Matsudaira, D. Baltimore and J. Darnell, **Molecular Cell Biology**, 4th Ed.,W.H. Freeman eds., New York: W.H. Freeman & Co Ltd, 2000.

# Chapter 6

# Brain Neuronal Cell Patterning on Modified Polymeric Surface by Negative-Ion Implantation

The brain neuronal cells or the central nerve in the primary culture need the positive-charge sites of the –NH– groups on the substrate surface as a binding site [1-3]. However, the modified polymeric surfaces of polystyrene and silicone rubber from the carbon negative-ion implantation technique have only the negative-charged sites of hydroxyl and carbonyl groups. The brain neuronal cells could not adhere on them and on the non-modified surfaces. The positive-charge sites can be enhanced by coating with a polycation polymers of poly-D-lysine (PDL) and polyethyleneimine (PEI) on the polymeric surfaces [1-4]. Therefore, the patterning of positive-charged site for brain neuronal cell adhesion is required. As described in Chapter 4, the selective adsorption ratios of PDL were not high, so that the neuronal cells could not respond such a difference. Then, the idea for patterning neuron adhesion is an application of the degradation of PDL layer coated on the polymeric surfaces by using negative-ion implantation. In this chapter, the pattern adhesions of brain neuronal cells on the positive-charged sites of PDL layer on spin-coated polystyrene (SCPS) modified by carbon negative-ion implantation were studied, after the fist section of 6.1 about brief descriptions of neuronal cells.

## 6.1 Neuron and Brain Neuronal Cells [5]

Neuron is a cell specialized to conduct electrochemical impulses called nerve impulses or action potentials. A typical neuron comprises a soma (cell body), several dendrites of short-branched fibers and an axon of long nerve fiber. In mammal, three major classes of neurons in the function are interneurons, sensory neurons and motor neurons. Details are as follows: (1) The interneurons in the central nervous system (CNS) are located in the spinal cord and the brain. Each of them has profusely branched dendrites for the function for receiving signal at synapses from the other neurons and a single long axon for the function of transmitting the signal at its terminus to other neurons. (2) The sensory neurons function to carry the nerve impulses from the receptor to the CNS of the brain and the spinal cord. Their cell bodies are located in the dorsal root ganglion near the spinal cord and their axons branches just after leaving the cell body. The

peripheral branch receives the nerve impulse from the axon of the sensory neurons to their sensory-neuron cell body and the central branch carry from the nerve impulse resulted in the cell body to the CNS. (3) The motor neurons function to innervate a muscle cell. Typically, the motor neurons have a single long axon extending from the cell body to the effector cell. In mammalian motor neurons, many electrically insulating sheaths of myelin usually cover all parts of the axon except at the nodes of Ranvier and the axon terminals.

In the operation system, nerve system can be classified into two types of the central nervous system (CNS) and the peripheral nervous system (PNS). The CNS consists of the spinal cord and the brain. The PNS consists of the sensory neurons and the motor neuron.

In this research, the neuron adhesion patterning on the polymeric surfaces by using carbon negative-ion implantation were confirmed by the cultivation of the real neurons of the CNS and the PNS. In this chapter, the patterned adhesion of the brain neuronal cells in the CNS was studied by culturing two kinds of the brain neuronal cells. Details of the brain neuronal cells, which were used, were described in this section. The adhesion patterns of the PNS neuron on the $C^-$-modified polymeric surfaces of SCPS and silicone rubber were studied by culturing and differentiating the mesenchymal stem cells. Details will be described in Chapter 7.

## Brain Neuronal Cell Lines

Brain neuronal cells, which form the central nervous system, include mostly neurons and glial cells [6]. Neurons or nerve cells perform the processing and storage of information such as action potential involved in brain function [6]. They communicate each other via synapses, where the axon terminal of one cell impinges upon a dendrite or soma of another [6]. Glial cells or neuroglias (glia) function to support in space and provide nutrition to neurons [6]. The characteristics and function of brain neuronal cells depend on the derived part, age and specie of the animal. The cells derived from the embryo have the great function for outgrowth of axon and dendrite to form the neuron network, comparing to those from the newborn baby and adult. However, the adhesion of the brain neuronal cells derived from all different age use the same mechanism. Then, the brain neuronal cells derived from newborn one could be used to study the adhesion of the brain cells.

In the experiment, two cell lines of newborn mouse brain neuronal and rat embryo brain cortex neuronal cells were cultured. At first, the newborn mouse brain neuronal cells were used to study the acceptable concentration of PDL on the $C^-$-implanted SCPS for the good adhesion properties. The rat embryo brain cortex neuronal cells were then used to study the suitable concentration of PDL for the patterned adhesion with the axon and dendrite outgrowth on the PDL surface patterned by carbon negative-ion implantation. The details of both of the brain

neuronal cells derived are as follows:

### 6.1.1 Newborn Mouse Brain Neuronal Cell

The newborn mouse brain neuronal cells were gathered from the different mice of 1-day newborn mouse and were cryopreserved by Dr. Junji Nakamura, Kyoto Univ. Hospital. The cells were derived from cortex and hippocampus of the newborn mouse. The preferred substrate is the polyethyleneimine-coated tissue culture polystyrene dish (PEI-coated TCPS) at concentration of 0.1% PEI in borate buffer saline. The primary culture of newborn mouse brain neuronal cells derived and immediately plated on the PEI-coated TCPS after 21 and 29 days *in vitro* are shown in Fig. 6.1. A lot of the single cell and small amount of neurospheres extended many axons (the long thick neurite) and dendrites (the short small branch neurite) as shown in Fig. 6.1(a), while the formation of brain tissue without outgrowth of axon and dendrite was found instead in Fig. 6.1(b). Thus, the newborn mouse brain neuronal cells showed both of the properties of the axon and dendrite outgrowth and the tissue formation, even in the cell culture *in vitro*. These cells could be used in the experiment of neuron adhesion.

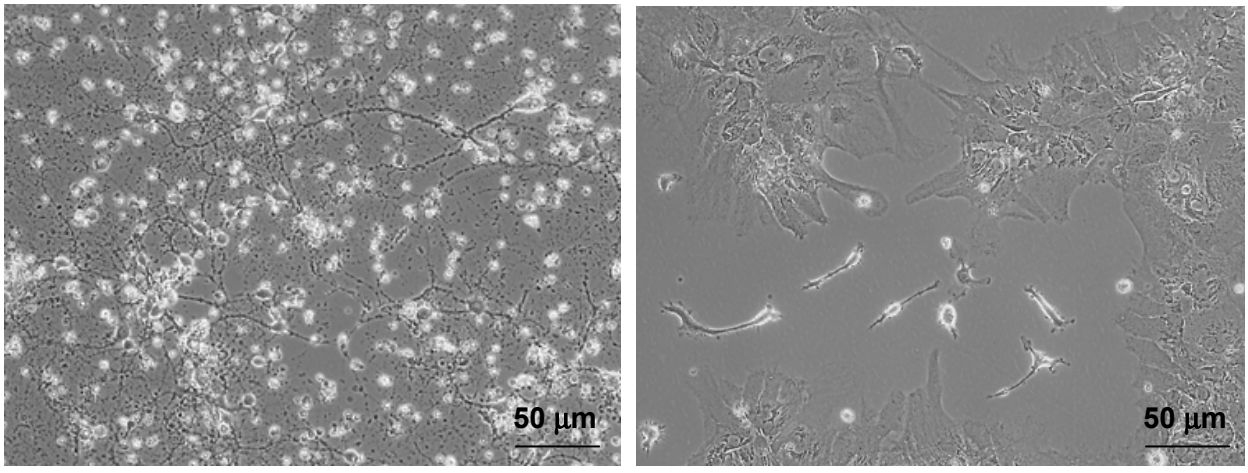


(a) 21 days *in vitro* (b) 29 days *in vitro*

Fig. 6.1 Primary culture of derived newborn mouse brain neuronal cells on PEI-coated TCPS after: (a) 21; and (b) 29 days *in vitro*.

### 6.1.2 Rat Embryo Brain Cortex Neuronal Cell

The rat brain cortex neuronal cells are obtained from a company of Cambrex bioscience Walkersville Inc. in catalog no. R-Cx-500. These cells were derived from rat embryo brain at 18 – 19 days. In usage, the company recommends the culture of this cell by using the coating

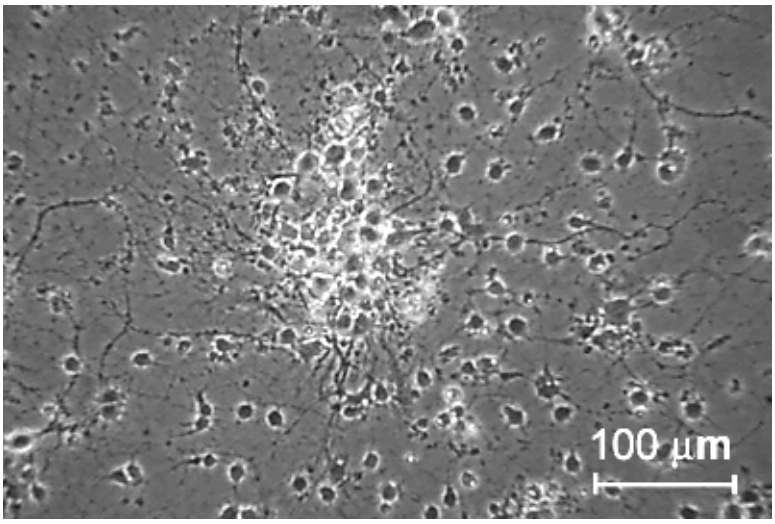


Fig. 6.2 Primary culture of rat brain cortex neuronal cells on PDL-coated TCPS after 16 days *in vitro*.

surface of the poly-D-lysine (PDL) with laminin at PDL concentration of 33 μg/ml in phosphate-buffered saline [7]. However, many researchers can success the cell culture by using alone coating surfaces of poly-D-lysine or poly-L-lysine [1-2]. The primary culture of rat embryo brain cortex neuronal cells on the PDL-coated TCPS at PDL concentration of 33 μg/ml after 16 days *in vitro* are shown in Fig. 6.2. The formations of neurite network are shown in Fig. 6.2. A lot of single cell and large size of neurospheres extended many axons (the long thick neurite) and dendrites (the short small branch neurite).

## 6.2 Carbon Negative-Ion Implantation and Degradation of PDL

As described in Chapter 3, the carbon negative-ion implantation can modify the surface by ion bombardment, sputtering the surface bonding to make the defect and then forming the oxygen functional group or the negative-charged site. Resulting from these phenomena, the idea of the carbon negative-ion implantation into the surface of PDL, which contains the positive-charged sites of the –NH– groups, to degrade the adhesion property of brain neuronal cell was created. The carbon negative-ion implantation was expected to decrease the number of the positive-charged sites and to increase the number of the negative-charge sites on PDL. The degradation of the adhesion pattern for the brain neuronal cells was expected to occur.

To confirm the idea, the $C^-$-implanted PDL surfaces were analyzed by XPS. The samples were prepared by the following process: (1) The SCPS film were dipped in the PDL in PBS solvent at the concentration of 33 μg/ml for 1 h and were dried at room temperature for 2 h. (2) Carbon negative ions were then implanted into the PDL-coated SCPS at energy of 10 keV

and ion doses of $3\times10^{14}$ and $3\times10^{15}$ ions/cm$^2$ as a half moon shape as shown in Chapter 4. (3) The unimplanted and $C^-$-implanted PDL surfaces were analyzed by XPS for evaluation of the remained PDL adsorption with the same analysis conditions as described in Chapter 4.

Modifications of atomic bonding state on the $C^-$-implanted PDL are shown in Fig. 6.3. From Fig. 6.3 (a), the main peak of XPS survey spectrum for unimplanted area almost was C 1s. Very small peaks of N 1s and O 1s were observed on both of the unimplanted and implanted surfaces, although the monomer structure of PDL contains nitrogen and oxygen atoms, excluding hydrogen atoms for about 22% and 11% per unit, respectively.

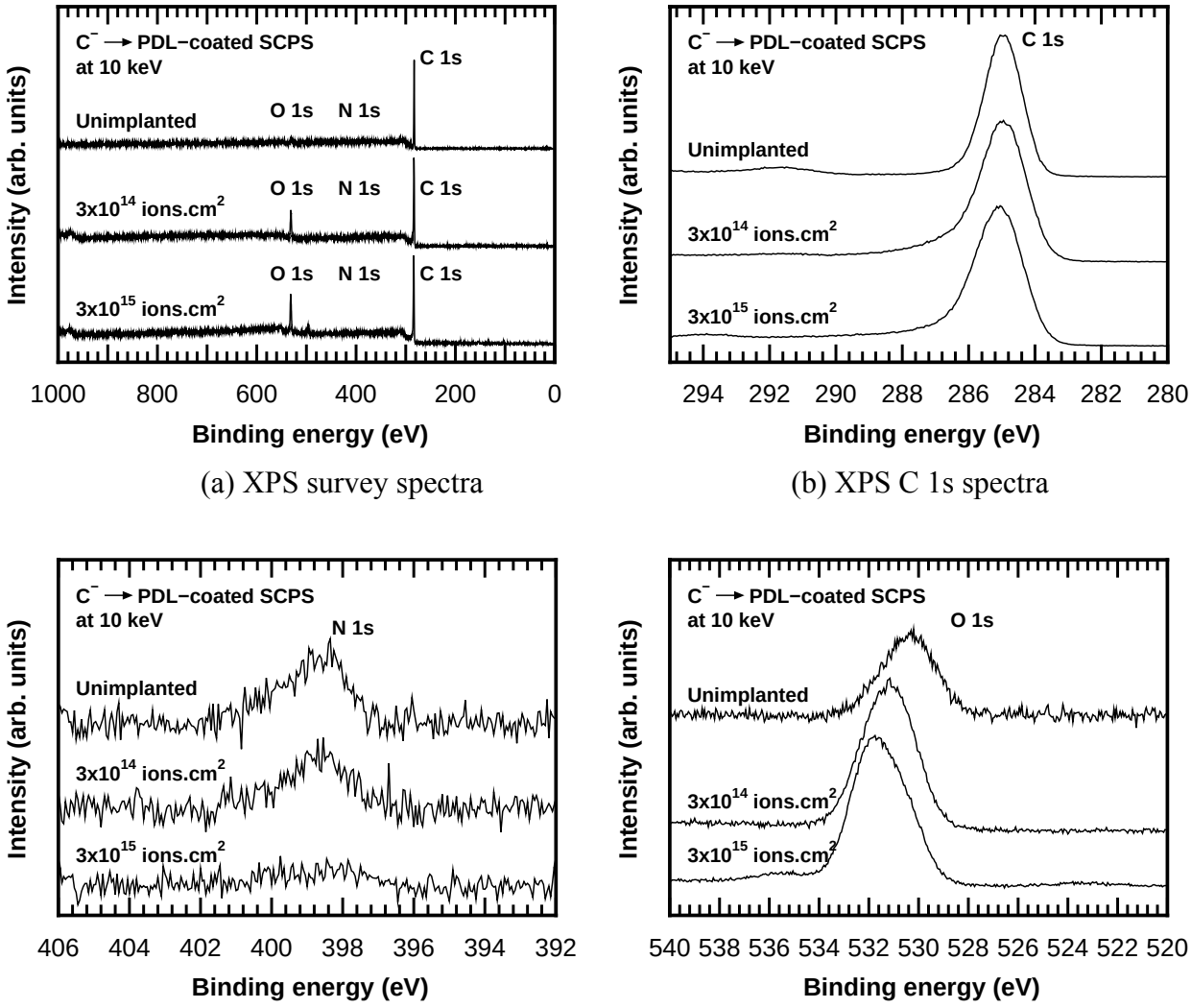


(a) XPS survey spectra

(b) XPS C 1s spectra

(c) XPS N 1s spectra

(d) XPS O 1s spectra

Fig. 6.3 XPS spectra of unimplanted and $C^-$-implanted PDL at 10 keV and $3\times10^{14}$ – $3\times10^{15}$ ions/cm$^2$ at the center implanted area: (a) survey spectra; (b) C 1s spectra; (c) N 1s spectra; and (d) O 1s spectra.

This is considered to be due to the following reasons; (1) very thinly coated PDL and (2) the decomposition of PDL during X-ray irradiation. In principle, the detected photoelectron within only 10 nm in depth can escape from the surface, so the depth resolution in XPS analysis almost is almost 10 nm at the maximum. From the results in Fig. 6.3 (b), the small peak of phenyl group, which is contained in the molecular form of polystyrene, at 291.6 eV in the XPS C 1s spectrum on the unimplanted area. That means the surface of SCPS could be observed during XPS analysis. Therefore, the very thinly layer of PDL less than 10 nm or the sparsely adsorption of PDL occurred. When considering to the decomposition of PDL during X-ray irradiation, the X-ray energy was 1486.6 eV that was much higher than the binding energy of the C-N bonds. So, the decomposition of the amino groups of PDL was possible. The binding energies of the other bonds of PDL were also much lower than the X-ray energy, but the X-ray irradiation did not affect the other atomic bond. Therefore, the small amount of nitrogen atom was considered from the thinly layer or the sparse adsorption of PDL.

In XPS survey spectra, the peak for O 1s gradually became clear in the spectra after increasing of the ion dose. Fig. 6.3 (b) shows a long tail around 285.0 eV in the XPS C 1s spectra and disappearance of the small peak of phenyl groups after the implantation. From the details in the XPS spectra of N 1s and O 1s in Figs. 6.3 (c) and (d), the nitrogen intensity decreased, contrastively the increase of oxygen intensity after carbon negative-ion implantation. The carbon negative ions cut all bonds of the carbon, the amine (C-NH), as well as the origin carbonyl (C=O), and sputtered them out. The dangling bonds of the carbon were then absorbed with oxygen atoms from the residual gas to form the oxygen functional groups of carbonyl (C=O) and hydroxyl (OH). That means the implantation decreased amount of the positive-charged sites and increased amount of negative-charged sites. The changes in the intensities were affected by the ion dose amount. After the implantation, the amount of nitrogen atoms decreased about 30% at dose of $3\times10^{14}$, and about 65% at dose of $3\times10^{15}$ ions/cm$^2$. The decrease of the amount of nitrogen atoms to about 50% is expected to occur at the implantation dose of $5\times10^{14}$ ions/cm$^2$.

As for evaluation, the carbon negative-ion implantation into the surface of positive-charged site material is promising for patterning neuron adhesion by the degradation effect. However, the results of XPS show the very thinly layer or the sparse adsorption of PDL on the non-treated surface of SCPS that might cause the sparse adhesion area. The suitable uniform layer of PDL for the clear neuron adhesion pattern is required. PDL prefer to be adsorbed on the hydrophilic surface as shown in Chapter 4. So, before coating the surface with PDL, the SCPS surfaces should be treated by using carbon negative-ion implantation. Then, the clear selectively patterned adhesion of the brain neuronal cells was obtained by the carbon negative-ion implantation into the uniform layer of PDL on the $C^-$-implanted SCPS. However, the suitable conditions of the PDL concentration for clearly selective uniform adhesion area and

the ion implantation for patterning non adhesion area were the concerned issues.

To solve the challenge issues, two experiments of brain neuronal cell culture were carried out. One is to find out the suitable PDL concentration of the coating solution to support a uniform adhesion as described in section 6.3. The other is to achieve the selective cell-adhesion pattern by culturing the real brain neuronal cells on the $C^-$-implanted PDL surface as described in section 6.4.

## 6.3 Effect of PDL Concentration on Brain Neuronal Cell-Adhesion Properties on PDL-Coated Modified Spin-Coated Polystyrene

In the study of the suitable coating concentration of PDL for the uniform layer, there are two concerned parameters; the PDL concentration and the surface wettability. As described in Chapter 4, the adsorption properties of PDL on the non-treated SCPS was not good. The small amount of PDL adsorbed on the non-treated SCPS increased with an increase in the concentration. The adsorption properties of PDL on the SCPS surface were improved by the carbon negative-ion implantation. The amounts of nitrogen atoms adsorption on the treated SCPS were higher than those on the non-treated one, and the different adsorption were almost 1.4 times for all coating concentrations of 0.5 – 50 μg/ml. Therefore, the surface treatment of SCPS was necessary to obtain a uniform layer of PDL. The amount of PDL adsorbed on the treated SCPS increased with an increase in the ion dose from $1\times10^{14}$ – $1\times10^{16}$ ions/cm$^2$ and saturated at dose from $3\times10^{15}$ ions/cm$^2$. The PDL adsorptions on the treated SCPS were improved by almost 1.4 times for all ion implantation doses of $1\times10^{14}$ – $1\times10^{16}$ ions/cm$^2$. So, in this work, the ion implantation dose of $3\times10^{15}$ ions/cm$^2$ was selected to modify the SCPS surface to be hydrophilic for the uniform adsorption of PDL.

### 6.3.1 Experiment

For finding out the suitable PDL concentration of the coating solution to support a uniform adhesion, the brain neuronal cells derived from newborn mouse were used to be cultured on the coating surfaces of PDL on the $C^-$-implanted SCPS. The description of the experiment for sample preparation, the primary culture process for the brain cells and the confirmation observation method are as follow:

## Sample Preparation

The SCPS surfaces were implanted by the carbon negative ions at 10 keV and $3\times10^{15}$ ions/cm$^2$ as a half moon shape area. The other operation condition of residual gas pressure and ion-current density were those described in Chapter2. After the implantation, the samples were sterilized by using the process as described in Chapters 5. The sterilized samples were dipped in the PDL solution in PBS solvent at the various concentrations of 1 – 33 μg/ml for 1 h. They were once rinsed by the sterilized DIW and were completely dried for 2 h at room temperature. The coated samples were fixed into the non-treated polystyrene dish (NTPS, Corning) by 0.33% agarose (Agarose 900, Dojindo Molecular Technologies, Inc.).

## Primary Culture Process

For the primary culture of the brain neuronal cells, the culture medium of the serum-free neurobasal medium (N-medium, Cat. no. 12348-017, lot no. #1214994, Gibco) containing 2% B-27 supplement (B27, Cat. no. 17504-044, lot no.#1219115, Gibco) were used. After fixing the sample, the culture medium was added into the dish. Then, the newborn mouse brain neuronal cells were cultured on the samples. The cryopreserved newborn mouse brain neuronal cells (courtesy of Dr. Junji Nakamura, Kyoto Univ. Hospital) were rapidly thawed by placing in a water bath pre-heated to 37℃. Then, the cells were gently transferred into a 15 ml centrifuge tube and the pre-warmed medium was immediately added onto the cells by drop-wise and rotating tube. The cell suspension was mixed by once pipetting and they were transferred to the sample dish, as well as on control dish of PDL-coated TCPS at 33 μg/ml. The cells were incubated for 4 h under 5% $CO_2$ at 37°C in incubator. After that, the cells started to adhere to surface. The medium was removed with leaving a small volume to ensure the wet condition, and the pre-warmed medium was then added. The cells were cultured for 22 days *in vitro*. The culture medium of each dish was exchanged by the fresh medium pre-warmed to 37°C every 4 days.

## Confirmation Observation

The adhesion properties of mouse brain neuronal cells on the PDL-coated surfaces of the $C^-$-implanted SCPS were observed by phase-contrast microscope (CK2, Olympus). Since the brain neuronal cells were compose of two cell lines; neuron and glial, the type of the adhered cells on the surface could not be classified by phase-contrast microscopy. To confirm the neuron adhesion properties of this newborn mouse brain neuronal cell, the immunofluorescent

techniques were applied. At 22 days *in vitro*, types of adhered cells were observed by fluorescent microscope (BX50, Olympus). Three different staining for identifications of the cell type, of the cell shape with their neurite outgrowth and of the adhered cell position were examined by using the different antibodies and dyes. The cell type was identified by the labeling of the neuron-specific enolase (NSE). The NSE is a glycolytic isoenzyme which is located in central and peripheral neurons and neuroendocrine cells. It can be used as an identifying molecular marker for all types of neurons [8]. The cell shape with their neurite outgrowth was identified by the labeling of the actin filaments (f-actin). The actin filaments or the fiber structures are the thin, flexible protein fibers formed by the polymerization of globular actin molecules, and they provide mechanical support, determine cell shape, and allow cell movement. Then, the staining of the actin filaments can be used as an identifying marker for determination of the cell shape. The adhered cell positions were identified by the labeling of the cell nucleus. The cells were coated with 1% agarose in PBS and were fixed with 4% formaldehyde in PBS for 5 min. Some parts of the cell membrane were dissolved with 0.2% Triton X-100 (335-01, Nacalai Tesque, Inc., Japan) in PBS for 10 min to allow the large dyne molecules access to the cell's interior. After the samples were rinsed twice with PBS, the cells were stained with polyclonal rabbit anti-NSE (Cat. no. 40500510, Quartett, Germany) in the bovine serum albumin (BSA, Cat. no. 309-00563, lot. no.#401-038, Wako Pure Chemical Industries Ltd., Japan) solution (5 mg BSA in 1 ml PBS) for 60 min, and then the excess of antibody were removed by rinsing three times with PBS. The labeled NSE was bound to fluorescent by the goat anti-rabbit-fluorescein isothiocyanate (FITC, Cat. no 234, Medical & Biological Laboratories, Japan) in BSA solution. The excess of this dye were removed by rinsing three times with PBS. The second staining for the f-actin was done with Texas Red-X phalloidin (Cat. no. T7471, Invitrogen, USA) in PBS for 45 min, then the samples were rinsed with PBS for three times. Finally, the cell nucleus were stained with 4', 6-Diamidino-2-phenylindole (DAPI, Sigma-aldrich, Japan) for 30 min, and rinsed with PBS for three times.

### 6.3.2 Results

From phase-contrast observation, after the newborn mouse brain neuronal cells were plated on the PDL surface for 4 h, no adhesion property was found. After 1 day *in vitro*, about 70% of the plated cells started to adhere on the PDL-coated surfaces of the $C^{-}$-implanted SCPS. After 2 days *in vitro*, some adhered cells presented the outgrowth of growth cone. After 4 days *in vitro*, the number of cell adhesions increased. The adhesion of single cell and some small neurospheres were found. No outgrowth of axon and dendrite was found.

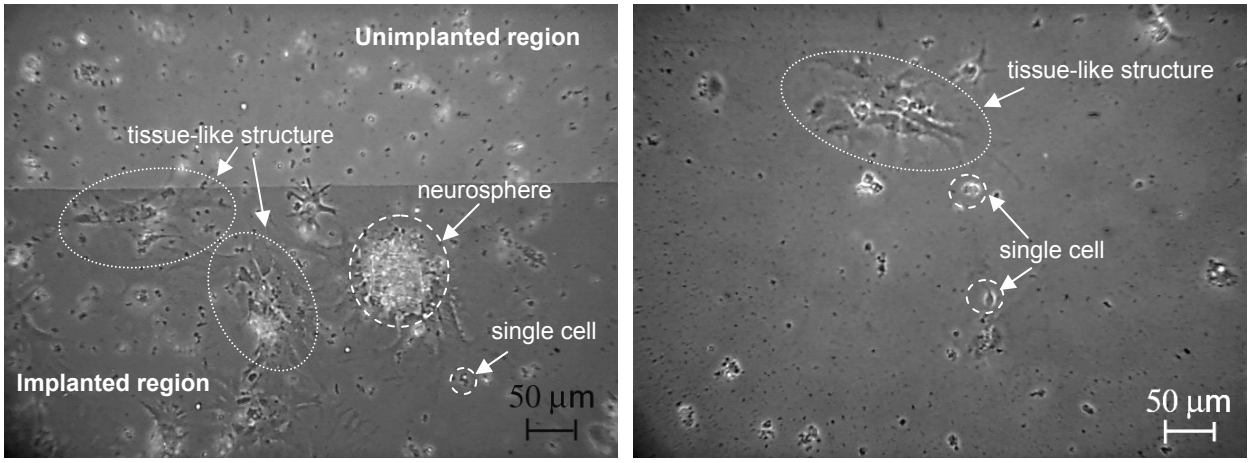


(a) PDL/C-SCPS (5 μg/ml) (b) Control of PDL/TCPS (33 μg/ml)

Fig. 6.4 Phase contrast micrographs of newborn mouse brain neuronal cells after 7 days *in vitro* on the PDL-coated surfaces of $C^-$-implanted SCPS (PDL/C-SCPS) at 10 keV and $3\times10^{15}$ ions/cm$^2$ as concentration of (a) 5 μg/ml and (b) on control.

After 7 – 15 days *in vitro*, the cluster of single cell started to form a tissue-like structure, which the shape was the same as shown in Fig. 6.1 (b). The adhesion properties of the newborn mouse brain neuronal cells on the PDL-coated SCPS at coating concentration of 5 μg/ml and at ion implantation conditions of 10 keV and $3\times10^{15}$ ions/cm$^2$ are shown in Fig. 6.4. In Fig. 6.4 (a), almost all the newborn mouse brain neuronal cells adhered on the implanted region. A lot of single cell and some neurospheres adhered on the PDL-coated implanted region. Moreover, the formations of the tissue were found on this region. The spread and formations of cells as the tissue were also found on control as shown in Fig. 6.4 (b). These tissue formations of cells were the same as those of cells on the PEI-coated TCPS dish as shown in Fig. 6.1 (b). This was the normal state of newborn mouse brain neuronal cell culture.

Similar to the results at coating concentration of 5 μg/ml, the adhesions of single cell and neurosphere and the formation of the tissue on the PDL-coated implanted region at the other coating concentration were also observed. However, some difference in cell density was found with various PDL coating concentration. The adhesion properties of the cells after 7 days *in vitro* on other PDL-coated surfaces at the different concentrations can be summarized. So, the numbers of adhered cells on the PDL-coated implanted region are shown in Fig. 6.5. The ratios in percent of selective adhesion between cells on the PDL-coated implanted region and on all regions are also shown in Fig. 6.5. Results show that the tendencies for both of the number of adhered cells and the selective adhesion ratio were as a function of PDL concentration. The number of adhered cells on the coating surfaces of the $C^-$-implanted region at 10 keV and $3\times10^{15}$ ions/cm$^2$ rapidly increased with an increase in the PDL concentrations from 1 to 5 μg/ml

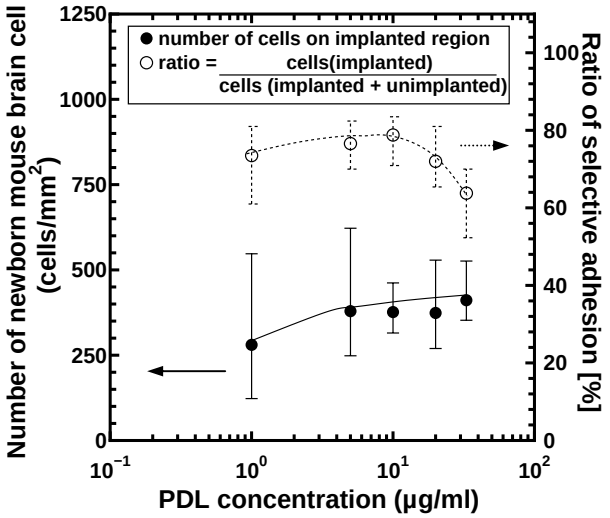


Fig. 6.5 Adhesion properties of newborn mouse brain neuronal cells for the number of adhered cells on the implanted region and the selective adhesion properties after 7 days *in vitro* on PDL/C-SCPS at 10 keV and $3\times10^{15}$ ions/cm$^2$ as a function of PDL concentration.

before saturated in the range of 5 – 33 μg/ml as shown in Fig. 6.5. The number of cells increased from 280 to 420 cells/mm$^2$. In the saturation range, the numbers of cells were 380 – 420 cells/mm$^2$. While the selective adhesion ratio of cells between the implanted and unimplanted regions calculated by proportion of the number of cells on implanted region and on both regions shows the different result. The selective adhesion ratio a little increased from 72% to 78% with an increase in the PDL concentrations from 1 to 10 μg/ml, and it decreased to 64% with an increase in concentration from 20 – 33 μg/ml as shown in Fig. 6.5. Therefore, the considered suitable PDL concentration for enhancing the number of adhesion cell with the acceptably selective adhesion ratio on the $C^-$-implanted region at 10 keV and $3\times10^{15}$ ions/cm$^2$ should be in the range of 5 – 20 μg/ml.

As for the immunofluorescent observation, the cells after 22 days *in vitro* were stained and labeled with dyes and antibody and the obtained results are shown in Fig. 6.6. The nucleus of all cells, which are neuron and glial cells, were labeled with the blue color of DAPI (Fig. 6.6 (b)). F-actin, axon and dendrite of cells were labeled by the red color bright of Texas Red (Fig. 6.6 (c)). The neuron-specific enolase of the neurons can be labeled by the green color bright of FITC (Fig. 6.6 (d)). In Fig 6.6, the newborn mouse brain neuronal cells were cultured on the PDL-coated implanted region at PDL concentration of 5 μg/ml and at ion implantation conditions of 10 keV and $3\times10^{15}$ ions/cm$^2$. Almost all the newborn mouse brain neuronal cells adhered on the implanted region. Although there were some adhered cells on the unimplanted region as described above, after long time culture almost all of them were detached. The adhered cells on the implanted region still survived. Fig. 6.6 (a) shows the phase-contrast micrograph of

the brain neuronal cell adhesion on only the implanted region. The nucleus of all neuronal cells were on the implanted region as shown in Fig. 6.6 (b). The labeled f-actin shows the structure of formed tissue as the walls including many filaments inside of these walls as shown in Fig. 6.6 (c). In Fig. 6.6 (d), the green-colored parts show the sites of the NSE of the neurons. The positions of the labeled nucleus, f-actin and NSE are closely corresponded each other in Fig. 6.6. It indicates that the adhered cells on the PDL-coated surface of the $C^-$-implanted SCPS are neurons.

From these observations, the newborn mouse brain neuronal cells sparsely adhered on the PDL layer of the non-treated SCPS. The uniform adhesions of the cells were found on the PDL layer of the $C^-$-implanted SCPS. This was corresponding to the previous expectation. The suitable PDL concentration for coating the $C^-$-implanted SCPS to enhance the uniform adhesion properties of the brain neuronal cells was in the concentration range of 5 – 20 μg/ml.

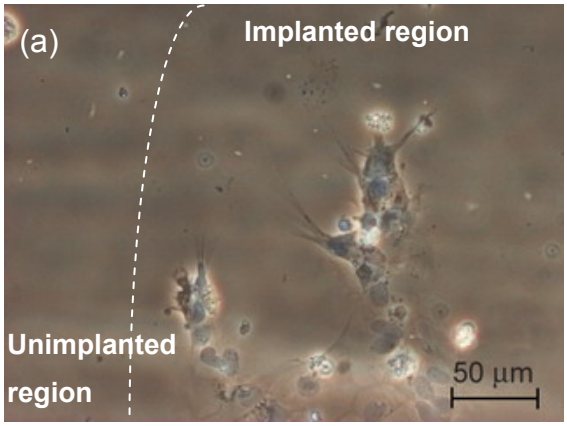


(a) PDL/C-SCPS at 5 μg/ml (optical image)

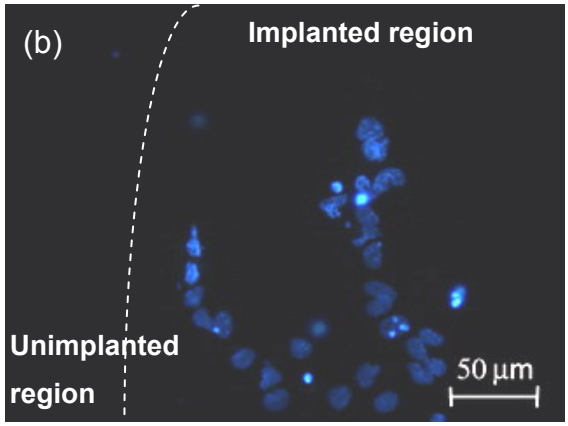


(b) PDL/C-SCPS at 5 μg/ml (nucleus)

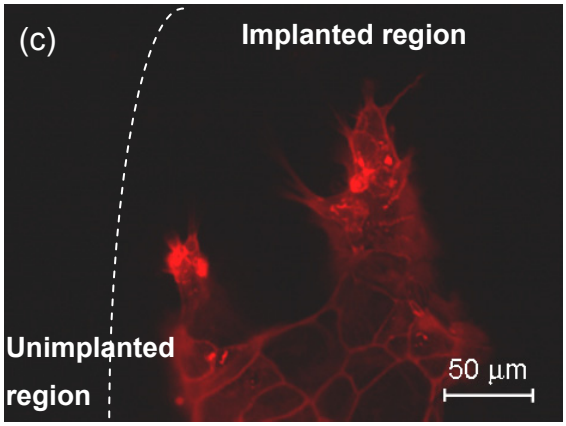


(c) PDL/C-SCPS at 5 μg/ml (f-actin)

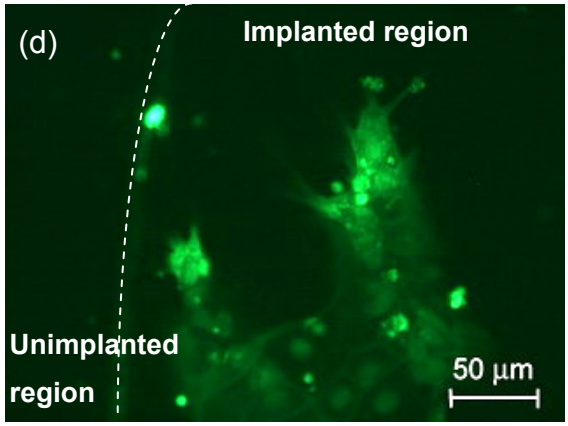


(d) PDL/C-SCPS at 5 μg/ml (NSE)

Fig. 6.6 Immunofluorescent micrographs of mouse brain neuronal cells at 22 days culture on the PDL-coated surfaces of $C^-$-implanted SCPS (PDL/C-SCPS) at 10 keV and $3\times10^{15}$ ions/cm$^2$ as coating with 5 μg/ml when: (a) optical image; (b) nucleus; (c) f-actin and (d) neuron-specific enolase (NSE).

## 6.4 Brain Neuronal Cell Patterning on PDL-Coated SCPS

From the description in section 6.2, the possibility to pattern the polycation polymeric surface by carbon negative-ion implantation was purposed. The carbon negative-ion implantation decreased the positive-charge sites and increased the negative-charge site on the surface coating of PDL on the unimplanted SCPS at a certain coating concentration of 33 μg/ml. From XPS analysis, the result shows that the PDL was sparsely adsorbed on the non-treated surface of SCPS. By pre-implantation into the SCPS before the PDL coating, the adsorption properties of PDL were improved and the suitable coating concentrations for the brain neuronal cell adhesion were 5 – 20 μg/ml as shown in section 6.3.2. For patterning the adhesion of the brain neuronal cells, there is no need to totally destroy the surface. Only 50% for the decrease of the amount of nitrogen atoms is expected to give an effect to the cell adhesion. To obtain the decrease of the nitrogen atoms for 50% at these obtained coating concentrations, therefore, the implantation dose of $1\times10^{14}$ ions/cm$^2$ was selected. From the description in sections 6.2 and 6.3, the selective adhesion patterning of the brain neuronal cells was expected to be obtained by the carbon negative-ion implantation into the uniform layer of PDL through the micro-pattern mask. The confirmation of the possibility to pattern the brain neuronal cell adhesion and the outgrowth of the axon and dendrite was studied in this section.

### 6.4.1 Experiment

For achievement of the selective cell-adhesion pattern of the real brain neuronal cells, the brain neuronal cells derived from embryo rat were cultured on the patterned PDL surfaces. The description of the experiment for sample preparation, the primary culture process for the brain cells and the confirmation observation method are as follow:

#### Sample Preparation

The preparation process of the patterning of the PDL-coated SCPS samples is shown in Fig. 6.7. The carbon negative-ion implantation was used twice in the preparation of the sample before and after PDL coating. Before the PDL coating, the carbon negative ions were implanted into SCPS at 10 keV and $3\times10^{15}$ ions/cm$^2$ without any mask to enhance the adsorption properties of PDL on SCPS. The implanted samples were first sterilized by using the process described in Chapters 5. After that, they were dipped in the PDL solution in PBS solvent at the coating concentrations of 5 – 20 μg/ml, which were the coating concentration for the uniform adhesion of the brain neuronal cells as shown in section 6.3.2. The coating process was those described in

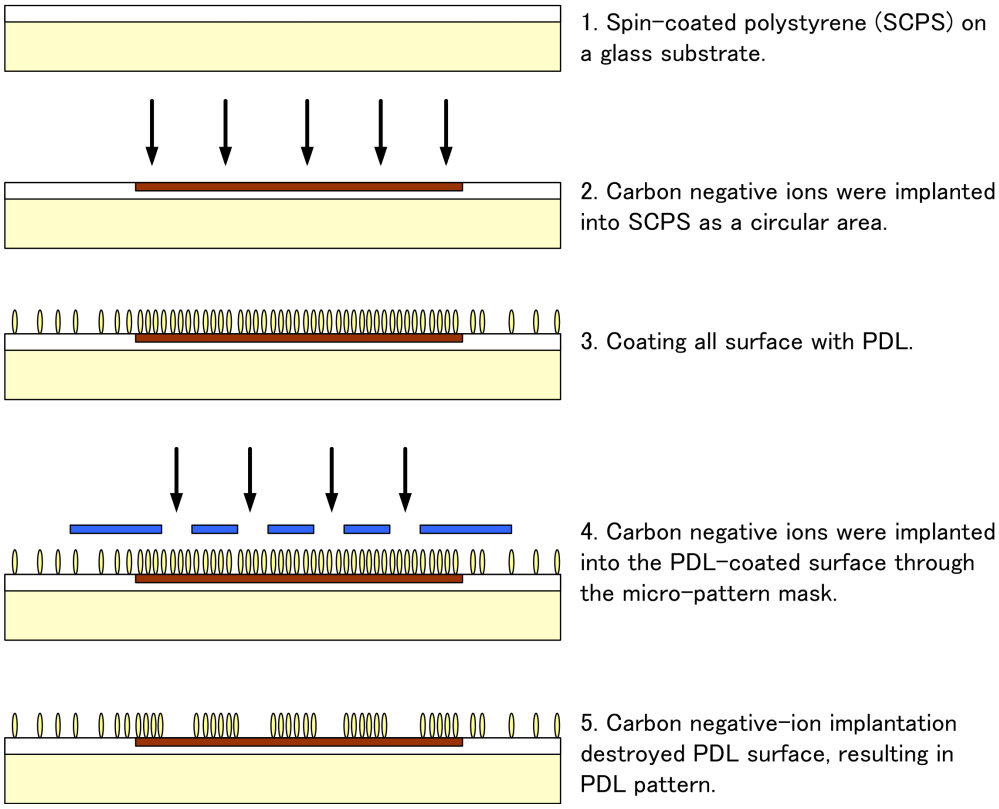


Fig. 6.7 Schematic diagram of PDL patterning by carbon negative-ion implantation.

section 6.3.1. After the PDL coating, the carbon negative ions were implanted into the coating surface of PDL through the micro-pattern mask to pattern the negative-charged sites region. The micro-pattern mask consists of many slit apertures with 50-µm width and 70-µm spacing. The applied ion energy and dose for patterning the surface were at 10 keV and $1\times10^{14}$ ions/cm$^2$. The other operation condition of residual gas pressure and ion-current density were those described in Chapter 2.

## Primary Culture Process

Before the cell culture, the samples were sterilized by using the irradiation of the ultra violet light in the clean bench for 1 night and were rinsed once by the sterilized de-ionized water. Then, they were set into the NTPS dish, and they were fixed by using 0.33% agarose. The rat embryo brain cortex neuronal cells (Cat. no.R-Cx-500, Cambrex bioscience Walkersville Inc.) were cultured on the patterned surface. The culture medium and the primary culture processes were those described in section 6.3.1. The rat embryo brain cortex neuronal cells were cultured for 23 days *in vitro*. The culture medium of each dish was exchanged by the fresh medium pre-warmed to 37°C every 4 days.

### Confirmation Observation

The adhesion properties of the cells were observed by the phase-contrast microscope (CK2, Olympus). Similar to the newborn mouse brain neuronal cells, the rat embryo brain cortex neuronal cells were also composed of two cell lines; neuron and glial. Therefore, the types of the adhered cells on the surface were classified by the immunofluorescent technique. At 23 days *in vitro*, types of adhered cells were observed by the fluorescent microscope (BX50, Olympus). The protocols for the immunofluorescent method observation were those described in section 6.3.1.

## 6.4.2 Results

Based on phase-contrast microscopy, the patterned adhesion of the rat embryo brain cortex neuronal cells and their growth from 4 h to 11 days *in vitro* is shown in Fig. 6.8. In Fig. 6.8 (a), after the neuronal cells were plated on the patterned PDL surface for 4 h, they started to adhere to the surface. No clearly selective adhesion of cells could be observed. After 1 day *in vitro*, the adhered cells presented the outgrowth of growth cone on some regions on the unmodified PDL surface as shown in Fig. 6.8 (b). The discrete adhesions of the neuronal cells obscurely were found on the areas corresponding to the complementary pattern to the implanted pattern. After 4 days *in vitro*, Fig. 6.8 (c) shows that the number of adhered cells increased and the cells extended the axons and dendrites along the areas of the complementary pattern. Small neuron network were found on the complementary pattern. The adhered cells on the discrete adhesive areas gradually increased in the number after 6 and 8 days *in vitro* (Figs. 6.8 (d) and (e)), and the adhesion pattern became much clear after 11 days *in vitro* (Fig. 6.8 (f)).

After 16 days *in vitro*, the patterned adhesion of the rat embryo brain neuronal cells could be obviously observed. The obtained result is shown in Fig. 6.9, where the sample preparation conditions were set at 10 keV – $3\times10^{15}$ ions/cm$^2$ for the pre-implantation, 5 μg/ml for the PDL coating concentration and 10 keV – $1\times10^{14}$ ions/cm$^2$ for the pattern implantation. Almost all of the cells with their axon and dendrite were found on the unmodified PDL regions of the pre-implanted SCPS. Those cells were composed of a lot of single cells and the neurospheres. The cells extended a lot of axon and dendrite along the areas of the complementary pattern. Some of single cells sparsely adhered on the unimplanted PDL surface of the non-pre-implanted SCPS area (data not shown here). No adhesion of the rat embryo brain cortex neuronal cells on the modified PDL by the pattern implantation was observed. At this coating concentration of 5 μg/ml, the clear selective adhesion pattern of rat brain cortex neuronal cells could be achieved on the unmodified PDL regions of the pre-implanted SCPS.

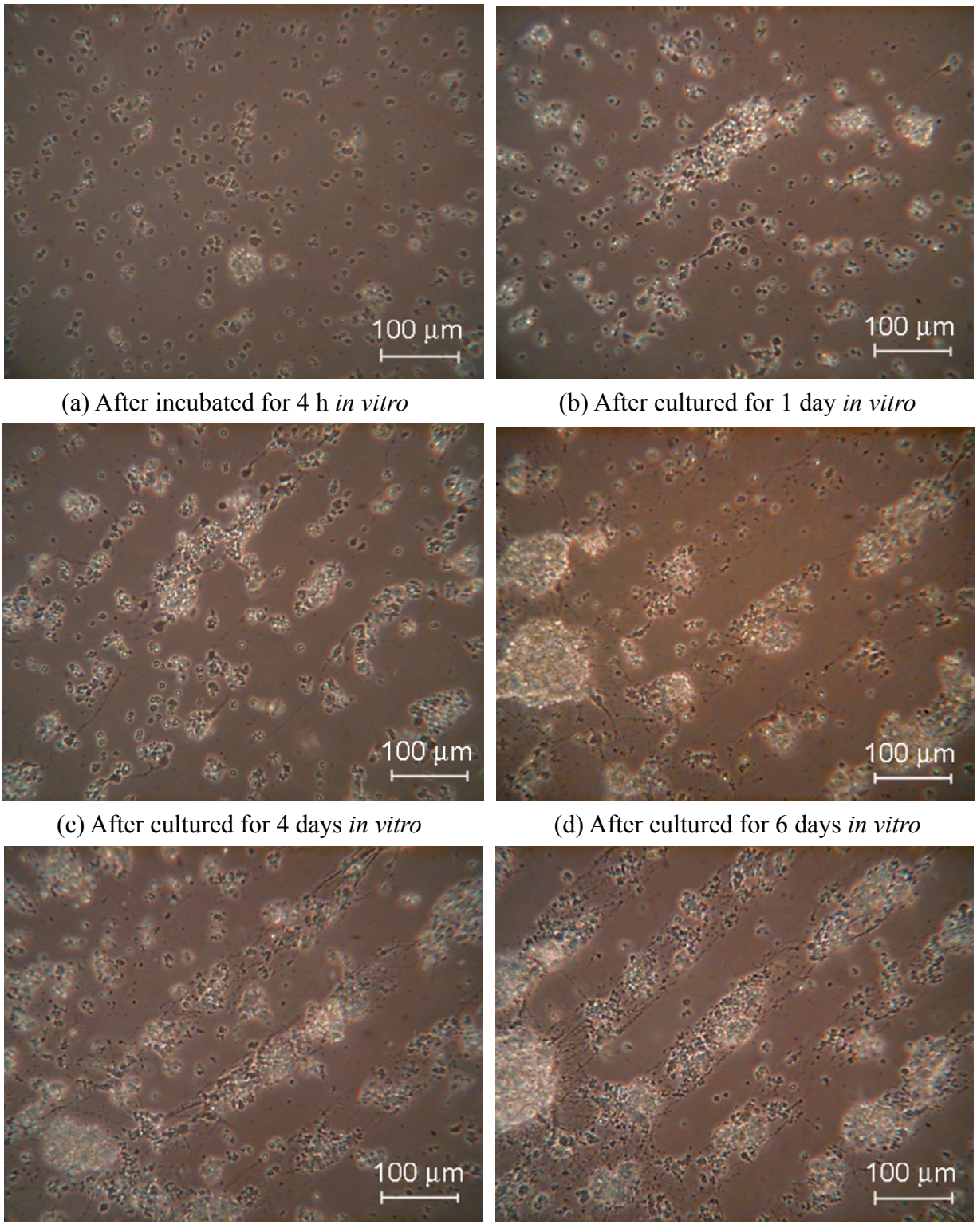


(a) After incubated for 4 h *in vitro*

(b) After cultured for 1 day *in vitro*

(c) After cultured for 4 days *in vitro*

(d) After cultured for 6 days *in vitro*

(e) After cultured for 8 days *in vitro*

(f) After cultured for 11 days *in vitro*

Fig. 6.8 Phase-contrast micrograph of rat embryo brain cortex neuronal cells on $C^{-}$-implanted PDL/SCPS at 5 µg/ml, 10 keV and $1\times10^{14}$ ions/cm$^2$ after cultured for: (a) 4 h; (b) 1 day; (c) 4 days; (d) 6 days; (e) 8 days; and (f) 11 days *in vitro*.

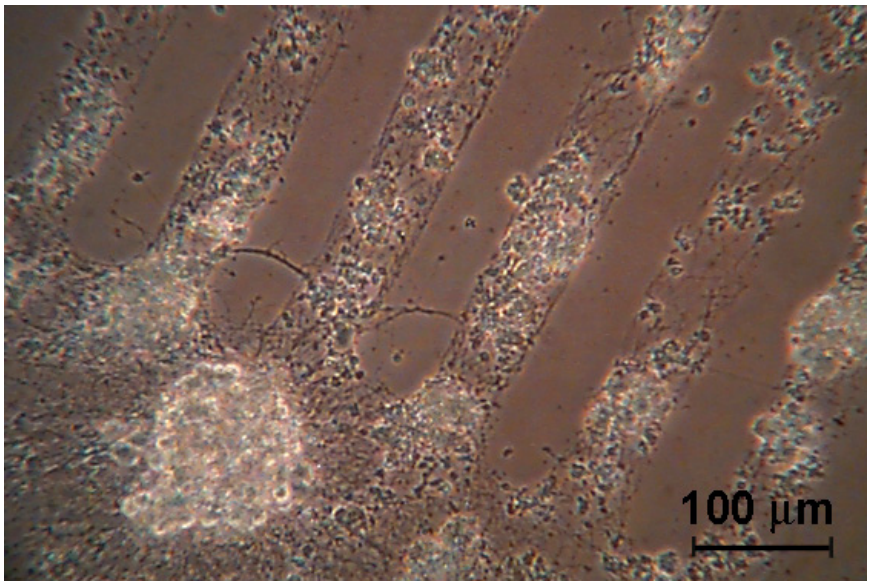


Fig. 6.9 Phase-contrast micrograph of rat embryo brain cortex neuronal cells patterned on $C^-$-implanted PDL/SCPS at 5 μg/ml, 10 keV and $1\times10^{14}$ ions/cm$^2$ after 16 days *in vitro*.

At other coating concentrations more than 10 μg/ml, the clear patterned adhesion of the rat embryo brain cortex neuronal cells could not be achieved. Although the cells also adhered and extend the axon and dendrite on the unmodified PDL regions of the pre-implanted SCPS, the number of adhesion cells was too small so that a clear patterned adhesion was not obtained. This reason is still unknown, but I considered that the reasons should be due to (1) the excess of PDL that floating in the culture medium and (2) the adsorption of the sputtered particle of PDL fragments on the unmodified PDL surface. From the former, the floating PDL might be adsorbed on the cell surface leading to cell death. From the latter, the fragments of PDL lost the brain neuronal cell adhesion properties. Therefore, the best PDL coating concentration in this experiment is considered to be 5 μg/ml.

Fig 6.10 shows the immunofluorescent micrographs of the selective adhesion pattern of the rat brain cortex neuronal cells after cultured for 23 days *in vitro*. The sample was prepared at the pre-implantation of 10 keV and $3\times10^{15}$ ions/cm$^2$, at the coating concentration of 5 μg/ml, and at pattern implantation of 10 keV and $1\times10^{14}$ ions/cm$^2$. Almost all of the brain neuronal cells adhered on the unmodified PDL region corresponding to the complementary pattern as shown in the optical micrographs of Figs. 6.10 (a) and (b) at the different magnifications of 10×10 and 10×20, respectively. However, some parts of neuronal cell adhesion pattern presented no cell adhesion. These parts were from the detachment of cell death. For long term *in vitro* (20 days), the noticeable observation showed the decrease in number of cells from cell death. Although the embryo brain neuronal cells can increase in the number *in vivo*, they could not do this function *in vitro*. Therefore, the vacant region from detachment of cell dead on some region of pattern was

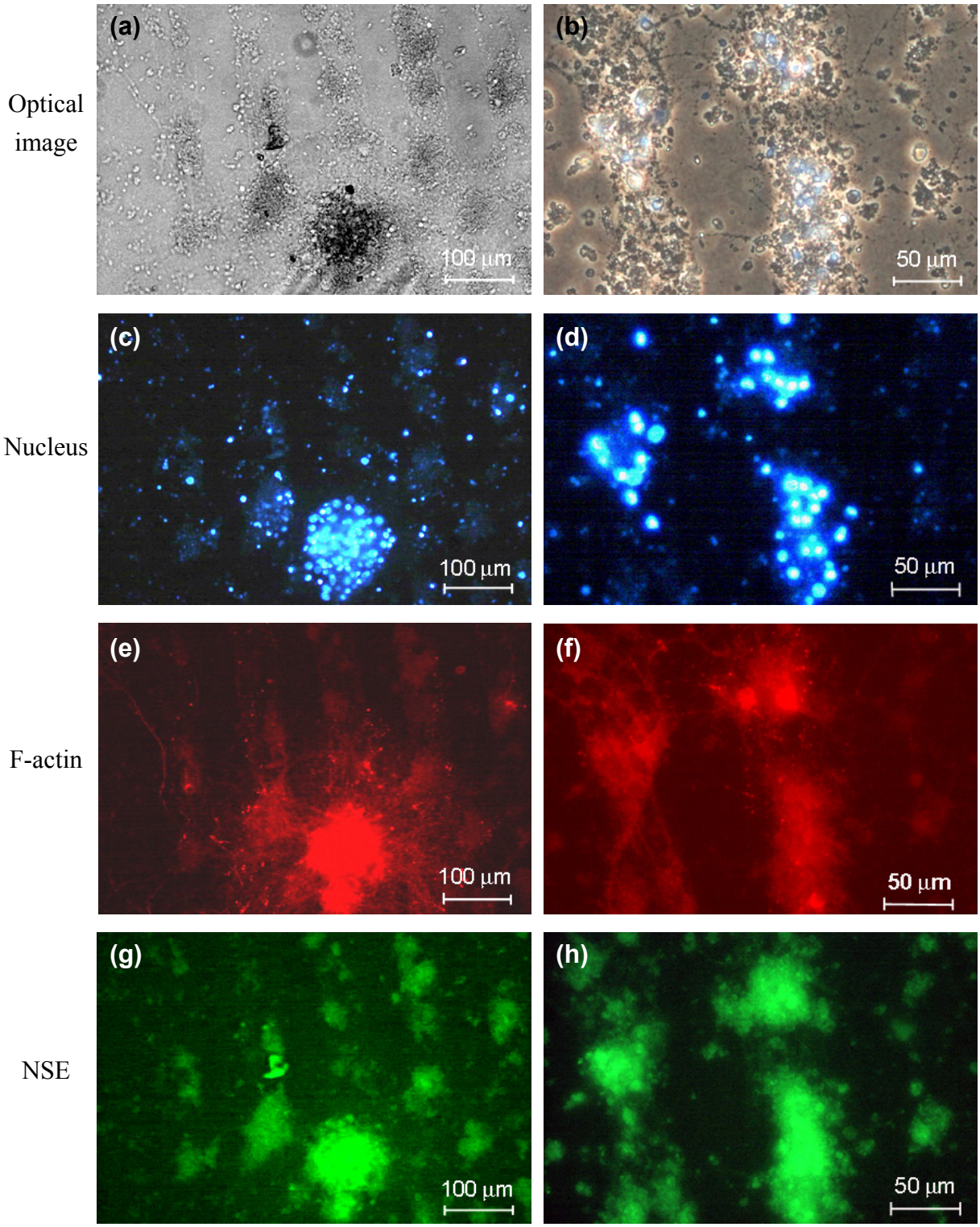


Fig. 6.10 Immunofluorescent micrographs of rat embryo brain cortex neuronal cells patterned on $C^-$-implanted PDL/SCPS at 5 μg/ml, 10 keV and $1\times10^{14}$ ions/cm$^2$ at 23 days *in vitro* with lens magnifications of 10×10 and 10×20 for: (a), (b) optical image; (c), (d) nucleus; (e), (f) f-actin, axon and dendrite; and (g), (h) neuron-specific enolase (NSE).

appeared. Figs. 6.10 (c) and (d) show the positions of nucleus in blue color by the staining of DAPI. These positions well also corresponded to the adhered cells on the complementary pattern. The fiber structures of f-actin, which labeled in red color of Texas Red-X phalloidin, were shown in Figs. 6.10 (e) and (f). The red-colored regions also well agreed with the cell images in Figs. 6.10 (a) and (b). In particular, the red fine line in the upper part of Fig. 6.10 (f) well corresponded to the neurite appeared in Fig. 6.10 (b). In Figs. 6.10 (g) and (h), the neuron-specific enolase (NSE) stained by FITC are shown in the green color. The green-colored regions agreed with the cell images in Figs. 6.910 (a) and (b). So, the adhered cells were neurons since the NSE is confined solely to neurons [8].

From all observation, the patterned adhesion of the brain neurons could be achieved by carbon negative-ion implantation at 10 keV and low dose of $1\times10^{14}$ ions/cm$^2$ on the PDL-coated SCPS as coating at concentration of 5 μg/ml. Therefore, the neuron adhesion patterning on the polystyrene can be achieved by carbon negative-ion implantation.

## 6.5 Summary

The primary culture of the brain neuronal cells requires only the positive-charged sites of amino group on the surface to binding and adhesion, and the carbon negative-ion implantation could modify the polymeric surface to be hydrophilic by formation of the negative-charged sites of carbonyl and hydroxyl group. Then, patterning the polymeric surface, which contains the positive-charge sites, is an alternative way to neuron arrangement on the pattern. For this purpose, two types of neuronal cells from newborn mouse brain cells and rat embryo brain cells were selected to study. The fundamental measurement of carbon negative-ion implantation for patterning surface was checked by evaluation of surface atomic binding state on the $C^-$-implanted PDL on the SCPS film by XPS. After ion implantation into the PDL surface, the change in XPS C1s spectra around 285.0 eV from the formation of C=O and OH groups were observed even if at low dose implantation. Decrease in nitrogen intensity with increase in oxygen intensity was also investigated. Changes in these intensities depended on the ion implantation dose. Then, the carbon negative-ion implantation into PDL for patterning positive-charged site could be done. The suitable concentration of PDL for selectivity and uniformity of neuron adhesion on the $C^-$-implanted SCPS at 10 keV and $3\times10^{15}$ ions/cm$^2$ was investigated by primary culture of the newborn mouse brain neuronal cells. The suitable concentration for neuron adhesion was in the range of 5 – 20 μg/ml. Based on these obtained suitable conditions, the patterned adhesion of rat embryo brain neuronal cells was studied by carbon negative-ion implantation at 10 keV and $1\times10^{14}$ ions/cm$^2$ through the micro-pattern mask. The patterned adhesion of neurons on the unimplanted region of PDL could be achieved as coating at

concentration of 5 μg/ml. From all observation, the neuron adhesion patterning on the polymeric surface could be achieved by negative-ion implantation.

## References


[1] E. Yavin and Z. Yavin, "Attachment and Culture of Dissociated Cells from Rat Embryo Cerebral Hemispheres on Polylysine-Coated Surface", J. Cell Biol, vol. 62, pp. 540-546, 1974.

[2] P. C. Letourneau "Possible Roles for Cell-to-Substratum Adhesion in Neuronal Morphogenesis", Dev Biol., vol. 44, no. 1, pp. 77-91, 1975.

[3] A.R. Vancha, S. Govindaraju, K.VL Parsa, M. Jasti, M. González-García, and R.P. Ballestero, "Use of Polyethyleneimine Polymer in Cell Culture as Attachment Factor and Lipofection Enhancer", BMC Biotechnology 2004, vol. 4, no. 23, Published online 2004, doi:10.1186/1472-6750-4-23.

[4] Y. Bledi, A.J. Domb and M. Linial, "Culturing Neuronal Cells on Surfaces Coated by a Novel Polyethyleneimine-Based Polymer", Brain Res. Protoc., vol. 5, issue 3, pp. 282-289, 2000.

[5] H. Lodish, A.Berk, L. S. Zipursky, P. Matsudaira, D. Baltimore and J. Darnell, **Molecular Cell Biology**, 4th Ed., W.H. Freeman eds., New York: W.H. Freeman & Co Ltd, 2002.

[6] **Principles of Neural Science**. E.R. Kandel, J.H. Schwartz, T.M. Jessell, eds., 4th ed., New York: McGraw-Hill, 2000.

[7] P. Liesi, D. Dahl, and A. Vaheri, "Neurons Cultured from Developing Rat Brain Attach and Spread Preferentially to Laminin", J. Neurosci. Res., vol. 11, pp. 241-251, 1984.

[8] T. Kirino, M.W. Brightman, W.H. Oertel, D.E. Schmechel and P.J. Marangos, "Neuron-Specific Enolase as an Index of Neuronal Regeneration and Reinnervation", J. Neurosci., vol. 3, no. 5, pp.915-923, 1983.

# Chapter 7

# Mesenchymal Stem Cell Patterning and Its Differentiation into Neuron

Stem cells not only retain the self renewal ability, but also the ability of unlimited potency to differentiate into a wide range of specialized cell types accounting to research on stem cells since 1960s [1-3] until now for application in medical therapies [4]. Three broad categories of mammalian stem cells are composed of the embryonic stem cells derived from blastocysts, adult stem cells found in adult tissues, and cord blood stem cells found in the umbilical cord. State-of the art medical therapy, a great deal of adult stem cell researches have focused on clarifying their capacity to self-renew indefinitely and their differentiation potential [5-7]. Mesenchymal stem cell (MSC), one of interesting adult stem cells, is on research since the potency of differentiation into neurons and other cells for support the nerve regeneration. It can be derived from the bone marrow [7-8] and from the umbilical cord blood [4] that no need to deconstruct the living body. In case of human clinical application, MSCs were derived from a small bone marrow specimen from a patient, expanded in the *in vitro* culture, and given back to the same patient for avoiding the problems associated with immune rejection of foreign transplanted cells or tissues. For nerve regeneration, culture for increase in the number and differentiation of MSC on polymeric surface is necessary. In addition, the adhesion patterning of MSCs on the polymeric surfaces and differentiation into neurons can be then the idea for artificial neuron network in future. This chapter describes the cell line of MSC in details, the patterning of MSC adhesion on polymeric surfaces of spin-coated polystyrene (SCPS) and silicone rubber (SR) by carbon negative-ion implantation and the differentiation of the adhered MSCs into neuronal cells on the pattern.

## 7.1 Mesenchymal Stem Cell (MSC)

Mesenchymal stem cells (MSC) are another well-characterized population of adult stem cells since they have been shown to differentiate into many cell lines in the multiple tissues such as adipocyte cells, cartilage, bone, tendon and ligaments, muscles cells, dermal cells and even neuron cells and $\beta$-pancreatic islets cells, depending to the culture conditions.

MSC or so-called marrow stroma cells were firstly reported by E. A. McCulloch and J.

E. Till in the early 1960s by finding the visible nodules in the spleens of the mice after injecting bone marrow cells into irradiated mice [8]. After E.A. McCulloch and J.E. Till progressed their works with A. Becker [1] and L. Siminovitch [2], they reported that the cells derived from bone marrow have capability of self-renewal, a crucial aspect of the functional definition of stem cells. Therefore, i*n vivo* and *in vitro* cultures of the multipotential adult stem cells of MSC have been recently studied for clinical applications since their characteristics of self–renewal and differentiation to many cell lines [5-7].

Woodbury *et al.* showed the differentiation induction into neuron-like cells in rat and human MSC by culturing with the special serum-free culture medium containing the $\beta$ -Mercaptoethanol (BME) [9-10]. They showed the neuron shape and the neuron gene express after induction of differentiation. However, there is a limitation of this induction method of differentiation into neuronal cells on the tissue culture polystyrene dish (TCPS) that the neuronal cells could be differentiated back into MSC, again, after remove BME for a time.

Fig. 7.1 shows the culture of rat MSC and their differentiation into neuronal cells on TCPS dish (Corning, USA). The confluence state of the undefined transparent shape of rat MSC from their spreading and flattening for adhering to the surface (Fig. 7.1 (a)) was differentiated into neuronal cell by the induction of 1 mM BME in the serum-free culture medium for 120 min, following Woodbury *et al.* [9] as described in details in section 7.4. The change in the undefined spread shape of rat MSC was induced by decrease in the spread adhesion area to be a defined round shape with size of around 20 μm with remaining some non decreased part as an outgrowth of neurite as shown in Fig. 7.1 (b). This outgrowth looked similar to the outgrowth of axon from the soma of neuron. The new shape of the differentiated MSC by induction of 1 mM BME almost looked like the neuron shape.

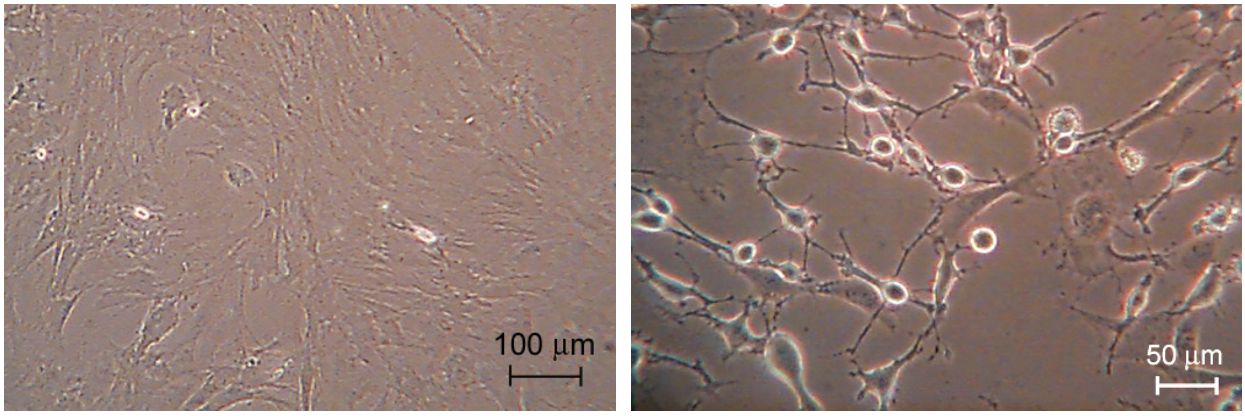


(a) The confluence state of rat MSC on TCPS (b) MSC differentiation into neuron-like cells

Fig. 7.1 Phase-contrast micrographs of MSC on TCPS dish: (a) at the confluence state; and (b) after differentiation into neuron-like cells by induction of 1 mM BME for 120 min.

Since MSC can adhere to normal TCPS, which consists of the hydrophilic surface of the hydroxyl and carbonyl groups, they should then adhere to the $C^-$-modified polymeric surface of SCPS and SR. Therefore, there is a possibility to pattern the adhesion of neuronal cells from the differentiation of MSC adhered on the $C^-$-patterned polymeric surface. In this work, the MSC derived from rat bone marrow were selected to study the MSC adhesion pattern and its differentiation into neuron-like cells on the $C^-$-implanted polymeric surfaces of SPCS and SR. The cultured cells were almost from the passage numbers of 1-3 since the differentiation potential dropped from the $6^{th}$ passage [11]. The suitable conditions of the ion implantation for the patterning adhesion of MSC on the $C^-$-implanted polymeric surface of SCPS and SR are described in sections 7.2 – 7.3, respectively. The differentiation of MSC adhered on the suitable $C^-$ patterned surfaces of SCPS and SR into neuron-like cells will be also described in section 7.4 – 7.5, respectively.

## 7.2 MSC-Adhesion Patterning of on $C^-$-Implanted SCPS

The suitable ion implantation conditions in dose and energy for MSC adhesion pattern with maintaining the characteristics of MSC and increasing their number during *in vitro* culture were investigated by culture of the rat mesenchymal stem cells on the $C^-$-modified SCPS. The carbon negative ions were implanted into the SCPS films on glass through a micro-pattern mask, which is consisted of many slit apertures with 50-μm width and 70-μm spacing, to pattern the implanted region. As for study of the suitable dose condition for the good adhesion patterning, the carbon negative ions were implanted at the set energy of 10 keV and at the various ion doses from $1\times10^{13}$ to $1\times10^{16}$ ions/cm$^2$. As for study of the suitable energy condition for the good adhesion patterning, the carbon negative ions were implanted at the suitable dose for cell adhesion patterning and at the various ion energies from 5 to 20 keV. The other operation condition of residual gas pressure and ion-current density were those described in Chapter 2.

All implanted samples were sterilized by 70% ethanol, were rinsed three times with the sterilized de-ionized water (DIW) and were rinsed once with the phosphate buffered saline (PBS) before cell culture. The sterilized samples were set into non-treated polystyrene dish (NTPS, Corning). The rat mesenchymal stem cells, derived from rat bone marrow, from the $1^{st}$ passage cells were lifted by incubation with trypsin (0.25%) and 1mM EDTA at 37°C for 4-5 min. The action of trypsin was stopped with the serum medium of Dulbecco's modified Eagle's medium (DMEM, Nissui, Japan) containing 5% heat-inactivated horse serum (HS, Gibco, New Zealand), 5% fetal bovine serum (FBS, Trace Scientific Ltd., Australia), sodium hydrogen carbonate (1.8 mg/ml, Wako, Japan) with antibiotic of penicillin G and streptomycin. The cells then were

collected with a 10 ml pipette into a sterilized 15-ml tube and centrifuged for 5 minutes at 500 rpm (Tabletop centrifuge 5200, Kubota). The supernatant was then removed, and the cells were resuspended again in the serum medium, and a uniform cell suspension was generated by gently pipetting the cells up and down in the pipette. The cells were then plated on the $C^-$-implanted SCPS in the serum medium for 10-16 days under 5% $CO_2$ at 37°C in incubator. The culture medium of each dish was exchanged by the fresh medium pre-warmed to 37°C every 4 days.

The adhesion properties of MSC on the $C^-$-implanted SCPS were observed by the phase-contrast microscope (CK2, Olympus) and by the fluorescence microscope (BX50, Olympus). The fluorescence microscopy was used to investigate the real position of cell nucleus. The cells were fixed with 4% formaldehyde in PBS for 5 min and were rinsed once with PBS. The cells were stained with 4', 6-Diamidino-2-phenylindole (DAPI, Sigma-aldrich, Japan) for 30 min, and rinsed with PBS for three times.

### 7.2.1 Effect of Ion Dose on MSC-Adhesion Properties

Since MSC adhesion on the surface needs the time for 24 – 48 h [10], the adhesion properties were investigated after culturing for 3 days. The adhesion properties of rat MSC on the $C^-$-implanted SCPS at the implantation energy of 10 keV are shown in Figs. 7.2 – 7.7.

Fig. 7.2 shows the culture of rat MSC adhesion patterned on the $C^-$-implanted SCPS at 10 keV and $1\times10^{15}$ ions/cm$^2$ after 3-day culture. MSC adhered and spread their body only on the implanted regions, where corresponding to the narrow dark stripe between the marked white lines. Some round-shape cells weakly adhered without spreading the body also on the unimplanted region. These cells could be removed after replacement of the culture medium. Therefore, the clear selective adhesion of rat MSC could be observed.

At low implantation dose of $1\times10^{13}$ ions/cm$^2$, after 3-day culture the weakly adhered MSC as a round-shape were randomly found on the $C^-$-implanted SCPS as shown in Fig. 7.3. Although the implanted region could not be seen in this figure, the adhesive position should be considered to be the implanted region due to the lowering of the contact angle after implantation. The region between the marked white lines is corresponding to the implanted region. The adhesion of the round-shaped cells almost aligned in this region. Similar to the results at low dose of $1\times10^{13}$ ions/cm$^2$, MSC also adhered as a round-shape on the $C^-$-implanted SCPS at $1\times10^{14}$ ions/cm$^2$ after 3-day culture. In addition, these round-shape adhesion and some spread adhesions of MSC as a pattern were observed on some areas of the $C^-$-implanted SCPS at $1\times10^{14}$ ions/cm$^2$ after 13-day culture as shown in Fig. 7.4 (b). This presented the more lowering of contact angle on some area of the implanted regions after long time culture, but it was not enough to obtain the suitable adhesion property. Therefore, the implantations at low dose of

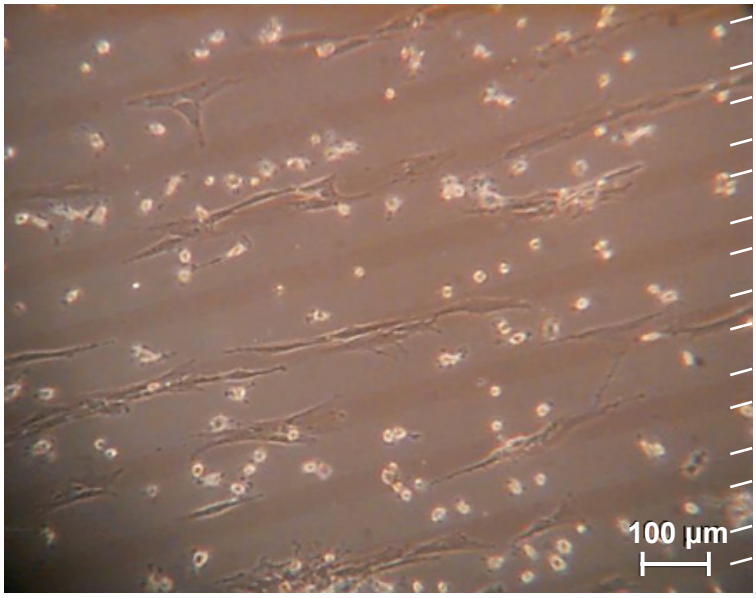


Fig. 7.2 Phase-contrast micrographs of MSC on the $C^-$-implanted SCPS at 10 keV and $1\times10^{15}$ ions/cm$^2$ after 3-day culture.

$1\times10^{13}$ – $1\times10^{14}$ ions/cm$^2$ were not suitable for adhesion of MSC.

After 3-day culture, MSC could adhere and spread their body along the region, corresponding to the implanted region since the lowering of contact angle, of $C^-$-implanted SCPS at $3\times10^{14}$ ions/cm$^2$ as shown in Fig. 7.5 (a). Some weakly adhesions of round-shape MSC were also found on the region between the spread adhesion regions. After 6-day culture, the spread adhered MSC along the implanted region increased their number, resulting in the confluent state of cells as an adhesion pattern as shown in Fig. 7.5 (b). Thus, the adhesion pattern

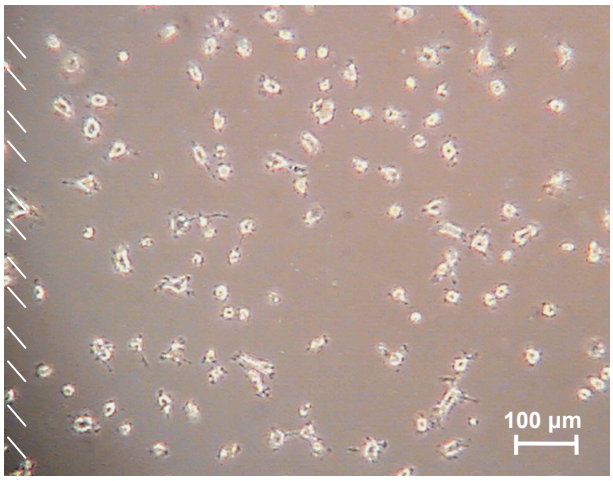


Fig. 7.3 Phase-contrast micrographs of MSC on the $C^-$-implanted SCPS at 10 keV and $1\times10^{13}$ ions/cm$^2$ after 3-day culture.

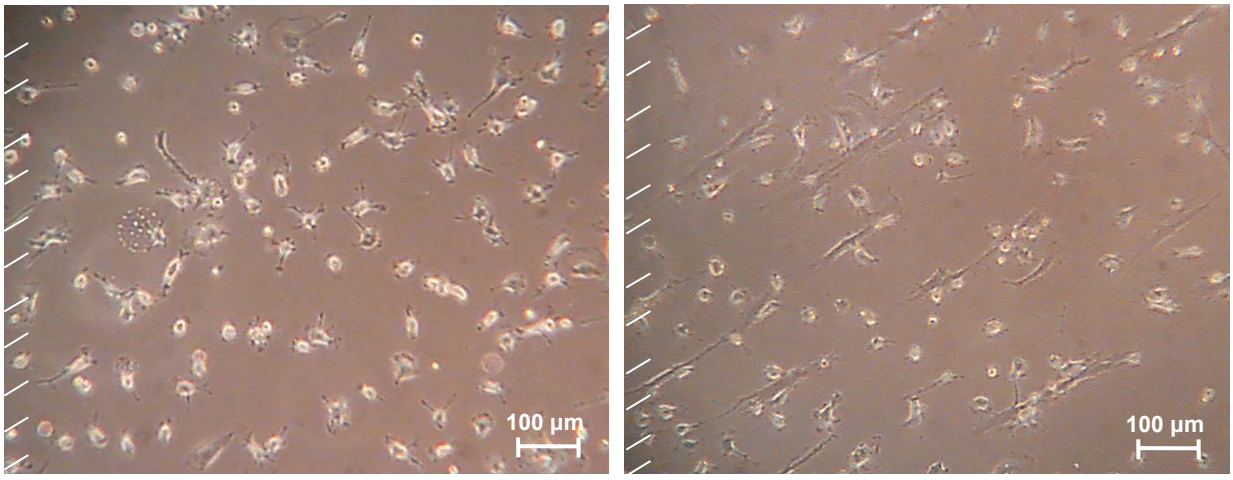


(a) Random round-shape adhesion of MSC (b) Selective spread adhesion of MSC

Fig. 7.4 Phase-contrast micrographs of MSC on the $C^-$-implanted SCPS at 10 keV and $1\times10^{14}$ ions/cm$^2$ after 13-day culture: (a) random round-shape adhesion; and (b) selective spread adhesion.

for MSC could be completely obtained on the $C^-$-implanted SCPS at implantation from dose of $3\times10^{14}$ ions/cm$^2$.

At implantation dose of $3\times10^{15}$ ions/cm$^2$, almost all of the spread adhered MSCs were also found on the implanted region of the $C^-$-implanted SCPS, but some of them also appeared on the unimplanted region after 3-day culture as shown in Fig. 7.6. The selective adhesion of MSC could not be obtained. This reason is considered to be due to the emitted gas particles from the implanted areas were adsorbed on the unimplanted areas and it led to the hydrophilic property on the unimplanted area. So, the cells could adhere on the unimplanted area. This

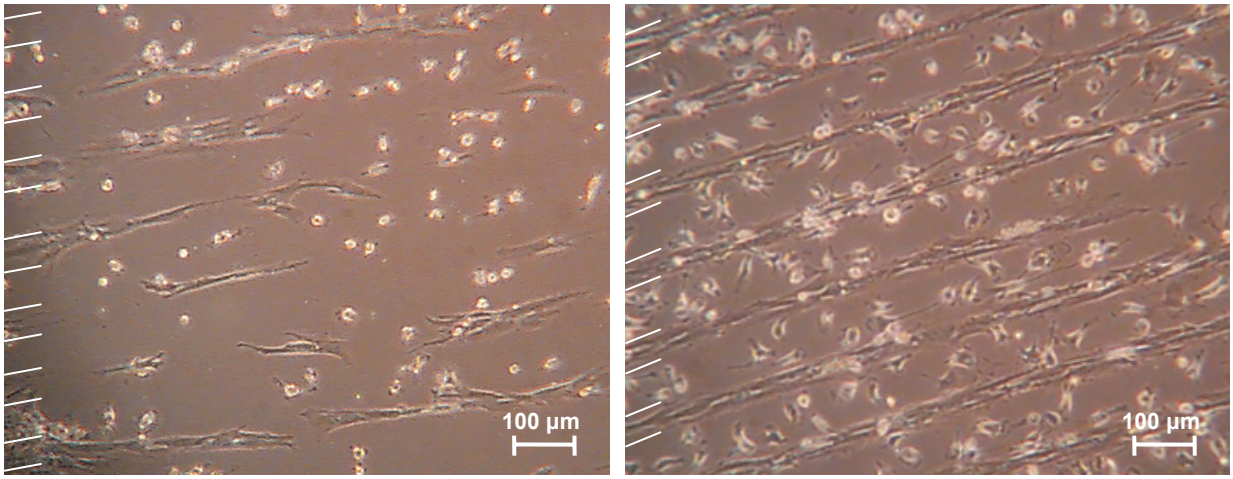


(a) Selective adhesion after 3-day culture (b) Confluence state after 6-day culture

Fig. 7.5 Phase-contrast micrographs of MSC on the $C^-$-implanted SCPS at 10 keV and $3\times10^{14}$ ions/cm$^2$: (a) selective adhesion after 3-day culture; and (b) confluence after 6-day culture.

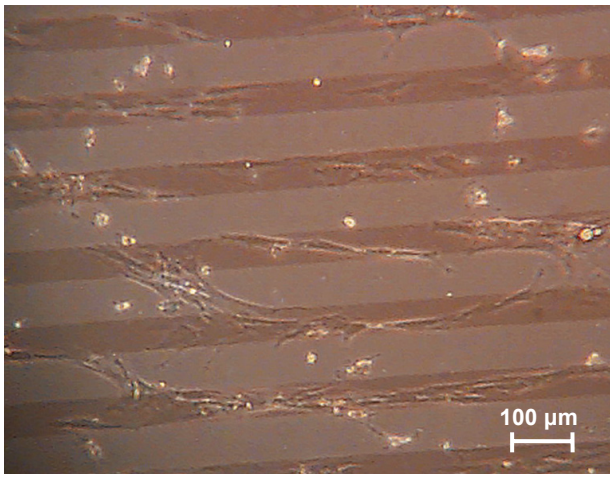


Fig. 7.6 Phase-contrast micrographs of MSC on the $C^-$-implanted SCPS at 10 keV and $3\times10^{15}$ ions/cm$^2$ after 3-day culture.

adsorption of the emitted gas particles had already described in Chapter 5. Similar to the implantation at this dose, there was no selective adhesion on the $C^-$-implanted SCPS at 10 keV and $1\times10^{16}$ ions/cm$^2$. Therefore, the adhesion pattern of MSC could not be obtained at the implantation dose of $3\times10^{15}$ – $10\times10^{16}$ ions/cm$^2$.

As for confirmation of the real position adhesion of nucleus, the immunofluorescent technique of DAPI with blue color was applied. The immunofluorescent micrographs of rat MSC on the $C^-$-implanted SCPS at $3\times10^{14}$ ions/cm$^2$ after 16-day culture is as shown in Fig. 7.7. From Fig. 7.7 (a) cell adhered and spread along the surfaces as a pattern on the $C^-$-implanted SCPS at 10 keV and $3\times10^{14}$ ions/cm$^2$. At this implantation dose, the implanted region could not be seen.

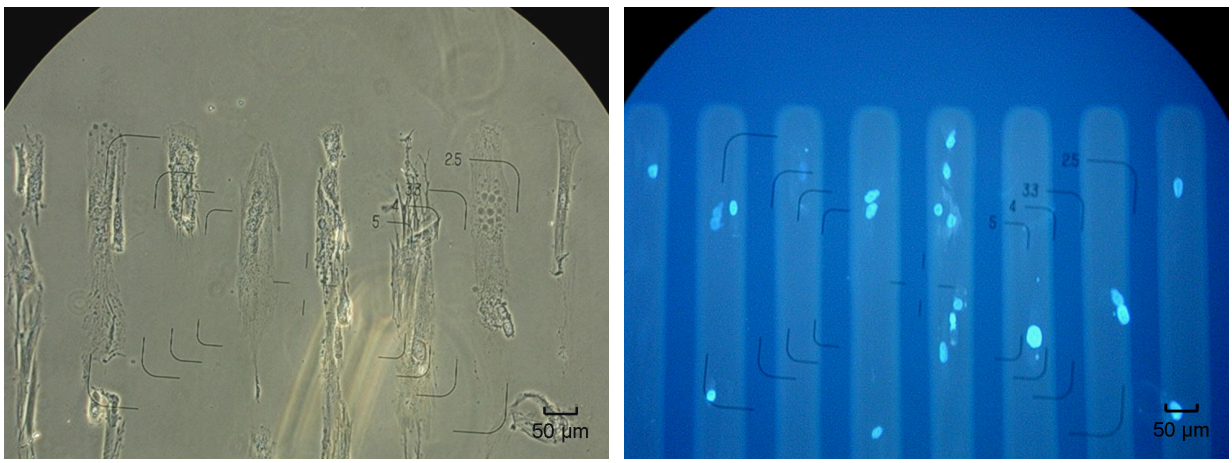


(a) Optical image (b) Nucleus

Fig. 7.7 Fluorescent micrographs of MSC on the implanted region of the $C^-$-implanted SCPS at 10 keV and $3\times10^{14}$ ions/cm$^2$: (a) optical image; and (b) nucleus.

The bright blue dot of DAPI showed that all cell nucleus were on the implanted region, corresponding to the bright stripe as shown in Fig. 7.7 (b). This confirmed that rat MSC adhered on the implanted region as the same as results at $1\times10^{15}$ ions/cm$^2$. The pattern of adhesion was on the implanted region. From all observations, the suitable dose condition for pattering of rat MSC adhesion on the $C^-$-implanted SCPS at 10 keV, therefore, were at $3\times10^{14}$ – $1\times10^{15}$ ions/cm$^2$.

### 7.2.2 Effect of Ion Energy on MSC-Adhesion Properties

For the study of the effect of the ion energy in the range of 5 – 20 keV, the SCPS were implanted at the certain dose of $3\times10^{14}$ ions/cm$^2$ that is the suitable dose for patterning the MSC adhesion.

Fig. 7.8 shows the phase-contrast micrographs of MSC cultured for 3 days on the

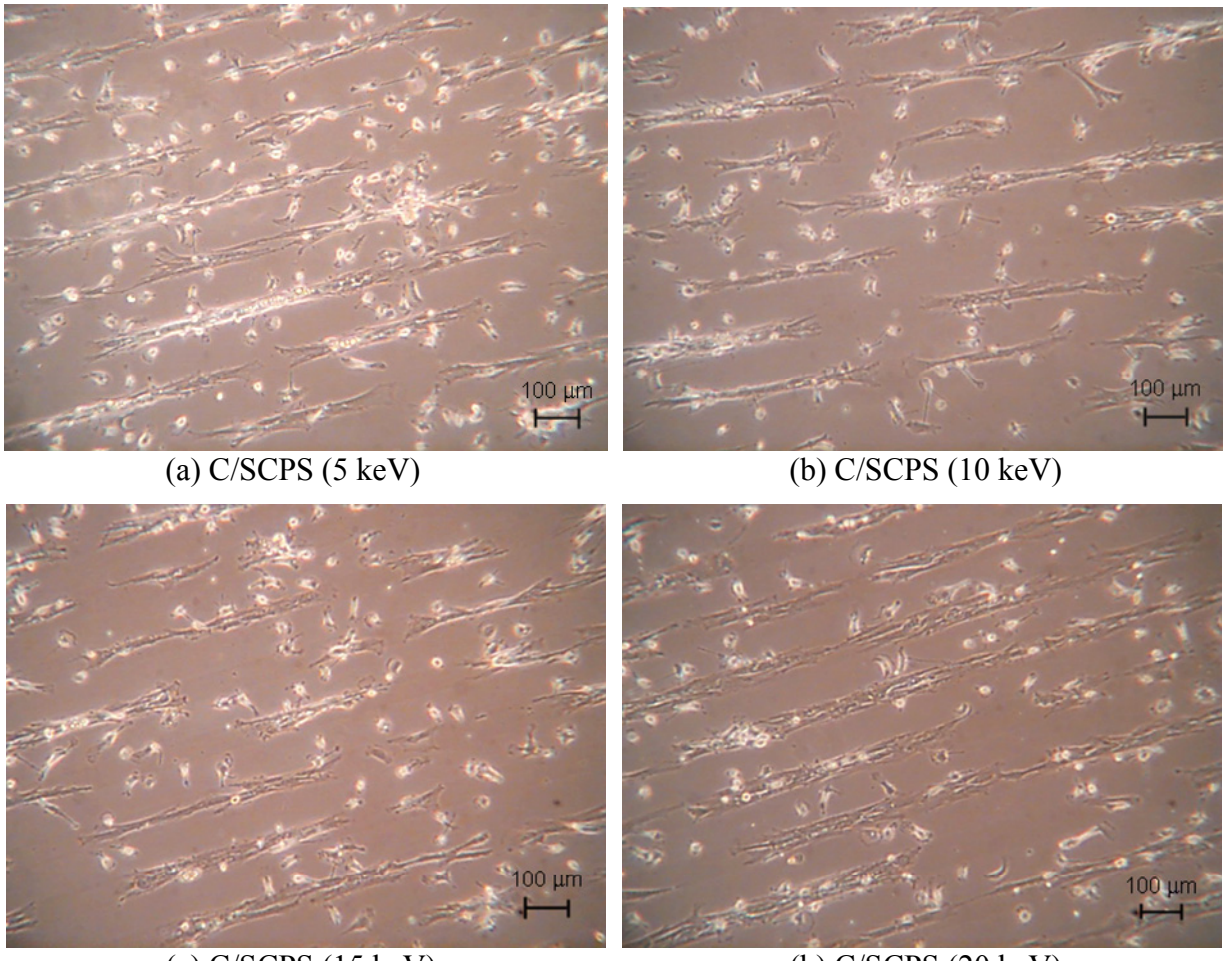


(a) C/SCPS (5 keV) (b) C/SCPS (10 keV)

(a) C/SCPS (15 keV) (b) C/SCPS (20 keV)

Fig. 7.8 Phase-contrast micrographs of MSC after 3-day culture on the $C^-$-implanted SCPS (C/SCPS) at $3\times10^{14}$ ions/cm$^2$ with: (a) 5; (b) 10; (c) 15; and (d) 20 keV.

$C^-$-implanted SCPS at $3\times10^{14}$ ions/cm$^2$ with various energies of 5 – 20 keV. The MSC adhered and spread their body on the implanted region of all energy implantations. Some round-shape MSC also appeared on the unimplanted region. The MSC of both selective spread adhesion and random round-shape adhesion increased their number. Replacement of the culture medium removed some of round-shape MSC. The spread adhered cell almost remained on the implanted region. After 6-day culture, the clear selective adhesions of MSCs were obtained on the implanted region and they are shown in Fig. 7.9, where the cells spread their bodies along the implanted region. The remained cells on the implanted region grew in the number, adhered along the implanted region and reached to the confluence state. Some round-shape MSC from the excess cells also appeared on the unimplanted region.

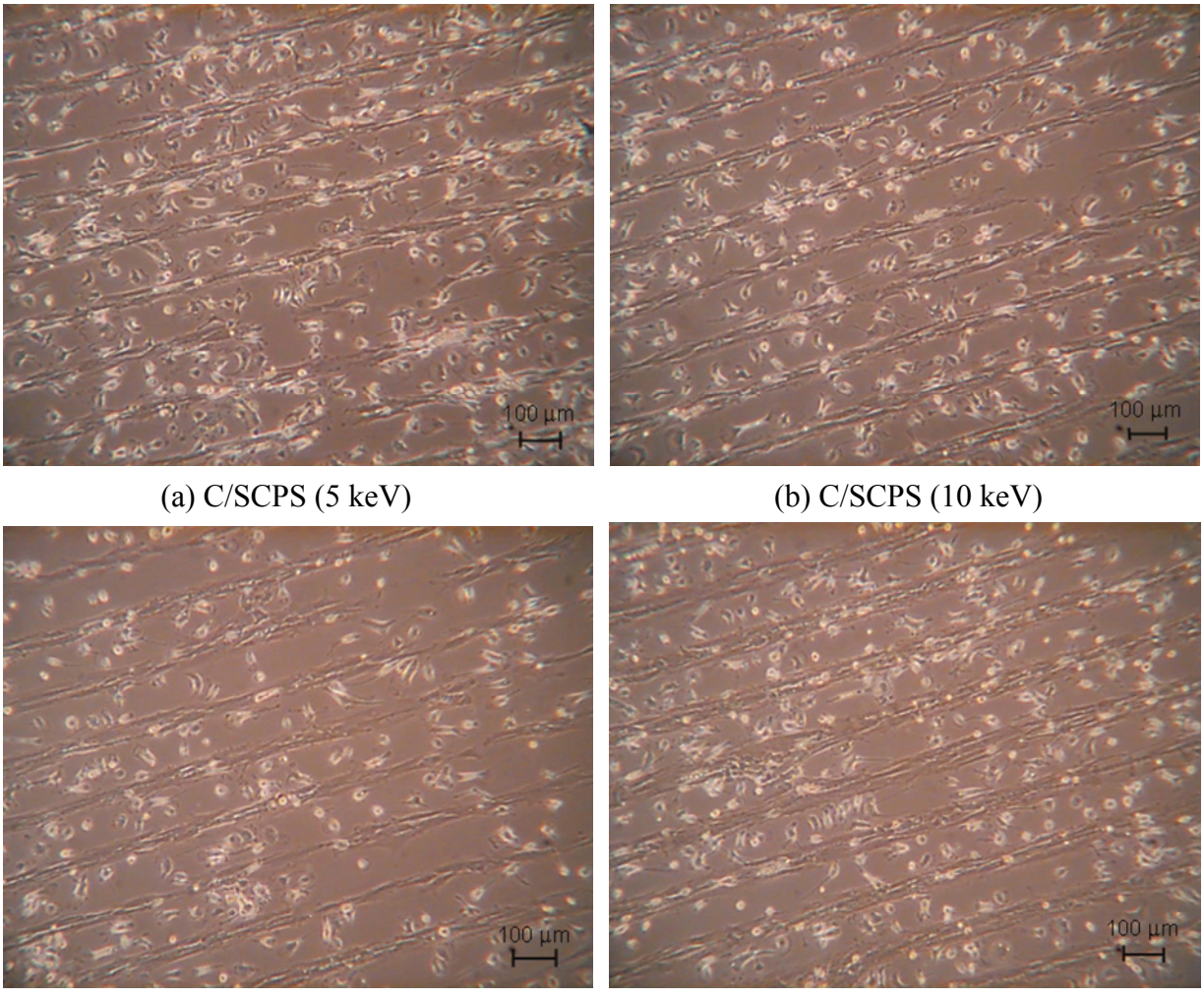


(a) C/SCPS (5 keV) (b) C/SCPS (10 keV)

(c) C/SCPS (15 keV) (d) C/SCPS (20 keV)

Fig. 7.9 Phase-contrast micrographs of MSC after 6-day culture at the confluence state on the $C^-$-implanted SCPS (C/SCPS) at $3\times10^{14}$ ions/cm$^2$ with: (a) 5; (b) 10; (c) 15; and (d) 20 keV.

As a result, there was insignificant different adhesion of MSC on the $C^-$-implanted SCPS at $3\times10^{14}$ ions/cm$^2$ with various energies of 5 – 20 keV. Therefore, there was no effect of implantation energy at this dose on the MSC adhesion patterning. All implantation energies of 5 – 20 keV at $3\times10^{14}$ ions/cm$^2$ were suitable for patterning the adhesion of rat MSC on SCPS.

## 7.3 MSC-Adhesion Patterning of on $C^-$-Implanted SR

The suitable ion implantation conditions in dose and energy for MSC adhesion pattern with maintaining the characteristics of MSC and increasing their number during *in vitro* culture were investigated by culture of the rat mesenchymal stem cells on the $C^-$-modified SR. SR sheets with the thickness of 0.5 mm were obtained from Wacom Electric co., ltd and from Fuji system. The carbon negative ions were implanted into the SR sheet through a micro-pattern mask to pattern the implanted region. As for study of the suitable dose condition for the good adhesion patterning, the carbon negative ions were implanted at the set energy of 10 keV and at the various ion doses from $1\times10^{13}$ to $1\times10^{16}$ ions/cm$^2$ through the previous micro-pattern mask, composed of many slit apertures with 50-μm width and 70-μm spacing. As for study of the suitable energy condition for the good adhesion patterning, the carbon negative ions were implanted at the suitable dose for cell adhesion patterning and at the various ion energies from 5 to 20 keV through the different micro-pattern mask, composed of many slit apertures with 50-μm width and 150-μm spacing.

All implanted samples were sterilized by 70% ethanol, were rinsed three times with the sterilized de-ionized water (DIW) and were rinsed once with the phosphate buffered saline (PBS) before cell culture. The sterilized samples were set into non-treated polystyrene dish (NTPS, Corning) by using 0.33% agarose (Agarose 900, Dojindo, Japan). The rat mesenchymal stem cells, derived from rat bone marrow, from the 3$^{rd}$ passage cells were lifted and were plated on the $C^-$-implanted SR by using the same process described in section 7.2. The cells were cultured on the $C^-$-implanted SR in the serum medium for 20 – 25 days under 5% $CO_2$ at 37°C in incubator. The culture medium of each dish was exchanged by the fresh medium pre-warmed to 37°C every 4 days.

The adhesion properties of rat MSC on $C^-$-implanted SR were observed by phase-contrast microscope (CK2, Olympus) and by fluorescence microscope (BX50, Olympus). Since the sheet surface of SR (Wacom Electric co., ltd) is fulfilled with many patterns, so the observation of position and shape for MSC from phase-contrast image was hardly to be done. The fluorescence microscopy was used to investigate the real adhesive position and the shape of MSC through labeling nucleus and actin-filament (F-actin). The cells were fixed with 4% formaldehyde in PBS for 5 min. Some parts of the cell membrane were dissolved with 0.2%

Triton X-100 (335-01, Nacalai Tesque, Inc., Japan) in PBS for 10 min to allow the large dyne molecules access to the cell's interior. After the samples were rinsed twice with PBS, F-actin of cells were stained with Texas Red-X phalloidin (Cat. no. T7471, Invitrogen, USA) in PBS for 45 min, then the samples were rinsed with PBS for three times. Nucleus of the cells were done with 4', 6-Diamidino-2- phenylindole (DAPI, Sigma-aldrich, Japan) for 30 min, and rinsed with PBS for three times.

### 7.3.1 Effect of Ion Dose on MSC-Adhesion Properties

As for observation of the suitable ion dose condition for patterning rat MSC adhesion on the $C^-$-implanted SR sheet, the SR sheets obtained from Wacom Electric co., ltd were used. The adhesion properties of rat MSC on the $C^-$-implanted SR sheets at the implantation energy of 10 keV are shown in Figs. 7.10 – 7.12.

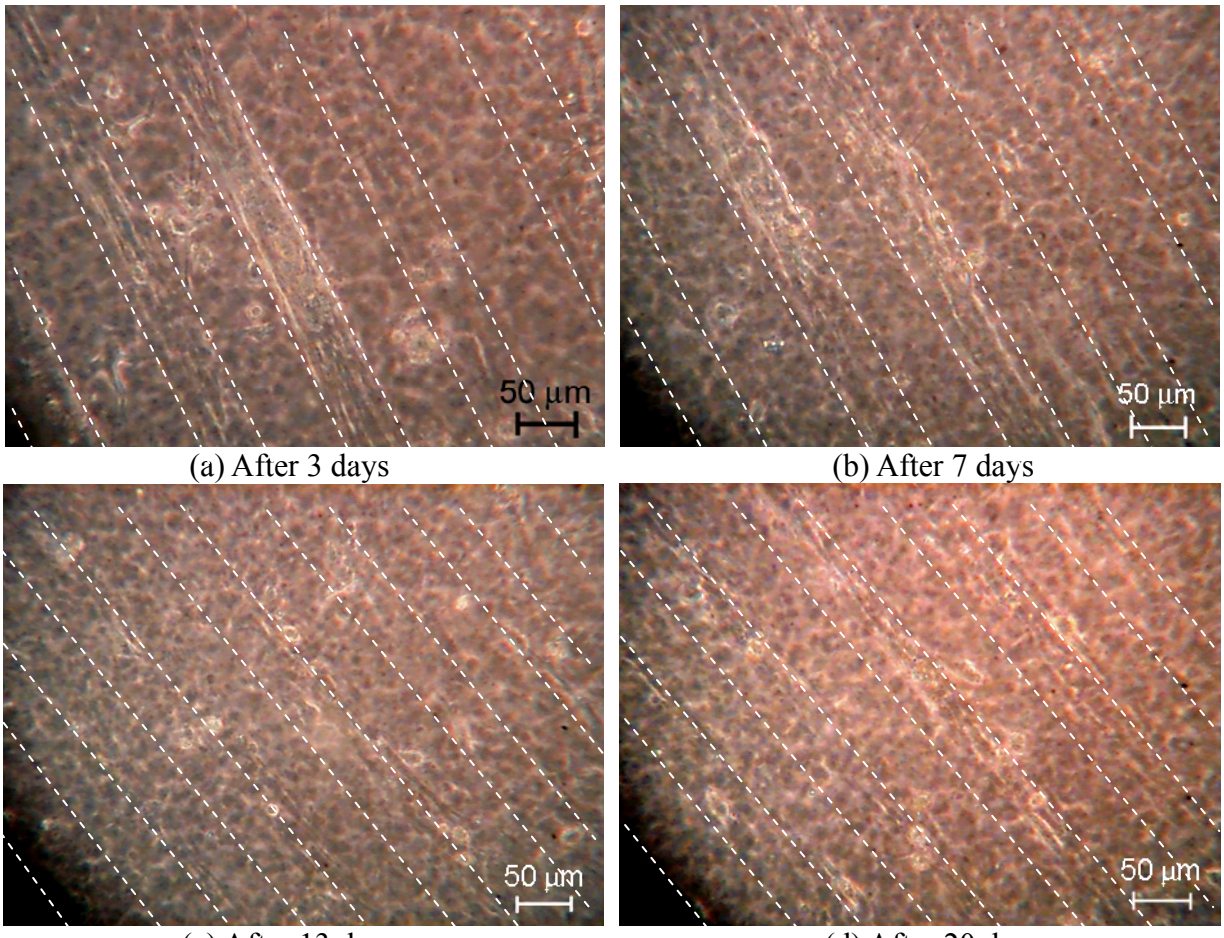


(a) After 3 days (b) After 7 days

(c) After 13 days (d) After 20 days

Fig. 7.10 Phase-contrast micrographs of MSC on the $C^-$-implanted SR (C/SR) at 10 keV and $3\times10^{15}$ ions/cm$^2$ after cultured for: (a) 3; (b) 7; (c) 13 and (d) 20 days.

Typical culture of rat MSC adhesion patterned on the $C^-$-implanted SR at 10 keV and $3\times10^{15}$ ions/cm$^2$ after cultured for 3 – 20 days is shown in Fig. 7.10. Generally, the implanted region on the normal transparent surface could be seen at the implantation dose from $1\times10^{15}$ ions/cm$^2$, but the sheet surface of SR (Wacom Electric co., ltd) is fulfilled with many patterns bringing to the invisible implanted region. Based on phase-contrast microscopy, the adhered MSC narrowly spread their body along the regions as a pattern. The maximum line width of the cell adhesion area was about 50 μm in width, corresponding to the slit aperture width of the applied micro-pattern mask. As described in Chapter 3, carbon negative-ion implantation into SR surface presented of lowering contact angle of SR from the modified hydrophilic bonding on the implanted region. The patterned adhesion area was, therefore, considered to be the implanted region. Not only the spread adhesion of MSC, but also some round-shape adhesion of cells was also found on the unimplanted region. However, this round-shape adhesion did not interfere patterning cell adhesion since the round-shape cells weakly adhered to surface and could be removed by only replacement of the culture medium. Only the adhered cells on the implanted region grew and increased in the number. Therefore, the MSC adhesion patterning on the implanted region of the $C^-$-implanted SR at 10 keV and $3\times10^{15}$ ions/cm$^2$ could be achieved.

The adhesions of MSC on the $C^-$-implanted SR at 10 keV and other doses are shown in Fig. 7.11. The negligible adhesion of round-shape MSC was observed on the $C^-$-implanted SR at $1\times10^{13}$ and $1\times10^{14}$ ions/cm$^2$ as shown in Figs. 7.11 (a) and (b), respectively. At implantation dose of $1\times10^{15}$ ions/cm$^2$, some spread adhesion of MSC along a region as a pattern were first to be observed as shown in Fig. 7.11 (c). However, these adhered cells could be removed during replacement of the culture medium. Then, the implantations into SR at low doses of $1\times10^{13}$ – $1\times10^{15}$ ions/cm$^2$ were not suitable to obtain the good adhesion properties for rat MSC. Comparing to the bond of C-C in SCPS, the back bone bond of Si-O in SR is very strong, so a lot of ion dose are required to cut the strong bonding for the surface modification from hydrophobic to be hydrophilic. The implantation in SR at low doses of $1\times10^{13}$ – $1\times10^{15}$ ions/cm$^2$ could not carry out such ability due to their no lowering and a small lowering of contact angle after dipping in DIW for 24 h as described in Chapter 3. At high dose of $1\times10^{16}$ ions/cm$^2$, the clear patterned adhesion of rat MSC was obtained as shown in Fig. 7.11 (d). Similar to the result at $3\times10^{15}$ ions/cm$^2$ as shown in Fig. 5.10, the cell adhesion areas should be the implanted region since the lowering of contact angle and the maximum line width as the line width of applied micro-pattern mask. The negligible round-shape adhesion of MSC was also found on the unimplanted region, but they did not interfere. The suitable ion dose conditions for patterning rat MSC adhesion on the $C^-$-implanted SR at 10 keV were at $3\times10^{15}$ – $1\times10^{16}$ ions/cm$^2$.

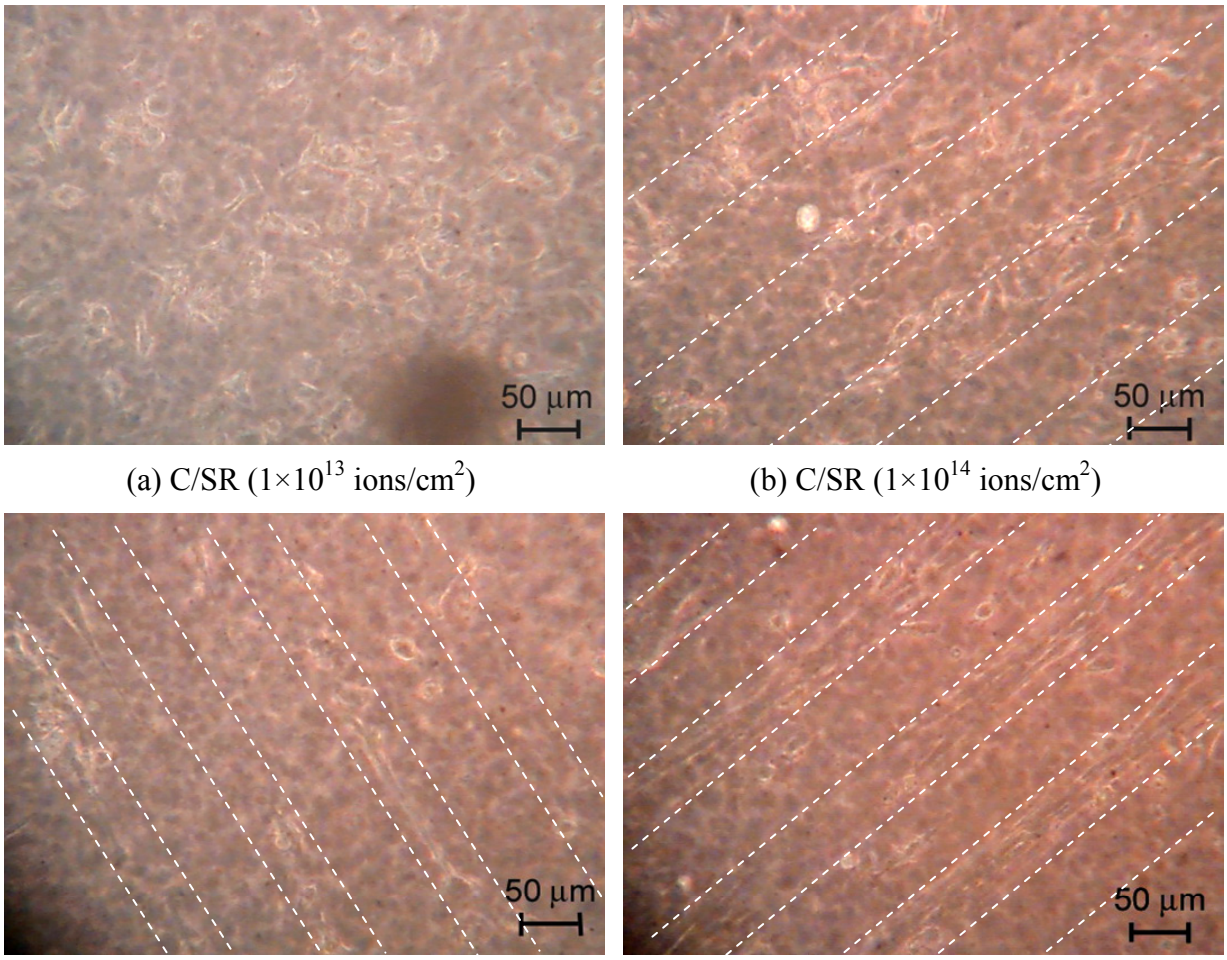


(a) C/SR ($1\times10^{13}$ ions/cm$^2$) (b) C/SR ($1\times10^{14}$ ions/cm$^2$)

(c) C/SR ($1\times10^{15}$ ions/cm$^2$) (d) C/SR ($1\times10^{16}$ ions/cm$^2$)

Fig. 7.11 Phase-contrast micrographs of MSC after 3-day culture on the $C^-$-implanted SR at 10 keV with: (a) $1\times10^{13}$; (b) $1\times10^{14}$; (c) $1\times10^{15}$; and (d) $1\times10^{16}$ ions/cm$^2$.

Since the sheet surface of this SR is fulfilled with many patterns, resulting in the invisible implanted region and in unclear cell adhesion. The immunofluorescent techniques of DAPI with blue color and Texas-red-X phalloidin with red color were applied to label the nucleus and the f-actin, indicating the cell adhesion shape. Based on fluorescent microscopy, rat MSC adhesion patterned on the implanted region of the $C^-$-implanted SR at 10 keV and $3\times10^{15}$ ions/cm$^2$ after 25-day culture is as shown in Fig. 7.12. The cells adhered and spread along the implanted pattern on the surfaces. These adhered and spread cells are shown in Fig. 7.12 (a), but it is difficult to identify the cells. The blue color of DAPI in Fig. 7.12 (b) shows the position of the nucleus. The fiber structures stained by the red color of Texas Red-X phalloidin are shown in Fig. 7.12 (c). It determined the shape of cells, and indicated that the implanted areas were covered by the adhesion of the cells. At the high ion dose of $1\times10^{16}$ ions/cm$^2$, the same selective adhesion of MSC was obtained.

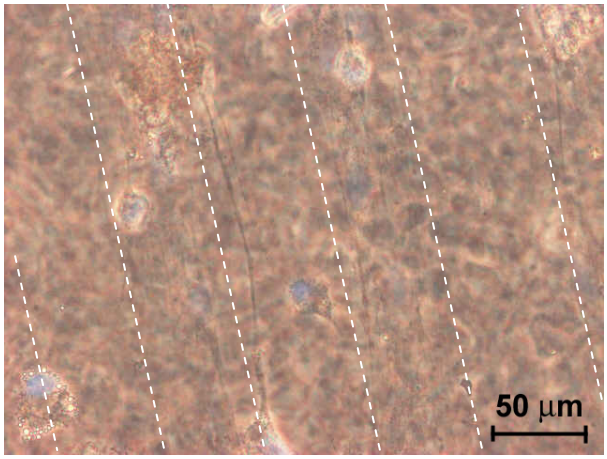


(a) Optical image

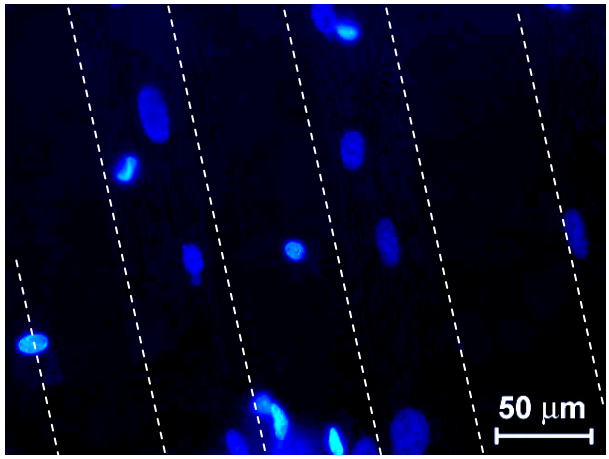


(b) Nucleus

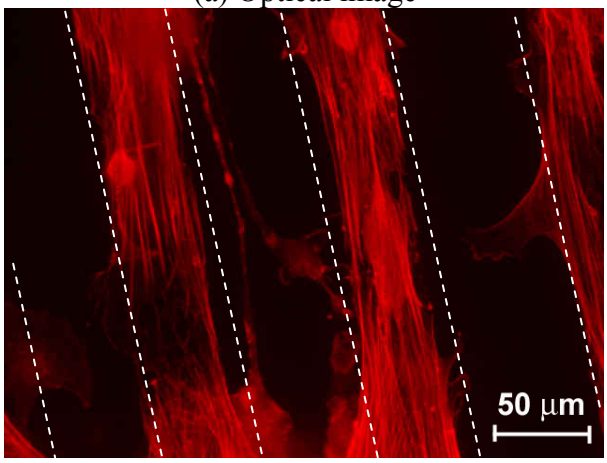


(c) F-actin

Fig. 7.12 Fluorescent micrographs of MSC on the implanted region of the $C^-$-implanted SR at 10 keV and $3\times10^{15}$ ions/cm$^2$: (a) optical image; (b) nucleus (bright blue dot); and (c) F-actin (bright red stripe).

From all observations, the suitable dose condition for pattering of rat MSC adhesion on the $C^-$-implanted SR at 10 keV, therefore, were at $3\times10^{15} - 1\times10^{16}$ ions/cm$^2$.

### 7.3.2 Effect of Ion Energy on MSC-Adhesion Properties

For the study of the effect of the ion energy in the range of 5 – 20 keV, the SR were implanted at the certain dose of $3\times10^{15}$ ions/cm$^2$ that is the suitable dose for patterning the MSC adhesion. In this work, the SR produced from Fuji system was selected. The different micro-pattern mask, consisted of slit apertures with 50-μm width and 150-μm spacing, was used.

Fig. 7.13 shows the adhesion of rat MSC after cultured for 3 days. Almost all of rat MSC selectively adhered and spread their body only on the implanted region of all energy implantations. The selective adhesions of MSC as a pattern on the implanted regions at all

energies of 5 – 20 keV were observed. However, the unclear patterns of MSC adhesion were also observed at 5 and at 20 keV. The sparsely patterned adhesion of rat MSC were found on the SR implanted at low energy of 5 keV (Fig. 7.13 (a)) due to the small amount of the adhered cells on the implanted region. At higher energy of 20 keV (Fig. 7.13 (d)), some spread adhesions of rat MSC on the unimplanted region were observed. Therefore, the nearly complete pattern after cultured for 3 days was obtained on the implantation SR at 10 – 15 keV.

The number of rat MSC increased and reached to the confluence state after cultured for 7 days. The cells cultured for 7 days on the samples implanted at various energies are shown in Figs. 7.14 and 7.15. The completely patterned adhesions of rat MSC at the confluence state on the implanted region of the $C^-$-implanted SR could be obtained at the implantation energies of 10 – 15 keV as shown in Figs. 7.14 (a) and (b), respectively.

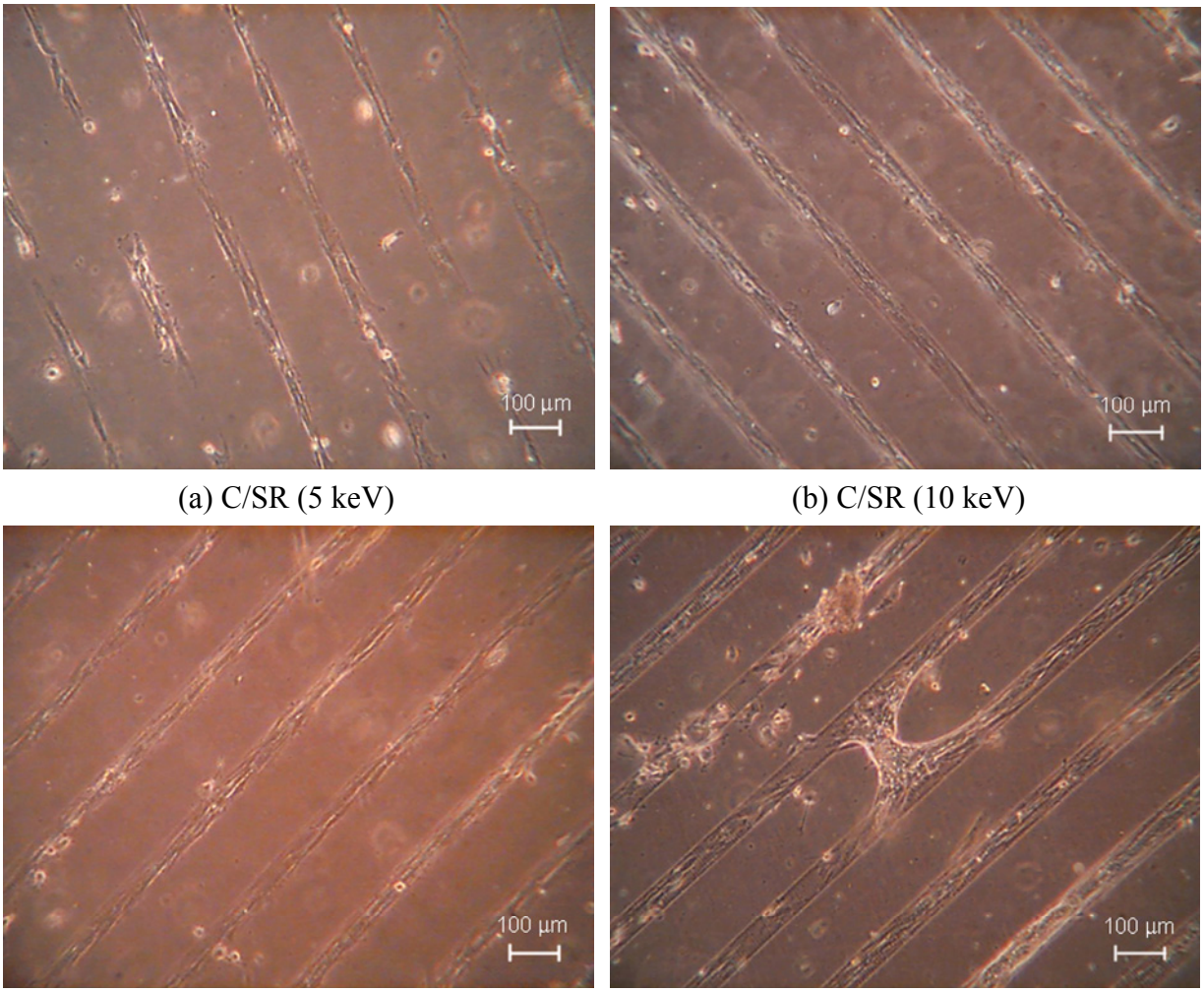


(a) C/SR (5 keV) (b) C/SR (10 keV)

(c) C/SR (15 keV) (d) C/SR (20 keV)

Fig. 7.13 Phase-contrast micrographs of MSC after 3-day culture on the $C^-$-implanted SR (C/SR) at $3\times10^{15}$ ions/cm$^2$ with: (a) 5; (b) 10; (c) 15; and (d) 20 keV.

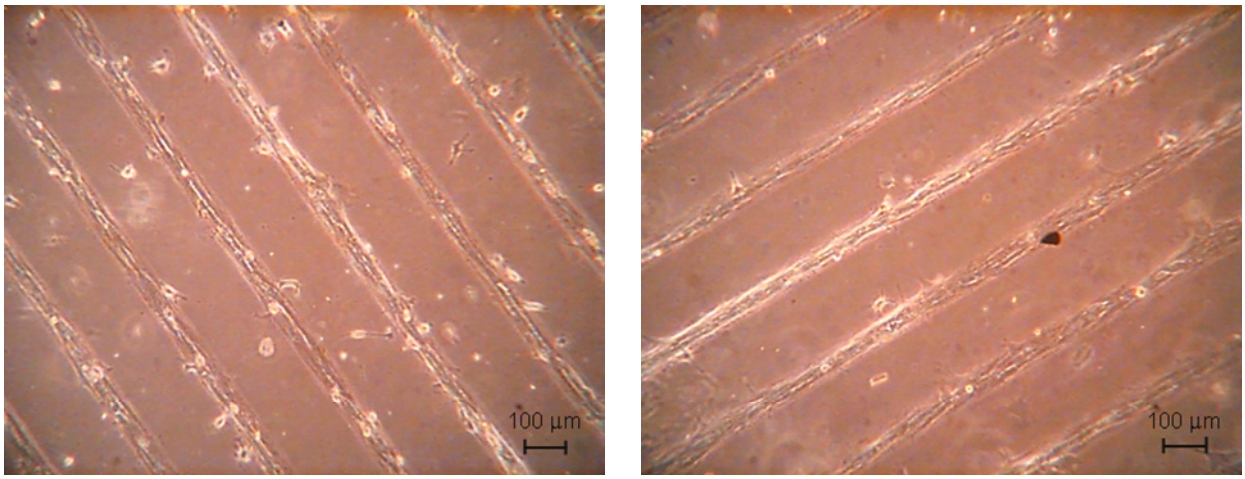


(a) C/SR (10 keV) (b) C/SR (15 keV)

Fig. 7.14 Phase-contrast micrographs of MSC after 7-day culture at the confluence state on the $C^-$-implanted SR (C/SR) at $3\times10^{15}$ ions/cm$^2$ with: (a) 10; and (b) 15 keV.

On the other hands, the incompletely patterned adhesions of rat MSC on the implanted region at low energy of 5 keV is shown in Fig. 7.15 (a). Some cells detachments appeared, even on the implanted region. This detachment might be due to the weak adhesion of cells on this implanted region. At high energy of 20 keV, almost all of the cells adhered on the implanted region, and some also adhered on the unimplanted region as shown in Fig. 7.15 (b). This might be considered to be due to the effect of the emitted gas particles. The emitted gas particles from the implanted areas at high energy increased more than that at low energy. Therefore, the adsorption of the emitted gas particles on the surface at high energy might influence on the cell

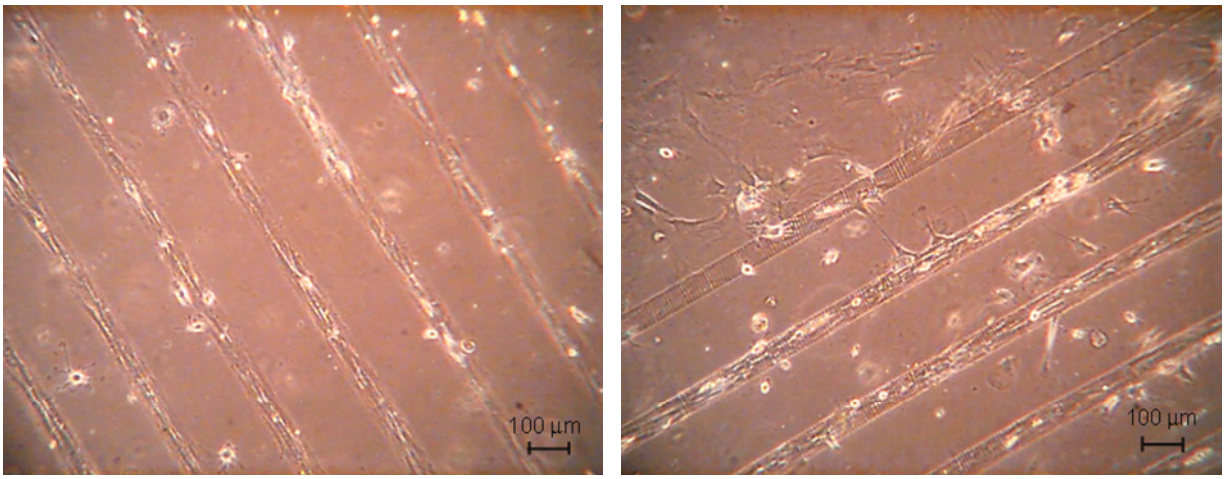


(a) C/SR (5 keV) (b) C/SR (20 keV)

Fig. 7.15 Phase-contrast micrographs of MSC after 7-day culture at the confluence state on the $C^-$-implanted SR (C/SR) at $3\times10^{15}$ ions/cm$^2$ with: (a) 5; and (b) 20 keV.

adhesion. At the confluence state, cells on the implanted region started to migrate and adhere on the unimplanted region. The non selective adhesion of rat MSC on the $C^-$-implanted SR at 20 keV started to be observed. The suitable implantation energy at $3\times10^{15}$ ions/cm$^2$ for pattering the adhesion of rat MSC on $C^-$-implanted SR was at 10 – 15 keV

## 7.4 Differentiation of MSC on $C^-$-Implanted SCPS

The differentiation of MSC on the $C^-$-implanted SCPS was examined, after obtaining the MSC adhesion patterning on the SCPS by the implantation at $3\times10^{14}$ ions/cm$^2$ and 10 keV. The process of differentiation induction in rat MSC into neuron-like cells follows the method using the $\beta$ −mercaptoethanol (BME) that was reported Woodbury *et al.* [9-10]. I proposed two different culture media of the pre-induction and the induction media. The pre-induction medium was for familiarizing the cells to BME without the differentiation induction. The effect of BME was suppressed by supplement of serum. The pre-induction medium was the serum medium of Dulbecco's modified Eagle's medium (DMEM, Nissui, Japan) containing 1 mM BME (BME, M3148, Sigma-aldrich, USA), 20% fetal bovine serum (FBS, Trace Scientific Ltd., Australia), sodium hydrogen carbonate (1.64 mg/ml, Wako, Japan), and antibiotic of penicillin G and streptomycin. The induction medium was for differentiation induction into neuron-liked cells. It was the serum-free medium of DMEM (Nissui, Japan) containing 1mM BME, sodium hydrogen carbonate (1.64 mg/ml, Wako, Japan), and antibiotic of penicillin G and streptomycin.

After the completely patterned adhesion of MSC on the $C^-$-implanted SCPS was obtained, the differentiation induction process was started. At first, the culture medium was replaced with the pre-induction medium, and the cells were incubated for 24 h. The pre-induction medium was removed and the cells were rinsed once with PBS. Just after adding the induction medium, the differentiation was induced. The induced differentiation was observed every 30 min by the phase-contrast microscope (CK2, Olympus). After rat MSC differentiated into neuron-like cells, the induction medium was removed and the cells were rinse once with PBS. The cells were then cultured in the serum-free neurobasal medium (Cat. no. 12348-017, lot no.#1214994, Gibco, USA) supplementing with B27 (Cat. no. 17504-044, lot no.#1219115, Gibco, USA) for 10 days.

Finally, the cells were observed by the fluorescent microscopy (BX50, Olympus). Double staining of the neuron-specific enolase (NSE) and nucleus on the differentiated cells were studied. The cells were coated with 1% agarose (Agarose 900, Dojindo, Japan) and were fixed with 4% formaldehyde in PBS for 5 min. Some parts of the cell membrane were dissolved with 0.2% Triton X-100 (335-01, Nacalai Tesque, Inc., Japan) in PBS for 10 min, and the samples were rinsed twice with PBS. The differentiated cells were stained with polyclonal rabbit

anti-NSE (Cat. no. 40500510, Quartett, Germany) in the bovine serum albumin (BSA, Cat. no. 309-00563, lot no.# 401-038, Wako Pure Chemical Industries Ltd., Japan) solution (5 mg BSA in 1 ml PBS) for 60 min, and then the excess antibody was removed by rinsing three times with PBS. The NSE was bound to fluorescent by the goat anti-rabbit-fluorescein isothiocyanate (FITC, Cat. no 234, Medical & Biological Laboratories, Japan) in BSA solution. The dye excess was removed by rinsing three times with PBS. After that the cells were again stained with DAPI for 30 min, and rinsed with PBS for three times.

The differentiation induction was applied for the patterned adhesion MSC on the $C^-$-implanted SCPS at $3\times10^{14}$ ions/cm$^2$ and 10 keV as shown in Fig. 7.5 (b). After the cells were cultured in the pre-induction medium for 24 h, the state of cells is shown in Fig. 7.16. The cells still adhered and spread their body along the implanted region. Any change in cell shape was not observed.

After replacement with the induction medium for 30 min, the cells started to decrease in size. The spread cells were sharply defined against each other within 60 min as shown in Fig. 7.17 (a). The cells gradually changed their shape to have a rounded cell body from 60 min to 120 min as shown in Fig. 7.17 (b). At the same time, the shapes for neuron-like cells with outgrowth of neurite were observed. After 180 min, almost all of the MSCs were differentiated into neuron-like cells, so the differentiation induction was stopped. The neuron-like cells were then cultured in the serum-free neurobasal medium supplementing with B27. The differentiation of rat MSC adhesion patterning on the $C^-$-implanted SCPS at $3\times10^{14}$ ions/cm$^2$ and 10 keV could then be completed.

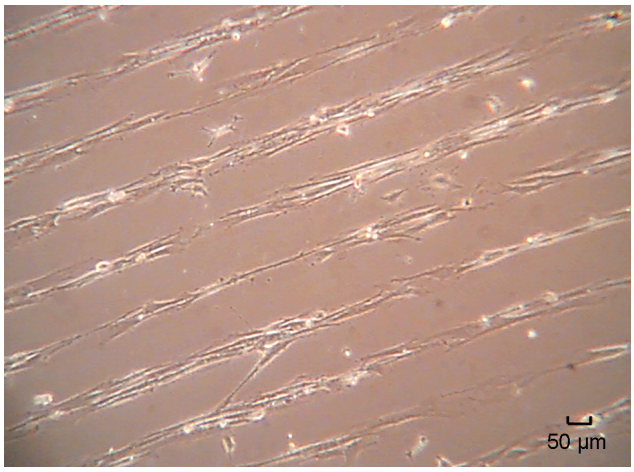


Fig. 7.16 Phase-contrast micrographs of MSC on the $C^-$-implanted SCPS at 10 keV and $3\times10^{14}$ ions/cm$^2$ after cultured in the pre-induction medium for 24 h.

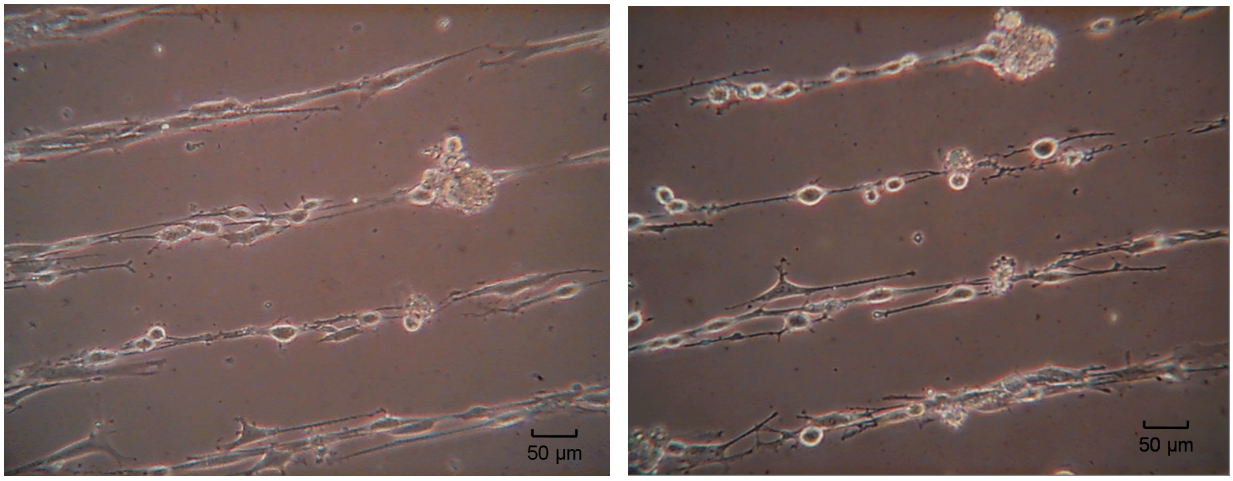


(a) C/SCPS (BME 1 mM for 60 min) (b) C/SCPS (BME 1 mM for 120 min)

Fig. 7.17 Phase-contrast micrographs of MSC differentiation into neuron on the $C^-$-implanted SCPS (C/SCPS) at 10 keV and $3\times10^{14}$ ions/cm$^2$ after supplement with 1 mM BME for: (a) 60; (b) 120 min.

After differentiation for 1 day, no differentiation back to MSC was observed as shown in Fig. 7.18 (a). The neuron-like cells still remained on the implanted region even if after differentiation for 10 days as shown in Fig. 7.18 (b).

In order to confirm the neuron differentiated from MSC, the immunofluorescent technique for labeling the neuron-specific enolase (NSE) characterizing neuron [12] was applied to the differentiated cells. The observed micrographs are shown in Fig. 7.19. The NSE labeled

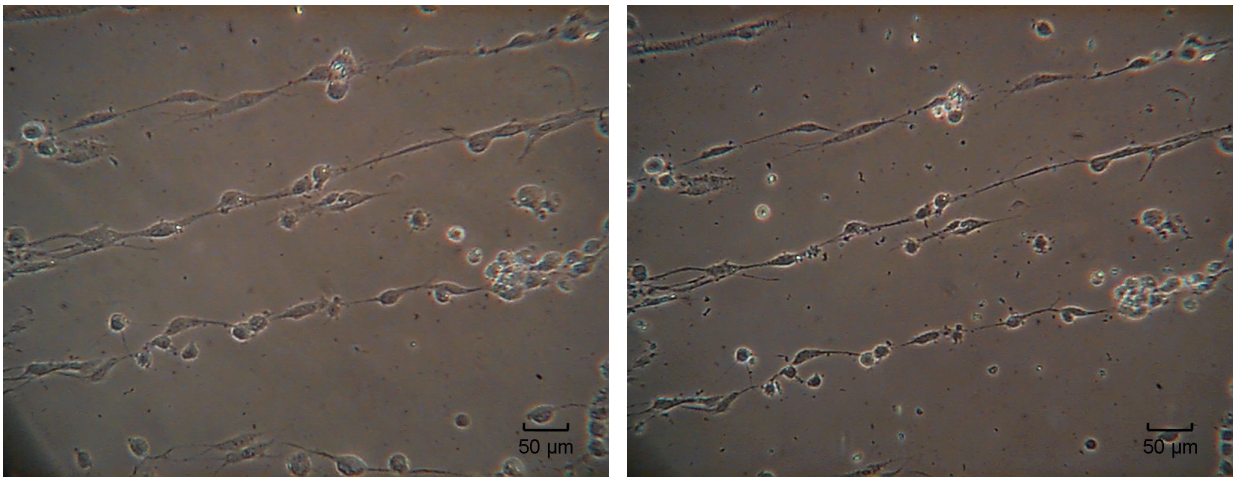


(a) C/SCPS (after differentiation for 1 day) (b) C/SCPS (after differentiation for 10 day)

Fig. 7.18 Phase-contrast micrographs of neuron-liked cells differentiated from rat MSC on the $C^-$-implanted SCPS (C/SCPS) at 10 keV and $3 \times 10^{14}$ ions/cm$^2$ after differentiation for (a) 1 day; and (b) 10 days.

with green color well agreed with the cells appeared in the phase-contrast micrograph of Fig. 7.19 (a). This means these cells were neurons. From Fig. 7.19 (b), the nucleus of cells were still observed after cultured in the neurobasal medium for 10 days. This means the cells were still alive, even if after differentiation for 10 days.

Therefore, the patterning of the neuronal cells from MSC differentiation could be achieved and be remained on the patterned polystyrene by carbon negative-ion implantation. So, the neuron network could be performed by the culture of MSC and differentiation into neuron on polystyrene patterned by carbon negative-ion implantation.

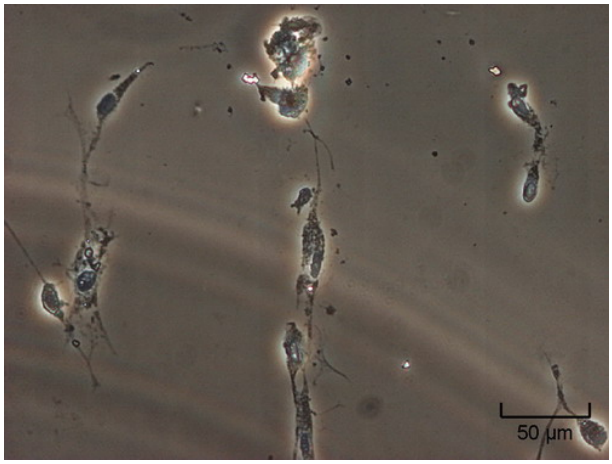


(a) Optical image

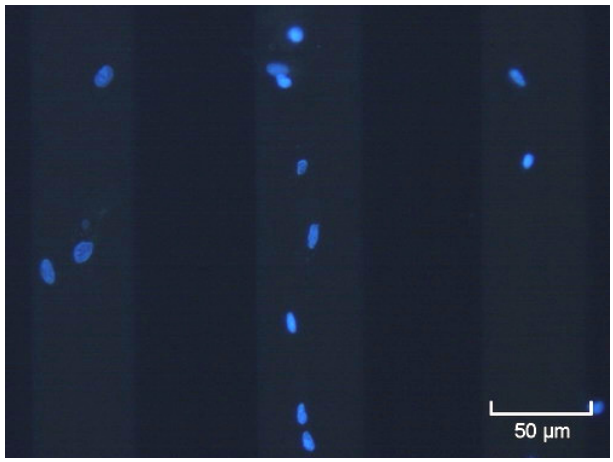


(b) Nucleus

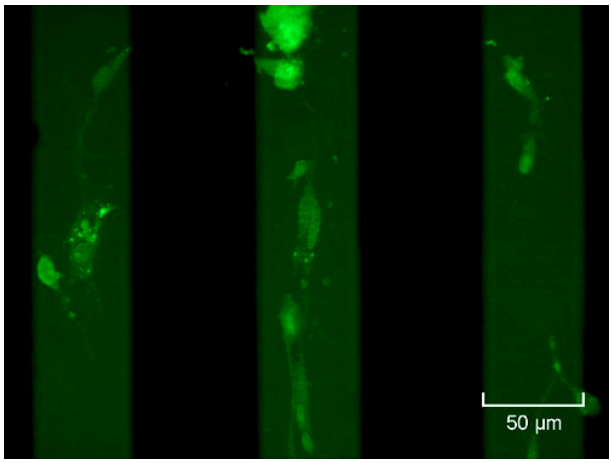


(c) NSE

Fig. 7.19 Fluorescent micrographs of neuron-liked cells differentiated from rat MSC on the implanted region of the $C^-$-implanted SCPS at 10 keV and $3\times10^{14}$ ions/cm$^2$: (a) optical image; (b) nucleus (bright blue dot); and (c) NSE (bright green mark).

## 7.5 Differentiation of MSC on $C^-$-Implanted SR

The MSC differentiation into neuron-like cells on the $C^-$-implanted SR was investigated. Carbon negative ions were implanted into SR from Fuji system at $3\times10^{15}$ ions/cm$^2$ and 10 keV, referred to the suitable dose and energy for the selective adhesion of rat MSC as described in section 7.3. The micro-pattern mask composed of many slit apertures with 50-μm width and 150-μm spacing was used. Rat MSC from the 1$^{st}$ passage were cultured on the $C^-$-implanted SR as described in sections 7.2.1 and 7.3.1. After cells became to the confluence state, they were differentiated with the same process as described in section 7.4.

The differentiation induction was applied for the patterned adhesion of MSC on the $C^-$-implanted SR at $3\times10^{15}$ ions/cm$^2$ and 10 keV as shown in Fig. 7.14 (a). Fig. 7.20 shows the state of the cells after cultured in pre-induction medium for 24 h. Any change in cell shape was not observed. After replacement with the induction medium for 30 min, the cells started to decrease in size. The spread cells were sharply defined against each other within 60 min. About 80% of adhere cells gradually changed their shape to have a rounded cell body from 60min to 180 min as shown in Figs. 7.21 (a) – (d). At the same time, the shapes for neuron-like cells with outgrowth of neurite were observed. The differentiation of rat MSC adhesion patterning on the $C^-$-implanted SR at $3\times10^{15}$ ions/cm$^2$ and 10 keV was observed. Therefore, the carbon negative-ion implantation into SR could pattern the adhesion of rat MSC and pattern their neuron-like cells from MSC differentiation. The differentiated cells were considered to be neuron, similar to the neurons on the $C^-$-implanted SCPS described in section 7.4.

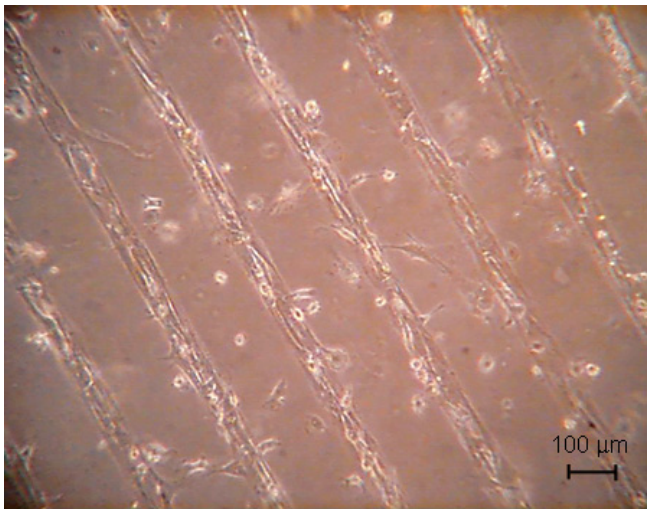


Fig. 7.20 Phase-contrast micrographs of MSC on the $C^-$-implanted SR (C/SR) at 10 keV and $3\times10^{15}$ ions/cm$^2$ after cultured in the pre-induction medium for 24 h.

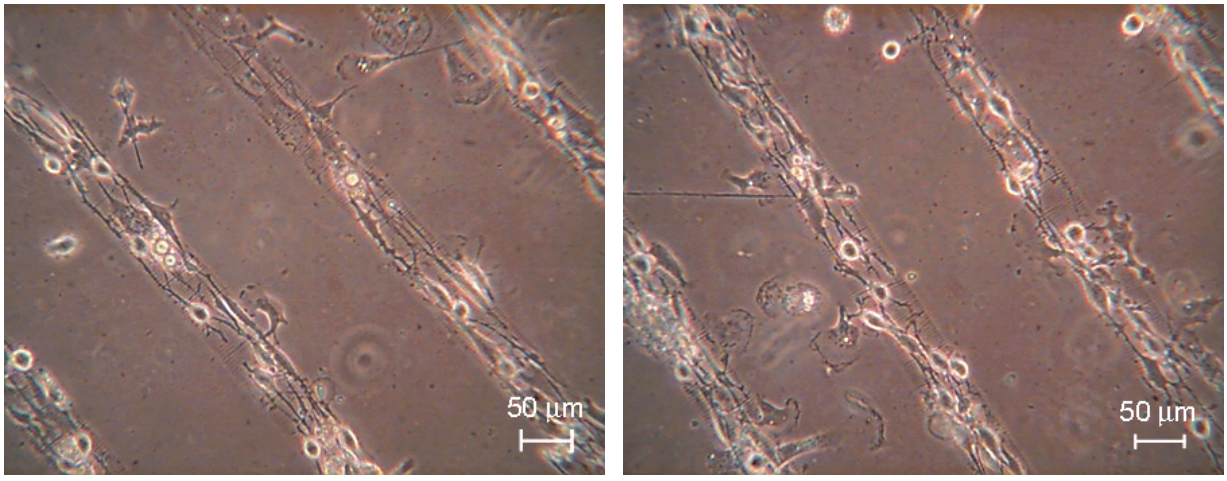


(a) C/SR (BME 1 mM for 60 min) (b) C/SR (BME 1 mM for 120 min)

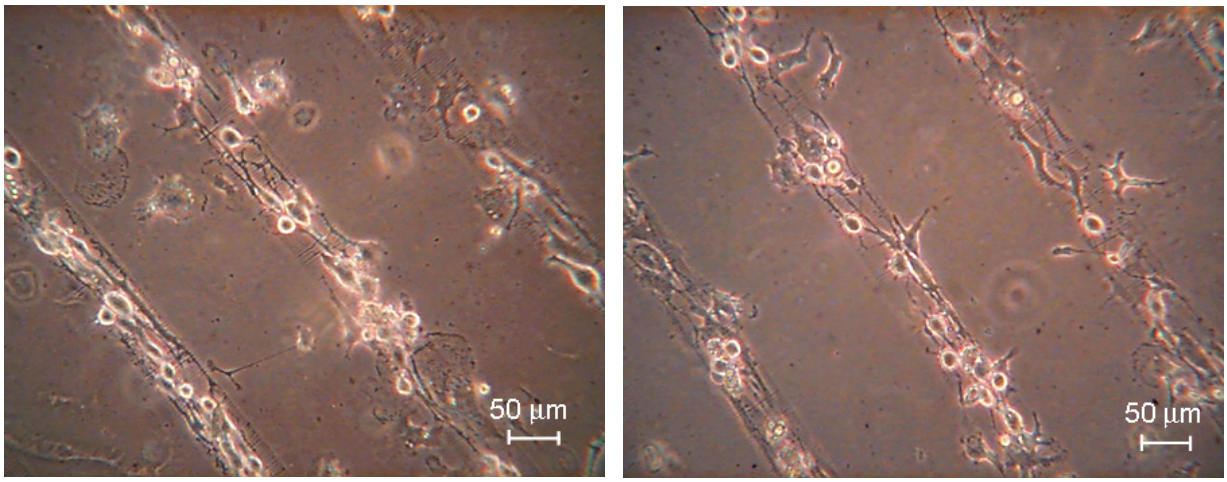


(a) C/SR (BME 1 mM for 150 min) (b) C/SR (BME 1 mM for 180 min)

Fig. 7.21 Phase-contrast micrographs of MSC differentiation into neuron on the $C^-$-implanted SR (C/SR) at 10 keV and $3\times10^{15}$ ions/cm$^2$ after supplement with 1 mM BME for: (a) 60; (b) 120; (c) 150; (d) and 180 min.

## 7.6 Summary

The multipotential mesenchymal stem cell (MSC) is attractive for research and clinical therapy, such as nerve regeneration, gene therapy etc., since their characteristics of self-renewal and differentiation into many cell lines, as well as in neuron. The artificial neuron network by differentiation of MSC is also possible. For this purpose, the suitable conditions for adhesion and differentiation on the pattern adhesion are necessary. In this chapter, the carbon negative ions were implanted into the polymeric surfaces of SCPS and SR for investigation of the fine pattern adhesion of rat MSC and the differentiation induction into neuron-like cells on this pattern.

The suitable dose for patterning MSC adhesion on the implanted region of the

$C^-$-implanted SCPS was at $3\times10^{14}$ – $1\times10^{15}$ ions/cm$^2$ for energies of 5 – 20 keV. That of the $C^-$-implanted SR was at $3\times10^{15}$ – $1\times10^{16}$ ions/cm$^2$ for energies of 10 – 15 keV. The difference in the suitable ion dose for MSC adhesion patterning on the SCPS and SR were 10 times. The reasons were still unknown, but they might be considered to be due to the different main chain bonding and the different elements in both polymeric materials. The requirement of the higher dose and energy to modify the surface of SR might be due to the tight bonding of Si-O in the main chain and the reflection of the implanted ions on SR. The suitable dose and energy for the good properties of rat MSC adhesions on the $C^-$-implanted surfaces of SCPS and SR can be summarized as shown in Tables 7.1 and 7.2. Comparing to the patterning of the adhesion of PC12h cells, the patterning of the MSC adhesion could be obtained by using a little different control in ion dose and energy. In case of the SCPS surface, the adhesion patterning of the MSC required a smaller implantation dose than that of PC12h cells for 10 times. This reason might be considered to be due to the characteristics of cell-self. There was no effect of the implantation energy at the suitable dose on the adhesion patterning of MSC and PC12h cells. In case of the SR surface, almost the same adhesion patterning of the MSC and PC12h cells were observed. From the PC12h cell culture, the fundamental assessments for control the patterning of the cell adhesion were obtained. Therefore, there is no need to culture the rat MSC at all ion implantation dose and energy. The tendency of the control condition of the implantation for the MSC adhesion patterning could be predicted by considering the tendency of the control condition for PC12h cell.

As for the differentiation into neuron, the rat MSCs were cultured on the $C^-$-implanted SCPS at $3\times10^{14}$ ions/cm$^2$ with 10 keV and on the $C^-$-implanted SR at $3\times10^{15}$ ions/cm$^2$ with 10 keV to obtain a clear selective adhesion pattern. After the cells grew to the confluence state, they were differentiated by using the induction of BME. The pattern of neuron differentiated from the adhered MSC could be achieved. The MSC ability to differentiation into neuron still retained on the implanted region and the patterning of the neuron-differentiated cells still remained on the implanted region. The formation of the neuron network could be achieved by the culture of MSC and its differentiation. Comparing to the patterning of the brain neuronal cells, the adhesion patterning of MSC and its neuron-differentiated cells were no need the coating of PDL on the surface. Moreover, the adhesion patterning of the MSC might have more advantage in the clinical applications since its great characteristic of differentiation into many kinds of cell lines.

Table 7.1 The rat MSC adhesion property on the $C^-$-implanted SCPS

| Energy (keV) | Adhesion property in the ion dose range (ions/cm$^2$) | | | | | |
|---|---|---|---|---|---|---|
| | $10^{13}$ | $10^{14}$ | | $10^{15}$ | | $10^{16}$ |
| | | 1 | 3 | 1 | 3 | |
| 5 | - | - | ○ | - | - | - |
| 10 | × | Δ | ○ | ○ | Δ | Δ |
| 15 | - | - | ○ | - | - | - |
| 20 | - | - | ○ | - | - | - |

Table 7.2 The rat MSC adhesion property on the $C^-$-implanted SR

| Energy (keV) | Adhesion property in the ion dose range (ions/cm$^2$) | | | | | |
|---|---|---|---|---|---|---|
| | $10^{13}$ | $10^{14}$ | | $10^{15}$ | | $10^{16}$ |
| | | 1 | 3 | 1 | 3 | |
| 5 | - | - | - | - | Δ | - |
| 10 | × | × | × | Δ | ○ | ○ |
| 15 | - | - | - | - | ○ | - |
| 20 | - | - | - | - | Δ | - |

## References


[1] A.J. Becker, E.A. McCulloch, J.E. Till, “Cytological Demonstration of the Clonal Nature of Spleen Colonies Derived from Transplanted Mouse Marrow Cells”, Nature vol. 197, pp. 452-454, 1963.

[2] L. Siminovitch, E.A.McCulloch, J.E.Till, “The Distribution of Colony-forming Cells among Spleen Colonies”, J. Cell. Comp. Phy., vol. 62, pp. 327-336, 1963.

[3] A.J. Friedenstein, U.F. Deriglasova, N.N. Kulagina, A.F. Panasuk, S.F. Rudakowa, E.A. Luria, I.A. Ruadkow, “Precursors for Fibroblasts in Different populations of Hematopoietic Cells as Detected by the *In Vitro* Colony Assay Method”, Exp. Hematol., vol. 2 (2) pp. 83-92, 1974.

[4] B.E. Tuch, “Stem Cells--a Clinical Update”, Aust. Fam. Physician, vol. 35 (9), pp. 719-21, 2006.

[5] R.L. Gardner, “Stem Cells: Potency, Plasticity and Public Perception”, J. Anat., vol. 200 (3), pp. 277-282, 2002.

[6] S. Bobis, D. Jarocha and M. Majka, “Mesenchymal stem cells: characteristics and clinical applications”, Folia Histochemica Et Cytobiologica, vol. 44, no. 4, pp. 215-230, 2006.

[7] SL.Gerson, “Mesenchymal Stem Cells: No Longer Second Class Marrow Citizens”, Nat Med., vol. 5, pp. 262–264, 1999.

[8] E.A. McCulloch, J.E. Till, “The Radiation Sensitivity of Normal Mouse Bone Marrow Cells, Determined by Quantitative Marrow Transplantaiton into Irradiated Mice”, Radiation Research, vol. 13, pp.115-125, 1960.

[9] D. Woodbury, E.J. Schwarz, D.J. Prockop, and I.B. Black, “Adult Rat and Human Bone Marrow Stromal Cells Differentiate into Neurons”, J.Neurosci. Res., vol. 61, pp. 364-370, 2000.

[10] D. Woodbury, K. Reynolds, I.B. Black, “Adult Bone Marrow Stromal Stem Cells Express Germline, Ectodermal, Endodermal, and Mesodermal Genes Prior to Neurogenesis”, J. Neurosci. Res., vol. 69, 6, 908-917, 2002.

[11] M.M. Bonab, K. Alimoghaddam, F. Talebian, S.H. Ghaffari, A. Ghavamzadeh, and B. Nikbi, “Aging of Mesenchymal Stem Cell *In Vitro*”, BMC Cell Biology 2006, vol. 7, no. 14, Published online 2006 March 10, doi:10.1186/1471-2121-7-14.

[12] T. Kirino, M.W. Brightman, W.H. Oertel, D.E. Schmechel and P.J. Marangos, “Neuron-Specific Enolase as an Index of Neuronal Regeneration and Reinnervation”, J. Neurosci., vol. 3, no. 5, pp.915-923, 1983.

# Chapter 8

# Conclusions and Prospects

## 8.1 Conclusions

This study aimed to study the immobilization and patterning of neuron adhesion on the polymeric surface by using carbon negative-ion implantation technique for future application in the biomedical remedies. For this purpose, I investigated (1) the effect of ion implantation on the physical surface properties, (2) the relation among the modified surface and the adsorption of adhesive proteins and cell-adhesion mechanism, and (3) the parameters to control the cell adhesion. As the polymeric materials in the medical field to be studied, the spin-coated polystyrene (SCPS) and silicone rubber (SR) were selected. Although both materials have a difference in the main chain structure, I obtained almost the same effect of the implantation on the modification of both polymer surfaces. The effects of the ion implantation into these polymeric surfaces on the physical surface property relating to the protein adsorption and cell adhesion were clarified. The new atomic bonding was studied by XPS analysis. The surface morphology was examined by AFM. The wettability was evaluated by contact angle measurement. The adsorption properties of adhesive protein on the modified surfaces were studied and were used to predict the cell-adhesion properties on each modified surface. The fundamental conditions for the control of the patterning of the cell adhesion and neurite outgrowth were studied by the cultivation of rat adrenal pheochromocytoma cells (PC12h) since its specific characteristics of neurite outgrowth similar to neuron ones and its strong ability to survival. Then, the adhesion patterning of the brain neuron and stem cell, as well as its neuronal-differentiated cell, was accomplished. The obtained results are summarized as follows.

In Chapter 3, the change in the physical surface properties, relating to the adsorption properties of adhesive proteins, after the implantation was described. XPS analysis showed the formation of new oxygen function groups of hydroxyl and carbonyl on the implanted surfaces from the ion-induced defects. These new bonds refer to the hydrophilicity for the wettability. The implantation changed the surface morphology of surface roughness. As for the implantation in to polystyrene at 10 keV and $3\times10^{15}$ ions/cm$^2$, the surface roughness within the acceptable value, which dose not interfere to the protein adsorption and to cell culture, was obtained. As for the implantation into SR at the same condition, the smoother surface was obtained. The wettability properties of the $C^-$-implanted surfaces of SCPS and SR were evaluated by measuring the

change in contact angle with using two different methods of the water drop method and the air bubble method. The circumstance dependence and time dependence on the change in contact angle were obtained by the air bubble method. The contact angles decreased with an increase in the ion dose for all implantation energies of 5 – 20 keV. There was little implantation effect of energy on the lowering of contact angle in cases of the $C^-$-implanted surfaces of SCPS and SR. By air bubble method, the lowering of the contact angles saturated in the dose order of $10^{15}$ ions/cm$^2$ for both implanted surfaces of SCPS and SR after dipping in the de-ionized water for 48 h. The lowest angle of both implanted surfaces of SCPS and SR took place at the dose of around $2\times10^{15} – 3\times10^{15}$ and at the dose of $1\times10^{16}$ ions/cm$^2$, respectively.

In Chapter 4, the evaluation of the adsorption properties of the adhesive proteins for cell adhesion on the modified surfaces of SCPS and SR to estimate and to predict the selective cell-adhesion properties was described. The important adhesive proteins of type-collagen, fibronectin (FN) and laminin (LN), and the polycation polymer of poly-D-lysine (PDL) were selected. By detecting the amounts of nitrogen atoms adsorbed on the surfaces with using XPS analysis, the adsorption properties were improved by carbon negative-ion implantation. The selective adsorption properties of each adhesive protein and PDL on each modified surface could be controlled by the coating concentration and the ion dose. A clear difference in the adsorption properties between the unimplanted and implanted regions of each modified surface was obtained, but it was not so high. Almost the selective adsorption ratios of each protein were 1.25 – 1.6 for the coating surface of the $C^-$-implanted SCPS and were 1.6 – 3.3 for the coating surface of the $C^-$-implanted SR.

In Chapter 5, the fundamental assessments for the patterning of PC12h-cell adhesion and neurite outgrowth were demonstrated. The carbon negative-ion implantation into polymeric surfaces of SCPS and SR could improve and control the properties of cell adhesion and neurite outgrowth. The clear selective cell-adhesion pattern was observed on the implanted region. The patterning of cell adhesion and neurite outgrowth could be controlled by the implantation conditions of ion dose, ion energy and implanted line width, and by the additional adhesive protein coating. The suitable implantation dose and energy for the properties of selective cell-adhesion and neurite outgrowth were dose order of $10^{15}$ ions/cm$^2$ and energies of 10 – 20 keV, respectively. The best condition was at dose of $3\times10^{15}$ ions/cm$^2$ and energy of 10 keV. As for the additional protein coating with the cell-adhesion properties, the additional protein coating on the implanted surface at the best implantation condition improved the cell adhesion property. The more improvement of the cell-adhesion pattern on the $C^-$-implanted SR was observed by coating with fibronectin at 1 μg/ml. As for the immobilization of cell adhesion and neurite outgrowth on the implanted SCPS at the best dose, the effective minimum line widths for the adhesion of single cell-body and single neurite outgrowth were about 5 and 2 μm, respectively.

They decreased with an increase in the implantation energy. The suitable line widths for the adhesion of the cell-body and for only outgrowth of neurite on the $C^-$−implanted SCPS was about 20 and 5 μm, respectively. As for a simple neuron network formation as a grid pattern on the $C^-$-implanted SCPS at 10 keV, the suitable dose was at $3\times10^{15}$ ions/cm$^2$.

In Chapter 6, the patterning of the brain neuronal cells was demonstrated. The brain neuronal cells can adhere only on the positive-charged site surface. Then, patterning the polymeric surface, which contains the positive-charge sites, is an alternative way to neuron arrangement on the pattern. The carbon negative-ion implantation could destroy the positive-charged site and increased the negative-charged site. The positive-charged sites can be enhanced on the surface of SCPS films by coating with PDL. The uniform layer of PDL for the uniform cell adhesion could be obtained on the treated SCPS at energy of 10 keV and dose of $3\times10^{15}$ ions/cm$^2$ at the suitable coating concentration in the range of 5 – 20 μg/ml. The clear selective patterned adhesion of the rat brain neuronal cells with their axon-dendrite outgrowth on the uniform layer of PDL at the coating concentration of 5 μg/ml was obtained by carbon negative-ion implantation at energy of 10 keV and dose of $1\times10^{14}$ ions/cm$^2$ through the micro-pattern mask.

In Chapter 7, the adhesion patterning of stem cell and neuron-differentiated cell from stem cell was successfully obtained. The culture of the multipotential mesenchymal stem cell (MSC) with having the characteristics of self-renewal and differentiation into many kinds of cell lines, especially into neuron, on the $C^-$-implanted surfaces was studied. The rat MSC could adhere and grow on the implanted region. The rat MSC adhesion properties on the $C^-$-implanted polymeric surface could be controlled by the ion dose and ion energy. The suitable dose for patterning of the rat MSC adhesion on the implanted region of the $C^-$-implanted SCPS was at $3\times10^{14}$ – $1\times10^{15}$ ions/cm$^2$ for energies of 5 – 20 keV. That of the $C^-$-implanted SR was at $3\times10^{15}$ – $1\times10^{16}$ ions/cm$^2$ for energies of 10 – 15 keV. As for the differentiation into neuron, the rat MSCs on the adhesion pattern on both implanted surfaces of SCPS and SR could be differentiated into neuronal cells by an induction of $\beta$-Mercaptoethanol (BME) at concentration of 1 mM within 180 min. The neuronal cells and their neurite were obtained on the implanted region. The pattern of neuronal cells from the MSC differentiation could be achieved.

From all investigations, the objectives have been accomplished successfully. The carbon negative-ion implantation can pattern and control the neuron adhesion and their neurite outgrowth on the polymeric surface. The simple neuron network could be fabricated. Adhesions of many kinds of cell lines could be patterned on the polymeric surface by using the techniques. I can pattern not only the adhesion of PC12h cell, but also that of the stem cell by controlling the implantation conditions of ion dose and ion energy.

## 8.2 Prospects

I believe that the present study could contribute to developments of the technologies for the bio-interfaces and the medical therapies such as the artificial bionic organs and the neurological disease treatments. For future studies, the prospects are as follows.

### Application for Developments of Bio-Interface Technology

From the controllability of the immobilization and formation of a simple neuron network pattern shown in Chapters 5 and 6, I can form more complicated neuron network pattern of the brain neuronal cells. For more additional studies of the memory mechanism in the brain function with using the present study, mimicking the brain signal function might be possible. When we use this application with the technologies for the fabrication of integrated circuit (IC), the brain chip or neurochip might be fabricated. These could be useful for the more development of the technologies for the bio-interfaces to fabrication of the artificial bionic organs such as artificial vision, bionic cochlea implant and thought-controlled bionic limbs.

### Application for Developments of Medical Therapy Technology

From the adhesion patterning of the stem cells and its neuronal-differentiated cells shown in Chapter 7, I can obtained that pattern adhesion of neuronal cells. If we study more about the stem cell differentiation, it is possible to the formation of peripheral nervous system on the pattern. This might be a very useful research for the nerve regeneration or for the treatment of neurological disease such as Alzheimer's disease, spinal cord injuries or Parkinson's disease.

Moreover, since stem cells can differentiate into many kinds of cells, many researchers are going to use this stem cell, especially MSC, for the treatment of type-1 diabetes and a number of tissue engineering applications. Some of them might need the adhesion patterning of stem cell on polymeric surface, so my work could also support them.

Therefore, the carbon negative-ion implantation into polymeric surface can be an advantage promising technique for these developments related to bio-interface applications in further.

# Addendum

## List of Publications

### I. Journals

(1) "Nerve Cell Attachment Properties on Spin-Coated Polystyrene Modified by Carbon Negative-Ion Implantation"
P. Sommani, H. Tsuji, H. Sato, T Kitamura, M. Hattori, Y. Gotoh and J. Ishikawa
Trans. Mater. Res. Soc. Japan, vol. 31, no. 3, pp. 673 - 676, 2006.

(2) "Neurite Outgrowth Properties on Spin-Coated Polystyrene Modified by Carbon Negative-Ion Implantation through Pattern Mask"
P. Sommani, H. Tsuji, H. Sato, T Kitamura, M. Hattori, Y. Gotoh and J. Ishikawa
Trans. Mater. Res. Soc. Japan, vol. 31, no. 3, pp. 669 - 672, 2006.

(3) "Minimum Line Width of Ion Beam-Modified Polystyrene by Negative Carbon Ions for Nerve-Cell Attachment and Neurite Extension"
P. Sommani, H. Tsuji, H. Sato, T. Kitamura, M. Hattori, Y. Gotoh, J. Ishikawa
Nucl. Instr. and Meth., B, vol. 257, pp. 118 - 121, 2007.

(4) "Immobilization of Extracellular Matrix on Polymeric Materials by Carbon-Negative-Ion Implantation"
H. Tsuji, P. Sommani, T. Muto, Y. Utagawa, S. Sakai, H. Sato, Y. Gotoh and J. Ishikawa
Nucl. Instr. and Meth., B, vol. 237, issue 1 – 2, pp. 459 - 464, 2005.

(5) "Nerve-Cell Attachment Properties of Polystyrene and Silicone Rubber Modified by Carbon Negative-Ion Implantation"
H. Tsuji, P. Sommani, T. Kitamura, M. Hattori, H. Sato, Y. Gotoh and J. Ishikawa
Surf. Coat. Tech., In Press, Available online 12 March 2007

### II. Domestic conference presentation

(1) "Selective Attachment Properties of Nerve Cells on C-implanted Polystyrene Films"
P. Sommani, H. Tsuji, M. Hattori, T. Kitamura, H. Sato, Y. Gotoh, and J. Ishikawa
Oral and poster presentation in the 66$^{th}$ Autumn Meeting 2005 of the JSAP and Related Societies, Sep. 7 – 11, 2005, Tokushima Univ., Tokushima, 8a-ZD-13.

(2) "Effect of C-implantation on Nerve-Cell Attachment to Polystyrene Films"
P. Sommani, H. Tsuji, T. Kitamura, M. Hattori, T. Yamada, H. Sato, Y. Gotoh, and J. Ishikawa
Oral presentation in the 46th annual symposium of the VSJ, Nov. 9 – 10, 2005, Mejiro Campus of Gakushuin Univ., Tokyo, 10P – 48.

(3) "Nerve Cell Attachment Properties on Spin-Coated Polystyrene Modified by Carbon Negative-Ion Implantation"
P. Sommani, H. Tsuji, H. Sato, T Kitamura, M. Hattori, Y. Gotoh and J. Ishikawa
Oral presentation in the 16th Symposium of the MRS-J – Advanced Materials Researches Cut Paths to Innovation lead the 21st century – Session K: Innovation Material Technologies Utilizing Ion Beam, Dec. 9 – 11, 2005, Nihon Univ., Tokyo, K2-O17-D.

(4) "Neurite Outgrowth Properties on Spin-Coated Polystyrene Modified by Carbon Negative-Ion Implantation through Pattern Mask"
P. Sommani, H. Tsuji, H. Sato, T Kitamura, M. Hattori, Y. Gotoh and J. Ishikawa
Poster presentation in the 16th Symposium of the MRS-J – Advanced Materials Researches Cut Paths to Innovation lead the 21st century – Session K: Innovation Material Technologies Utilizing Ion Beam, Dec. 9 – 11, 2005, Nihon Univ., Tokyo, K2-P14-D.

(5) "Study of Nerve Growth Property on Polystyrene Surface Implanted by Carbon-Negative-Ions"
M. Hattori, H. Tsuji, T. Kitamura, P. Sommani, H. Sato, Y. Gotoh, and J. Ishikawa
Oral presentation in the 53rd Spring Meeting 2006 of the JSAP and Related Societies, March 22 – 26, 2006, Musashi Institute of Technology's Setagaya Campus, Tokyo, 24a-F-1.

(6) "Effect of Modified-Region Width of C-Implanted Polystyrene Films on Nerve-Cell Attachment"
P. Sommani, H. Tsuji, T. Yamada, M. Hattori, T. Kitamura, H. Sato, Y. Gotoh, and J. Ishikawa
Oral presentation in the 53rd Spring Meeting 2006 of the JSAP and Related Societies, March 22 – 26, 2006, Musashi Institute of Technology's Setagaya Campus, Tokyo, 24a-F-2.

(7) "Estimation of Protein Adsorption on Spin Coated Polystyrene Implanted Carbon Negative Ion"
T. Yamada, H. Tsuji, P. Sommani, M. Hattori, Y. Gotoh, and J. Ishikawa
Oral presentation in the 67th Autumn Meeting 2006 of the JSAP and Related Societies, Aug. 29 – Sep.1 2006, Biwako-Kusatsu Campus (BKC) of Ritsumeikan Univ., Shiga, 29a-K-8.

(8) "Selective Attachment Properties of Mesenchymal Stem Cells on C-Implanted Silicone Rubber"
P. Sommani, H. Tsuji, M. Hattori, T. Yamada, H. Sato, Y. Gotoh, and J. Ishikawa
Oral presentation in the 67th Autumn Meeting 2006 of the JSAP and Related Societies, Aug. 29 – Sep.1 2006, Biwako-Kusatsu Campus (BKC) of Ritsumeikan Univ., Shiga, 29a-K-9.

(9) "Observation of Surface Modification of Silicone Rubber for Mesenchymal Stem Cell Attachment by Carbon Negative Ion Implantation"
P. Sommani, H. Tsuji, M. Hattori, T. Yamada, H. Kojima, H. Sato, Y. Gotoh, and J. Ishikawa

Poster presentation in the 47th annual symposium of the VSJ, Nov. 7 – 9, 2006, Osaka Univ., Osaka, 8P – 46.

(10) "Estimation of Protein Adsorption on Polymer Material by Carbon-Negative Ion Implantation"
T. Yamada, H. Tsuji, M. Hattori, P. Sommani, H. Sato, Y. Gotoh, and J. Ishikawa
Oral presentation in the 47th annual symposium of the VSJ, Nov. 7 – 9, 2006, Osaka Univ., Osaka, 8Ba-4.

(11) "Mesenchymal Stem Cell Attachment Properties on Silicone Rubber Modified by Carbon Negative-ion Implantation"
P. Sommani, H. Tsuji, H. Sato, M. Hattori, T. Yamada, Y. Gotoh, and J. Ishikawa
Oral presentation in the 17th Symposium of the MRS-J – Advanced Materials Researches Cut Paths to Innovation – Session K: Innovation Material Technologies Utilizing Ion Beam, Dec. 8 – 10, 2006, Nihon Univ., Tokyo, K-04-D.

(12) "Modification Limit in Line Width of Carbon Negative-Ion Implantation onto Polystyrene Surface for Nerve-Cell Attachment and Neurite Outgrowth"
H. Tsuji, P. Sommani, M. Hattori, T. Yamada, H. Sato, Y. Gotoh, J. Ishikawa
Poster presentation in the 17th Symposium of the MRS-J – Advanced Materials Researches Cut Paths to Innovation – Session K: Innovation Material Technologies Utilizing Ion Beam, Dec. 8 – 10, 2006, Nihon Univ., Tokyo, K-P02-D.

(13) "Protein Adsorption Properties on Silicone Rubber Modified by Carbon Negative-ion Implantation"
P. Sommani, H. Tsuji, H. Sato, M. Hattori, T. Yamada, Y. Gotoh, and J. Ishikawa
Poster presentation in the 17th Symposium of the MRS-J – Advanced Materials Researches Cut Paths to Innovation – Session K: Innovation Material Technologies Utilizing Ion Beam, Dec. 8 – 10, 2006, Nihon Univ., Tokyo, K-P03-D.

(14) "Control of Mesenchymal Stem Cell (MSC) Attachment on Spin Coated Polystyrene Implanted Carbon Negative Ion In"
T. Yamada, H. Tsuji, P. Sommani, M. Hattori, Y. Gotoh, and J. Ishikawa
Oral presentation in the 54th Spring Meeting 2007 of the JSAP and Related Societies, March 27 – 30, 2007, Sagamihara Campus of Aoyama Gakuin Univ., Kanakawa, 28a-ZV-8.

(15) "Patterned Adhesion of Neuron Cells on Poly-D-Lysine Modified by $C^-$-Implantation"
P. Sommani, H. Tsuji, M. Hattori, T. Yamada, H. Kojima, H. Sato, Y. Gotoh, and J. Ishikawa
Oral presentation in the 54th Spring Meeting 2007 of the JSAP and Related Societies, March 27 – 30, 2007, Sagamihara Campus of Aoyama Gakuin Univ., Kanakawa, 28a-ZV-9.

## III. International conference presentation

(1) "Nerve-Cell Attachment Properties of Polystyrene and Silicone Rubber Modified by Carbon Negative-Ion Implantation"
H. Tsuji, P. Sommani, T. Kitamura, M. Hattori, H. Sato, Y. Gotoh and J. Ishikawa
Poster presentation in the 14th International Conference on SMMIB 2005, Sep. 04 – 09, 2005, Kusadasi, Turkey, IA-P7.

(2) "Minimum Line Width of Ion Beam-Modified Polystyrene by Negative Carbon Ions for Nerve-Cell Attachment and Neurite Extension"
P. Sommani, H. Tsuji, H. Sato, T. Kitamura, M. Hattori, Y. Gotoh, J. Ishikawa
Poster presentation in the 15th International Conference on IBMM 2006, Sep. 18 – 22, 2006, Taormina, Italy, P-291.

(3) "Negative-Ion Beam Modification of Polystyrene Surface for Preferential Nerve-Cell Attachment and Neurite Extension"
H. Tsuji, P. Sommani, H. Sato, T. Kitamura, M. Hattori, Y. Gotoh, J. Ishikawa
Poster presentation in the 15th International Conference on IBMM 2006, Sep. 18 – 22, 2006, Taormina, Italy, P-261.